APTAMER BASED LAB-ON-A-CHIP BIOSENSOR FOR SELECTIVE DETECTION

OF FOODBORNE PATHOGEN, *LISTERIA* SPP., IN FOOD PRODUCTS

A Thesis

by

RAMINDERDEEP KAUR SIDHU

Submitted to the Office of Graduate and Professional Studies of
Texas A&M University
in partial fulfillment of the requirements for the degree of

MASTER OF SCIENCE

Chair of Committee,   Carmen Gomes
Committee Members,   Rosana Moreira
                                    Arum Han
Head of Department,   Steve Searcy

December 2015

Major Subject: Biological and Agricultural Engineering

ABSTRACT

This research investigated impedimetric lab-on-a-chip biosensors for selective detection of foodborne pathogen, *Listeria* spp., using aptamers. *Listeria* was chosen as a model target due to its impact on the agricultural and food industries. The overall research goal of this project is to bridge the gap to address the need for real-time, highly sensitive and reliable biosensing platforms to meet the demands of on-site analysis of food products. The research objective was to develop a miniaturized aptamer biosensor that was designed and fabricated to carry out the detection of the bacteria in a simple and practical way. Miniaturization of the sensor enhanced the sensitivity and response time and allowed integration of various functionalities as a lab-on-a-chip platform. The research methods utilized the bottom-up approach of nanotechnology and dielectrophoresis techniques to improve the performance of miniaturized sensor. Pt-IMEs were functionalized with internalin A aptamers for selective binding of internalins in the cell membrane of the target bacteria, *Listeria* spp., via metal-thiol self-assembly. The aptamer biosensor was validated by taking measurements to detect foodborne pathogen, *Listeria monocytogenes*, in an off-the-shelf food product, i.e. vegetable broth at bacteria concentrations ranging from 10 to 10^7 CFU/mL. The sensitivity value was calculated to be 186.51 Ω/log(CFU/mL)] with the detection limit of 4.82 ± 0.01 CFU/mL within 12 min, which is one of the lowest detection limits reported to date.

The combination of biosensor miniaturization, aptamer functionalization of electrodes, electrochemical impedance spectroscopy and dielectrophoresis techniques for selective detection of *Listeria* spp. bacteria enhanced response time, limit of detection,

range of bacteria concentration, sensitivity and selectivity over other published

biosensors. The developed aptasensor could be easily employed for the detection of

other foodborne pathogenic bacteria to ensure food safety and public health.

DEDICATION

To my husband, Mohammad Mayyas

ACKNOWLEDGEMENTS

TABLE OF CONTENTS

LIST OF TABLES

CHAPTER I

INTRODUCTION AND LITERATURE REVIEW

1.1   Rationale and Significance

1.1.1   Need for pathogenic detection using biosensor in food safety

The Centers for Disease Control and Prevention (CDC) has estimated that up to

48 million illnesses, 128,000 hospitalizations, and 3,000 deaths each year in the United

States are caused by foodborne pathogens (CDC, 2011b, 2013a). Regardless of strict

controls and regulations to prevent foodborne pathogens in our food supply network,

there is an increase in foodborne infections incidence that continues to be an important

public health problem in the United States (CDC, 2013b). Detection methods that are

fast, sensitive, and require little expertise or training are especially desirable for "point of

care" (i.e., non-laboratory) settings (Duncan, 2011). Lab-on-a-chip based biosensors

serve as portable diagnostic tools that are being integrated with various bioassay

operations that allow the devices to rapidly sense pathogenic bacteria for field

applications such as environmental monitoring (Dutse & Yusof, 2011). The traditional

methods including total viable counts (TVC) or aerobic plate counts (APC), enzyme-

linked immunosorbent assay (ELISA), and polymerase chain reaction (PCR), real-time

PCR (rtPCR) in the food industry that are used to detect foodborne pathogens are

laborious, time consuming and expensive (Alocilja & Radke, 2003). *To date, few rapid,*

sensitive, and portable biosensors have been demonstrated in field conditions for food

safety applications. Thus, real-time, highly sensitive and reliable biosensing methods are

needed to detect pathogens in food products to ensure public health and promote food safety.

1.1.2 Significance of the designed lab-on-a-chip aptamer based biosensor

This research project contributed to the area of lab-on- chip biosensing applications through the study of aptamer functionalized electrodes and integration of dielectrophoresis techniques for real-time sensing of foodborne pathogenic bacteria. Viable and non-viable bacteria were distinguished using DEP assisted aptamer based biosesnor and it can be further used by the food industry to determine whether a serious threat is purposed by live or dead bacteria after a sterilization process and to validate other intervention processes. For instance, dead *Listeria monocytogenes* does not cause harm or fatal threats so it is vital to detect live bacteria. While many research groups are working on aptamer based biosensors or aptasensors to selectively detect the targeted pathogens and other are using dielectrophoresis techniques to attract and capture the bacteria to the working electrodes, *this project represented the first attempt to combine these two methods: functionalized electrodes with aptamers and combined electrochemical impedance spectroscopy and dielectrophoresis techniques, in a biosensor for selective capture of pathogens to ultimately improve biosensor's response time, sensitivity and detection limits.*

1.2 Research Overview and Objectives

The research goal of this project was to develop a miniaturized and portable aptamer based biosensor to detect foodborne pathogen, *Listeria* spp*.,* in food products. The technical merit of this study was in the design of a miniaturized aptamer-based

biosensor to achieve the following functions: i) ability to capture bacteria in suspension onto an interdigitated microelectrode array electrodes functionalized with optimum concentration of *Listeria*-aptamers, ii) enhanced capture of target bacteria using dielectrophoresis techniques, iv) ability to distinguish between viable and non-viable bacteria, v) ability to detect *Listeria* in food samples (vegetable broth) and in the presence of other interferents.

Hypothesis: Aptamer based *miniaturized* biosensor would feature enhanced sensitivity and response time to capture and detect *Listeria* spp. in food products.

This miniaturized aptasensor platform is expected to significantly improve the field of pathogenic detection due to the limitation of conventional technologies. The research objectives would bridge this gap by addressing a need for on-site analysis to meet the demands of current food processors and regulatory agencies. The research plan was to accomplish the following objectives:

(1) Evaluate the performance matrix of multiple interdigitated biosensor using electrode surface area and sensitivity analysis

(2) Functionalize platinum electrode with *Listeria monocytogenes* aptamers for selective binding of Internalin A in the cell membrane of the target bacteria, *L. innocua* and *L. monocytogenes.*

(3) Determine the miniaturized aptamer biosensor response to bacteria detection, *Listeria innocua,* based on electrochemical impedance spectroscopy.

(4) Evaluate the aptamer biosensor using dielectrophoresis techniques to detect foodborne bacteria, *Listeria innocua.*

3

(5) Determine the aptamer biosensor response to viable and non-viable *Listeria innocua* using dielectrophoresis and electrochemical impedance spectroscopy techniques.

(6) Evaluate the aptamer biosensor selectivity for *Listeria innocua* using *Staphylococcus aureus* as an interferent using dielectrophoresis and electrochemical impedance spectroscopy techniques.

(7) Validate aptasensor for analysis of foodborne pathogen, *Listeria monocytogenes*, in off-the-shelf food product, i.e. vegetable broth.

The thesis is organized to address the above objectives as follows: Chapter II addresses objective (1), Chapter III addresses objectives (2) & (3), Chapter IV addresses objectives (4) to (7), Chapter V concludes the final results, and Chapter VI provides future recommendations. The milestones of this project are summarized in the time-line schematic in Appendix A.

1.3   Background and Literature Review

Despite strict regulations to control the presence of foodborne pathogens in our food supply, there is an increasing incidence of illnesses and deaths from contaminated foods resulting in estimated cost of $14.6 - $16.3 billion per year (Anekwe & Hoffmann, 2013). Foodborne bacteria such as *Listeria monocytogenes* can have profound negative effects on humans including fatal infectious diseases. *Listeria monocytogenes,* for example, is one of the most common foodborne pathogens that cause infections globally, and it is the third leading cause of death from food poisoning (Cartwright et al., 2013). A person with *Listeriosis* usually has fever and muscle aches, sometimes preceded by

4

diarrhea or other gastrointestinal symptoms, but it can also lead to more serious clinical symptoms such as sepsis in the immune-comprised patients, stillbirth and miscarriages in pregnant women, meningoencephalitis in infants and adults, and febrile gastroenteritis (Schlech & Acheson, 2000). *Listeria monocytogenes* is identified as a common foodborne pathogens found in milk and dairy products, various meats and meat products, seafood and fish products, and more recently in fresh produce that cause approximately 1,600 illnesses, and 260 deaths each year in the United States, according to the Centers for Disease Control and Prevention (CDC, 2011b, 2013a). The most recent outbreaks of *Listeriosis* were associated with Blue Bell ice cream products in February 2015 when the pathogenic bacteria were isolated in chocolate chip country cookie sandwiches and great divide bars (CDC, 2015a). In September 2015, multistate outbreak of *Listeriosis* was linked to soft cheeses distributed by Karoun Dairies, Inc. (CDC, 2015c). In 2014, *Listeriosis* outbreaks were linked with dairy products from Roos Foods, cheese from Oasis Brands, Inc., prepackaged caramel apples from Bidart Bros., sprouts from Wholesome Soy Products, Inc., (CDC, 2014a, 2014b, 2015b, 2015d). The largest *Listeriosis* outbreak in U.S. history occurred in 2011 associated with cantaloupe from Jensen Farms. Centers for disease control and prevention (CDC) reported 147 illnesses, 33 deaths, and 1 miscarriage occurred among residents of 28 states (CDC, 2011a). Thus, the ability to determine whether foods are contaminated with foodborne pathogens remains an important research goal.

1.3.1 Conventional methods for detection of bacterial pathogens

L. monocytogenes is a Gram-positive, non-spore-forming, facultative anaerobic rod that can adapt to and grow in a wide range of environmental conditions, including refrigeration temperatures (2-4 ℃) and acidic and high salt environments (Gandhi & Chikindas, 2007). Currently, the detection and identification of foodborne pathogens in food industry is determined by conventional techniques such as aerobic plate counts (APC) or total viable count (TVC), enzyme-linked immunosorbent assay (ELISA), and polymerase chain reaction (PCR). APC or TVC are the oldest bacterial detection techniques that use selective media in order to detect a particular bacteria species. The selected media can contain inhibitors to stop or delay the growth of non-targeted strains and optical methods, mainly ocular inspection, are used to count growing colonies of specific bacteria (Lazcka, Del Campo, & Munoz, 2007). TVC or APC methods are accurate but expensive and time consuming requiring 5-7 days for complete analysis, requiring a pre-enrichment step (Yoon & Kim, 2012). For example, standard method NF EN ISO 11290-1 for the detection of *L. monocytogenes* relies on the ability of bacteria to multiply to visible colonies that can take up to 7 days to yield results (Leonard et al., 2003). An advantage of APC or TVC is that it detect viable bacteria. The disadvantage of APC or TVC methods is that viable bacteria can enter in dormancy state where they become non-culturable (viable-but non-culturable (VBNC)), therefore leading to underestimation of bacterial count or failure to isolate pathogen from a contaminated sample (Velusamy, Arshak, Korostynska, Oliwa, & Adley, 2010). Some faster methods to detect *L. monocytogenes* include ALOA® by AES laboratorie that can reduce the

6

detection time to 3 days using a chromogenic medium in conjunction with a *Listeria* monodisk (Artault, Blind, Delaval, Dureuil, & Gaillard, 2001). Another method developed by Vermicon Identification Technology (VIT®) consist of a commercial test system based on fluorescently labeled gene probes that took 27 hours to complete the analysis (Stephan, Schumacher, & Zychowska, 2003).

ELISA typically uses a sandwich structure, which involves the immobilization of the antigen-specific antibody on the substrate and then antigen is added to form an antigen antibody complex. The complex is then exposed to the second antibody, which binds to the antibody portion of the complex creating a sandwich structure. The signal is detected based on an enzyme attached to the second antibody, which converts to a measurable color once second antibody is attached to the antibody antigen complex (Lazcka et al., 2007). PCR is a nucleic acid amplification technology based on isolation, amplification and quantification of a short DNA sequence including the targeted bacteria's genetic material (Lazcka et al., 2007). ELISA can detect the pathogens faster but it has low affinity and poor stability as compared to colony counting and PCR, because it requires multiple steps of reagent addition and rinsing (Yoon & Kim, 2012). The ELISA system including *Listeria*-tek and a direct immunofluorescence kit (DIR) was used to detect *Listeria* using milk, meat, and cheese samples with total assay time of 48-72 hours (Nayak, Kotian, Marathe, & Chakravortty, 2009). However, ELISA is not reliable in distinguishing between viable and non-viable bacteria cells (Wang, He, & Shi, 2007). Advantages of PCR techniques include accuracy (10-20 hours analysis); however, sensitivity of the polymerase enzyme to environmental contaminants,

generations of false positives through the detection of naked nucleic acids, and difficulties in quantification are limiting factors for the use of PCR for the direct detection of microbial contamination (Leonard et al., 2003). Due to the small DNA fragment needed for detection, PCR results may be based on DNA from non-viable cells (Wang et al., 2007). Therefore, PCR cannot distinguish between viable and non-viable cells. PCR based detection of *Listeria spp.* in food samples are reported in studies done by Shearer, Strapp, and Joerger (2001), Hoffman, Gall, Norton, and Wiedmann (2003), and Murphy, McLauchlin, Ohai, and Grant (2007). Real-time PCR (rtPCR) is faster than PCR, but from industrial point of view it is not cost effective and requires trained technicians for analysis. These existing detection methods are performed in a microbiology laboratory and are time-consuming; therefore, not suitable for on-site analysis to meet the demands of current food processors and regulatory agencies (Alocilja & Radke, 2003). Hence, real-time, highly sensitive, reliable, and accurate portable technologies to detect pathogens in food products are in high demand.

1.3.2 Biosensors

In recent years, intensive research studies of rapid-screening methods for food safety have been focused on development of biosensor platforms for reliable and faster results than conventional techniques. Biosensor is an integrated bioreceptor-transducer device which is able to detect a chemical or biological target using a biological recognition element and translate the information using a measurable signal, i.e., electrical, optical, mass- or temperature-based (Thévenot, Toth, Durst, & Wilson, 2001). A bioreceptors or the biological recognition elements are the molecular species that

utilizes a biochemical mechanism for recognition, which is a key to specificity for

biosensor technologies. The biorecognition elements can include antibody/antigen,

enzymes, nucleic acids/DNA, cellular structures/cells, biomimetic and bacterio-phage

(phage) (Velusamy et al., 2010). The biochemical mechanism used by the biorecognition

element to recognize the target analyte generates biological interactions that are

converted into measurable electrical signals by the transducer for an electrochemical

biosensor. The electrical signal is amplified by the signal processor that can be easily

interpreted; the acquired signal is based on the waveform input signal, which is

computed by any shift changes in the waveform input signal. The wide variety of

bioreceptors and transducers that can be used to detect analyte provides flexibility for

biosensors that can be implemented in wide variety of clinical diagnostics, food analysis,

and environmental monitoring applications (Velusamy et al., 2010).

The biosensor research and development area started with the defining paper by

Clark reporting his invention of the oxygen electrodes in 1955. The first generation

glucose oxidase (GOx) biosensor was introduction in 1962 by Clark and Lyons which

led to quick explosion in biosensor research field (Grieshaber, MacKenzie, Voeroes, &

Reimhult, 2008). The oxygen levels were measured in a solution by first immobilizing a

thin layer of glucose oxidase enzyme over an oxygen electrode. The device monitored

the oxygen change consumed by the enzyme-catalyzed reaction at oxygen electrode and

compared the differential current by using a counter electrode (Wang, 2001). Since the

development of the first glucose biosensor many other sensing technologies and

biosensing devices has been developed because biosensors offer many advantages

including faster detection time, target specificity, real-time data collection, and simplified sample preparations (Arora, Sindhu, Dilbaghi, & Chaudhury, 2011; Grieshaber et al., 2008). The biosensors used for the detection of foodborne pathogens can be classified into three categories including optical, piezoelectric, and electrochemical.

1.3.2.1 Optical-based biosensors

Optical biosensor utilized optical properties changes as the sensing transduction signal to detect the molecular interactions between the biological recognition element and the target analyte. Two types of detection methods can be realized in optical biosensing 1) fluorescence-based detection and 2) label-free detection. Fluorescence-based detection is measured by the intensity of labeled target analyte or biorecognition element tagged with dyes or fluorescent proteins. The intensity indicates the presence of the target molecules and the strength of interaction between the recognition element and the target molecule (Velusamy et al., 2010). Green fluorescent protein (GFP) was shown to detect *Listeria monocytogenes* by inserting the GFP inside the bacteria cells (Fortineau et al., 2000). This method requires laborious labeling process that can interfere with the function of a biomolecule and the number of fluorophores cannot be controlled making quantitative analysis challenging (Fan et al., 2008).

The direct detection of the targeted bacteria or analyte due to change in electrical properties of the electrode surface when the targeted bacteria or analyte interact with the functionalized surface of biosensor is consider to be label-free. Labels including fluorophores, magnetic beads, and active enzymes are not required for electrochemical

measurements (Daniels & Pourmand, 2007). One label-free optical detection technique

is based on the measurement of refractive index (RI) induced by biomolecular

interactions between the targeted bacteria and bioreceptor, which is proportional to the

sample concentration or surface density instead of total sample mass (Fan et al., 2008;

Leonard et al., 2003). Surface plasmon resonance (SPR) is a widely used label-free

optical technique, which depends on the dielectric properties of the medium adjacent to

the metal surface affected by the binding of targeted molecules to the surface, which

changes the incident angle at a given wavelength (Tokarskyy & Marshall, 2008).

BIAcoreAB developed SPR commercial system to detect *Escherichia coli* O157:H7

bacteria using antibodies with the detection limit of 5 x 10^7 CFU/mL (Tokarskyy &

Marshall, 2008). *L. monocytogenes* was also detected using BIAcore 3000 biosensor

using polyclonal antibody with detection limit of 1 x 10^5 CFU/mL in 30 minutes. *L.

monocytogenes* and antibody were incubated followed by separation of free unbound

antibody with a stepwise centrifugation process. The response was inversely

proportional to the cell concentration when free antibody was passed over an anti-Fab

ligand-coated sensor chip surface. The signal was detected by measuring the proportion

of unbound antibody, thus inversely estimating the amount of analyte present and an

indirect estimation of cell concentration was determined (Leonard, Hearty, Quinn, &

O'Kennedy, 2004). The advantages of optical biosensors include that they are not

affected by electromagnetic interference, capable of remote sensing, and can provide

multiplexed detection within a single device (Fan et al., 2008). The disadvantages of

using SPR-based biosensors is that they are sensitive to ambient temperature drift and to

maximize the performance of the biosensor this parameter should be controlled, expensive to perform, and the equipment currently available is large in size (Lazcka et al., 2007).

1.3.2.2 Piezoelectric biosensors

Piezoelectric biosensors are another group of sensors used in pathogenic microorganism detection that are mass sensitive detectors generating and transmitting acoustic waves that operate on the basis of an oscillating crystal that resonates at a fundamental frequency (Arora et al., 2011). The crystal oscillations at its natural resonant frequency are caused by two excitation electrodes that apply electrical field to a sandwiched crystal between the electrodes. The crystals are coated with the biorecognition elements and when exposed to the targeted molecule a change in resonant frequency of the crystal occurs, which correlates to mass changes at the crystal surface (Leonard et al., 2003). The advantages of piezoelectric biosensors include that they are label-free, sensitive, low-cost, easy to use, and on-line analysis for antigen-antibody interactions (Leonard et al., 2003).

Quartz crystal microbalance (QCM) is the most common type of piezoelectric biosensors. Generally, QCM consist of a thin disk of AT (single rotation cut at $\varphi = 0°, \theta = 34°$) cut quartz, which is cut at an angle of +35° 15' along the z-axis (Leonard et al., 2003). Su and Li (2004) demonstrated QCM biosensor for *E. coli* O157:H7 detection based on immobilized antibodies on an AT-cut quartz crystal Au electrode surface. Antibodies were attached onto the surface via either protein-A or NHS ester derived from 6-mercaptohexadecanoic acid (MHDA) and frequency shift detected

from the biosensor resonant frequency was correlated to the bacteria concentration. The

QCM biosensor detected *E. coli* O157:H7 in the range of $10^3 - 10^8$ CFU/mL within 30-

50 minutes. In another study by Babacan, Pivarnik, Letcher, and Rand (2002), protein A

antibody was immobilized on the surface of QCM biosensor for the detection of

Salmonella Typhimurium with the low detection limit of 10^6 CFU/mL in 40 minutes.

The disadvantages of piezoelectric biosensors are associated with long incubation times

between bacteria and antibodies, crystal surface regeneration problems due to number of

washing and drying steps (Leonard et al., 2003).

1.3.2.3   Electrochemical biosensors

Electrochemical biosensors are the most studied for a broad spectrum of

applications due to the inherent advantages of their robustness, easy miniaturization, low

detection limits, small analyte volumes, and simplicity to use, as exemplified by the

Clark-type glucose biosensor discussed above (Grieshaber et al., 2008). The method

designed for direct monitoring of bio-recognition element and antigen interactions

without the need for labeling has been attractive as an alternative to the traditional

methods. The label-free methods provide faster detection methods when combined with

the bio-recognition elements such as monoclonal antibodies, aptamers, or enzymes

(Prodromidis, 2010; Tokarskyy & Marshall, 2008). Electrochemical biosensors are able

to detect the targeted bacteria by sensing the changes in the electrical properties caused

by biochemical reactions (Grieshaber et al., 2008). Based on the electrical parameters

such as current, potential, conductance, and impedance; electrochemical biosensors can

be classified into amperometric, potentiometric, conductometric, and impedimetric, respectively.

Amperometric biosensor detects the targeted analyte by measuring the current generated by reduction and oxidation of an electroactive species due to molecular interaction of biorecognition element and analyte at the working electrode. The applied potential is maintained between working and reference electrodes. The potential is the driving force for the oxidation and reduction reaction of an electroactive species (Velusamy et al., 2010). There are numerous amperometric biosensors employed to detect foodborne pathogens including a *L. monocytogenes* study by Chemburu, Wilkins, and Abdel-Hamid (2005) that detected 50 CFU/mL in milk and chicken extract samples within 30 minutes. Amperometric biosensors offer the advantage that they are sensitive, small, robust, economical rapid and portable. However, these sensors can suffer from poor selectivity and require electroactive species oxidation or reductions for detection to occur which can be limiting depending of the analyte (Leonard et al., 2003).

Potentiometric biosensor uses ion selective electrodes to detect the targeted bacteria by an enzyme-catalyzed reaction that generates or consumes a species. The potentiometric device consists of a perm-selective outer layer and a bioactive material such as enzyme that measures the electrical potential difference or electromotive force (EMF) between two electrodes at near zero current that provides logarithmic concentration dependent response (Leonard et al., 2003; Velusamy et al., 2010). The commonly used potentiometric devices include filed effect transistor (FET). The advantages of potentiometric biosensors are that they are portable, inexpensive, and

14

facilitate continuous monitoring in, *in situ* conditions (Arora et al., 2011). There are only few potentiometric devices that have been used to detect foodborne pathogens because of their limited flexibility to change the biorecognition element based on Debye screening length (λ_D). Debye screening is defined as a distance where moving charge carriers screen out of the external electric filed and electrical potential difference should take place within λ_D normally less than 10 nm. If using biorecognition element such as antibodies in FET devices, the biomolecular interactions occur beyond 10 nm from the gate surface due to the height of antibody. Therefore, these interactions would be beyond the Debye screening length to measure any electrical potential differences (Lee, Kim, & Kim, 2009). *E. coli* O157:H7 has been reported to be detected by potentiometric device by Ercole, Del Gallo, Mosiello, Baccella, and Lepidi (2003) with detection limit of 10 CFU/mL in 1.5 hours using blended lettuce, sliced carrots, and arugula in a stomacher to form liquid medium.

Conductometric based biosensors detects analytes by measuring the electrical conductivity that corresponds to a change in the ionic species concentrations. The conductometric device consists of two metal electrodes separated by known distance and alternating current (AC) voltage is applied across the electrodes to monitor the change in conductance between two electrodes during interactions between biorecognition element and targeted bacteria (Velusamy et al., 2010). Muhammad-Tahir and Alocilja (2003) developed conductometric biosensor to detect *E. coli* spp. with the lower detection limit of 7.9 x 10^1 CFU/mL in 10 minutes. Nutrient broth from Difco Laboratories (Detroit, MI) was used for *E. coli* enrichment and was serially diluted in 0.1% of peptone water to

15

obtain varying concentrations of the bacteria. The advantage of conductometric based biosensor is that no reference electrode is required; they are suitable for miniaturization and mass production using thin-film technology. The disadvantage of using this type of biosensor is that the sensitivity of the measurement is hindered by the parallel conductance of the sample solution (Thévenot et al., 2001).

Finally impedimetric based biosensors measures the impedance change in a response to small amplitude sinusoidal excitation input when the molecular interactions take place at the surface of the working electrode. Unlike potentiometric and conductometric biosensors, there is no need for charge transfer between electrode and analyte/biorecognition agent such as an oxidation/reduction reaction or charged analyte to measure electrical properties at the electrode surface. Impedance is solely based on the attachment of analyte to the surface of the electrode and its effect on the electrical properties of the biosensor (Leonard et al., 2003). Therefore, providing direct measurements due to molecular interactions between the analyte and surface of the electrode by monitoring electrical properties. The development of impedimetric biosensors has been widely employed to detect foodborne pathogens in recent years (Yang & Bashir, 2008). Impedimetric electrochemical biosensors drew a lot of attention in past decade because these sensors are considered as promising candidates for on-site applications due to their ease of miniaturization, label-free capabilities, low cost, and the ability to integrate into multi-array or microprocessor-controlled diagnostic tools, and to control remotely (Prodromidis, 2010).

1.3.3 Electrochemical impedance based biosensors

Impedance based biosensors uses electrochemical impedance spectroscopy technique (EIS) to detect the target analyte, such as foodborne pathogenic bacteria. EIS is an alternating current method that describes the response of the electrochemical cell by measuring current to a small amplitude sinusoidal voltage signal as a function of frequency (Prodromidis, 2010). The resulting current sine-wave shifts in time with respect to the input voltage sine wave which can be described as a ratio $V(t)/I(t)$ defined as impedance (Z) in Ohms. The ratio can be written as:

$$Z = \frac{V(t)}{I(t)} = \frac{1}{Y} = \frac{V_o \sin(2\pi f t)}{I_o \sin(2\pi f t + \phi)} \tag{1.1}$$

where V_o (Volts) and I_o (Amperes) are the maximum voltage and current signals, f (Hz) is the frequency, t is time (seconds), ϕ (degrees) is the phase shift between the voltage-time and current-time functions, Y is the complex conductance or admittance (Siemens) (Y. Wang, Ye, Z.,Ying, Y., 2012). Impedance is a complex value that depends on multiple factors in an electrochemical cell such as electrode kinetics, redox reactions, diffusion phenomena and molecular interactions at the electrode surface. These factors can be described by the impedance modulus, $|Z| = \sqrt{(Z')^2 + (Z'')^2}$, where Z' is the real part and Z'' is the imaginary part of the complex impedance modulus measured in Ohms (Lasseter, Cai, & Hamers, 2004). EIS is evaluated using either Nyquist or Bode plots. In Nyquist plot, the imaginary impedance component Z'' is plotted against the real impedance component Z' and in Bode plot, impedance modulus $|Z|$ and the phase shift

17

ϕ are plotted against the logarithm of the excitation frequency (Y. Wang, Ye, Z.,Ying, Y., 2012). The broad frequency range from anywhere between 1 Hz to 1 MHz could be applied for EIS analysis and Nyquist and Bode plots are generated to understand the behavior of the biosensor over a range of frequencies. Bode plots produce total impedance modulus versus log frequency over a broad applied frequency range, which can be used to identify significant total impedance changes between the bare and target-analyte on an analyte concentration dependence manner. Nyquist plots are further used to confirm significant impedance changes between the bare and target-analyte samples at different analyte concentrations by comparing the imaginary impedance component Z'' and the real impedance component Z' over an applied frequency range (Dastider, Barizuddin, Dweik, & Almasri, 2013).

Impedance biosensors have been designed for a number of biorecognition elements but the most common for detecting foodborne pathogens are antibodies. Impedimetric based biosensors that are directly immobilized by the antibodies on the surface of the biosensor electrodes to capture targeted bacteria are called impedimetric immunosensors. The attachment of the bacteria cells onto the antibodies is monitored by the change in electrical properties over a range of frequency due to insulating properties of the cell membrane (Y. Wang, Ye, Z.,Ying, Y., 2012). Direct immobilization of antibodies is called label-free detection to measure the impedance changes caused by antibody-antigen interactions, which provides faster detection time, low cost, simple detection protocols, and high specificity over the indirect methods. Indirect methods can

18

include pre-concentration steps of the bacteria cells onto the surface of the electrodes without the use of a biorecognition element.

Other biorecognition elements such as aptamers, bacteriophages, and lectins have been also used to detect pathogenic bacteria in impedimetric biosensors. The sensitivity of impedimetric sensors compared to other sensors was considered to be lower, however; over the last decade it has been improved by using miniaturized interdigitated microelectrodes array (IMEs) to enhance the detection limits (sensitivity). Yang, Li, and Erf (2004a) developed an electrochemical impedance immunosensor by immobilizing anti-*E. coli* antibodies onto the surface of IMEs for the detection of *E. coli* O157:H7 with the detection limit of 10^6 CFU/mL in the presence of ferrocyanide $[Fe(CN)_6]^{3-/4-}$ redox solutions. Impedance based biosensors offer rapid, portable, and inexpensive detection of foodborne pathogenic bacteria. The impedimetric biosensors have many advantages including that they are label-free simplifying assembly process and lowering the cost, rapid with detection time generally lower than 30 minutes and provides miniaturization realization helping to improve the sensitivity and minimize the testing sample volumes. Although impedimetric biosensor offer so many advantages yet there is no commercial product based on impedance biosensors that have launched successfully in the biosensing market for foodborne pathogens detection. The limitation in label-free biosensors is the poor affinity (i.e.; pathogen binding to capture probe) in complex solutions. Due to this limitation, biosensors have failed to compete with PCR and ELISA in applied pathogen detection within the food industry. To date, no reliable, rapid, sensors have been demonstrated in field conditions for food safety applications that can

19

detect as few as 1 viable target cell in 25 g of food. Therefore, further efforts should be continued to develop commercial products based on impedance biosensors to detect foodborne pathogenic bacteria with improved stability, reduced volume, increased sensitivity and lower costs (Wang, Ye, & Ying, 2012).

1.3.4   Interdigitated microelectrodes array in impedance measurements

Miniaturized impedance biosensors based on lab-on chip systems utilize microfabrication techniques to fabricate microelectrode arrays (Dutse & Yusof, 2011). In biosensing, microelectrodes have been used for various sensing devices due to small ohmic potential drop, fast establishment of steady-state signals, faster response time, and increased signal-to-noise ratio (Cohen & Kunz, 2000; Kim et al., 2004; Zoski, 2006). Micro-fabrication techniques can be used to produce microelectrodes with the variation of sizes and/or shapes as compared to conventional methods that are limited to one size and/or shape. More specifically, interdigitated microelectrode arrays (IMEs) can be fabricated using lithography techniques allowing controlled dimensions of the microelectrodes to study electrochemical behavior. IMEs are defined as alternating microelectrodes connected to one another that are separated by known distance (Varshney & Li, 2007).

There are several design parameters that could affect the sensitivity of the interdigitated microelectrodes array including width, height, gap, and material. These parameters determine the electrode performance in an electrochemical cell and changing one parameter can have positive effect in one aspect and negative effect in another. For example, when increasing an electrode width can increase the surface area of the

electrode to allow more target binding, however; it can also increase the signal-to-noise ratio (Stulík, Amatore, Holub, Marecek, & Kutner, 2000). In principle, IMEs have three main advantages over conventional electrodes for biosensing: (1) an enhanced sensitivity over conventional macro electrodes due to sub-micron electrode width and spacing, therefore increasing the surface area; (2) fabrication by lithographic techniques allowing reproducible and low cost devices; and (3) direct biosensing using impedimetric methods instead of fluorescent, enzymatic or electrochemical labels (4) enhanced portability (Laureyn et al., 2000).

1.3.5   Aptamer based impedance biosensors

Nucleic acid aptamers are artificial short single stranded oligonucleotides, either DNA or RNA, that are selected by combinatorial libraries which can bind to target molecule with high affinity. Aptamers are selected through *in vitro* process known as systematic evolution of ligands by exponential enrichment (SELEX) (Song, Wang, Li, Fan, & Zhao, 2008). SELEX is a chemical selection method that uses a randomized oligonucleotides library (10^{13} to 10^{15} fragments) mixed with the target bacteria or molecule to amplify and isolate the bound oligonucleotides sequence to the targeted molecule. This amplification and isolation process is performed by using polymerase chain reaction. The amplified sequences are repeated through multiple cycles, 6-20 rounds, by mixing with the targeted molecule until high affinity and high specificity aptamer sequence is achieved (Stoltenburg, Reinemann, & Strehlitz, 2007). The affinity of aptamers for their targets is comparable to, and in some instances higher than, monoclonal antibodies that have been used for detecting the target analyte, such as

21

bacteria. As compare to antibodies aptamers offer many advantages: 1) aptamers are composed of nucleic acids that are chemically synthesized with high purity avoiding batch-to-batch variations; 2) during the synthesis process aptamers can be modified with different functional groups such as –HS, -NH$_2$, and biotin that can immobilized onto the electrode surface based on user specific applications; 3) aptamers are highly stable and reusable after simple thermal melting of the DNA duplex allowing for biosensor regeneration (Y. Wang, Ye, Z.,Ying, Y., 2012).

Nucleic acid aptamers based impedimetric biosensors contain immobilized nucleic acid that captures target analyte by matching its complementary base pair sequences and transform the biorecognition molecule into impedance signal. In recent years, aptamer based biosensor technology platform is creating interest because it promises equally reliable results in a shorter time than aforementioned traditional detection methods. Due to aptamers inherent advantages of simple production, easy storage, good reproducibility, target versatility, easy modification, and convenient regeneration, they are considered to be ideal biorecognition elements for biosensor applications (Kärkkäinen et al., 2011). Recent efforts have expanded the library of aptamers for common foodborne pathogens; therefore, aptamers are being used to construct biosensors called aptasensors.

A number of aptasensors devices have been developed for monitoring various foodborne pathogens including *Salmonella* Typhimurium with detection of 600 CFU/mL in phosphate buffer saline solution within 10 minutes by Labib et al. (2012). Another study performed by Wu et al. (2012) detected *Escherichia coli* O157:H7 with a detection

22

range of $10^4 – 10^8$ CFU/mL in 2 hours using fecal samples. In another study by Ohk,

Koo, Sen, Yamamoto, and Bhunia (2010), *L. monocytogenes* was detected with a

detection limit of 10^3 CFU/mL in pure solution and 10^2 CFU/25 g of food sample after

18 hours. Luo et al. (2012) developed an aptasensor for the detection of *E. coli* O111

with detection limit of 1.1 x 10^2 CFU/mL in phosphate buffer saline and 3.1 x 10^2

CFU/mL in milk within 3.5 hours. However, to date, few, rapid, sensitive aptasensors for

Listeria detection have been demonstrated in field conditions for monitoring food safety.

1.3.6   Dielectrophoresis based impedance biosensors

In addition to aptasensors, researchers have also used dielectrophoretic

impedance measurement (DEPIM) technique with biosensors to improve the capture

efficiency of foodborne pathogens. Dielectrophoresis, DEP, can overcome the detection

limit due to limited physical sensitivities of the transducers and low immune-capture

efficiency of the immobilized antibodies on the electrode surfaces (Suehiro, Ohtsubo,

Hatano, & Hara, 2006; Yang, 2009). DEP has been used to manipulate biological cells

for filtering, focusing, sorting, and trapping in desired position and orientation (Cheng,

Chang, Hou, & Chang, 2007).

Dielectrophoresis is a mechanism where at a given alternating excitation input,

interdigitated microelectrodes generates electrostatic force-field that attracts the

polarized bacteria close to the force-field (Suehiro et al., 2006; Yang, 2009).

Dielectrophoresis is the electrokinetic motion of dielectrically polarized particles in non-

uniform electrical fields (Yang, 2009). Most biological cells or bacteria behave as

dielectric particles in external fields, DEP can attract polarized particles to the high field,

23

in order to trap bacteria onto an interdigitated microelectrode chip (Suehiro, Hatano, Shutou, & Hara, 2005). The trapped bacteria onto the surface of the electrodes increase the impedance of the biosensor and consequently sensitivity.

Interdigitated microelectrode arrays (IMEs) has been proven to be the most suitable for dielectrophoresis for its relative ease of micro-scale generation and structuring of an electric field. The advantage of integrated dielectrophoresis is that it provides speed, flexibility, controllability and ease of application to automation (Li & Bashir, 2002). The study conducted by Yang (2009) of DEP assisted techniques has shown two significant functions in the biochip platforms using IMEs to improve the detection (i) DEP can concentrate bacterial cells from the suspension to different locations on the chip surface, which make it very useful in manipulating bacterial cells in biosensors and biochips; (ii) DEP can make bacterial cells in close contact with the immobilized antibodies on the chip surface, which can effectively improve the immuno-capture efficiency (Yang, 2009).

DEP assisted bacteria detection has been used for various IMEs devices including the detection of *E. coli* (Cheng et al., 2007; Suehiro, Hamada, Noutomi, Shutou, & Hara, 2003; Suehiro et al., 2005; Suehiro, Noutomi, Shutou, & Hara, 2003; Suehiro et al., 2006), *L. monocytogenes* (Koo et al., 2009), and *Salmonella* (Yang, 2009). The lowest detected bacteria concentration among these studies was 10^2 CFU/mL using optical methods to measure the bacteria capture efficiency suspended in DI water by applying DEP signal for 15 min.

DEP has also been employed for the separation of viable and non-viable cells, and it can be further used in the food industry to determine whether a serious threat is purposed by live or dead bacteria after a sterilization process and to validate other intervention processes. DEP can separate live and dead bacteria utilizing the difference of dielectric properties between live and dead bacteria cells, which are different due to increased cell porosity of dead bacteria (Li & Bashir, 2002). For instance, dead *Listeria monocytogenes* does not cause harm or fatal threats so it is vital to detect live bacteria. There are various studies that demonstrate the separation or detection of viable and non-viable bacteria (Li & Bashir, 2002; Suehiro, Hamada, et al., 2003). These studies use optical method to detect the separation of viable and non-viable *Escherichia coli* cells with the lowest concentration of 10^5 CFU/mL suspended in DI water with applied DEP signal for 5 minutes

The performance criteria of a biosensor include sensitivity, selectivity, range, limit of detection and response time. These performance parameters are not specific to biosensor type, but generalized to the detection of the target analyte and it is applicable to any analytical method. Sensitivity is described by the change in response that results from a unit change in concentration of an individual analyte. Selectivity is biosensor's ability to distinguish different pathogens/analytes present in the solution (Thévenot et al., 2001). Limit of detection refers to the range of the bacteria/analyte concentration that biosensor can detect. The lower detection limits can be determined as a signal/noise ratio of 3, where noise is defined as the standard deviation of the control test without bacteria/analyte (J. Wang, 2006). The response time of the biosensor is based on the time

taken to prepare a sample and its ability to obtain a detectable signal. Biosensor range

could be determined based on the detectable linear response signal obtained over a range

of bacteria/analyte concentration, i.e., biosensor should be able to discriminate between

the response signal over a bacteria/analyte concentration range (J. Wang, 2006). In other

words, the linear range of a concentration dependence is referred to as the biosensor

dynamic range (Cunningham, 1998).

CHAPTER II

BIOSENSOR FABRICATION AND DEVICE COMPATIBILITY

2.1 Overview

Biosensors based on lab-on-a-chip for bacteria detection have been emerging as a viable alternative to traditional techniques such as total viable counts (TVC), enzyme-linked immunosorbent assay (ELISA), and polymerase chain reaction (PCR). The traditional methods are time consuming, expensive, and require specialized facilities and trained personnel. Impedance biosensors based on lab-on-a-chip system have been used for the detection of pathogenic bacteria using interdigitated microelectrodes array to achieve enhanced sensitivity and response time. In this study, an optimized design based on multiple interdigitated microelectrodes (IMEs) array was used for the detection of pathogenic bacteria. The IME based biosensor was fabricated using the Aggiefab facility at Texas A&M University (College Station, TX).

The electrode performance of multiple interdigitated microelectrodes (IMEs) array based biosensor was characterized by using electrochemical techniques including cyclic voltammetry and direct current potential amperometry measurements of reversible redox species. IMEs with different geometric electrode gap were fabricated by microfabrication lithographic techniques. All electrode measurements were performed via a 3 electrode set-up with Ag/AgCl as reference electrode. The electroactive surface area (ESA) of designed 25, 50, 100 μm IMEs was calculated from cyclic voltammagrams using Randles-Sevick equations with values of 0.7181 ± 0.0196, 0.1436 ± 0.0018, and 0.0718 ± 0.0024 cm^2, respectively. Cyclic voltammetry was carried out in

4mM $Fe(CN)_6$/1M KNO_3 solutions at a switching potential of 750 mV with 10 seconds quiet time at scan rates from 10, 20, 50, 75, and 100 mV·s^{-1}. The sensitivity was calculated from DCPA using H_2O_2 (0.58 M increments in phosphate buffered saline, PBS, pH 7.4 at room temperature) with the values of 21.39 ± 0.1335 and 5 ± 0.0298 μA mM^{-1} for 50 and 100 μm IMEs, respectively. A direct relationship was observed between surface area and sensitivity. Based on highest sensitivity results, 50 μm IME device was chosen to further functionalize with aptamers (*Listeria monocytogenes*-aptamers) via metal-thiol self-assembly for *Listeria* spp. detection.

2.2 Introduction

Listeria monocytogenes have caused major food pathogenic outbreaks globally and it is identified as third leading cause of death from food contamination (Cartwright et al., 2013). Current methods to detect foodborne pathogens are laborious and can take several days to produce results. These methods include total viable counts (TVC), enzyme-linked immunosorbent assay (ELISA), and polymerase chain reaction (PCR). Real-time PCR (rtPCR) is faster than PCR, but it is expensive and requires trained technicians for data analysis (Yoon & Kim, 2012). As a result, there is a demand for a real-time, highly sensitive, reliable, and accurate portable technologies to detect pathogens in food products.

Electrochemical biosensors referred as amperometric, potentiometric, conductimetric, or impedimetric have been developed in recent years for rapid, sensitive, selective detection of foodborne pathogenic bacteria to ensure food safety and security (Wang et al., 2012). Impedance based electrochemical biosensors uses the change in

electrical properties of materials in response to a sinusoidal potential excitation signal with small amplitude measuring current (Prodromidis, 2010) . Impedimetric biosensors works based on the impedance change due to binding of target molecules to the capture probes including antibodies, DNA, proteins, and other biorecognition elements immobilized on the surface of the electrodes (Radke & Alocilja, 2005a; Varshney & Li, 2009).

Impedimetric biosensors based on lab-on chip systems utilize microfabrication techniques to fabricate interdigitated microelectrodes array (Dutse & Yusof, 2011). Interdigitated comb fingers consist of a series of parallel microband electrodes connected together in alternating sequence to form an array. Interdigitated microelectrodes array have been integrated with impedance biosensors in order to miniaturize the conventional electrodes and enhance the sensitivity (Varshney & Li, 2009). In biosensing, microelectrodes have been used for various sensing devices due to small ohmic (iR) drop, fast establishment of steady-state mass transfer, and small capacitive charging currents (Cohen & Kunz, 2000; Kim et al., 2004). Microfabrication techniques can be used to produce microelectrodes with the variation of sizes and/or shapes as compared to conventional methods that are limited to one size and/or shape. More specifically, interdigitated microelectrodes (IMEs) can be fabricated using lithography techniques allowing controlled dimensions of the microelectrodes to study electrochemical behavior. In principle, IMEs have three main advantages over conventional electrodes for biosensing: (1) an enhanced sensitivity over conventional macro electrodes due to sub micron electrode width and spacing, therefore increasing the surface area; (2) the

fabrication by lithographic techniques allowing reproducible and low cost devices; and (3) direct biosensing using impedimetric methods instead of fluorescent, enzymatic or electrochemical labels (4) enhanced portability (Laureyn et al., 2000).

Various IMEs designs have been implemented in biosensor's design for detection of the targeted bacteria. The design parameters that affect the overall principle of the IMEs sensitivity and selectivity include electrode width, height, and length, spacing between electrodes, and electrode material. The use of the material depends on the intended application, ionic species involved, and inertness of the material to the environment, and fabrication ease and suitability. Several materials have been used for impedance detection of IMEs such as platinum (Pt), gold (Au), and titanium oxide (TiO_2) (Gómez-Sjöberg, Morisette, & Bashir, 2005; Gómez, Bashir, & Bhunia, 2002; Radke & Alocilja, 2004; R. Wang, Ruan, Kanayeva, Lassiter, & Li, 2008). Platinum was used to design the electrodes in this study due to its inert properties, excellent sensitivity for ferrocyanide oxidation and reduction reactions, and most importantly the ease of fabrication onto the silicon dioxide substrate. A study shown by (Min & Baeumner, 2004) demonstrated that there is no significant effect of number of electrodes on signal to noise (S/N) ratio as compared to the other parameters because signal value is proportional to the surface area of the entire IMEs array, whereas background noise is proportional to the area of the electrodes only (Varshney & Li, 2009). Therefore, increasing the number of electrodes will also increase the background noise leading to no change in the S/N ratio. Therefore, fixed active area of 0.81 cm^2 was used for multiple electrode gaps in this study. The S/N ratio was increased by using optimal

height of 70 – 140 nm for ferrocyanide redox reactions, according to (Min & Baeumner, 2004) studies. The electrode height of 100 nm was achieved in this study using platinum deposition. The ratio of the gap size between electrodes to the width of each electrode is key to increasing the sensitivity for the detection of redox species among the other design parameters. Several electrode gaps and widths have been used for IMEs to study the detection of pathogenic bacteria (Varshney & Li, 2009). In this study, electrode gaps of 15, 25, 50, and 100 μm with electrode width were investigated based on the size of the targeted bacteria between 2 and 4 μm and limitation of the mylar mask resolution used for the fabrication of the IMEs. The sensitivity of electrode width and gap size was determined in this study.

Several impedance-based biosensors have been developed for the detection of pathogenic bacteria based on interdigitated microelectrodes array using specific and non-specific bio-recognition elements immobilized onto the surface of the IMEs. For instance, Yang et al. (2004a) showed IMEs coated surface with anti-*Escherichia coli* antibodies for the detection of *E. coli* O157:H7. The detection range of the biosensor was 4.36×10^5 to 4.36×10^8 CFU/mL measured in the presence of ferri/ferrocyanide solution. Radke and Alocilja (2004) used open gold interdigitated microelectrode array chip with immobilized antibodies to detect *E. coli* O157:H7 by performing impedance measurements by immersing the electrodes into a known concentration of bacteria suspended in peptone water. The biosensor was found to be sensitive for the detection range from 10^5 to 10^7 CFU/mL. The minimum detection limit of the sensor was improved from 10^5 to 10^4 CFU/mL using the same methodology and electrode setup in

pure cultures and romaine lettuce wash water. The immobilized antibodies on the electrode surface were selective for the detection of target bacteria, *E. coli* O157:H7, in the presence of non-target bacteria, *Salmonella infantis* (Radke & Alocilja, 2005a, 2005b). The use of a biorecognition element directly on the surface of the interdigitated microelectrodes provides specificity to the biosensor by bringing the targeted bacteria within few nanometers of the sensing electrodes maximizing the effect that the targeted bacteria has on impedance (Varshney & Li, 2009).

Another method for detecting pathogenic bacteria cells with IMEs includes the use of magnetic beads coated with bio-recognition elements, instead of their immobilization onto the surface of the electrodes, for specific separation and concentration of cells before impedance measurements (Varshney & Li, 2009). Varshney and Li (2007) demonstrated a label-free impedance biosensor based on gold IMEs to detect *E. coli* O157:H7 in food samples that were separated by using magnetic nanoparticle-antibody conjugates (MNAC) functionalized with anti-*E. coli* antibodies before applying impedance. After the separation of conjugated targeted bacteria and antibody using magnetic beads, the bacteria cells were resuspended in a mannitol solution and uniformly spread on to the IMEs surface by placing a magnet underneath the microchip. This impedance biosensor based on IMEs and MNAC was able to detect a minimum of 7.4×10^4 and 8.0×10^5 CFU/mL of *E. coli* O157:H7 in pure culture and ground beef samples, respectively. To further improve the detection limit of the target bacteria, *E. coli* O157:H7, the same techniques were used in a microfluidic device embedded with gold IMEs; where a small volume of 60 nL was used to detect the

bacterial cells (Varshney, Li, Srinivasan, & Tung, 2007). This further improved

impedance biosensor was able to detect a minimum of 1.6×10^2 and 1.2×10^3 CFU/mL

of *E. coli* O157:H7 in pure culture and ground beef samples, respectively; with detection

time of 35 minutes from sampling bacteria from food matrix to measurement.

Interdigitated microelectrodes array have been used for foodborne bacteria

detection based on metabolites produced as a result of bacterial growth by measuring the

change in the electrical conductivity of the medium during growth of microorganism.

Gomez et al. (2002) showed a platinum IMEs embedded in a flow cell to detect

metabolic activity of live and heat-killed bacterial cells in a low conductivity medium

specifically designed to maximize the change in conductance of the medium due to

growth of *L. innocua, E. coli, L. monocytogenes*. After 2 hours of off-chip incubation at

37°C, the limit of detection of live cells distinguished from the same number of heat-

killed cells in low conductivity medium was 100 cells for *L. innocua*, 200 cells for *L.

monocytogenes*, and 40 cells for *E. coli*. Yang et al. (2004b) designed an open (non-

microfluidic) IMEs device used for the detection of *Salmonella* Typhimurium in milk

samples using selective medium as a pre-enrichment growth and also to determine the

specificity of the biosensor to the targeted bacteria. The impedance system was able to

detect a range of *S*. Typhimurium from 4.8 to 5.4 x 10^5 CFU/mL after a pre-enrichment

growth step of 9.3 and 2.2 hours, respectively. The biosensor selectivity was determined

in the presence of *L. monocytogenes*, *E. coli* O157:H7, and *Pseudomonas aeruginosa*

with selective medium consisting of selenite cystein broth supplemented with

trimethylamine oxide and mannitol, for *S*. Typhimurium.

Even though there have been many studies on using IMEs-based biosensors to detect foodborne pathogens, to date, no reliable, rapid, sensors have been demonstrated in field conditions for food safety applications that can detect as few as 1 viable target cell in 25 g of food. The main goal of this study was to design and fabricate platinum interdigitated microelectrodes (IMEs) array to miniaturize the biosensor in order to enhance sensitivity while using aptamers as the biorecognition element, on the surface of the electrodes for capture and detection of *Listeria* spp. in food products. In order to achieve this goal the first step was to optimize the IMEs design. IMEs with various electrode gap geometries were fabricated and the electrodes' performance was characterized by electrochemical techniques including cyclic voltammetry and direct current potential amperometry.

2.3   Materials and Methods

2.3.1   Chemicals, reagents, and equipment

Silicon wafer (4 inches) with wet thermal oxide thickness of 90 and 300 nm with the resistivity of 0.001-0.005 Ohm-cm was purchased from University Wafer (Fremont, CA). Platinum pellets, Pt, 99.99% pure, 1/8" diameter were obtained from Kurt J. Lesker (Jefferson Hills, PA). LOR 3A, non UV sensitive polymer, was purchased from MicroChem (Newton, MA). AZ 5214 E-positive photoresist, AZ 726 MIF-standard photoresist developer, AZ 400T-photoresist stripper were purchased from EMD Performance Materials (Sommerville, NJ). Mylar mask was ordered from CAD/Art Services, Inc (Bandon, OR). Potassium ferrocyanide trihydrate was purchased from Ward's Science (Rochester, NY) and potassium nitrate was purchased from Alfa Aesar

(Ward Hill, MA). Hydrogen peroxide (3 wt %) was purchased from a local HEB store (College Station, TX). Silver conductive epoxy was purchased from Allied Electronics (Austin, TX). Silver/silver chloride (Ag/AgCl) standard reference electrode and platinum auxiliary electrodes were purchased from BASi (West Lafayette, IN). Verteq photoresist spinner, Karl Suss MA6 mask aligner, Lesker PVD 75 e-beam evaporator, dicing saw, and hotplate were used to fabricate the interdigitated microelectrode array biosensor at the Aggiefab facility at Texas A&M University (College Station, TX). CHI 600E potentiostat (Austin, TX) with CHI6044e software was used for electrochemical analysis. Bruker Dektak Profilometer (Tucson, Arizona) was used to measure the features on the wafer.

The biosensor was fabricated using a platinum array of interdigitated microelectrodes (IME) commonly referred to as comb fingers connected to a larger contact pad on each side of the silicon dioxide substrate and silver conductive was used to perform the wire bonding for analytical testing. The thickness of wet thermal oxide is 90 and 300 nm on 4 inches silicon wafer. Table 2.1 lists the elements of the biosensor. The layout for the IME design was drawn in *DraftSight* (Waltham, MA) as shown in Figure 2.1. The electrodes were consisted of four different type of electrode gap including 15, 25, 50, and 100 μm. The electrode gap was considered based on the size of target bacteria cell and the best electrode gap was chosen based on sensitivity and effective electrode surface area. Thus, there were eight devices in total with two replicas for each Si wafer. Each interdigitated microelectrodes array width was 25 μm with total active area of 0.81 cm^2 and bonding pads 200 x 200 μm. Within the total active area of

0.81 cm^2, the number of electrodes changed for each IMEs with different electrode gap.

Table 2.1. Elements of biosensor design consisting of a platinum array of interdigitated microelectrodes.

Element	Dimensions
Substrate	4" SiO$_2$ wafer with thermal oxide layer
Active area	0.81 cm^2
Electrode width	25 μm
Electrode gap	15, 25, 50, and 100 μm
Bonding pads	2 mm x 2 mm
Metal layers	Ti-15 nm & Pt-100 nm
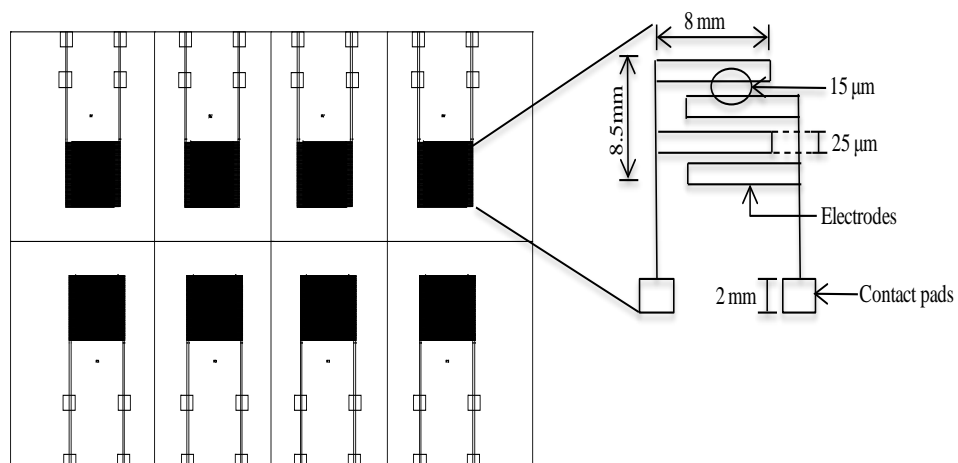
Figure 2.1. Interdigitated microelectrodes array sensor layout.

2.3.2   Fabrication method

The fabrication process consisted of several steps of photolithography processing including dual layer lift-off and electro-deposition requiring one layer mask step. Mylar mask was used to delineate interdigitated microelectrodes array and bonding pads. The fabrication process is shown in Figure 2.2, a cross-sectional view of the IMEs using dual layer lift off process. The fabrication process consisted of first coating the wafer with positive photoresist by using a spin coater to coat 1.5 microns of LOR 3A and AZ5214E. LOR 3A, non UV-sensitive, photoresist was used for dual layer liftoff. AZ5214E positive photoresist and UV-sensitive was used to coat on top of LOR 3A. Soft bake step was performed after each coating to ensure the adhesion of each photoresist to the wafer. UV exposure was performed to delineate the desired pattern for IMEs with the exposure dosage of 90 mJ/cm^2 for 25 seconds using soft contact. The wafer was developed in AZ5214E developer to outline the microelectrode pattern with the bonding pads using one layer mask step. Since, positive photoresist was used; the UV exposure dissolved the photoresist and opened the desired pattern area on the silicon wafer for the metal deposition as depicted in Figure 2.2. After inspecting the wafer under the microscope, electron beam evaporation system (e-beam evaporator) was used to deposit the two metals, titanium (Ti) and platinum (Pt). Ti was deposited as a sacrificial layer to achieve adhesion of platinum layer with the thickness of 15 nm of Ti and 100 nm of Pt. Finally, liftoff step was performed to strip photoresist with AZ 400T resist remover from the unexposed wafer surface. Appendix A and B explains the detailed process of dual layer lift-off and platinum electrode deposition.

37

Next, dicing saw with diamond blade was used to dice the fabricated biosensor chips before the wire bonding step. Spindle speed of 25 krpm and 0.5 mm/s forward cut blade speed was used to dice the microchips. AZ5214E, photoresist was coated on the fabricated sensors before dicing. The microchips were first cleaned with photoresist remover, and then washed with 100% pure ethanol and DI water for 2 minutes before attaching the wires with the conductive silver epoxy to the bonding pads followed by curing at 65 °C for one hour in the oven.
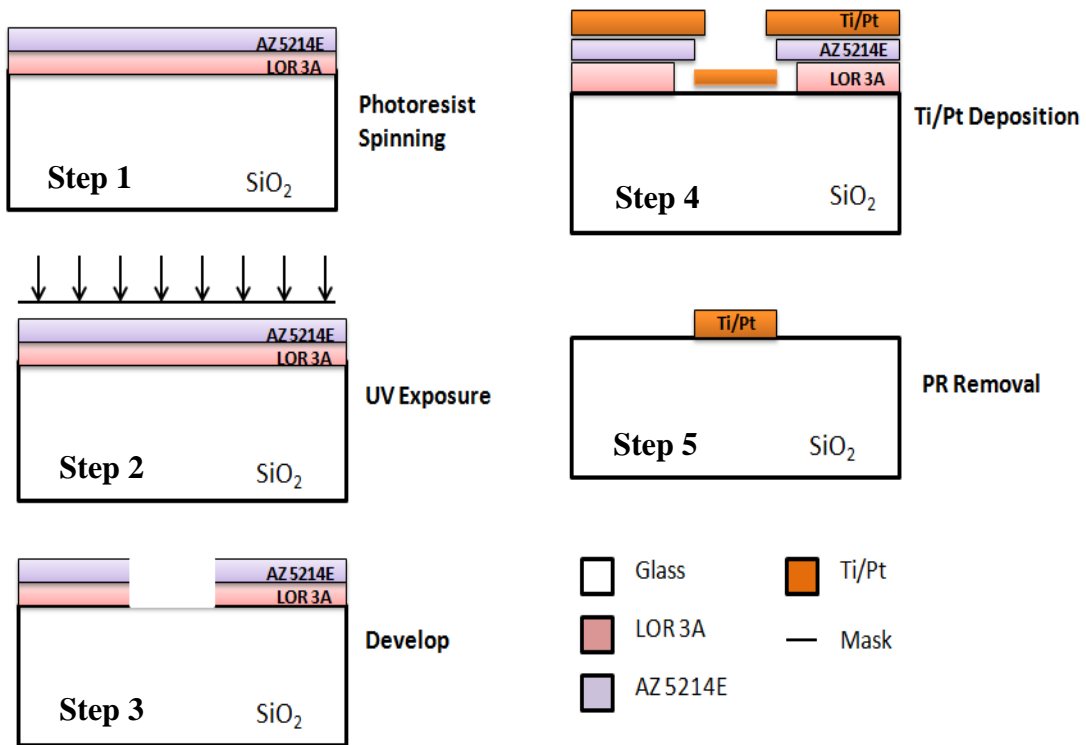
Figure 2.2. Fabrication process of interdigitated microelectrodes (IMEs) on Si substrate.

2.3.3 Cyclic voltammetry method

Cyclic Voltammetry (CV) was used to understand the electrochemical behavior of interdigitated microelectrodes (IMEs) array biosensor. CV is widely used technique to study a reversible redox couple reaction which consists of sweeping the potential of a working electrode immersed in an electrolyte solution and measuring the resulting current. The potential of a working electrode is controlled versus a reference electrode, i.e. silver/silver chloride (Ag/AgCl), which increases linearly with a fixed scan rate or a slope in a triangular waveform as shown in Figure 2.3. The triangular potential sweeps the potential between two values known as switching potentials causing forward and reverse scans. During a forward and reserve scan, oxidation current and oxidation current peaks can be determined at a fixed potential. The oxidative current peak is followed by a sharp decrease due to electron transport diffusion limited and similar trend is observed under the reductive current peak (Kissinger & Heineman, 1983; Rahimi & Mikkelsen, 2011; Van Benschoten, Lewis, Heineman, Roston, & Kissinger, 1983). The output signal, potential versus current, is shown in the Figure 2.3 below.

A

B
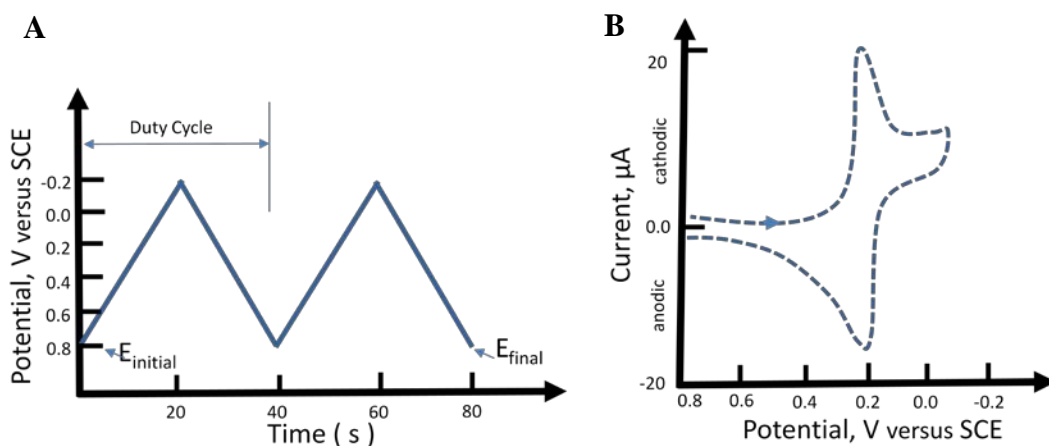
Figure 2.3. (A) Typical excitation signal for cyclic voltammetry, a triangular potential waveform with switching potential at 0.8 and -0.2 V versus reference electrode. (B) Typical cyclic voltammogram of ferrocyanide redox species.

CV was performed using a three-electrode cell (C-3) potentiostat, CHI 600E, at room temperature. In this study, CV of three different geometric IMEs was performed to measure the surface area with gap size of 25, 50, and 100 μm. One of the two interdigitated array electrodes was connected to the working electrode, and the other was connected to the counter electrode, and to Ag/AgCl, which was used as a reference electrode; and all electrodes were connected to the potentiostat. The platinum working electrode was used to apply the potential to the electrolyte solution to study the charge transfer behavior at the Pt electrode. The Pt counter electrode was used to pass the current to balance the charge added or removed at the working electrode, thus completing the electrochemical circuit. Silver/Silver chloride (Ag/AgCl) was used to measure and control the potential of working electrode. CV of different geometric IMEs

was carried out to determine the surface area in 4mM $Fe(CN)_6$/1M KNO_3 solution at a switching potential of 0.75 V versus a Ag/AgCl reference electrode with 10 seconds quiet time at scan rates from 10, 20, 50, 75, and 100 $mV.s^{-1}$. The electroactive surface area of a IMEs was evaluated by redox peaks, current vs. potential plots and Randles-Sevcik Equation 2.1 (Vanegas et al., 2014)

$$i_p = \left(2.69 \times 10^5\right) n^{3/2} D^{1/2} C A v^{1/2} \qquad (2.1)$$

where i_p (A) is the reduction peak obtained from the cyclic voltammogram, n is the number of transferred electrons in the redox reaction, D is the diffusion coefficient (6.70 x 10^{-6} $cm^2 s^{-1}$), C is the molar concentration of ferricyanide solution (4 mM), A is the electroactive surface area (cm^2) of the electrode and v is the potential scan rate (V s^{-1}). The value of n is equal to one for CV using $Fe\ (CN)_6^{3-}$ with the following half reaction taking place at the electrode (Vanegas et al., 2014):

$$Fe(CN)_6^{3-} + e^- \xrightarrow{yields} Fe(CN)_6^{4-} \qquad (2.2)$$
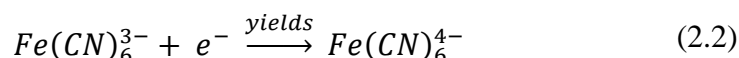
The slope k can be obtained from Equation 2.1 by linear relationship between i_p and $v^{1/2}$. Cottrell plot (i_p versus $v^{1/2}$) with linear regression gives the value of k and electroactive surface area (A, cm^2) can be expressed as (Vanegas et al., 2014):

$$A = k/((2.69\ x\ 10^5)n^{3/2}D^{1/2}C) \qquad (2.3)$$

A series of scan rates are used and the corresponding i_p values are recorded to obtain the Cottrell plots and electroactive surface area of the interdigitated microelectrodes (IMEs) array biosensor.

2.3.4 Direct current potential amperometry method

DC potential amperometry (DCPA) was used to demonstrate the sensitivity of the biosensor. A constant voltage is applied to the working electrode versus reference electrode and the resulting current-time dependence was measured. Potential amperometry was conducted in phosphate buffered saline (PBS) solution with pH of 7.4 at a constant potential of +500 mV versus Ag/AgCl reference electrode. All electrode chemical measurements were performed in 15 mL PBS via a 3-electrode set-up using platinum working and counter electrodes and Ag/AgCl as reference electrode. Successive 2 μL aliquots of H_2O_2 were injected to the PBS to increase the H_2O_2 concentration by 0.584 M increments while the redox current associated with the oxidation of H_2O_2 was measured at a working potential of 500 mV. The working potential (+500 mV) was chosen to ensure desirable amperometric sensitivity and a low probability of oxidizing interference compounds (Shi et al., 2011). The current output was measured at constant potential while successively injecting hydrogen peroxide (H_2O_2) in the stirred working solution (450 rpm) at 2 minutes intervals to allow the electrical signal to reach steady state (Vanegas et al., 2014). The i-t curves (current vs. time) from potential amperometry were used to evaluate the performance of the different geometric IMEs biosensors in terms of sensitivity and response time. Sensitivity was calculated from the slope of the linear portion of concentration versus current curves (μA mM^{-1}) (Vanegas et al., 2014).

The electrode electroactive surface area and sensitivity were used to determine performance of the IMEs and to compare the efficiency of different IMEs geometries by calculating current density defined as (Vanegas et al., 2014):

$$K = i/A \qquad (2.4)$$

where K is the current density ($\mu A \; mM^{-1} \; cm^{-2}$), i is the amperometric sensitivity ($\mu A \; mM^{-1}$) and A is the electroactive surface area of the electrode.

2.3.5   Statistical analysis

JMP v. 11 Software (SAS Institute, Cary, NC) was used for all statistical analyses. Means, error bars and standard deviations were calculated based on triplicate tests. Differences between variables i.e., electrode surface area and sensitivity among three electrode gap sizes, were tested for significance using one-way analysis of variance (ANOVA) and significantly different means ($p < 0.05$) are separated using Tukey's Honestly Significant Differences (HSD) test.

2.4   Results and Discussion

2.4.1   Biosensor fabrication results

Figure 2.4 shows the fabricated wafer and diced biosensor with attached wire bonds. Interdigitated electrodes with three different electrode gaps including 25, 50, and 100 µm were successfully fabricated. Table 2.2 shows the dimensions on the fabricated biosensors with multiple interdigitated microelectrodes array and Figure 2.5 shows the profilometer measurements. However, electrode gap with 15 µm showed to have short-circuited connection between interdigitated electrodes by making a conductive path across two electrodes of different combs. This was due to fabrication limitations of

mylar mask resolution. Therefore, interdigitated electrodes with gap size of 25, 50, and

100 μm were used to further characterize electrodes' performance.
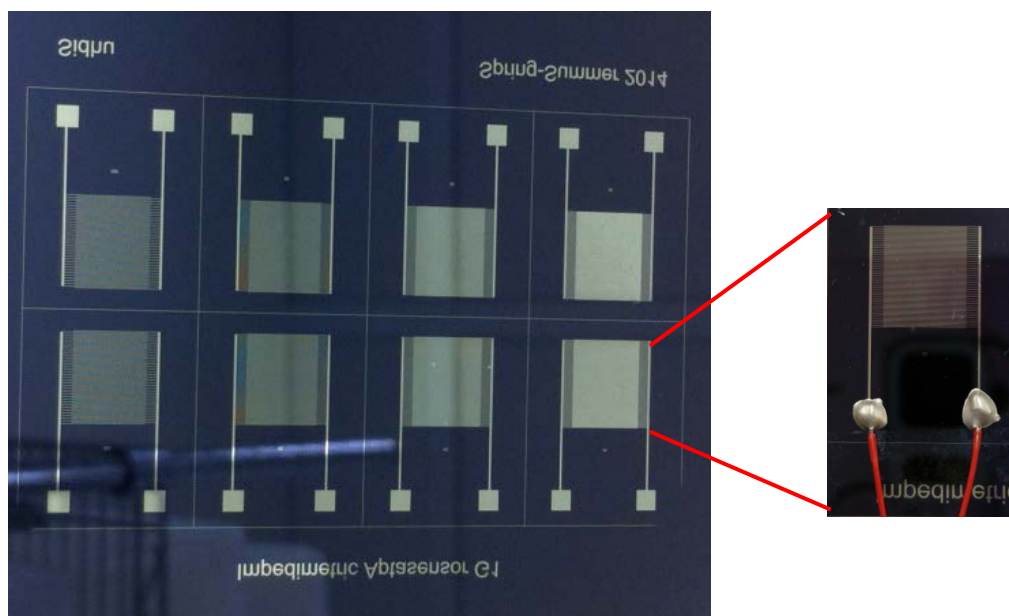
Figure 2.4. Fabricated IMEs on silicon dioxide wafer and diced biosensor with wire bonding.
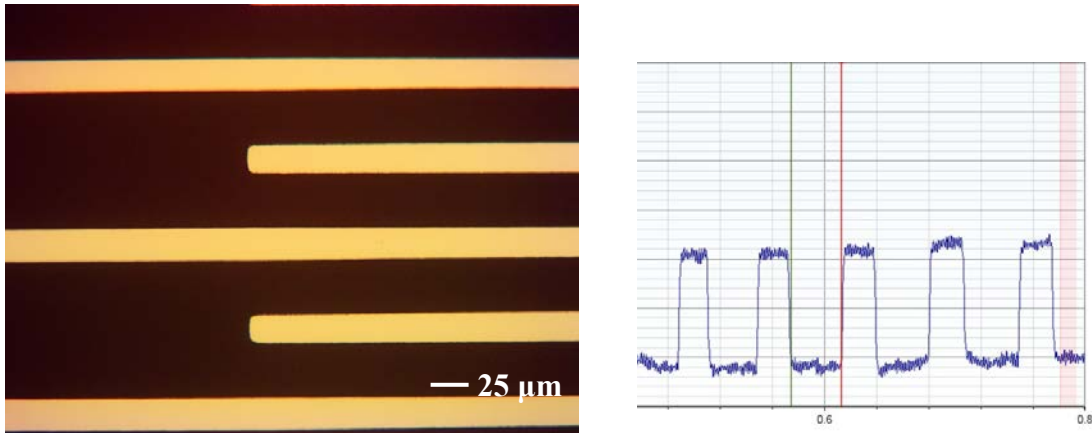
Figure 2.5. The gap size of 50 µm interdigitated electrode array with Dektak profilometer (Tucson, AZ) measurement.

Table 2.2. Dimensions after biosensor fabrication.

Element	Design dimensions (µm)	Profilometer measurements
Electrode gap	25	12-15 µm
Electrode gap	50	35-40 µm
Electrode gap	100	82-87 µm
Electrode width	25	22-27 µm
Ti & Pt thickness	n/a	110 - 115 nm

2.4.2   Cyclic voltammetry results

2.4.2.1   Comparison of electroactive surface area (ESA)

Cyclic voltammetry (CV) of potassium ferricyanide at bare Pt microelectrodes of three different geometries in KNO_3 supporting electrolyte was performed to estimate the electroactive surface area. The potential scan was cycled between -0.75 V and +0.75 V versus an Ag/AgCl reference electrode at varying scan rates of 10, 20, 50, 75, and 100 mV/s. The cyclic voltammograms for the bare electrodes of each electrode gap size followed expected trends as shown in Figure 2.6 A, Figure 2.7 A, and Figure 2.8 A. The CVs exhibited a sigmoid curve, a response characteristic of a reversible couple with well-defined redox peaks and indicating diffusion controlled reaction at the electrode-solution interface in which the diffusion layer is smaller than the surface area of the microelectrode (Vanegas et al., 2014). Cottrell plots were prepared using the oxidation peak with the corresponding scan rates as shown in Figure 2.6 B, Figure 2.7 B, and Figure 2.8 B to calculate the electroactive surface area of each electrode gap size. The trend of these plots was linear indicating that as the scan rate was increased, oxidation peak was also increased. The slope was obtained from Cottrell plots and Equation 2.1 was used to calculate the electroactive surface area of each biosensor (IMEs) with different electrode gap.
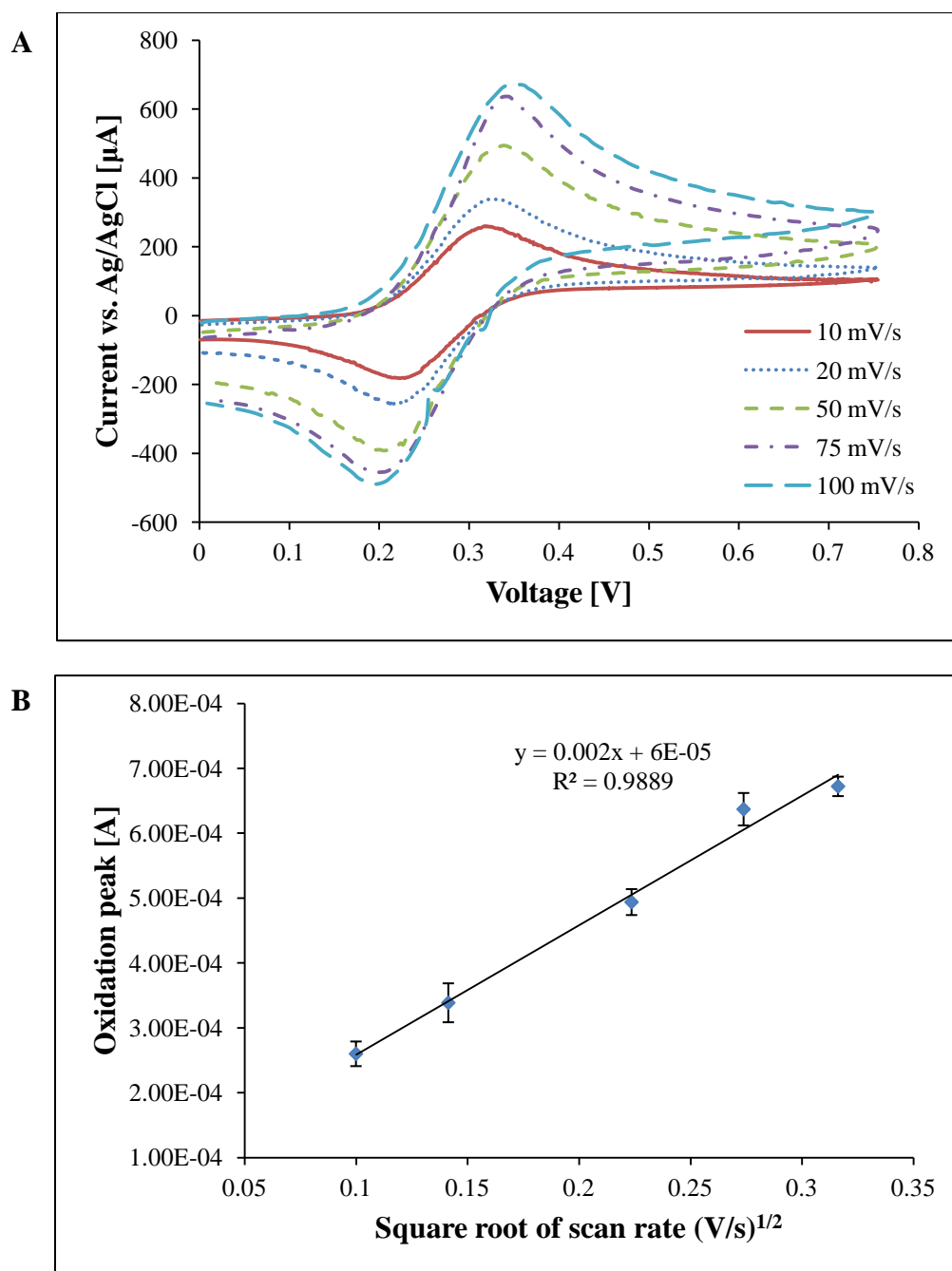
Figure 2.6. (A) Representative CV of bare 25 μm Pt-IMEs device in 4 mM $Fe(CN)_6^{3-}$ / 1 M KNO$_3$ at different voltage scan rates. (B) Characteristic Cottrell plot of a bare 25 μm Pt-IMEs.
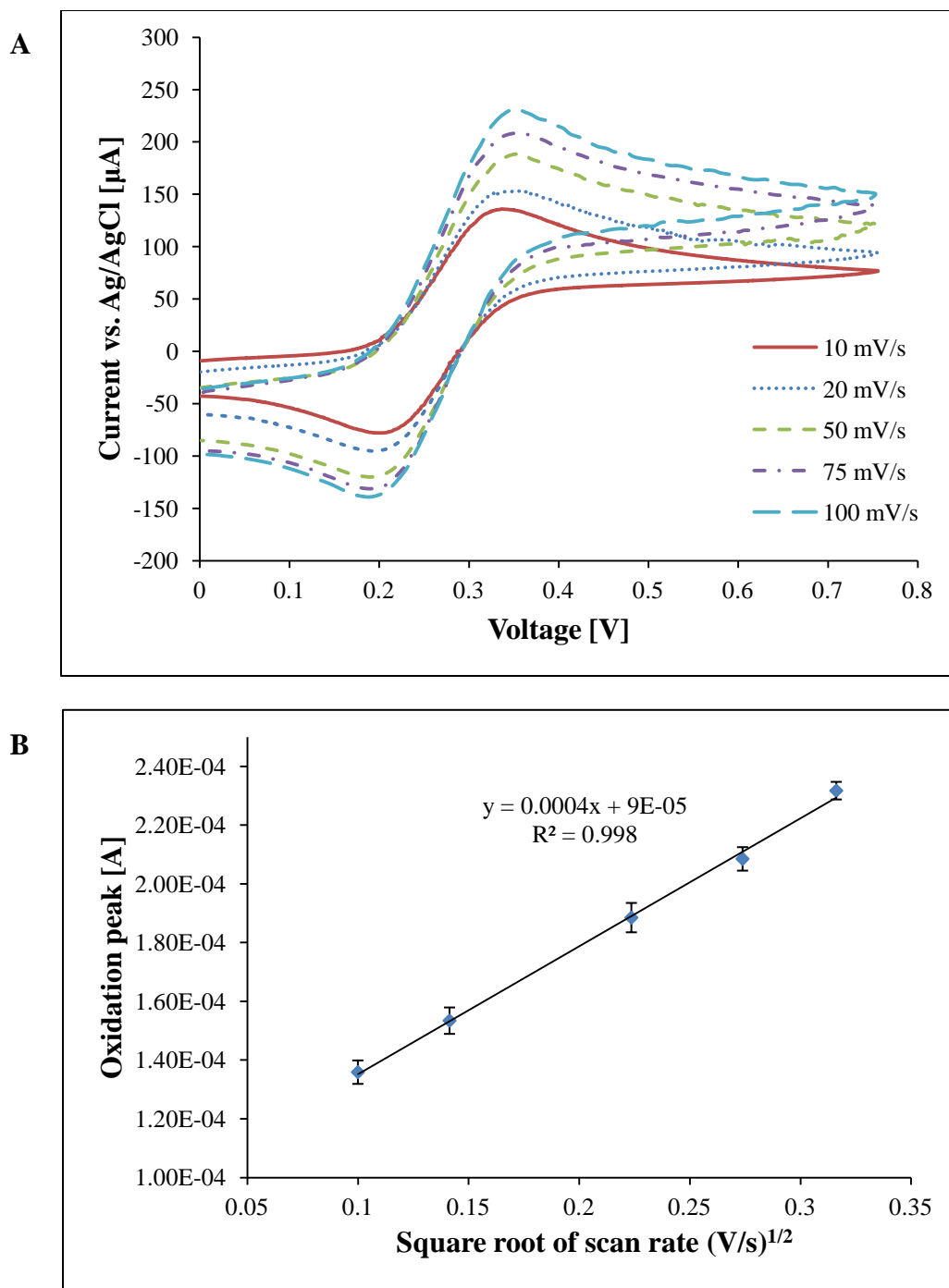
Figure 2.7. (A) Representative CV of bare 50 μm Pt-IMEs device in 4 mM $Fe(CN)_6^{3-}$ / 1 M KNO_3 at different voltage scan rates. (B) Characteristic Cottrell plot of a bare 50 μm Pt-IMEs.

48
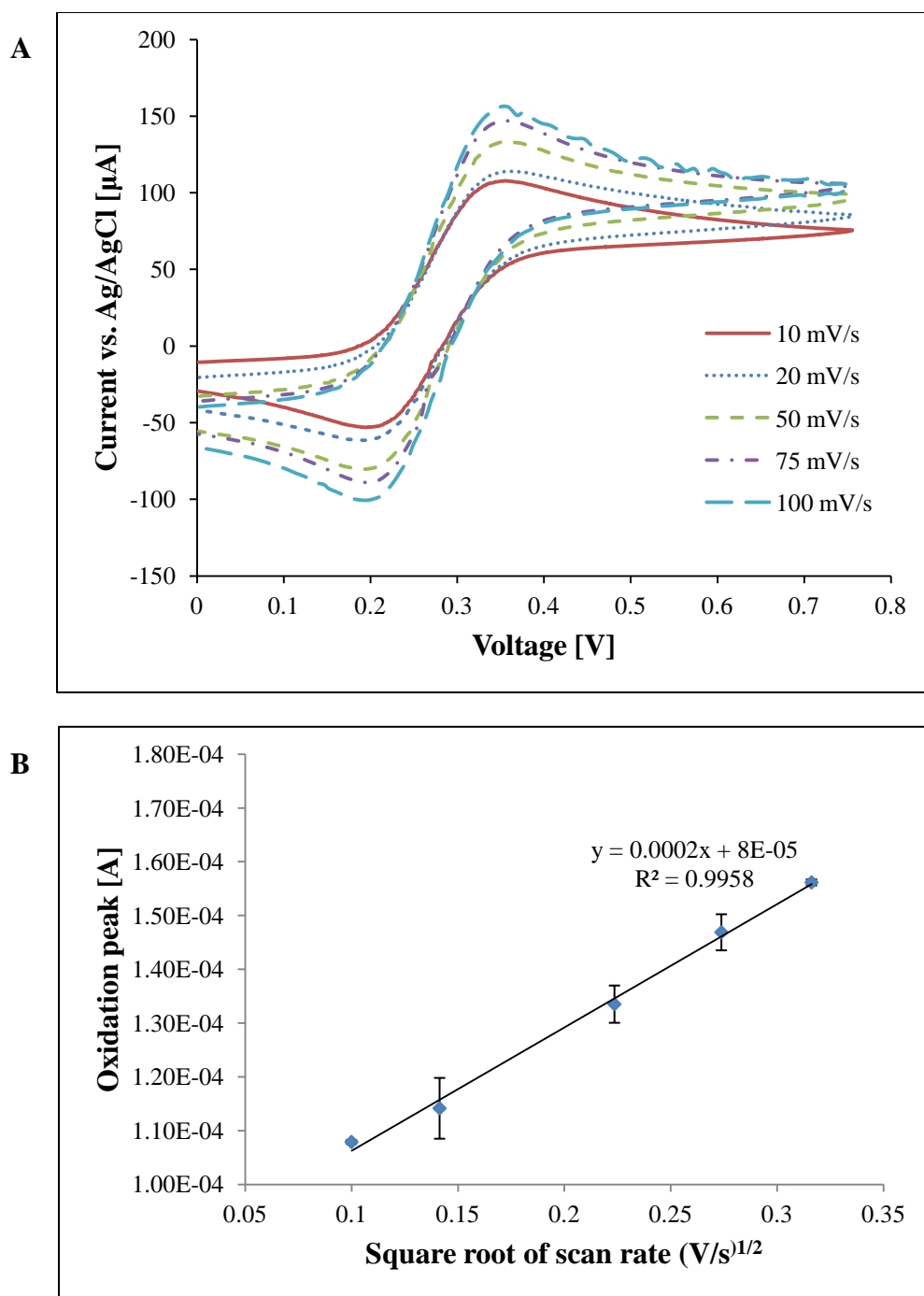
Figure 2.8. (A) Representative CV of bare 100 μm Pt-IMEs device in 4 mM $Fe(CN)_6^{3-}$ / 1 M KNO$_3$ at different voltage scan rates. (B) Characteristic Cottrell plot of a bare 100 μm Pt-IMEs.

49

The electroactive surface area of 25, 50, and 100 μm IMEs were 0.7181 ± 0.0196 cm^2, 0.1436 ± 0.0018 cm^2, and 0.0718 ± 0.0024 cm^2, respectively. The electroactive surface area of 25 μm was significantly larger than 100 μm electrode gap showing one order of magnitude difference due to higher number of platinum comb fingers. The electroactive surface area of IMEs including 25, 50, and 100 μm significantly increased ($p < 0.05$) as the electrode gap size decreased. Thus, the cyclic voltammetry analysis demonstrated that the electroactive surface area (ESA) was influenced by the electrode gap size.

The CV data showed that as the electrode gap size increased, the oxidation current values decreased. The oxidation peaks at the scan rate of 100 mV/s for 25, 50, and 100 μm microelectrode gaps were 672 ± 6.18 , 232 ± 5.20, and 156 ± 0.96 μA, respectively. The calculated electroactive surface areas and the oxidation peak currents indicated that the resistance of 100 μm micro electrode gap device is significantly higher ($p < 0.05$) than the 25 and 50 μm. Figure 2.9 shows a comparison of electroactive surface area in the presence of potassium ferrocyanide reversible redox couples. The electrode's electroactive surface areas of three gap sizes were significantly different based on $p < 0.05$. These results reflect that the numbers of electrodes were decreased as the electrode gap was increased. The electrode gap size of 100 μm had less number of electrodes as compared to 25 and 50 μm given that the electrode width (25 μm) and active area (0.81 cm^2) in the sensor layout remained the same for all electrodes. Therefore, the electroactive surface area (ESA) results are in agreement with the fabricated electrode area.
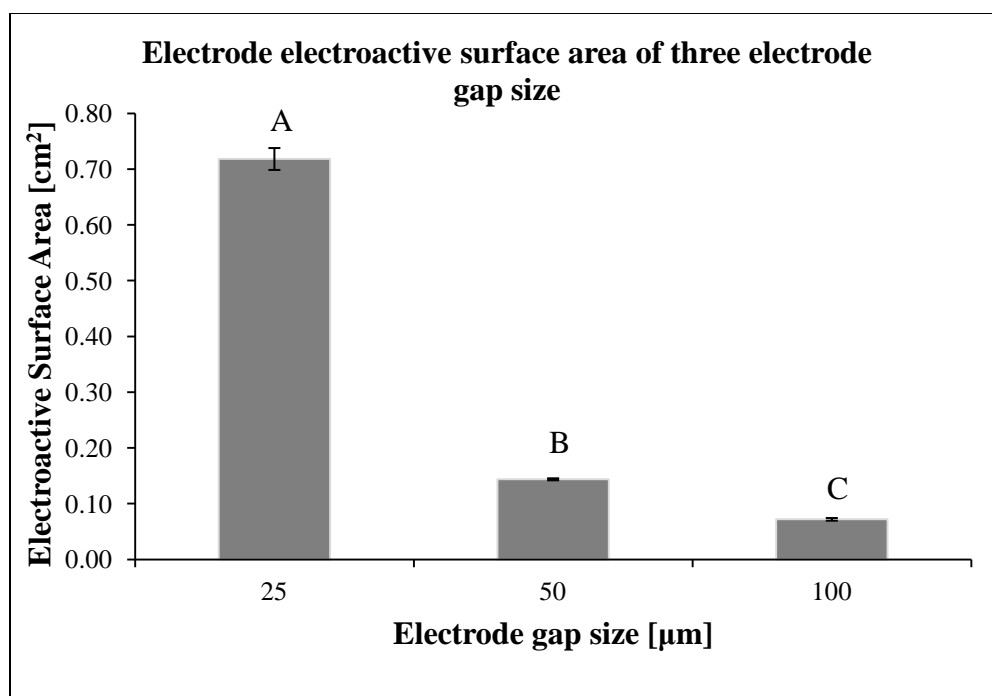
Figure 2.9. Comparison of electroactive surface area (ESA) of multiple interdigitated microelectrodes array electrode gap sizes. Surface area columns that display different letters above their error bars represent significantly different values among three electrode gap size ($p < 0.05$). Error bars denotes the standard error of the arithmetic mean of three replicates.

2.4.3 Direct current potential amperometry results

The electrocatalytic activity of the three different devices was characterized in terms of the amperometric sensitivity to H_2O_2; since H_2O_2 is the electroactive intermediate for oxidase-based biosensors (Elzanowska, Abu-Irhayem, Skrzynecka, & Birss, 2004). The detection of H_2O_2 is important in various applications such as glucose oxidase (GOx), in which H_2O_2 is produced in an enzymatic reaction involving glucose and molecular oxygen (Wang, 2001). The reaction at the electrode can be described as

51

below:

$$H_2O_2 \xrightarrow{electrode} O_2 + 2H^+ + 2e^-$$ (2.5)
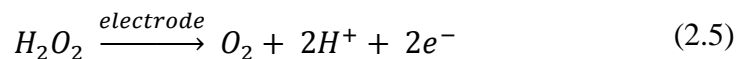
A typical dynamic potential amperometry curve of bare Pt electrodes for 50 and 100 μm are displayed in Figure 2.10A and Figure 2.11A. The amperometric sensitivity was calculated using the slope of linear regression for current and H_2O_2 concentration as illustrated in Figure 2.10B and Figure 2.11B. The average sensitivity values of 50 and 100 μm IMEs devices were 21.39 ± 0.1335 μA/mM and 5.36 ± 0.0298 μA/mM, respectively. The sensitivity values of the two electrode gaps were significantly different at $p < 0.05$. The response time of both devices was less than 5 s showing a stable response. The sensitivity of 50 μm IMEs device was significantly higher than 100 μm IMEs device as expected from the cyclic voltammetry data. Higher electroactive surface area of the electrodes was directly related to the higher sensitivity of the sensor. The current density was also calculated using Equation 2.4 that exhibits 148.96 ± 20.15 μA mM^{-1} cm^{-2} for 50 μm IMEs device and 74.65 ± 2.40 μA mM^{-1} cm^{-2} for 100 μm IMEs devices. The 50 μm electrode gap size exhibited excellent sensing properties with surface area of 0.1436 ± 0.0018 cm^2 and current density of 148.96 ± 20.15 μA mM^{-1}.

Note that the amperometric sensitivity data was not reported for 25 μm electrode gap due to charge overflow error from the CHI 600E potentiostat/impedance analyzer (Austin, TX) while increasing the concentration of H_2O_2. This indicates that the instrumentation was unable to read the current response from the 25 μm IMEs device due to high current density passing through the electrodes. The sensitivity defined by the CHI manufacturer is current/voltage (A/V) and ranges from $1x10^{-12}$ to $1x10^{-1}$ (CH Instruments User Manual, 2014). The A/V value at 25 μm electrode gap exceeded the $1x10^{-1}$ and, therefore, the system read current overflow error. An instrument that would cover larger range of current can be used to detect the changes at the 25 μm electrode gap or a current divider setup can be implemented to reduce the current flow between the electrodes.
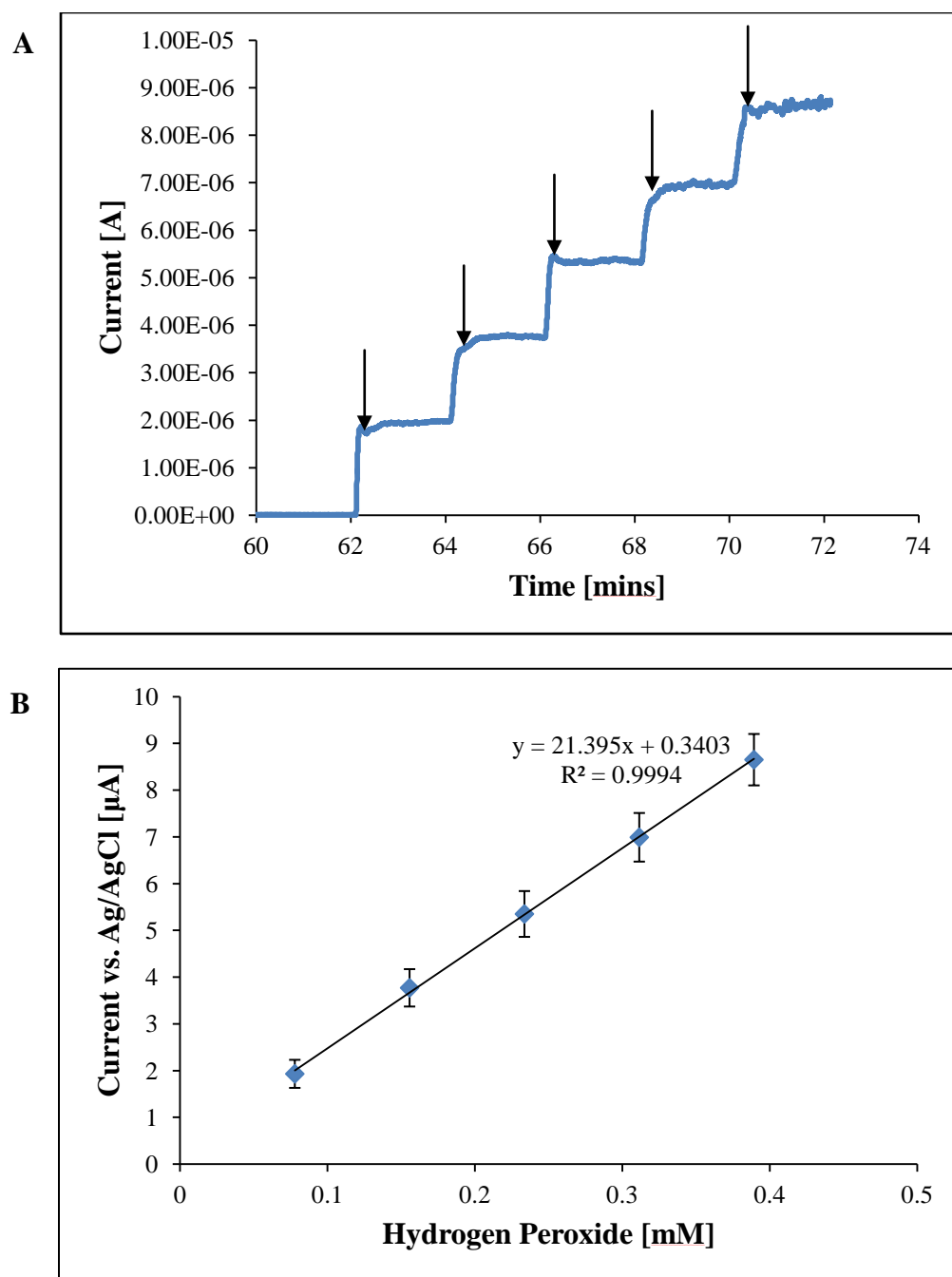
Figure 2.10. (A) Representative amperometric sensing of bare 50 μm Pt-IMEs device in 15 mL PBS (pH 7.4) at working potential of 500 mV. The current response to 2 μL successive injections of 0.584 M H_2O_2 (injection times are indicated by vertical arrows). (B) Characteristic Cottrell plot of a bare 50 μm Pt-IMEs.

54
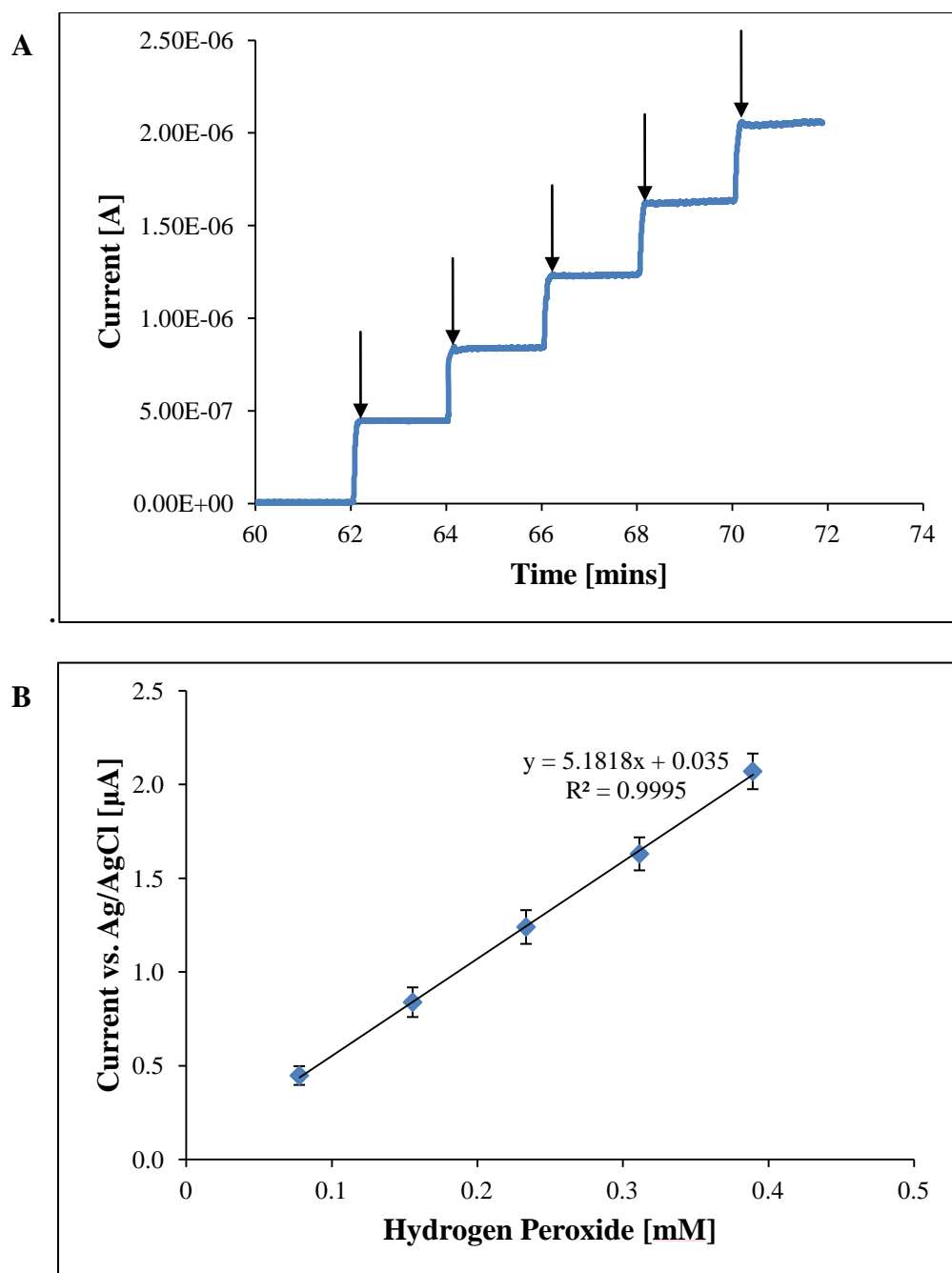
Figure 2.11. (A) Representative amperometric sensing of bare 100 μm Pt-IMEs device in 15 mL PBS (pH 7.4) at working potential of 500 mV. The current response to 2 μL successive injections of 0.584 M H_2O_2 (injection times are indicated by vertical arrows). (B) Characteristic Cottrell plot of a bare 100 μm.

Table 2.3 summarizes the performance characteristics of the three electrode gap sizes using cyclic voltammetry and potential amperometry techniques. Electrode's electroactive surface area, sensitivity and current density were calculated to identify the best sensor design to continue on further studies on biosensor design for the detection of the bacteria pathogen.

Table 2.3. Summary of electroactive surface area, sensitivity and current density of three bare Pt IMEs.

Electrode gap (μm)	Surface Area (cm^2)	Sensitivity (μA mM^{-1})	Current Density (μA mM^{-1} cm^{-2})
25	0.7181$_a$ ± 0.0196	NR	NR
50	0.1436$_b$ ± 0.0018	21.39$_a$ ± 0.1335	148.96$_a$ ± 20.15
100	0.0718$_c$ ± 0.0024	5.360$_b$ ± 0.0298	74.65$_b$ ± 2.40

NR = Not reported due to charge overflow.
[a,b] Means within a column which are not followed by a common superscript letter are significantly different ($p < 0.05$). Values are shown as the mean ± standard deviation of three independent repetitions.

These results shows that the interdigitated microelectrodes array with 50 μm was able to detect the current response with the highest sensitivity as compare to 100 μm electrode gaps. Macroelectrode studies performed by Chaturvedi et al. (2014) using Pt/Ir working electrode (BASI MF-2013, 1.6 mm diameter, 7.5 cm length, 6 mm shaft diameter, CTFE plastic body) reported the electroactive surface area (ESA) and sensitivity based on similar techniques followed in this study. The electrode surface was modified using nanoceria-platinum-graphene (nPt-RGO-nCe-nPt) nanocomposites to enhance the ESA and sensitivity of the biosensor. Cyclic voltammetry was used to

determine the ESA in 4 mM $Fe(CN)_6^{3-}$ / 1 M KNO$_3$ and direct current potential

amperometry was used to calculate the sensitivity of the metal-graphene hybrid

nanocomposites by injecting hydrogen peroxide. The reported values for ESA and

sensitivity were 0.062 ± 1.5 cm^2, and 11.1 ± 1.5 (μA mM^{-1}), respectively. These results

show that the ESA and sensitivity values have drastically improved by changing the

electrode size and geometries to micro-scale when compared to the macro-scale as

observed for the interdigitated microelectrodes array.

In this study, the current response controlled by H$_2$O$_2$ concentration is suggested to

be analogous to expected response to bacteria concentration. The ionic concentration of

the medium or solution conductivity changes by adding hydrogen peroxide

concentration which would be analogous to adding live bacteria which changes the

solution conductivity. The device characteristic were defined by current response in a

standard electrolyte solution to understand the behavior of IMEs.

2.5   Conclusions

In this work, Pt-based IMEs biosensors with different electrode size gap were

fabricated and characterized using cyclic voltammetry (CV) measurements of reversible

redox species in potassium ferrocyanide and direct current potential amperometry

(DCPA) in phosphate buffered saline solution . The bottom-up microfabrication

techniques were used to fabricate the IMEs based biosensors with microelectrode gap of

15, 25, 50, and 100 μm. The IMEs devices with 15 μm were not used due to the

fabrication limitation of mylar mask. These characterization tools allowed the

understanding of sensing response of biosensor relative to the solution concentration and

electrode gaps. As the surface area increased, the sensitivity of the biosensor also increased.

The potentiostat was unable to read current response due to high current density flow on the electrode surface of IME device with 25 μm electrode gap.The trend in enhanced sensitivity over the conventional macro electrodes was due to the sub-micron electrode width and spacing, therefore increasing the electroactive surface area and sensitivity as compared to the aforementioned results in a study performed by Chaturvedi et al. (2014). The best suitable electrode design was 50 μm IMEs based on the electroactive surface area and highest sensitivity results. Therefore, 50 μm IMEs biosensor was selected to be used in the following Chapter III to carry out further experimentation by functionalizing electrodes with aptamers to capture and detect the targeted bacteria.

CHAPTER III

BIOSENSOR FUNCTIONALIZATION WITH APTAMERS AND

IMPEDIMETRIC DETECTION OF *LISTERIA* SPP.

3.1 Overview

Impedance biosensors based on lab-on-a-chip system have been used for the detection of pathogenic bacteria using interdigitated microelectrodes array to achieve enhanced sensitivity and response time. The traditional methods including total viable counts (TVC), enzyme-linked immunosorbent assay (ELISA), and polymerase chain reaction (PCR) are time consuming, expensive, and require specialized facilities and trained personnel. Optimized designed for lab-on-a-chip biosensor was selected as discussed in Chapter II for bacteria detection. Interdigitated microelectrodes (IMEs) array with electrode gap size of 50 μm was used and functionalized with *Listeria monocytogenes* aptamers, selective to protein internalin A, via metal-thiol self-assembly for *Listeria* spp. detection. Six aptamer concentrations including 100, 150, 200, 300, 400, and 800 nM were reduced using dithiothreitol (DTT) protocol and functionalized on the IMEs surface. Electrochemical impedance spectroscopy analysis was used to characterize the biosensor and detect *Listeria* spp. without the need for label amplification and pre-concentration steps reducing the detection time. The optimized aptamer concentration of 800 nM was selected to capture the bacteria through protein binding. The aptasensor was developed to detect wide range of bacteria concentration from 10 to 10^6 CFU/mL. The aptasensor was capable to detect bacteria concentration at lower limit of 5.39 ± 0.21 CFU/ml with sensitivity of 268.1 ± 25.40 (Ohms/log

59

[CFU/mL]) in 17 min. The aptamer based biosensor offers a portable, rapid and sensitive alternative for food safety applications.

3.2   Introduction

In recent years, many studies on rapid-screening methods for food safety have been focused on development of biosensor platforms for reliable and faster results than conventional techniques such as aerobic plate counting (APC), enzyme-linked immunosorbent assay (ELISA), and polymerase chain reaction (PCR) (Wang et al., 2012). A number of devices have recently been developed for monitoring foodborne pathogens based on immobilization of capture agents, i.e., the bio-recognition element component of a biosensor, such as aptamers (Iliuk, Hu, & Tao, 2011; Song et al., 2008). Aptamers are synthetic oligonucleotides, either DNA or RNA, that have an ability to bind specifically to target molecule or bacteria such as cell surface proteins, extracellular biomolecules, or viruses (Kärkkäinen et al., 2011; Torres-Chavolla & Alocilja, 2009). Aptamers are selected through a *in vitro* process known as systematic evolution of ligands by exponential enrichment (SELEX) (Song et al., 2008). SELEX is a chemical selection method which is based on random RNA or ssDNA oligonucleotide library consisting of a multitude of fragments (10^{13} to 10^{15}) with different sequences. The SELEX procedure can be summarized by the repetition of successive steps consisting of selection (binding, partition, and elution), amplification, and conditioning (Stoltenburg et al., 2007). In the first SELEX process, the oligonucleotide library and the target molecules are incubated for binding. The target-bound oligonucleotides are isolated by several stringent washing steps and eluted. Subsequently, target-bound oligonucleotides

are amplified by polymerase chain reaction. Finally, amplified sequences are used for

the conditioning step, which is a repetition of the selection round. Multiple cycles of

selection rounds, 6 to 20 SELEX rounds, are performed to achieve three-dimensional

structures that are highly affine and target-specific aptamers (Shangguan, Tang,

Mallikaratchy, Xiao, & Tan, 2007; Stoltenburg et al., 2007). Due to aptamers inherent

advantages of simple production, easy storage, good reproducibility, target versatility,

easy modification, and convenient regeneration, they are considered to be ideal

recognition elements for biosensor applications (Kärkkäinen et al., 2011). Recent efforts

have expanded the library of aptamers for common foodborne pathogens; therefore,

aptamers are being used to construct biosensors called aptasensors.

Aptasensor has been designed to detect various pathogens including an aptamer-

based sensor, which was developed utilizing impedimetric detection of *Salmonella*

Typhimurium via aptamers self-assembly onto a gold nanoparticle-modified screen-

printed carbon electrode (Labib et al., 2012). Another aptamer-based biosensor was

developed using gold nanoparticles for detection of *Escherichia coli* O157:H7 based on

colorimetric detection (Wu et al., 2012). An antibody-aptamer functionalized fiber-optic

biosensor for detection of *Listeria monocytogenes* in food was designed with detection

limit of 10^3 CFU/ml in pure solution and 10^2 CFU/25g of food sample (Ohk et al., 2010).

A gold electrode aptamer-based sensor was designed for *E. coli* O111 detection based on

a target-induced aptamers displacement strategy with detection limit of 1.1 x 10^2

CFU/ml in phosphate buffer saline and 3.1 x 10^2 CFU/ml in milk (Luo et al., 2012).

However, to date, few, rapid, sensitive aptasensors for Listeria *detection have been demonstrated in field conditions for monitoring food safety.*

Electrochemical impedance spectroscopy (EIS) technique has been employed for the detection of foodborne pathogens over other categories such as optical based biosensors that require light (e.g., surface Plasmon resonance or fluorescence) and piezoelectric biosensors that use mechanical motion (e.g., quartz crystal microbalance or resonant cantilever) due to their low cost, low power, ease of miniaturization, portability, simplicity, faster, response, and label-free detection capabilities (Daniels & Pourmand, 2007). EIS is used to monitor the impedance change at the electrode-solution interface when the target analyte interacts with the functionalized surface of the electrodes designed to capture it. Impedance changes occur due to change in electrical properties at the electrode surface solely due to the presence of the target analyte (Daniels & Pourmand, 2007). Impedance based biosensors do not require special reagents and are preferred for label-free detection of target bacteria.

EIS is an alternating current (AC) method that describes the response of an electrochemical cell to a small amplitude sinusoidal voltage signal as a function of frequency. The output is measured in impedance (Z) defined as the ratio $V(t)/I(t)$ resulting from current sine wave, which differs in time (phase shift) with respect to the perturbing (voltage) wave (Prodromidis, 2010). The measured impedance can be demonstrated by the following Equation 1.1:

$$Z = \frac{E_t}{I_t} = \frac{E_0 \sin(\omega t)}{I_0 \sin(\omega t + \phi)}$$ (3.1)

where E_0 is the potential at time t, E_0 (Volts) is the amplitude of the signal, and ω

(radians/s) is the radial frequency. The relationship between radial frequency ω and

frequency, f, can be expressed as $\omega = 2\pi f$. The response signal, I_t, is shifted in phase

(ϕ) and has a different amplitude than I_0 (Amperes), (Gamry Instruments Application

Note, 2007).

The total impedance accounts for the combined opposition of all the components

within the electrochemical cell (resistors, capacitors, inductors) to the flow of electrons

and ions (Prodromidis, 2010). In this study, aptamers, as the biorecognition element, are

used to functionalize the interdigitated microelectrode array for selective binding of

Internalin A in the cell membrane of the target bacteria, *Listeria* spp. Internalin A

(In1A), a surface protein, is one of the major invasion proteins involved in pathogenesis

that represent a complex family of leucine-rich-repeat-containing protein that interacts

with E-cadherin leading to bacteria growth in the host cells (Ohk et al., 2010). In1A is

found in all *L. monocytogenes* strains and serves as a molecular marker for the detection

of the pathogenic bacteria (Bierne, Sabet, Personnic, & Cossart, 2007). Aptamer specific

for In1A was used in this research to detect *Listeria innocua*. *Listeria innocua*, is a non-

pathogenic microorganism, which has been shown to be an excellent surrogate for

Listeria monocytogenes (Buzrul & Alpas, 2004). In this study, the optimization of

various aptamer concentrations loading on the surface of IMEs was determined based on

the saturation point derived from the electrochemical impedance analysis. Optimized

aptamer concentration was used at saturation point to cover the maximum surface area of

the interdigitated microelectrodes array to maximize the capture of the bacteria cells and consequently biosensor performance. Furthermore, optimized aptamer concentration was used to evaluate the response of miniaturized aptasensor to detect *Listeria innocua* in phosphate buffered solution. Aptasensor performance parameters were measured and compared to current published biosensors.

3.3   Materials and Methods

3.3.1   Chemicals, reagents, and equipment

Listeria monocytogenes thiol SS-C6 aptamers that target protein Internalin A (A8, 5′-ATC CAT GGG GCG GAG ATG AGG GGG AGG AGG GCG GGT ACC CGG TTG AT-3′, 47 mers) were purchased from GeneLink (Hawthrone, NY). Ethylenediaminetetraacetic acid (EDTA), disodium salt, dihydrate was purchased from EMD Performance Materials (Sommerville, NJ). Potassium chloride (KCl) and sodium chloride were purchased from EM Science (Hatfield, PA). TRIS (Hydroxymetyl)aminomethane, potassium phosphate dibasic (K_2HPO_4), and sodium phosphate monobasic monohydrate (Na_2HPO_4) were obtained from J.T.Baker Chemical (Phillipsburg, NJ). Sodium phosphate monobasic monohydrate ($H_2NaO_4P.H_2O$) was purchased from Sigma Aldrich (St. Louis, MO). Potassium ferrocyanide trihydrate ($K_4Fe(CN)_6.3H_2O$) was purchased from Ward's Science (Rochester, NY). Sulfuric acid and hydrogen peroxide were purchased from Avantor Performance Materials (Center Valley, PA). DL-Dithiothreitol was obtained from Sigma Aldrich (St. Louis, MO). Sodium acetate ($NaC_2H_3O_2.3H_2O$) was purchased from MCB Reagents (Cincinnati, OH). Lab-line squaroid 3618 vacuum oven (Grand Island, NY), Cody ultrasonic cleaner

CD-2800 (Beijing, China), and VWR Scientific Model V centrifuge (Houston, TX), were used to perform the thiol modified oligo disulfide reduction protocol. CHI 600E potentiostat/impedance analyzer and CHI6044e software (CH Instruments, Austin, TX) were used to analyze electrochemical response of aptamer functionalized electrodes and the detection of *Listeria* spp. Tryptose phosphate broth (TPB) and buffered peptone water (BPW) were purchased from HiMedia (Mumbai, India). Oxford *Listeria*-selective agar and Oxford *Listeria*-selective supplement were purchased from EMD Performance Materials (Sommerville, NJ).

3.3.2   Disulfide reduction of thiol modified aptamers

Thiol labeled aptamers for *L. monocytogenes* consisted of 47-mer and it targets the internalin A (InlA) protein (Labib et al., 2012); the 3' end was modified with a terminal thiol group. Studies by Ohk et al. (2010) shows a gel purification of the 47-mer aptamer with a thiol terminus and 6 carbon spacer at the 3' end for adsorption to platinum. The design of thiolated aptamers consists of three segments: (1) a thiol (-SH) or disulfide (-SSR) terminus, (2) a linker or spacer, i.e. –S-H-$(CH_2)_6$OH, and (3) the aptamer sequence (Balamurugan, Obubuafo, Soper, & Spivak, 2008).

GeneLink (Hawthrone, NY) supplied oligonucleotides in desalted, lyophilized, and disulfide form. Disulfide thiol modifier, dithiol phosphoramidite (DTPA) was used by the manufacturer leading to the addition of two thiol groups. Disulfide modified *Listeria* thiol aptamers are reduced using the dithiothreitol (DTT) reduction protocol provided by the manufacturer (GeneLink, 2011). Briefly, DTT was used to form two free thiols from disulfide bonds by preparing 100 mM DTT solution in sodium

phosphate buffer, (pH 8.3 –8.5). In 2 mL eppendorf tube, 400 µL of 100 mM DTT

solution was directly added to thiol aptamers and left at room temperature for 1 hr to

reduce the thiol groups. In order to remove the traces of DTT in thiolated aptamers 50

µL of 3 M sodium acetate (pH 5.2) was added and mixed properly using a vortex.

Ethanol precipitation was used to separate the thiolated aptamer from the solution.

Absolute ethanol (1.5 mL) was added, vortexed, and stored at -80 ^{o}C for 20 minutes. The

thiolated aptamers were obtained in pellet form after centrifugation at 12,000 rpm for 10

minutes. The supernant was discarded and the pellet was vacuum dried at room

temperature and 30 in Hg pressure for 20 minutes to remove any traces of solvents.

Drying the pellet completely was crucial in order to re-dissolve the aptamers in the 10

mM TriS, 1mM EDTA, pH 7.5 buffer (TE buffer). Figure 3.1 illustrates the reduction of

disulfide bonds to thiol bonds using DTT protocol.

The aptamers were reconstituted in TE buffer following the manufacturer's

protocol (GeneLink, 2004). In order to make a stock solution of 100 µM of thiolated

aptamers, 27 µL was dissolved in TE buffer solution and stored at -80°C for further

dilutions.
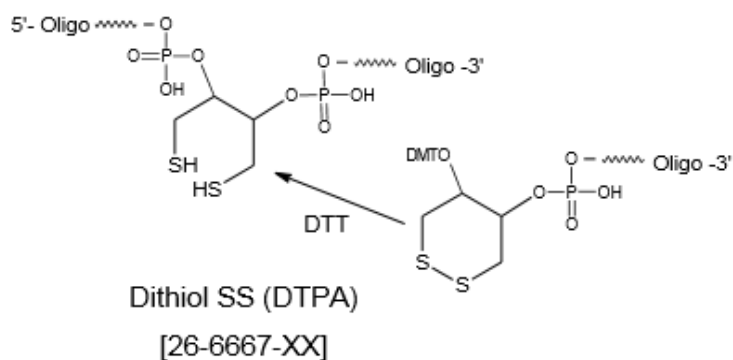
Figure 3.1. DTT reduction of disulfide bonds to two thiol bonds. The molecular diagram was obtained from GeneLink (Hawthorne, NY) (GeneLink, 2014).

3.3.3 Aptamer functionalization onto interdigitated microelectrode array

The aptamers were attached to the platinum IMEs surface using the sulfur atoms of the thiol group forming a self-assembled monolayers (SAM) (Balamurugan et al., 2008) as shown in figure 3.1. The mechanism of aptamer attachment via SAMs is through covalent adsorption in the thiol form (aptamer-linker-SH). Figure 3.2 illustrates the schematic of aptamer attachment to the interdigitated microelectrode array. The advantage of using a direct Pt-SH bond to the IMEs includes a rapid covalent reaction and formation of a stable monolayer (Zhang & Yadavalli, 2011).
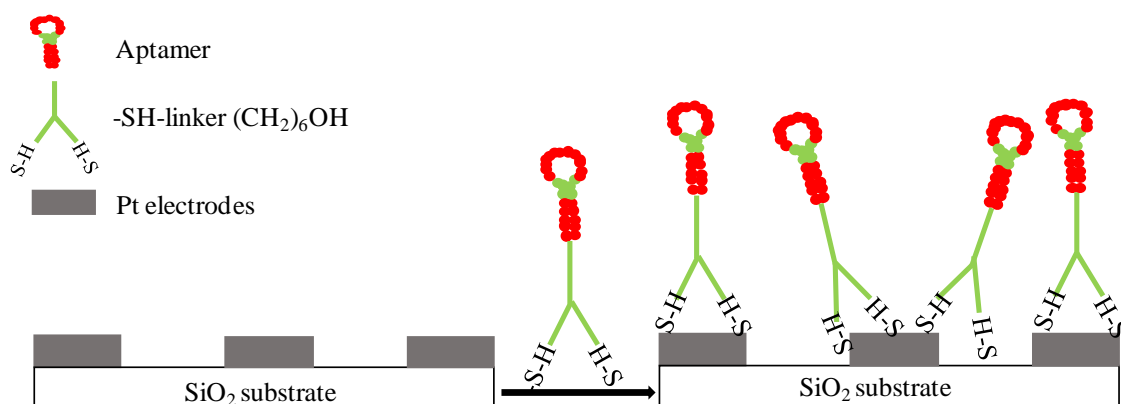
Figure 3.2. Schematic of *Listeria monocytogenes* aptamers attachment to the platinum IMEs.

The platinum IMEs were first cleaned with piranha solution with the ratio of 3:1 concentrated sulfuric acid to hydrogen peroxide. Piranha solution was used to remove all the organic residues from the surface of the IMEs. The biosensor microchip was immersed in the solution for one minute without exposing the bonding pads with the silver conductive epoxy. If the silver conducting epoxy was exposed to the piranha solution, it would decompose the organic epoxy comprising the integrity of the electrical connection. The biosensor microchip was thoroughly washed with DI water for one minute to ensure proper removal of piranha solution residues from the surface. Following cleaning, the microchip was air dried and used for functionalization of the aptamers. The stock solution of 100 µM *Listeria monocytogenes* aptamers was further diluted to various concentrations of 100, 150, 200, 300, 400, and 800 nM in 10 mM TriS, 1mM EDTA, pH 7.5 buffer (TE buffer). Then, 65 µL of each concentration was used to

functionalize the biosensor by drop coating and air drying for two hours inside a biosafety cabinet. Thiol-terminated aptamers were attached to the platinum electrodes by self assembling on the surface via covalent adsorption. After two hours, the unbound aptamers were washed off in 10 mL PBS solution (pH 7.4) followed by DI water rinsing. The aptamer coated biosensor was used immediately for further testing. For each loading of aptamer concentration, IMEs biosensor was cleaned with piranha solution and loaded with the desired concentration. The impedance value of bare Pt-IMEs was measured before loading the biosensor with each aptamer concentration. The impedance values of bare Pt-IMEs were used to confirm the adsorption of the thiolated aptamers onto the surface of the IMEs by comparing the impedance values before and after the aptamer coating.

3.3.4   Bacteria culturing

Prior to use, *Listeria innocua* (NRCC B33076) cultures were stored at -80°C. The bacteria was resuscitated by removing 100 μL of an inoculum from the frozen culture and incubated in TPB for 24 hours at 37°C. Two successive transfers were performed in TPB media for 24 hours at 37°C. After the initial three transfers, to ensure the working culture was at the desired bacterial concentration of $10^7 - 10^8$ CFU/mL, weekly transfers were made in TPB, incubated for 24 h at 37°C, and kept in the refrigerator at 5°C. Further, serial dilutions were made to achieve 10^7-10 CFU/mL in 9 mL BPW. The dilutions were spread-plated onto Oxford *Listeria*-selective agar plates supplemented with Oxford *Listeria*-selective supplement and incubated at 37°C for 24 h

to count the bacteria colonies during each testing to ensure the correct bacterial

concentrations.

3.3.5   Electrochemical Impedance Spectroscopy

3.3.5.1   Optimization of the aptamer loading concentration

Electrochemical impedance spectroscopy (EIS) is an alternating current (AC)

method that describes the response of an electrochemical cell to a small amplitude

sinusoidal voltage signal as a function of frequency. The output signal can be described

as impedance (Z, Ohms) in terms of voltage (V, Volts) and current (I, Amperes),

$Z = V / I$, which is a complex number defined as $Z = Z' + iZ''$. Z' is a real in-phase

component of the total impedance which measures the resistance of the electrochemical

cell whereas Z'' is an imaginary out-of-phase component that is associated with the

capacitance of the cell (Lasseter et al., 2004).

The operating principle was based on the interdigitated microelectrodes (IMEs)

array fabricated on the silicon dioxide surface, which functioned as the electrical

transducer of the biosensor. The IMEs were functionalized with *Listeria monocytogenes*

aptamers via covalent adsorption, which consisted of the biological transducer of the

biosensor. When the aptamer based biosensor was tested in a solution, the presence of

aptamers on the biosensor surface caused the impedance to change across the IMEs. This

impedance change was measured and correlated to the various aptamer concentrations

that were loaded onto the IMEs surface to determine the saturation point.

The total impedance measured across IMEs accounts for the combined

opposition of all the components within the electrochemical cell (resistors, capacitors,

70

inductors) to the flow of current (Prodromidis, 2010). Further, these components can be explained by the physical interactions occurring on the surface of IMEs caused by the molecular interactions of the aptamers with the IMEs and the solution (Yang & Li, 2005).

In this study, electrical impedance spectroscopy (EIS) was carried out in a solution of PBS (pH 7.4) using a two -electrode setup on CHI 600E potentiostat/impedance analyzer. One of the two interdigitated array electrodes (IMEs) was connected to the working electrode, and the other IMEs was connected to the reference and counter electrodes of the CHI 600E potentiostat/impedance analyzer. Figure 3.3 shows the experimental setup for the electrochemical impedance spectroscopy analysis method. A sine-modulated AC potential of 100 mV was applied across the IMEs and impedance was measured for a frequency range of 1 Hz to 100 kHz at 30 points per decade. Bode plot (log frequency versus impedance) and Nyquist plot (imaginary versus real impedance) were generated to analyze the aptamer functionalization at various concentrations. The saturation point was determined by comparing the impedance value at each concentration relative to the bare platinum interdigitated microelectrode array.

Working,
Reference &
Counter electrodes

Exposed bonding
pads

PBS solution level

Pt-IMEs
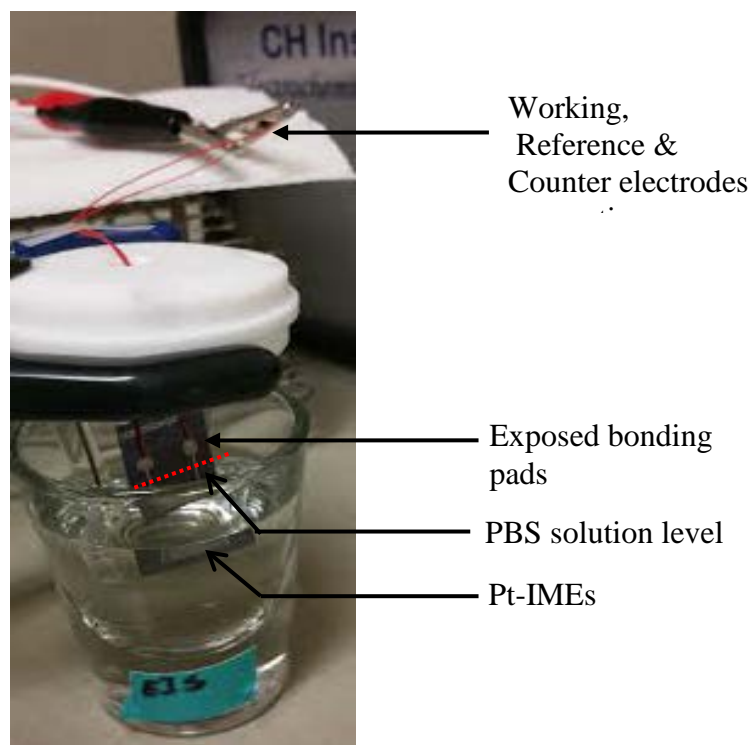
Figure 3.3. Detection of *Listeria* spp. using IMEs aptasensor.

Electrochemical impedance analysis was used to characterize the aptamer based

biosensor response with increasing concentration of *Listeria* spp., *Listeria innocua*

(NRCC B33076), from 10 to 10^6 CFU/mL. Aptamer functionalized IMEs impedance

without bacteria addition was measured and established as a baseline to detect the

impedance difference after introducing the bacteria cells. The applied potential was 100

mV (AC) with a frequency range of 1 Hz to 100 kHz at 30 points per decade. PBS (pH

7.4) was used to run the analysis with functionalized IMEs immersed in 17 mL PBS

solution. The bacteria cells at each concentration were immobilized on the aptamer

coated IMEs for 15 minutes to allow successful binding to the aptamers. During this

time the solution was stirred at 450 rpm using magnetic stirrer at room temperature. The

bacteria cells were added incrementally onto the aptamer coated IMEs from the diluted

bacteria concentration in BPW solution. The desired volume of 17 μL from BPW

solution was added to 17 mL PBS to achieve the bacteria concentration ranging from 10

to 10^6 CFU/ml. The impedance measurements were taken after the stirring was turned

off and solution was stagnant. The bonding pads were not exposed to the PBS solution.

The capacitor stabilizer was turned on in the CHI6044e software and the electrodes were

grounded in order to minimize the charge buildup onto the surface of the electrodes.

Nyquist plots (imaginary impedance versus real impedance) and Bode plots (impedance

vs. frequency) were generated to analyze the total impedance response of the biosensor

with increasing bacteria concentration from 10 to 10^6 CFU/mL. The total impedance

change was correlated to the bacteria concentration by measuring the baseline of the

aptamer coated IMEs without bacteria. The difference in impedance was calculated as

the change in impedance at the bacteria concentration from the baseline and plotted as a

calibration curve to determine the sensitivity, range, and lower detection limits of the

aptamer based biosensor. The total impedance was measured at 1 Hz based on the

spectrum of EIS scan from 1 Hz to 100 kHz.

3.3.6 Statistical analysis

JMP v. 11 Software (SAS Institute, Cary, NC) was used for all statistical

analyses. Means, error bars and standard deviations were calculated based on triplicate

tests. Differences between variables was tested for significance using one-way analysis

of variance (ANOVA) and significantly different means ($p < 0.05$) was separated using

Tukey's Honestly Significant Differences (HSD) test. The lower detection limits were determined as a signal/noise ratio of 3, where noise was defined as the standard deviation of the aptamer coated platinum interdigitated microelectrode array without bacteria as a control test. Sensitivity was determined from the linear correlation of impedance change versus bacteria concentration. Biosensor range was determined based on the detectable impedance signal obtained over a range of bacteria concentration from 10 to 10^6 CFU/mL (Tolba et al., 2012; J. Wang, 2006).Impedance change was measured from the baseline of the biosensor defined as impedance determined at aptamer coated IMEs without bacteria. Detection time was measured based on the time allowed for the bacteria to interact with functionalized aptamer coated IMEs (15 minutes) and time to run EIS scan from 1 Hz to 100 kHz (2 minutes).

3.4   Results and Discussion

3.4.1   Characterization of aptamer loading onto the interdigitated microelectrode

Aptamer functionalized IMEs were characterized by electrochemical impedance spectroscopy (EIS). EIS was used to describe the response of platinum interdigitated microelectrodes biosensor (Pt-IMEs) as a result of low amplitude sinusoidal signal with sweeping frequency range of 1 Hz to 100 kHz. The characterization of SAMs at the electrode surface due to increasing aptamer concentrations were carried out using impedance magnitude measured in PBS solution.

The adsorption of the thiolated aptamers, also known as the molecular interface, onto the IMEs were expected to obstruct the current flow in the presence of buffer solution, therefore increasing the resistance on the surface of electrodes. This

phenomenon was measured using the impedance value which can describe the contributions of aptamer binding to the platinum interdigitated microelectrodes. The total impedance plotted in Figure 3.4 can be written in real and imaginary parts of the impedance as $|Z| = \sqrt{(Z')^2 + (Z'')^2}$ (Lasseter et al., 2004). Z is the total impedance measured in Ohms, Z' is the real resistance measured in Ohms and Z'' is the imaginary part also measured in Ohms.

Bode plot in Figure 3.4 demonstrates the behavior of the aptamer biosensor at different aptamer loading over the entire frequency range from 1 Hz to 100 kHz. The inset shows the impedance values for different aptamer loading at 1 Hz frequency. This data was also presented in an alternative form using the Nyquist plot as shown in Figure 3.5. As mentioned earlier, Nyquist plots were used to show real and imaginary impedance values which reflect the resistance and capacitance of the electrochemical cell; respectively, over the entire range of frequency spectrum (1 Hz to 100 kHz). Due to the intricate 3D structures of aptamers, the bimolecular interfaces (i.e., aptamer and buffer solution) were combined in total impedance, which represents the physical interactions of Pt-IMEs, the aptamer, and the buffer solution.
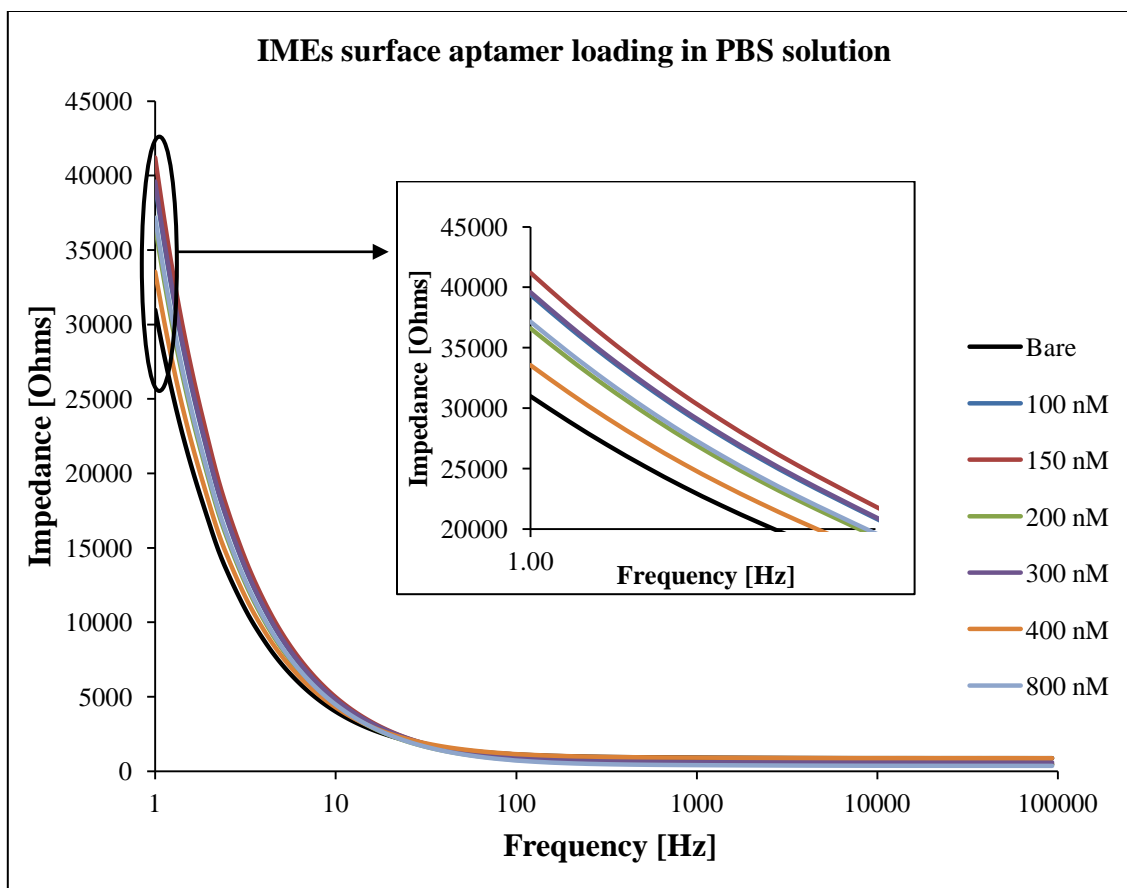
Figure 3.4. EIS analysis (total impedance vs. frequency) of aptamer loading at various concentrations onto IMEs in PBS solution over the frequency spectrum ranging from 1 Hz to 100 kHz. The inset shows the impedance values for various aptamer loading concentrations at 1 Hz.
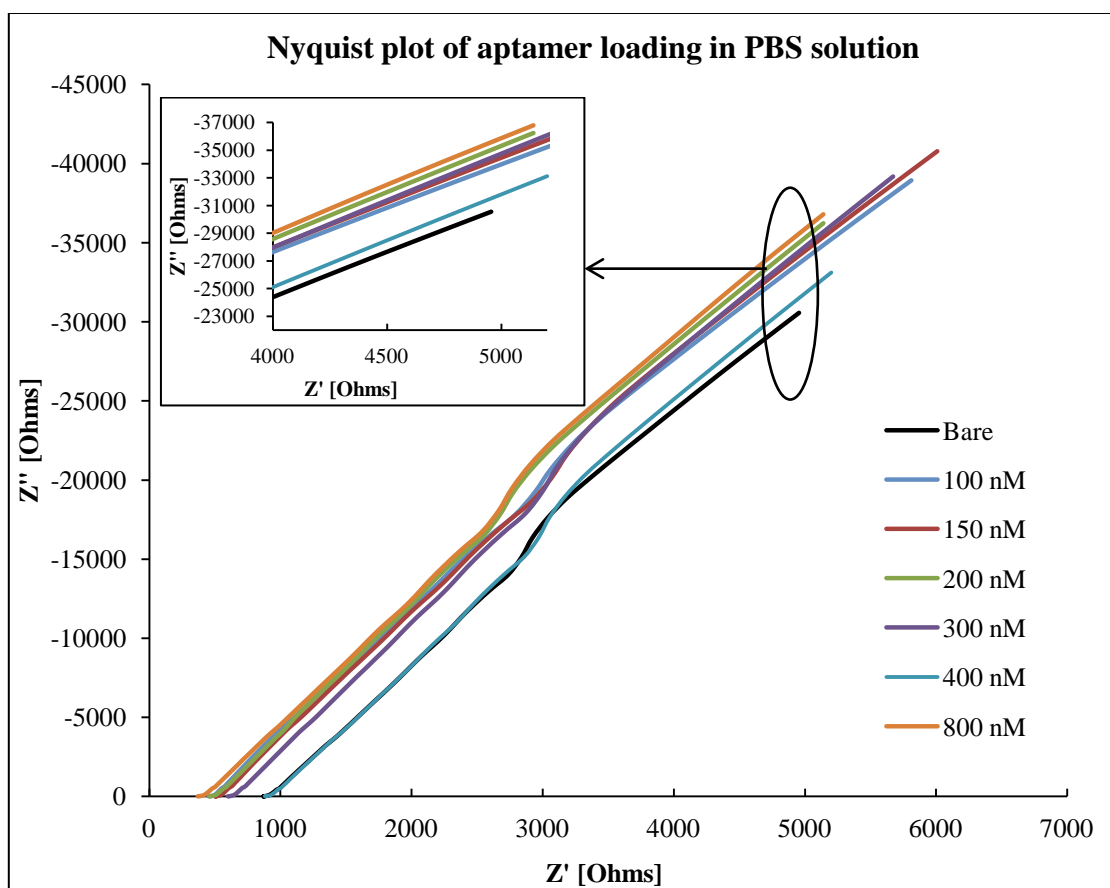
Figure 3.5. Nyquist plot of aptamer loading at various concentrations in PBS solution over the frequency spectrum ranging from 1 Hz to 100 kHz. The inset shows the impedance values for various aptamer loading concentrations at 1 Hz. Z' is real impedance in Ohms and Z'' is imaginary impedance in Ohms representing resistance and capacitance of the biosensor.

The physical interactions in the electrochemical cell between electrodes surface, analyte, and solution could be explained by the Randles equivalent circuit model shown in Figure 3.6. The circuit includes ohmic resistance of the solution (R_s), Warburg impedance (Z_W), double layer capacitance (C_{dl}), and electron transfer resistance (R_{ct}). Ideally, Z_W and R_s are not affected by the electrode surface modifications because these

components represent the properties of the bulk solution and diffusion of the redox

probe; whereas C_{dl} and R_{ct} are affected by the electrode surface modifications because

they are related to the dielectric and insulating features at the electrode and solution

interface (Yang & Li, 2005; Yang, Li, & Erf, 2004a).
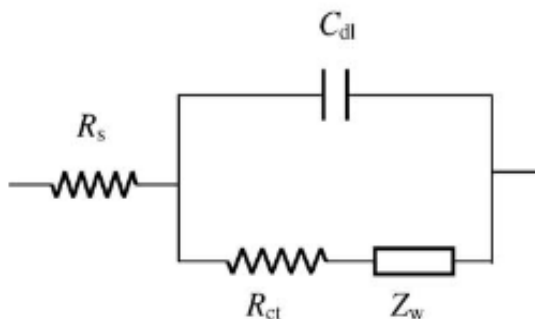
Figure 3.6. The Randles equivalent circuit model for the EIS measurements with the Pt-IMEs. C_{dl} represents double layer capacitance; R_{ct} is the electron transfer resistance; Z_W is the Warburg impedance; R_s represents the resistance of the solution.

The above circuit model could be used to study the impedance response of the

biosensor for the aptamer coated IMEs and the interaction between aptamer surface and

bacteria. Based on the study by Yang and Li (2005) the Randles equivalent circuit was

used to fit the data to determine the circuit components based on the interdigitated

microelectrode array immobilized with antibody to detect $E.\ coli$. In their study, the

solution resistance and Warburg impedance remained relatively unchanged, 0.038% and

8.2% respectively, when the bare surface of the electrode was modified. However, these

two circuit components may change when bacteria is introduced into the solution

depending on the bacteria concentration and type of solution. The double layer and

charge transfer resistance were changed significantly with 12.5% and 80.1% when the

electrode surface was modified with antibody. The same principle could apply to the

biosensor used in our study and Table 3.1 summarizes the expected changes in the

circuit components relative to the bare electrode in PBS solution.

Table 3.1. Expected outcome based on the aptamer coated IMEs and bacteria
interactions.

Circuit Component	Surface modification (aptamer coating)	Injection of bacteria into the solution
R_s (Ω)	Unchanged	Small changes
Z_W ($\Omega\,s^{1/2}$)	Unchanged	Small or large changes
C_{dl} (μF)	Changed	Changed
R_{ct} (Ω)	Changed	Changed

Typically, fitting the measurements of the total impedance into the circuit model

such as, Figure 3.6, requires tuning the circuit components such that the error between

the predicted and measured impedance is minimized by several constraints such as

fixing components' values. For example in Table 3.1 one could use an optimization

software to fit the measured impedance for fixed values of R_s and Z_W while tuning C_{dl}

and R_{ct}. Theoretically, there are multiple solutions for this problem and the results may

significantly vary depending on the search algorithm used in the optimization regardless

of the fit quality. Moreover, when the number of varying components increases in the

circuit, the number of possible solutions will further increase. This is exactly analogous

to the aptamer coating of Pt-IMEs or/and the injection of the bacteria into the solution

where all the circuit components (R_s, Z_W, C_{dl}, and R_{ct}) are changing in the optimization model. Prior to coating the IMEs with aptamers the circuit model in Figure 3.6 was fitted to the EIS data of the bare Pt-IMEs in PBS solution. The optimal values of the circuitry were obtained from CHI6044e software based on the best-fit between EIS measurements and simulated circuit with a reported total error value of 7.03%. The circuit components' (R_s, Z_W, C_{dl}, and R_{ct}) values for the Pt-IMEs were 88.26 Ω, 1.95 x 10^{-3} Ω s$^{1/2}$, 1.093 x 10^{-5} μF, 3410 Ω, respectively. After loading the Pt-IMEs with 800 nM aptamer concentration, the new circuit components for the EIS measurements were obtained from the CHI6044e software. Table 3.2 shows the parameters obtained to fit the model described in Figure 3.6. The EIS data for 800 nM aptamer concentration was run twice under the same optimization constraints; however, the results were not conclusive. Therefore, optimization is not a trivial problem and further studies are required to understand the equivalent circuit model needed to understand the dynamic system of aptamer coating, interaction of bacteria at the IMEs and aptamer surface and in the PBS solution.

Table 3.2. Optimization parameters using CHI6044e software for 800 nM aptamer loading onto IMEs.

Run	Optimization error %	R_s (Ω)	R_{ct} (Ω)	Z_W (Ω s$^{1/2}$)	C_{dl} (μF)
Optimization 1	6.88	95.71	3.89 x 10^4	5.017	7.69 x 10^{-6}
Optimization 2	6.96	95.66	2.86 x 10^5	8.83 x 10^7	8.29 x 10^{-5}

At frequencies above 1 kHz, the impedance vs. log frequency curves converged to impedance values lower than 885 Ohms for six aptamer concentration loadings (100, 150, 200, 300, 400, 800 nM) and also for the bare IMEs. This impedance convergence is shown in Figure 3.4 by the overlapping curves seen after 10 Hz. The same results were observed from the Nyquist plot in Figure 3.5, which shows increasing frequencies in the direction from right to left for each treatment on the Nyquist plot. The real and imaginary impedance values were overlapped at 100, 150, 200, 400, and 800 nM aptamer concentrations. The inset in Figure 3.5 shows the real versus imaginary impedance values at lower frequencies below 10 Hz.

Figure 3.4 and Figure 3.5 established that at frequencies below 10 Hz the impedance response to the aptamer loading had high and distinct values due to the addition of the aptamer deposition onto the electrodes, with the aptamers being responsible for the resistance increase on the electrode surface. The results indicated that the total impedance of the system increased, which is an expected trend due to increase in resistance as thiolated aptamers were adsorbed onto the electrode surface. Formation of SAMs of the thiolated aptamer onto the IMEs surface substantially increased the impedance values at 100, 150, 200, 300, 400, and 800 nM as compared to the bare IMEs indicating the formation of dense layers. The impedance value is significantly higher ($p < 0.05$) than the bare Pt-IMEs at any given aptamer concentration loading (Figure 3.4 and Figure 3.5).

In contrast, at higher frequencies the relationship between the total impedance value and the aptamer loading were not strongly correlated in distinct patterns as shown

in Figure 3.4, Figure 3.5, and Figure 3.7. These results showed that the impedance was decreased with no distinctive trend as the aptamers were loaded onto the surface of the IMEs as compared to Figure 3.8 which shows a distinct trend and biosensor reaching steady state with the impedance values. Figure 3.7 shows the total impedance values at 1, 10, 100 kHz. These frequencies were chosen to show impedance values at different frequency magnitudes over the entire frequency spectrum. The difference in impedance values of six aptamer concentrations relative to the bare Pt-IMEs were significantly decreased ($p < 0.05$) with the exception of 400 nM, which showed no significant difference ($p > 0.05$) from the bare Pt-IMEs. The impedance difference among 100, 150, 200, 300, and 400 nM were negligible. Aptamer loading generated no distinct pattern and the biosensor did not reach any steady state at 1, 10, and 100 kHz as shown in Figure 3.7. Moreover, at each aptamer concentration there is no difference among total impedance values at 1, 10, and 100 kHz. Therefore, the comparison at the higher frequencies did not provide a good indication on how the aptamers were deposited onto the electrode surface. Similar results of overlapping curves at higher frequencies for Bode and Nyquist plots were obtained based on the studies by Dastider et al. (2013) and Radke and Alocilja (2004). These studies explained that the high frequency above 1 kHz might correspond to the ohmic resistance of the solution, which is indicated by the convergence of the impedance curves shown in Figure 3.4. The biosensor was able to detect the electrical signal at low frequencies below 10 Hz induced by the adsorbed layer of thiolated aptamers onto the IMEs. The presence of aptamers on the IMEs surface caused the impedance change due to the formation of SAMs, which inhibited the current

flow between the biosensor IMEs. Based on these results, the frequency of 1 Hz was

selected to determine the saturation limit of the aptamer loading as it showed the most

distinguishable impedance changes among the treatments (Figure 3.4 and Figure 3.5).
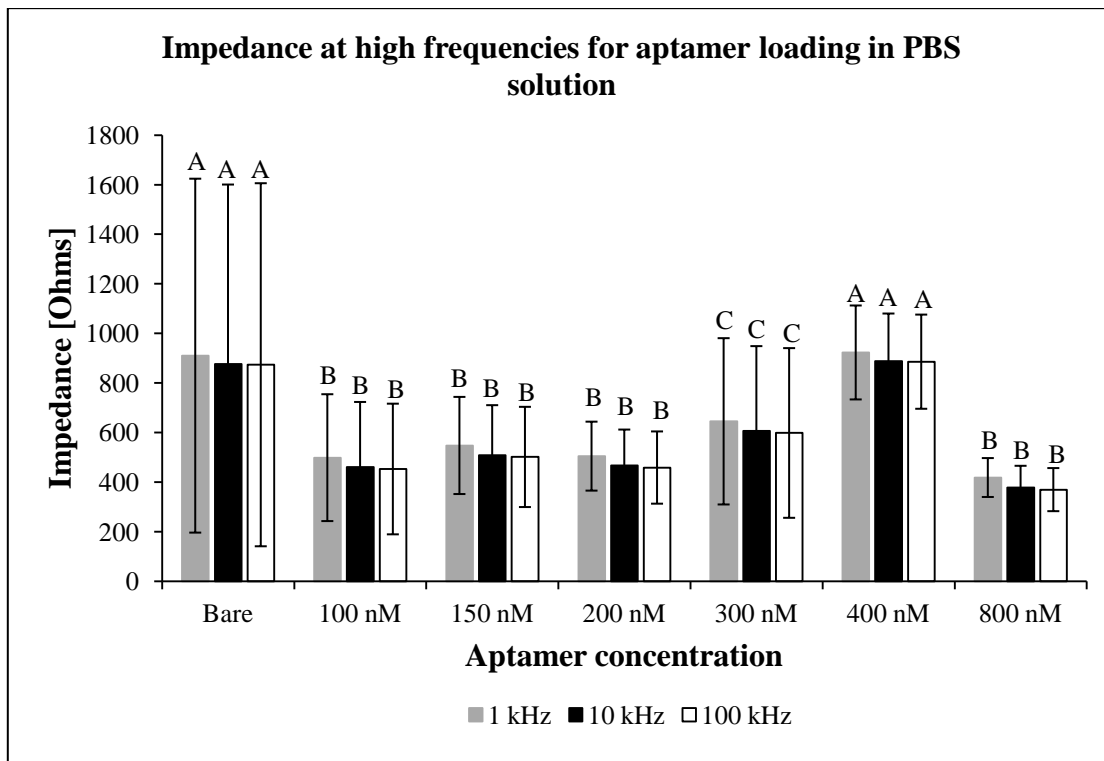
Figure 3.7. Impedance values at higher frequencies for various aptamer concentrations in
PBS solution at 1, 10, 100 kHz. Error bars were based on the standard deviations of
means in triplicate tests. Different letters indicate significance at $P < 0.05$.

When the aptamer based biosensor was tested in PBS solution, the presence of

aptamers on the biosensor surface caused the impedance to change across the IMEs. This

impedance change was measured and correlated to the various aptamer concentrations

that were loaded onto the IMEs surface to determine the saturation point at the selected

frequency of 1 Hz. Figure 3.8 illustrated the impedance magnitude at 1 Hz used to

determine the saturation point of aptamer loading. The impedance values versus the

aptamer concentrations were plotted at each concentration.
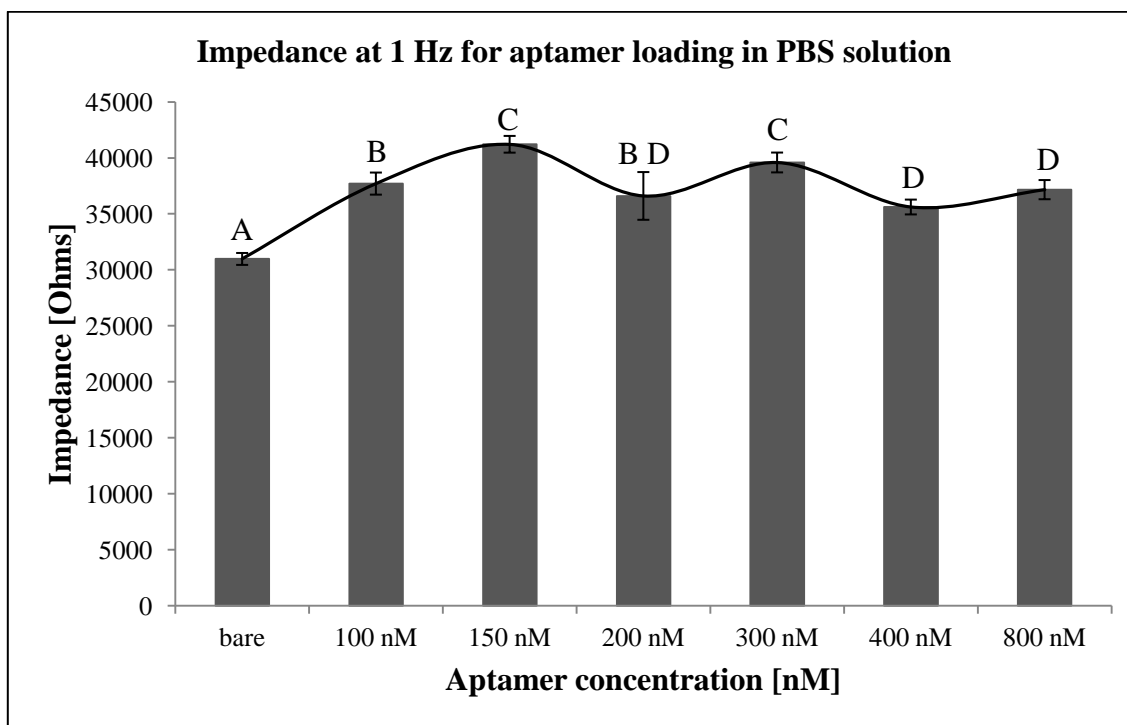
Figure 3.8. EIS analysis at 1 Hz for aptamer loading onto interdigitated microelectrodes array in PBS solution at 1 Hz. Error bars were based on the standard deviations of means in triplicate tests. Different letters indicate significance at $P < 0.05$.

The impedance values of six aptamer concentrations loading were significantly

higher ($p < 0.05$) than the bare Pt-IMEs shown in Figure 3.8. The significant increase (P

< 0.05) in the impedance values relative to the bare Pt-IMEs demonstrated that the

aptamers were successfully adsorbed onto the surface of the IMEs biosensor. The

impedance values started to saturate at 300 nM and the IMEs biosensor reached steady

state between 400 and 800 nM where the difference was between 15 to 20% relative to

the bare. The measured impedance values of the biosensor at each aptamer concentration

(100, 150, 200, 300, 400, 800 nM) is due to the double layer capacitance of the IMEs

and aptamer interface, solution resistance, and charge transfer resistance from the bulk

solution. These variables can change slightly and these variabilities could be caused by

the IMEs cleaning process or the random aptamer attachment to electrode surface.

Although the ideal trend of the impedance response to aptamer loading should follow an

asymptomatically converging function until it reaches saturation, due to the

aforementioned variables, the impedance response possesses dynamics that shows slight

fluctuations in Figure 3.8. However, the dynamic system described in the Figure 3.8 has

reached steady state values between 400 and 800 nM. The 800 nM aptamer

concentration is a safer design parameter, which guarantees that the electrodes are fully

coated with *Listeria monocytogenes* aptamers. Additional experiments were performed

to confirm the aptamer loading selection and it is shown in Figure 3.9. The experiments

were conducted in 5mM $Fe(CN)_6^{3-}$ / 100 mM KCl solution using the same procedures

described in section 3.3.5.1 and to test the hypothesis that the impedance saturate at

800nM in a solution different than PBS. The aptamer concentration ranging from 100 to

3200 nM was selected to understand the behavior of the aptamer coated IMEs for

concentrations above 800 nM. This analysis in 5mM $Fe(CN)_6^{3-}$ / 100 mM KCl solution,

shown in Figure 3.9, confirms our hypothesis, where no significant changes ($P > 0.05$) in impedance response were measured above 800 nM aptamer loading, reaching saturation.

Figure 3.8 and Figure 3.9 showed that the biosensor reached the maximum loading of the bio-recognition element, aptamers, onto the platinum interdigitated microelectrode array at 800 nM. Hence, 800 nM aptamer loading was chosen to coat the biosensor for *Listeria* spp. detection based on the results discussed in this section. Furthermore, EIS analysis showed to have the ability to sense the covalent binding of the thiolated aptamers onto the IMEs surface without the use of any kind of labels and directly converted the SAMs formation into measurable electrical signal. EIS analysis have been used in previous studies to determine binding affinity constants, K_D, of enzymes and antibodies among other compounds due to its label-free capabilities (Daniels & Pourmand, 2007).
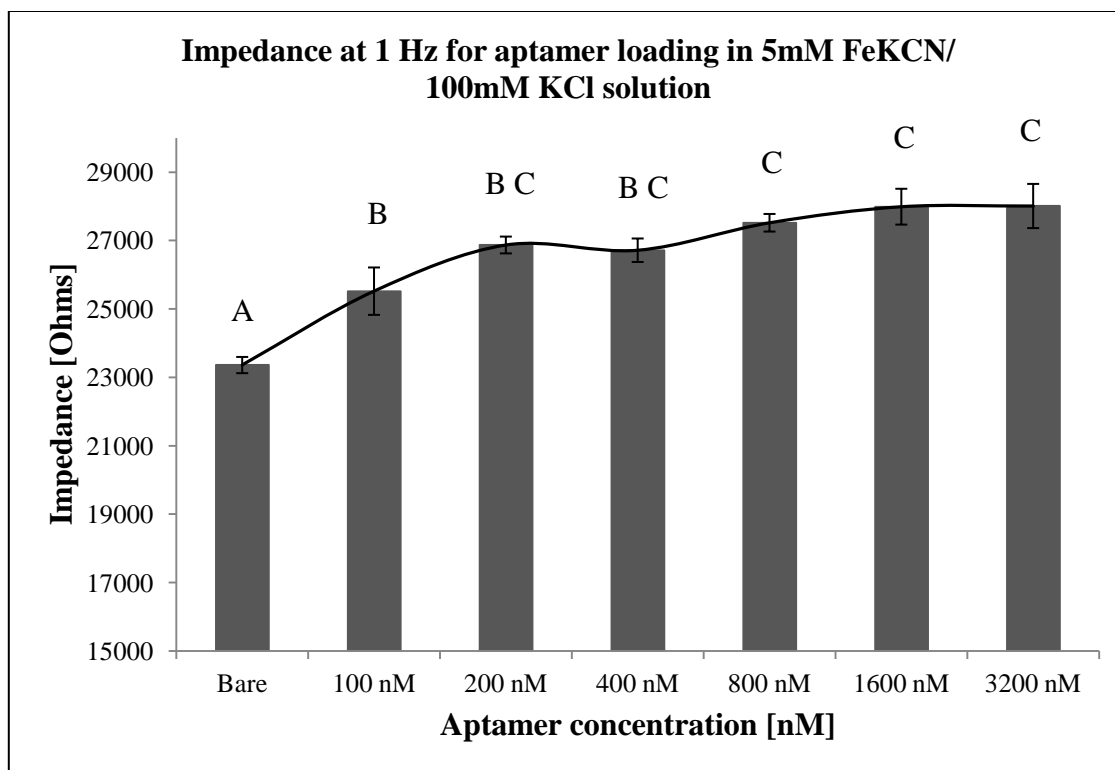
Figure 3.9. EIS analysis at 1 Hz for aptamer loading onto interdigitated microelectrodes array in 5mM $Fe(CN)_6^{3-}$ / 100 mM KCl solution at 1 Hz. Different letters indicate significance at $P < 0.05$.

3.4.2 Detection of *Listeria* spp. using IMEs aptasensor

Listeria innocua is commonly used as a non-pathogenic surrogate organism for

Listeria monocytogenes due to their genetic and metabolic similarities and importance to

the food industry (Buzrul & Alpas, 2004; Milillo et al., 2012). The operating principle

of functionalized IMEs with aptamers were discussed in section 3.3.5.1, the same

principle was applied to understand the behavior of the *Listeria monocytogenes* aptamers

binding to the membrane protein of *Listeria* spp. (i.e., internalin A) to the. This binding

added another element to the electrochemical cell further increasing the impedance from the aptamer coated IMEs by obstructing the current flow.

Figure 3.10 was obtained from the measured total impedance versus log frequency. The inset shows that the aptamer-bacteria binding resulted in increased impedance as the bacteria concentration was increased at the frequency of 1 Hz. The impedance values were measured at 1 Hz for the reasons mentioned above, which resulted in impedance increase with the increase in bacteria concentration. At low frequency, 1 Hz, the impedance values were directly proportional to the increasing concentration of the bacteria cells whereas at the higher frequencies the values were independent of the bacteria concentration and showed no significant difference ($P > 0.05$). Figure 3.11 shows the Nyquist plot for the entire frequency range of 1 Hz to 100 kHz and the inset depicts the real and imaginary impedances at lower frequencies. The direction of increasing frequencies is from right to left on the Nyquist plot (Figure 3.11). The overlapping of impedance values at higher frequencies above 1 kHz in Figure 3.10 andFigure 3.11 showed no distinct pattern whereas at lower frequencies below 10 Hz the impedance values were increased ($p < 0.05$) as the bacteria concentration was increased.

Hence, the impedance values at 1 Hz were used to determine biosensor performance's parameters, i.e., range, sensitivity, detection time, and limit of detection calculations.
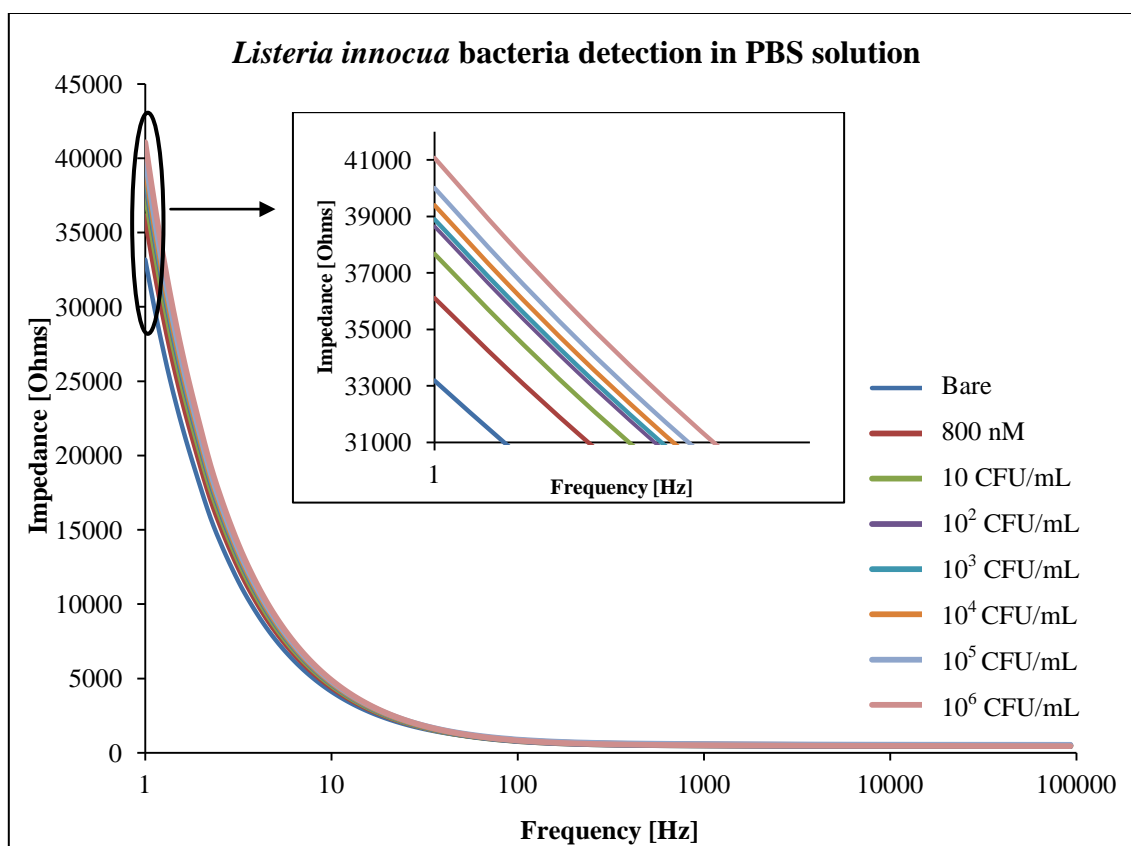
Figure 3.10. Detection of *L. innocua* using aptamer coated IMEs in PBS solution over the frequency spectrum ranging from 1 Hz to 100 kHz. Bacteria concentration ranged from 10 to 10^6 CFU/mL. The inset showed the total impedance values at 1 Hz.
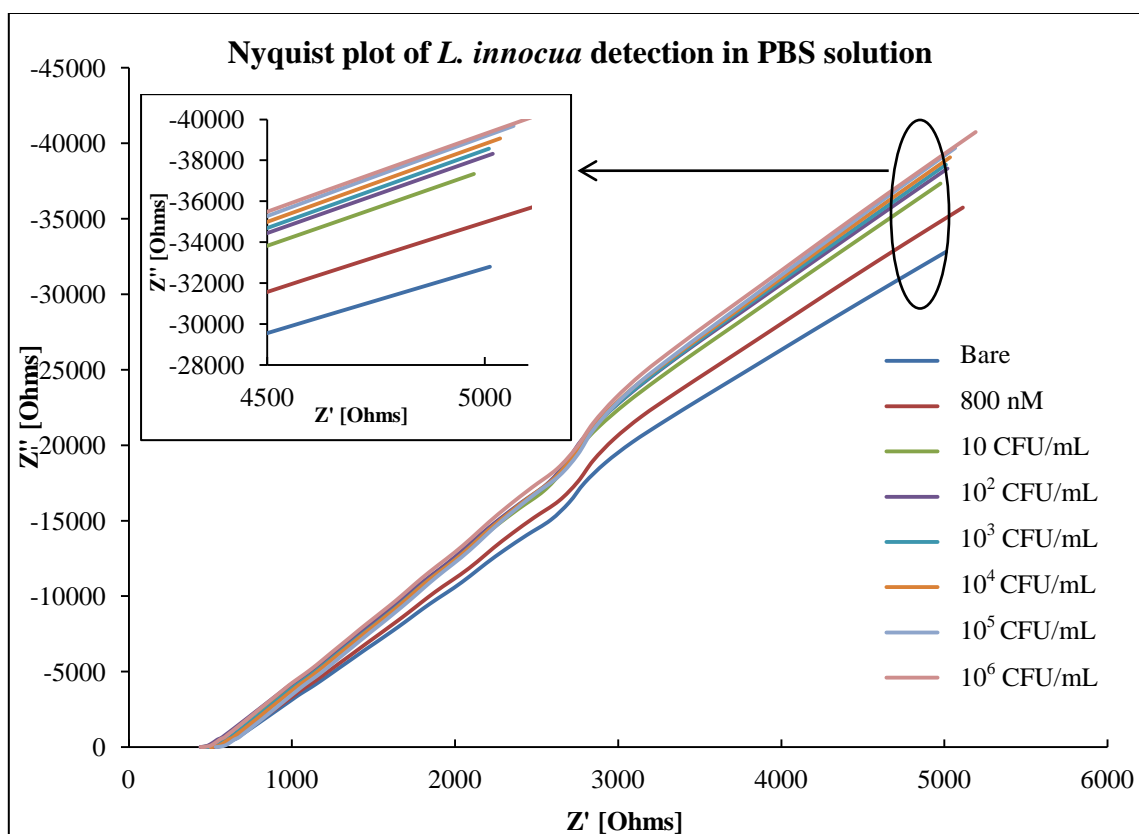
Figure 3.11. Nyquist plot of *L. innocua* detection in PBS solution over the frequency spectrum ranging from 1 Hz to 100 kHz. Bacteria concentration ranged from 10 to 10^6 CFU/mL. The inset shows the impedance values below 10 Hz. Z' is real impedance and Z'' is imaginary impedance representing resistance and capacitance of the biosensor.

The aptamer coated IME impedance was used to calculate the difference between impedances after the bacteria was introduced. The capture of the bacteria onto the modified IMEs with aptamer was further illustrated in Figure 3.12 through the normalized impedance change (NIC) percentage calculated based on the Equation (3.2) below:

$$NIC = \frac{Z_{bacteria} - Z_{aptamer}}{Z_{aptamer}} *100 \qquad (3.2)$$

Figure 3.12 was obtained based on the normalized impedance change versus log bacteria concentration. The NIC value caused by the bacteria was found to increase linearly with the number of cells present in the solution that would bind to the biosensor surface. For *Listeria innocua* detection, a linear relationship was found between the NIC (%) and the logarithmic concentration of bacteria, $C_{L.innocua}$ in (CFU/mL), which was depicted by the following equation: $NIC = 0.7424 \log (C_{L.innocua}) + 2.7941; R^2 = 0.9653.$

The sensitivity value was calculated to be 0.7424 ± 0.0703 ($NIC/\log[CFU/ml]$) from the linear regression. The experimental data confirmed the hypothesis that the modified IMEs with *Listeria monocytogenes* aptamers for selective binding of *Listeria* spp. were able detect the *Listeria* cells. The *Listeria monocytogenes* aptamers were designed to target *Listeria* spp. protein, internalin A which is located at the membrane surface, allowing the aptamer binding sites to capture the bacteria at the sensor surface; therefore increasing the impedance on the surface of the interdigitated microelectrodes (Ohk et al., 2010). The change in the impedance of the sensor is directly proportional to the number of bacteria immobilized on the sensor's surface. The increased NIC as seen in the Figure 3.12 confirmed that the resistance of the aptamer coated interdigitated microelectrodes was increased due to increasing concentration of bacterial cells in the PBS solution.

Normalized impedance change versus *Listeria innocua* concentration

$y = 0.7424 \log(C_{L.\ innocua}) + 2.7941$
$R^2 = 0.9653$
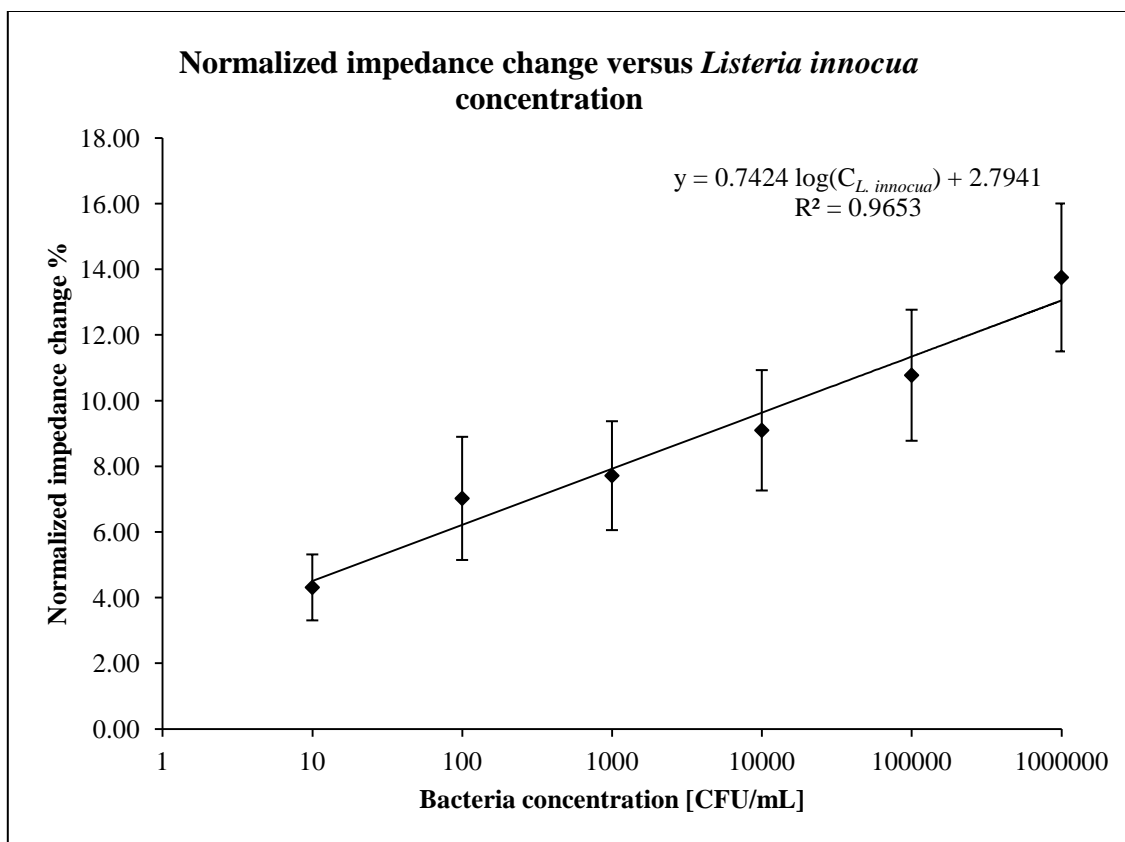
Figure 3.12. Normalized impedance change (%) versus *Listeria innocua* concentration ranging from 10 to 10^6 CFU/mL in PBS measured at 1 Hz using aptamer coated IMEs. Error bars were based on the standard deviations of means from triplicate tests.

A calibration curve for detection of *Listeria innocua* was obtained by plotting impedance difference (ΔZ) versus logarithm of bacteria concentration. Impedance difference was calculated using Equation 3.3:

$$\Delta Z = \frac{Z_{bacteria} - Z_{aptamer}}{Z_{aptamer}} \qquad (3.3)$$

where $Z_{bacteria}$ the total impedance (Ohms) measured for a given bacteria concentration

and $Z_{aptamer}$ is the total impedance (Ohms) measured without bacteria and it was

considered the baseline of the aptamer coated IMEs biosensor.

The results are shown in Figure 3.13 as a function of total impedance difference

at 1 Hz for six bacteria concentration whereas figure 3.12 normalized the impedance

difference by multiplying by 100. Figure 3.13 demonstrated a linear relationship found

between ΔZ (Ohms) and the bacteria concentration, $C_{L.innocua}$ in log (CFU/ml), to be

depicted by the following equation $\Delta Z = 268.1 \log (C_{L.innocua}) + 1009; R^2 = 0.9653$. The

sensitivity was determined to be 268.1 ± 25.40 (Ohms/log [CFU/mL]). The lower

detection limit (LDL) was calculated based on the signal/noise of 3 where noise is

defined as measured impedance, $Z_{aptamer}$ (control experiment), which is the aptamer

coated IMEs without the bacteria. . The LDL Equation 3.4 was used as described below:

$$LDL = [(3S_D + Z_{aptamer}) - b] / m \qquad (3.4)$$

where m is the slope and b is y-intercept of the linear calibration plot shown in Figure

3.13, S_D is the impedance ($Z_{aptamer}$) standard deviation of the control experiment (Tolba

et al., 2012; J. Wang, 2006). The lower detection limit and its standard deviation of the

aptasensor for *L. innocua* were found to be 5.39 ± 0.21 CFU/mL. The total detection

time from introducing the bacteria samples to impedance measurements was 17 minutes.

The protein binding of bacterial cells to the aptamer surface was allowed for 15 minutes

while stirring the solution at 450 rpm at room temperature, followed by the EIS analysis

which in average would take 2 min. These results indicated that the aptasensor was

capable of detecting *L. innocua,* at a significantly low detection limit using a linear

calibration curve throughout a wide range of bacteria concentration without the need for

labels or pre-concentration, therefore, decreasing the detection time.

Impedance difference versus *Listeria innocua* concentration

$\Delta Z = 268.1\log(C_{L.innocua}) + 1009$
$R^2 = 0.9653$
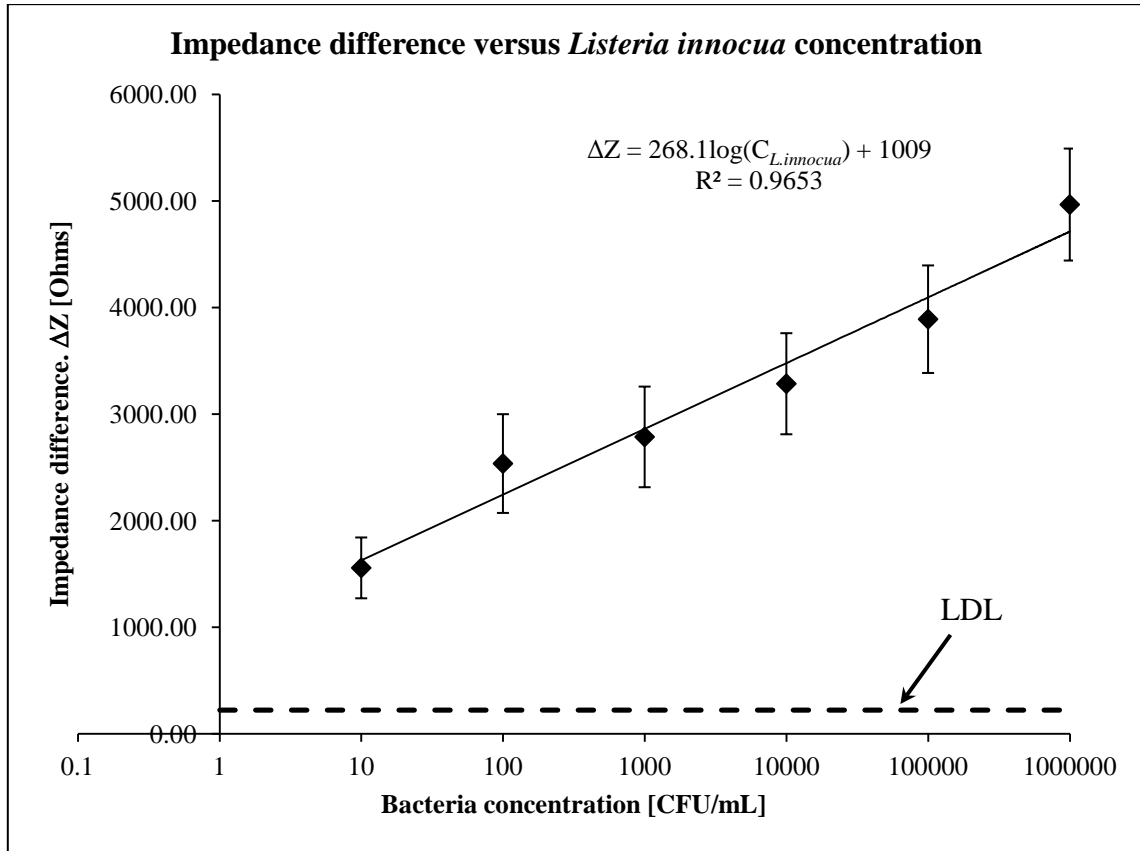
Figure 3.13. Detection of *L. innocua* in PBS solution using aptamers functionalized IMEs through impedance changes measured at 1 Hz. *Listeria innocua* concentration ranged from 10 to 10^6 CFU/mL. Error bars were based on the standard deviations of means in triplicate tests. Lower detection limit (LDL) line was determined based on signal/noise ratio multiplied by 3.

The total impedance Bode and Nyquist plots, sensitivity, and lower limit

detection results demonstrated the binding of *L. innocua* to *Listeria monocytogenes*

aptamers-functionalized IMEs. The combination of specific protein biorecognition via

covalently adsorbed aptamers onto the surface of electrodes with EIS detection method

provided a sensitive, rapid, and label-free biosensor. The developed miniaturized

aptamer based biosensor was able to monitor direct electrochemical changes using

impedance to detect bacteria attachment to the aptamers. The developed impedance

aptasensor to capture *Listeria* spp. had lower detection limit, higher sensitivity, and

shorter detection time as compared to the biosensors reported in the literature shown in

Table 3.3. Table 3.3 summarized the impedance based biosensors used to detect *Listeria*

spp. on various electrode types. The study by (R. Wang et al., 2008) showed the

detection range from 10^2 to 10^7 CFU/mL for *Listeria monocytogenes*; however, no linear

correlation was found for this bacteria range. The studies performed in the past used

antibodies or growth medium in order to detect *Listeria* as compared to the aptamers

which offer the advantage of chemical synthesis with high purity avoiding batch-to-

batch variations and longer shelf-life (Wang et al., 2012). The study performed by Tolba

et al. (2012) reported an impedimetric biosensor using the cell wall binding domain

(CBD) of bacteriophage-encoded peptidoglycan hydrolases (endolysin) immobilized on

a gold screen printed electrode (SPE) using amine-coupled chemistry for the detection of

Listeria bacteria cells in PBS solution. The disadvantage of this method was that it

required long pre-conditioning steps for the electrodes of 16 hours immersing in a 1 mM

ethanolic solution of 11-mercaptoundecanoic acid (MUA) at room temperature in order

to detect the bacteria (Tolba et al., 2012). Furthermore, the linear range and detection

limits reported are for significantly high bacteria concentrations (10^4 to 10^9 CFU/mL)

that do not meet the required detection levels in the food industry (below 10 CFU/mL).

Table 3.3. Comparison of lab-on-a-chip impedimetric biosensors for detection of
Listeria spp.

Biosensor type	Impedance detection technique	Detection time	Limit of detection [CFU/mL]	Bacteria range [CFU/mL]	Reference
Flow cell with embedded Pt-IMEs	Metabolites produced by bacterial cells as a result of growth in Tris-Gly-Dext (no biorecognition element)	2 hrs	$1.9 \times 10^7 – L.$ *innocua* $3.80 \times 10^7 – L.$ *monocytogenes*	10^7 to 10^9	(Gómez et al., 2002)
TiO$_2$ nanowire bundle microelectrodes	Biorecognition element – antibodies (Abs)	50 minutes	4.7×10^2	10^2 to 10^7	(R. Wang et al., 2008)
Gold screen printed electrodes (SPE)	Immobilization of biorecognition element-Endolysin on SPE	30 minutes	1.1×10^4 – pure bacteria culture 1.1×10^5 – 2% milk	10^4 to 10^9	(Tolba et al., 2012)
Pt-IMEs	Biorecognition element – *Listeria monocytogenes* aptamers	17 minutes	5.39	10^1 to 10^6	This study

3.5 Conclusions

An impedimetric aptasensor was developed using miniaturized interdigitated

microelectrodes (IMEs) array with the biorecognition element, *Listeria monocytogenes*

aptamers, for rapid, sensitive and lower detection limit of *Listeria* spp. in PBS solution.

The loading of aptamer onto the IMEs surface was optimized using covalently

adsorption and EIS analysis. *Listeria monocytogenes* aptamers were reduced using DTT

reduction protocol and six aptamer concentration were functionalized onto the IMEs

surface. The aptamer based biosensor was saturated at 800 nM, which was used to

functionalize the IMEs surface to detect the targeted bacteria. Electrochemical

impedance spectroscopy analysis was able to detect the surface modification due to

aptamers attachment and protein binding of *Listeria innocua*; providing a direct

technique for *Listeria* spp. detection without the need for label amplification or sample

pre-concentration steps. The aptasensor was capable to detect bacteria throughout a

wide range of bacteria concentration from 10 to 10^6 CFU/mL with a sensitivity value of

268.1 ± 25.40 (Ohms/log [CFU/mL]) and lower detection limit of 5.39 ± 0.21 CFU/mL

in 17 min, which are lower than the values reported previously in the literature. In this

study, real-time, highly sensitive, rapid and portable aptamer based biosensor was

demonstrated to detect *Listeria* spp. and could be used in future food safety applications.

The developed biosensor could be implemented in field conditions to detect foodborne

pathogens in food products to ensure public health and to promote food safety.

CHAPTER IV

APTASENSOR ASSISTED WITH DIELECTROPHORESIS FOR ENHANCED

BACTERIA DETECTION

4.1 Overview

Dielectrophoresis (DEP) technique has been used in combination with label-free impedimetric biosensors to improve the capture efficiency of the target bacteria and ultimately detection. However, there is still a need to reduce detection limits for real-time, highly sensitive and reliable biosensing platforms to meet the demands of on-site analysis of food products. Furthermore, DEP can be used to distinguish between live and dead bacteria in the food industry to determine whether a serious threat is purposed by live or dead bacteria after a sterilization process and to validate other intervention processes. The primary goal of this chapter was to develop a method based on the DEP mechanism to detect and distinguish between viable and non-viable bacteria. The optimal operating settings of the biosensor were determined by varying the frequencies ranging from 0.5, 1, 10, 100, 600 kHz to 1 MHz. The non-viable *Listeria innocua* and *Staphylococcus aureus* were used based on the hypothesis that the *Listeria monocytogenes* aptamers were selective to only viable *Listeria spp*. Chapter II demonstrated that these aptamers, which bind to membrane protein internalin A, were able to detect viable *Listeria* cells. Optimal DEP force at 10 kHz frequency and 4.24 V_{pp} (peak-to-peak voltage) was applied to conduct the experiments for viability and selectivity. EIS analysis from 1 Hz to 100 kHz at 100 mV amplitude was applied to determine the total impedance of the biosensor in the experiments. The normalized

impedance percent change was calculated over three frequency regions from low (500 – 1000 Hz) to medium (1 – 600 kHz) to high (600 – 1000 kHz) for bacteria concentration of 10, 10^2, and 10^4 CFU/mL. Normalized impedance change of 14.13 % was found to be in 1 – 600 kHz frequency region for the three bacteria concentrations and it demonstrated maximum bacteria capture efficiency. These results showed that DEP force enhanced the bacteria capture efficiency. Based on these results, the combination of DEP-EIS techniques were used to detect the aptamer selectivity for viable and non-viable bacteria. Heat inactivated *Listeria innocua* was used to determine the biosensor response to non-viable bacteria in buffered peptone water. The developed aptasensor assisted with DEP was able to detect the viable and non-viable bacteria by using impedance difference measurement analysis with sensitivity values for viable *Listeria* spp. of 17.37 Ω/log(CFU/mL)] with lower detection limit of 7.44 ± 0.075 CFU/mL within 12 minutes. *S. aureus* was used as an interferent to detect *Listeria* spp. in BPW solution over the bacteria concentration range of 10 – 10^6 CFU/mL. The developed biosensor showed that it was capable of distinguishing the two bacteria using impedance difference analysis with *Listeria* spp. sensitivity value of 91.28 Ω/log(CFU/mL)]. The lower detection limit was calculated to be 5.68 ± 0.025 CFU/mL for viable *Listeria* spp. within 12 minutes. The impedance based biosensor was also used to detect *Listeria monocytogenes* in off-the-shelf product, vegetable broth, at the same DEP-EIS conditions used for viability and selectivity methods with the detection limit of 4.82 ± 0.01 CFU/mL in 12 min for bacteria ranging from 10 to 10^7 CFU/mL, with one of the lowest detection limits and detection times reported to date.

4.2   Introduction

In chapter III, electrochemical impedance spectroscopy (EIS) analysis was able to detect *Listeria innocua* by measuring impedance changes at the electrodes surface and by using aptamers as the biorecognition element. The total impedance value of the biosensor significantly increased as the bacteria concentration ranging from 10 to 10^6 CFU/mL increased. Furthermore, the method described in Chapter III followed the traditional test techniques where biosensors are typically immersed in a large solution volume containing bacteria (17 mL phosphate buffer saline). In particular, the biosensor was freely immersed in the solution and its surface was not in the direction of bacteria sedimentation, i.e., electrodes were positioned vertically instead of horizontally. Therefore, bacteria attachment was probabilistic and dependent on the kinematics of bacteria in the solution. To overcome these shortcomings, microfluidic channels are often used to increase the concentration of bacteria at the biosensor's surface. However, using microfluidic channels in biosensors can limit the shelf-life of the device by making more difficult to reuse or clean the biosensor. Further microfluidic device requires an additional fabrication process, such as PDMS (polydimethylsiloxane) molding.

Toward these challenges, this chapter aimed to improve the detection method of the aptamer-functionalized biosensor by using reduced sample volumes and dielectrophoresis (DEP) at an optimized frequency signal to improve the capture process. DEP act as magnet to polarized bacteria, however; the DEP electrostatic field size is typically narrow, and would only collect polarized bacteria that are at a close distance to the electrodes surface. This provides an improvement over the capture

100

process discussed in Chapter III. In addition, sampling a smaller volume contained in a chamber enabled the design of a portable device. Furthermore, with a reduced volume there is a reduction in bacteria exposure and contamination compared to a larger sample volume. In Chapter III, the capture mechanism was based on the random movement of bacteria without external force. The aptasensor provided a strong attachment using aptamers but did not attract the bacteria from solution to the surface.

Dielectrophoresis (DEP) techniques have been used in addition to label-free impedimetric methods to improve the capture efficiency of foodborne pathogens. Previous studies have used DEP to overcome the detection limit due to limited physical sensitivities of the transducers and low immune-capture efficiency of the immobilized antibodies on the electrode surfaces (Suehiro et al., 2006; Yang, 2009). DEP has been used to manipulate biological cells for filtering, focusing, sorting, and trapping in desired position and orientation (Cheng et al., 2007). Several other methods have been used for manipulation, concentration, and separation of biological particles that use various kinds of physical forces from mechanical, hydrodynamic, ultrasonic, optical, and electro-magnetic principles (Li & Bashir, 2002). Among these methods, dielectrophoresis techniques are proved to be the most suitable on micro-fabricated electrodes because of its relative ease of micro-scale generation and structuring of an electric field on the microchips (Li & Bashir, 2002).

Dielectrophoresis is the electrokinetic motion of dielectrically polarized particles in non-uniform external electric fields, DEP can attract polarized particles to the electric field, in order to trap bacteria onto an interdigitated microelectrode chip (Suehiro

101

et al., 2005). The trapped bacteria onto the surface of the electrodes increase the

impedance of the biosensor and consequently improve detection. In particular, when a

non-uniform form AC electrical field is applied, DEP forces occur on bacteria cells that

interact with field-induced electrical polarization (Li & Bashir, 2002). The time-

averaged DEP force exerted by the electrodes on a dielectric sphere in a medium can be

represented in Equation 4.1 as:

$$F = 2\pi \varepsilon_0 \varepsilon_m r^3 \text{Re}[f_{cm}] \nabla |E_{rms}|^2 \qquad (4.1)$$

where ε_0 [C/Vm] is the vaccumm dielectric constant, ε_m [C/Vm] is the permittivity of

the particle, r [µm] is the particle radius (in this case bacterial radius), E_{rms} [V/m] is the

root mean square value of the electric field (Yang, 2012). $Re[f_{cm}]$ is the real part of the

Clausius-Mossotti factor (f_{cm}) defined Equation(4.2 as:

$$f_{CM} = \frac{\varepsilon_p^* - \varepsilon_m^*}{\varepsilon_p^* + 2\varepsilon_m^*} \qquad (4.2)$$

where $\varepsilon_p^* = (\varepsilon_p - j\sigma_p)$ and $\varepsilon_m^* = (\varepsilon_m - j\sigma_m)/\omega$ are defined as the relative complex

permittivities of the particle and the medium, respectively; σ [S/m] is the conductivity, ε

[C/Vm] is the permittivity, ω [radians/s] is the angular frequency of the applied electric

field, and $j = \sqrt{-1}$ (Yang, 2012). The force acting on the particle is varied by the

frequency, which is indicated by the real part of frequency dependent term $\text{Re}[f_{cm}]$. A

particle can experience positive or negative DEP forces depending on the particle

relative polarization with respect to the suspending medium, for example, the particle

will experience positive DEP when $\text{Re}[f_{cm}] > 0$ moving the particle towards stronger

102

electrical field region. Whereas, a particle will experience negative DEP when

$\text{Re}[f_{cm}] < 0$ moving the particle towards weaker electrical field region (Li & Bashir,

2002; Yang, 2009).

DEP assisted bacteria detection has been used for various devices including the

detection of *Escherichia coli*, *L. monocytogenes*, and *Salmonella*. (Gómez-Sjöberg et al.,

2005) studied the detection of the *Listeria* cells using interdigitated microelectrode array

(IMEs) biosensor that incorporated DEP as a trapping tool to collect bacteria into a

microfluidic chamber followed by impedance measurements of bacteria growth. The

biosensor contained two sets of IMEs, one set was used to concentrate and capture the

bacteria cells from a main channel into a small chamber (400 pL) using dielectrophoresis

and the other set of IMEs was for monitoring the impedance change in the small

chamber by detecting bacteria's metabolic activity. The bacteria were incubated in the

small chamber for a minimum of 12 hours at 37° C in Luria-Bertani (LB) broth. The

bacteria's metabolism detection was based on impedance method and was conducted for

1 hour after the incubation time with the bacteria ranging from 10^4 to 10^5 CFU/mL with

lower detection limit of 8.0 x 10^4 CFU/mL. In other studies by (Yang, 2009) and (Koo et

al., 2009), DEP technique was used to effectively enhance the antibody capture

efficiency in biosensor/biochip platforms to improve the detection of bacteria cells. The

immuno-capture efficiencies of antibodies immobilized on solid surfaces to bacteria

cells are generally considered very low ranging from 0.01 to 16% so DEP technique has

been used to enhance the capture efficiency (Yang, 2012). For example, DEP enhanced

immunocapture of *Salmonella* cells were used on a non-flow IMEs based biosensor and

the bacteria cells were captured by the immobilized antibodies on the surface of IMEs in a study performed byYang (2009). DEP signal was applied for 15 or 30 minutes to capture the bacteria cells and then the immune-captured bacteria cells were detected by the sandwich format ELISA (enzyme-linked immunosorbent assay) and quantitative signal was produced by absorbance measurements at 450 nm. The lower detection limit on chip ELISA detection with DEP assistance was 5.0 x 10^4 CFU/mL for bacteria ranging from 10^4 to 10^7 CFU/mL within ~1 hour. The immuno-capture efficiency with DEP enhancement was 3-5 folds higher (64.7 – 105.2%) compared to without DEP. (Koo et al., 2009) reported a DEP enhanced biosensor based on IMEs for the detection of *Listeria monocytogenes* by immobilizing a heat shock protein 60 (Hsp60) onto the surface of the electrodes. The capture efficiency was increased 60% when DEP force was applied for 5 minutes at the beginning of the final 1 hour incubation step at room temperature. The bacteria cells were detected by fluorescence microscopy images after normalizing the cell counts from nine images. The lower detection range was 10^7 CFU/mL for the bacteria concentration ranging from 10^6 to 10^7 CFU/mL.

According to the studies by (Yang, 2009) and (Koo et al., 2009) DEP assisted immuno-capture techniques have showed two significant functions in the biochip platforms to improve the detection (i) DEP can concentrate bacterial cells from the suspension to different locations on the chip surface, which make it very useful in manipulating bacterial cells in biosensors and biochips; (ii) DEP can make bacterial cells in close contact with the immobilized antibodies on the chip surface, which can

effectively improve the immuno-capture efficiency and ultimately detection (Yang, 2012).

DEP has also been employed to study the selective capture of viable bacteria in combination with IMEs based biosensing platforms. Viability test studies the separation of the viable and non-viable cells, which could play an important role in the food industry to determine whether live or dead bacteria purpose a serious threat after a sterilization process. For instance, dead *Listeria* does not purpose harm or fatal threats to consumers, so it is vital to detect live bacteria. Both live and dead bacteria exhibit different electrical properties and polarization boundaries depending on the applied frequency. The bacterium cell membrane consists of a thin lipid bi-layer, which contains many proteins making it highly insulating with conductivity values of approximately 10^{-7} S/m whereas the conductivity values of the cell interior (i.e., cytoplasma) would be approximately 1 S/m due to the presence of many dissolved charged molecules. The conductivity of dead bacteria cell membrane could increase by a factor of 10^4 due to an increase in the permeability of the cell membrane and free exchange of cell contents with external medium through small pores (Li & Bashir, 2002). There are few studies that demonstrate the selective separation or detection of viable and non-viable bacteria. For example, (Li & Bashir, 2002) used DEP force to separate live and dead *Listeria innocua* onto IMEs by utilizing the difference of electrical properties between live and dead cells. The separation efficiency was determined by counting the live and dead cells collecting at the electrodes and the viability of the cells was characterized by a rapid epifluorescence staining method. The dielectrophoretic separation of live and heat-

105

treated *L. innocua* cells was achieved in DI water with the efficiency of 0% at bacteria concentration of 10^5 CFU/mL within 20 minutes. In other study by (Suehiro, Hamada, et al., 2003), reported detection of viable and non-viable *E. coli* strain K12 bacteria onto interdigitated microelectrode arrays. The working principle was based on the difference of the electrical properties of live and dead bacteria. Optimal frequency of 1 MHz was determined at fixed voltage magnitude (3 V peak-to-peak) at which only viable type bacteria could be trapped. Using this DEP technique selective trapping of viable bacteria was measured by using impedance (conductance, μS) with the lower detection range of 5 x 10^5 CFU/mL from bacteria concentration ranging from 10^5 to 10^6 CFU/mL within 15 minutes.

The lowest detection limit using DEP techniques of foodborne pathogen bacteria was reported to be 10^2 CFU/mL for *E. coli* by (Suehiro et al., 2005) with detection time of 3 hours. Lower detection time has been reported within 15 minutes for foodborne pathogen bacteria; however, with high bacteria concentration of 10^5 CFU/mL (Suehiro, Noutomi, et al., 2003). Therefore, further studies are needed to improve both the detection limit and time using DEP techniques. DEP is desirable in bacteria detection due to its easy implementation with miniaturized biosensor devices, non-destructive methods during the detection of the bacteria, and most importantly it can be used to manipulate, concentrate, separate or trap bacteria in the desired area for detection. *To date no biosensors based on IMEs have been reported that are integrated with DEP technique and aptamers for the rapid, sensitive and reliable detection of foodborne pathogens*.

In this study, dielectrophoresis (DEP) is used as a mechanism that generates electrostatic force-field that attracts the polarized bacteria close to the force-field using IMEs coated with aptamers. The hypothesis behind using DEP was that aptamer coated electrodes would provide a strong binding that maintains the trapped bacteria attached close to the electrode surface when the DEP signal is removed; therefore, increasing the impedance. The increase in the impedance was measured using EIS. The purpose of EIS test was to determine if significant amount of bacteria was deposited and remained attached to the surface after each DEP test. The number of bacteria, which are attracted from the solution to the surface of aptamer coated IMEs depends on potential magnitude (peak-to-peak voltage), frequency, and shape of input signal. Commonly used DEP signal is a sinusoidal input, which proved to have a good overall trapping efficiency (Cheng et al., 2007; Li & Bashir, 2002; Yang, 2009). Generally, in a linear model, the frequency magnitude of the input signal affects the strength of the electrostatic field output as given in Equation 4.1. In this study, bacteria capture efficiency was studied by DEP force applied at several high frequencies from 0.5, 1, 10, 100, 600 kHz to 1 MHz at fixed potential magnitude of peak-to-peak voltage of 4.24 V_{pp} for 30 minutes. Optimal frequency and time was selected based on impedance signals reaching steady state.

Selectivity of aptamer to viable and non-viable *Listeria* spp. was evaluated in this study and also biosensor response was investigated in the presence of interferent bacteria, *Staphylococcus aureus*. A unique combination of DEP-EIS technique was used to determine the biosensor response to the viable bacteria and selectivity experiments based on optimal frequency (10 kHz) and time (10 minutes). Comparative methods were

107

developed to test the hypothesis that the IMEs functionalized with *Listeria monocytogenes* aptamer would only establish a strong binding with *Listeria* spp.. DEP technique was used to improve the capture efficiency by attracting bacteria to the surface of aptamer-coated IMEs. Finally, DEP force was applied to detect *Listeria monocytogenes* in vegetable broth using 10 kHz for 10 minutes at peak-to-peak voltage of 4.24 V_{pp}.

4.3   Materials and Methods

4.3.1   Materials and equipment

Detailed descriptions of chemicals and equipment used for the aptamer biosensor fabrication are listed in Chapter II from 2.3.1 through 2.3.3 sections. Buffered peptone water (BPW) was purchased from HiMedia (Mumbai, India). *Staphylococcus aureus* (ATTC 25923) and *L. monocytogenes* Scott A 46 (ATCC 15313) were purchased from American Type Culture Collection and cultured in tryptic soy broth (TSB) bought from HiMedia (Mumbai, India). Oxford *Listeria*-selective agar and Oxford *Listeria*-selective supplement were purchased from EMD Performance Materials (Sommerville, NJ). Petrifilms were purchased from (3M aerobic plate count, St. Paul, MN). Vegetable broth was purchased from a local grocery store, H-E-B (College Station, TX). Autoclave from Sanyo (Westbury, NY) Model MLS-3751/3751L was used for thermal sterilization of the bacteria. Sulfuric acid and hydrogen peroxide were purchased from Avantor Performance Materials (Center Valley, PA). Surebonder (Wauconda, IL) hot glue gun and glue sticks were used for small volume chamber. Silicone rubber was purchased from Momentive Performance Materials Inc. (Huntersville, NC) to attach the biosensor

with cured hot glue. DeWalt blade (1/4"-1/2") was purchased from DeWalt Industrial

Tool Co. (Towson, MD) to cut a slit in an acrylic plastic container (Oklahoma City, OK)

with 1" width and 1" height . CHI 600E potentiostat/impedance analyzer and CHI6044e

software (Austin, TX) was used to analyze the electrochemical response of static DEP-

EIS and dynamic DEP modes. Marker Gene Live: Dead/cytotoxicity assay kit was

purchased from Marker Gene technologies, Inc (Eugene, OR). Microscopy and imaging

center facility at Texas A&M University (College Station, TX) was used for microscopy

imaging. Zeiss Axiophot (Thornwood, NY) was used with Plan Apochromat 25x/0.8

dipping objective lens from Zeiss microscopy (Thornwood, NY).

4.3.2   Theory and application of EIS and DEP-EIS

A unique combination of dielectrophoresis and electrochemical impedance

spectroscopy (EIS) measurements was developed to improve capture efficiency of the

targeted bacteria. In this study, bacteria capture efficiency was studied based on

impedance changes that can be described based on two modes 1) static DEP-EIS

technique, where the biosensor device impedance was measured after the DEP signal

was turned off, and 2) dynamic DEP impedance technique, where the biosensor device

impedance was measured during active DEP test.

4.3.2.1   Static DEP-EIS method

EIS impedance measurements were carried out following the DEP tests. The

DEP was conducted for excitation signal input of various sinusoidal frequencies at fixed

amplitude of 1.5 V_{pp}. The purpose of this test was to measure the change of total

impedance of the aptamer based biosensor due to entrapment of bacteria while DEP

signal was turned off. Then, the magnitude of impedance was measured at low frequency, 1 Hz, to determine if significant amount of bacteria was deposited and remained attached to the biosensor surface after each DEP frequency test. The experiment started with measuring EIS impedance of biosensor for a fixed volume, v_0, of buffered peptone water (BPW) solution without bacteria. DEP signal was applied across the electrodes for a fixed runtime at frequencies input of 500 Hz, 1, 10, 100, 600 kHz and 1 MHz expressed as $\{f_i = i = 1,...,n\}$. Then, the BPW solution was replaced with a fixed volume (v_0) containing bacteria and EIS scan was ran. DEP signal of known frequency (f_i) was applied across the electrodes and then the signal was turned off. A quick EIS test scan was conducted to cover a range of frequency from 1 Hz to 1 MHz. Following the EIS test, another DEP test signal at frequency f_{i+1} was fed to the biosensor. The process was repeated to cover all the DEP frequencies ranging from 500 Hz, 1, 10, 100, 600 kHz and 1 MHz. Finally, the previous steps were repeated for several bacteria concentrations of 10^2, 10^3, and 10^4 CFU/mL. Figure 4.1 demonstrates the predictive behavior of bacteria alignment onto the aptamer coated IMEs in a successive DEP-EIS test that could be based on the following mechanisms:

a. The spatial distribution of bacteria within the vicinity of interdigitated microelectrodes (IMEs) in Figure 4.1b is a function of electrostatic field, which means impedance is a function of frequency input and can be related to Equation 5.1.

b. The alignment of the bacteria due to applied DEP force could be illustrated as Figure 4.1c. This would reflect an increase in binding between aptamer and

bacteria, consequently; an increase in bacteria numbers attached to the ligand site
(aptamer binding site for Internalin A protein of bacteria) would increase the
total impedance of the biosensor as seen in Chapter III. The overall impedance of
the device would increase because the surface resistance of the IMEs would
increase by obstructing the current flow. On the other side Figure 4.1d shows that
if applied DEP force had no effect on the alignment of the bacteria then the
capture would be just based on random attachment to the aptamer functionalized
IMEs as shown in Figure 4.1a. Impedance change would be similar with and
without DEP force.

c. The number of attached bacteria to the aptamers may increase while frequency is
changed from one value f_i to another f_{i+1}. The total impedance signal may
follow one of the following responses during the frequency change:

   i. No change to the impedance as the frequency is increased from f_i to f_{i+1}.
   This would mean that during this step the bacteria accumulation on the
   aptamer surface reached a saturation point or peak point at f_i.

   ii. Decrease of the impedance as frequency is increased. This would mean
   that there is no peak or saturation point and reflect that binding strength
   between bacteria- aptamer and aptamer-IMEs might be weak. This could
   happen because change in frequency might disassemble the attached
   aptamers or bacteria on the surfaces of IMEs.

   iii. Increase of impedance as frequency is increased. This would mean that
   changing in frequency is an additive process where bacteria would be

able to attach to the open ligand sites as the electrostatic forces are
increased in magnitude. This is depicted in Figure 4.1e, where an increase
in frequency from f_i to f_{i+1} has led to an accumulation of bacteria to the
aptamers coated IMEs.

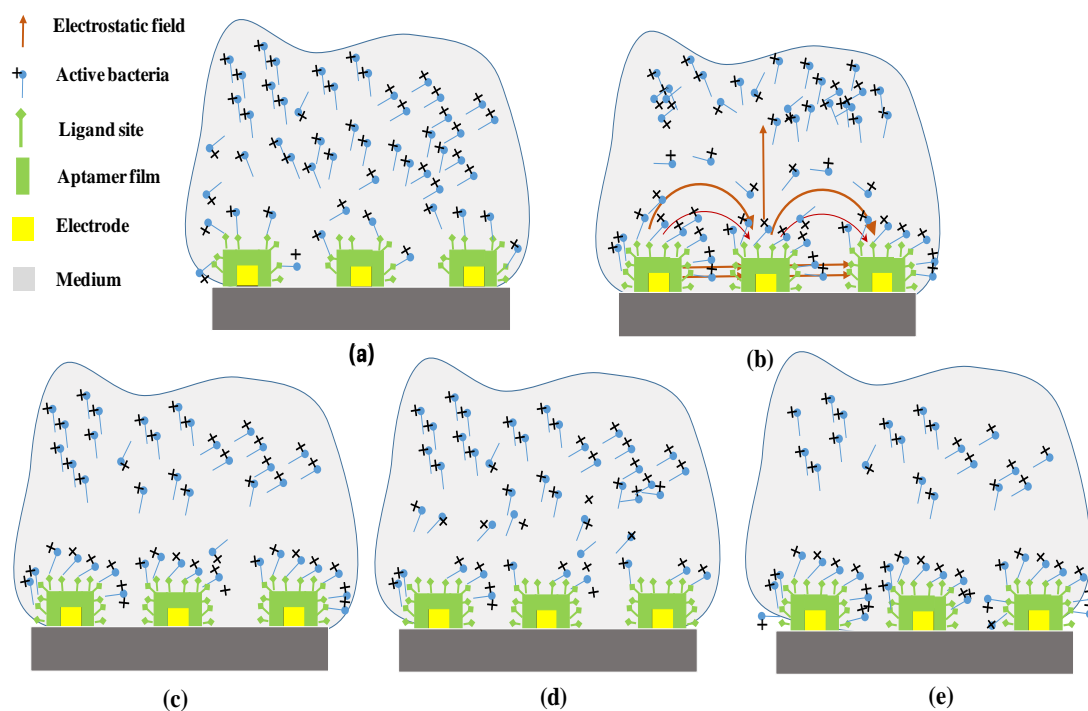Figure 4.1. Schematics of bacteria alignment and binding to aptamer in a successive
DEP-EIS test. (a) Suspended bacteria. (b) Alignment of bacteria during DEP signal at
frequency of f_i. (c) Bacteria alignment after DEP signal at f_i was removed. (d)
Realignment of bacteria following DEP signal of frequency f_{i+1}. (e) Realignment of
bacteria following removal of DEP signal of frequency f_{i+1}.

4.3.2.2   Dynamic DEP impedance method

The bacteria alignment, described in Figure 4.1 is a highly dynamic and probabilistic system whose measured impedance is instantaneous, i.e., time dependent. The time-response of a biosensor depends on the time taken by the bacteria cells to bind to the aptamer functionalized Pt-IMEs and the electrical field generated by DEP forces. The electrical field generated by DEP forces was shown to be effective at small distances above the electrode surface measured in microns for IME and particle sizes of 2-4 μm dispersion (Park, Zhang, Wang, & Yang, 2011). To optimize the capture of the bacteria, smaller volumes would allow larger number of bacteria to be concentrated in an effective electrical field as compared to using larger solution volume. Therefore, a small chamber was designed for the DEP testing.

Furthermore, the goal of this study was to monitor the impedance signal for a time period (Δt) until the dynamic system reaches steady state. This would determine the runtime of the DEP-EIS test. The value of impedance would follow the same argument made previously for DEP-EIS technique discussion except that in dynamic DEP impedance technique instantaneous impedance was measured, i.e., the dynamic impedance response. Figure 4.2 shows the schematic of the dynamic system with sinusoidal input and the real-time impedance measurement output. This impedance was recorded while running the DEP experiments as discussed in Section 4.4.2. The small volume chamber is discussed in Section 4.3.3.
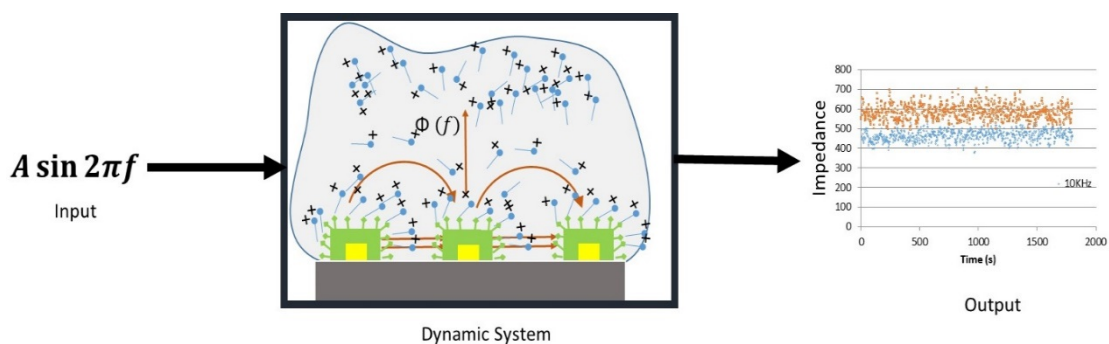
Figure 4.2. DEP dynamic model.

Given the complexity of bacteria movement discussed earlier, the optimal operating conditions of biosensor were determined using static DEP-EIS and dynamic DEP modes. As mentioned above in static DEP-EIS mode the biosensor impedance was measured after the DEP signal was turned off and in the dynamic DEP mode the biosensor impedance was measured during active DEP test. The DEP frequency magnitude and time based on biosensor performance was determined to further perform viability and selectivity tests (*S. aureus* and vegetable broth experiments) discussed in 4.3.6, 4.3.7, and 4.3.8, respectively. The frequency was selected among 500 Hz, 1, 10, 100, 600 kHz and 1 MHz.

4.3.3   Aptamer coated interdigitated microelectrodes and biosensor assembly

Aptamer stock solution preparation and immobilization onto the interdigitated electrodes (Pt-IMEs) was described in Chapter III section 3.3.3 expect that, for this study dip coating was used instead of drop coating the aptamers. Initially, the IMEs were cleaned with the piranha solution with the ratio of 3:1 concentrated sulfuric acid to

114

hydrogen peroxide. Piranha solution was used to remove all the organic residues from the surface of the IMEs. The IMEs were immersed in the piranha solution for one minute without exposing the bonding pads with the silver conductive epoxy. The IMEs were thoroughly washed with DI water for one minute to ensure proper removal of piranha solution residues from the surface. After, cleaning IMEs were air dried and used for functionalization with the aptamers. The stock solution of 100 μM *Listeria monocytogenes* aptamers (Genelink, Hawthrone, NY) was further diluted to 800 nM aptamer concentration in TE (10 mM Tris, 1mM EDTA, pH 7.5) solution. IMEs were dip coated in the 800 nM aptamer solution using 85 μL solution overnight under refrigeration at 5°C. Thiol terminated aptamers were attached to the Pt-IMEs by self assembling on the surface via covalent adsorption. The unbound aptamers were rinsed in 10 mL of PBS followed by DI water completing the biosensor assembly.

In this study, smaller volume of solution was spread on the top of Pt-IMEs to reduce the time for bacteria cells to concentrate and assemble onto aptamer functionalized IMEs. The dispensed solution formed an ellipsoid shape because of the hydrophobic forces between the solution and the silicon substrate. In addition, smaller volume was used because the spatial distribution of DEP force above the electrodes is dependent on the applied electric field and the dispersion of particles. The small volume chamber was designed as shown in Figure 4.3. Briefly, a slit was cut with a sharp blade to fit the biosensor into an acrylic plastic chamber to hold 400 μL. The chamber was filled with hot glue (silicone-based) up to 2 mm to the surface of the plastic chamber. The biosensor was inserted through the slit after the hot glue hardened (approximately 10 minutes).

115

Then, the biosensor microchip was attached to the cured glue (silicone-based) using silicone rubber to create a micro-chamber to hold liquid sample for bacterial detection testing using dielectrophoresis techniques.
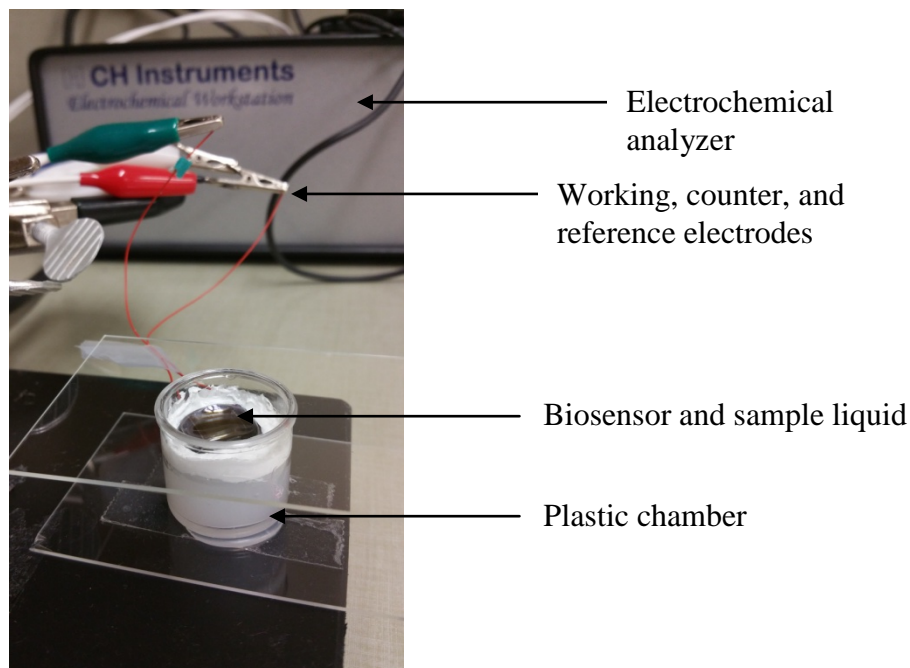
Figure 4.3. Small volume biosensor chamber and biosensor microchip connected to electrochemical analyzer.

4.3.4 Bacteria culturing

Prior to use, *Listeria monocytogenes* (ATCC 15313), *Listeria innocua* (NRCC B33076), and *Staphylococcus aureus* (ATTC 25923) cultures were stored at -80°C. *Listeria monocytogenes* and *Listeria innocua* bacteria were resuscitated by removing 100 µL of an inoculum from the frozen culture and incubated in TPB for 24 hours at

37°C. Two successive transfers were performed in TPB media for 24 hours at 37°C. After the initial three transfers, to ensure the working culture was at the desired bacterial concentration of $10^7 - 10^8$ CFU/mL, weekly transfers were made in TPB, incubated for 24 h at 37°C, and kept in the refrigerator at 5°C. Further, serial dilutions were made to achieve 10^7-10 CFU/mL in 9 mL BPW. The dilutions were spread-plated onto Oxford *Listeria*-selective agar plates supplemented with Oxford *Listeria*-selective supplement and incubated at 37°C for 24 h to count the bacteria colonies during each testing to ensure the correct bacterial concentrations. *Staphylococcus aureus* (ATTC 25923) was cultured as described for *Listeria* spp. expect tryptic soy broth (TSB) was used for growth broth and serial dilution was plated on petrifilms. Petrifilms was incubated for 24 hours at 37°C before counting the colony growth to ensure the correct bacteria concentrations. Thermal sterilization cycle (121°C for 15 min) was used to inactivate *L. innocua* (NRCC B33076) bacteria cells. Similarly, vegetable broth was sterilized using thermal sterilization cycle (121°C for 15 min) prior to testing.

4.3.5 Detection of *Listeria innocua* using combined DEP-EIS experiment

A unique combination of dielectrophoresis and electrochemical impedance spectroscopy measurements were developed to determine the capture efficiency of the targeted bacteria. DEP-EIS techniques were applied using CHI 600E potentiostat/impedance analyzer with CHI6044e software (Austin, TX). DEP-EIS were conducted in BPW solution and experimental setup included the small volume chamber to hold sample liquid with three electrode configuration. One of the two interdigitated array electrodes was connected to the working electrode, and the other was connected to

the reference and counter electrodes on the impedance analyzer. The IMEs were functionalized with thiolated aptamer as discussed in Section 4.3.3. The capacitor stabilizer was turned on in the CHI6044e software and the electrodes were grounded in order to minimize the charge buildup onto the surface of the electrodes.

DEP was applied with the peak-to-peak voltage of 4.24 V_{pp} for 30 minutes at 500 Hz, 1 kHz, 10 kHz, 100 kHz, 600 kHz, and 1 MHz. The impedance-time method was selected in CHI6044e software to run DEP experiments. The test was run for 30 minutes and steady state signal of DEP was studied to determine the time for the subsequent tests for viability and selectivity (for *S. aureus* and *Listeria monocytogenes* in vegetable broth). For EIS analysis, a sine-modulated AC potential of 100 mV was applied across the IMEs and impedance was measured for a frequency range of 1 Hz to 1 MHz at 12 points per decade. EIS plot (log frequency versus impedance) and Nyquist plot (imaginary versus real impedance) were generated to analyze the bacteria capture efficiency ranging from 10 to 10^7 CFU/ml at various frequencies.

DEP-EIS experiments were designed by first applying the DEP signal followed by measuring the impedance signal. Initially, BPW solution without bacteria at a fixed volume of 350 μL was first tested without applying DEP force and total impedance was measured with EIS scan. After that DEP signal was applied across the electrodes for 30 minutes at a frequency input of 500 Hz, 1, 10, 100, 600 kHz or 1 MHz expressed as $\{f_i = i = 1,...,n\}$. Then, BPW solution was replaced with 10 CFU/mL bacteria concentration suspended in 350 μL BPW and DEP-EIS analysis was run. DEP signal of known frequency (f_i) was applied across the electrodes and then the signal was turned

118

off. A quick EIS test scan was conducted to cover a range of frequency from 1 Hz to 1 MHz. Following the EIS test, another DEP test signal at frequency f_{i+1} was applied to the biosensor. The process was repeated to cover all the DEP frequencies ranging from 500 Hz, 1, 10, 100, 600 kHz to 1 MHz. Finally, these steps were repeated for bacteria concentrations of 10, 10^2 and 10^4 CFU/mL using a freshly functionalized biosensor microchip for each concentration.

4.3.6   Aptasensor selectivity to viable and non-viable *Listeria innocua* experiment

A combination of DEP-EIS techniques was implemented to determine aptamer based biosensor response to viable versus non-viable bacteria. However, only EIS data was used to analyze the results to determine the aptamer selectivity to the viable versus non-viable bacteria cells. The frequency of 10 kHz for 10 minutes was determined for DEP signal input as discussed in Section 4.4.2. DEP was applied with the peak to peak voltage of 4.24 V_{pp}. The total impedance of viable and non-viable bacteria was determined using optimal 800 nM aptamer concentration for IMEs. EIS test was run at frequency range of 1 Hz to 1 MHz at 12 points per decade and 100 mV potential.

The viability test procedures were developed considering that the non-viable bacteria had higher conductivity than viable bacteria (Li & Bashir, 2002). The rationale behind developing a viability protocol was that the non-viable bacteria would not attach to the aptamers due to denaturing of Internalin A (In1A) protein on the cell membrane of the bacteria since *Listeria monocytogenes* aptamers were selected to recognize In1A to capture the bacteria. Therefore, adding non-viable before viable bacteria allowed to test the difference between total impedance change in the same experiment, i.e.; without

119

using a new sensor. In theory, the increase in impedance signal would be higher for viable cells than for non-viable cells. The following procedures were used to run the viability test:

1. DEP signal with the peak to peak voltage of 4.24 V_{pp} was applied to a small BPW solution volume (350 µL) without bacteria at the optimal frequency of 10 kHz was applied for 10 minutes. EIS scan, at frequency range of 1 Hz to 1 MHz at 12 points per decade and 100 mV potential, was run after DEP signal was turned off to establish the baseline of the biosensor after DEP-EIS test.

2. The selectivity of the aptamer to non-viable bacteria, *L. inoccua*, was determined by adding 50 µL to the initial volume, 350 µL, followed by DEP and EIS scan (DEP-EIS test). The impedance change measured from the baseline would be due to the presence of non-viable bacteria in the solution and/or attached to the aptamers coated IMEs.

3. BPW solution with non-viable bacteria was removed and the biosensor was rinsed with DI water. Next, BPW solution, 350 µL, without bacteria was added and DEP-EIS test was performed, to this solution to record a new baseline. This step was performed to remove the bacteria from the solution making sure the impedance change measured was only due to the bacteria that were in direct contact with the aptamer coated-electrodes.

4. Viable, *L. innocua* was added to 350 µL and a final DEP-EIS test was performed. The impedance change measured from the new baseline would be due to the

presence of viable bacteria in the solution and/or attached to the aptamers coated

IMEs.

5. BPW with viable bacteria solution from step 4 was removed and the device was

    rinsed with DI water. Following, BPW solution, 350 µL, without bacteria was

    added and DEP-EIS test was performed. This step was performed to remove the

    bacteria from the solution making sure the impedance change measured is only

    due to the bacteria that is in direct contact with the aptamer coated IMEs.

6. These procedures were repeated for various bacteria concentrations, i.e.; 10, 100,

    and 1000 CFU/mL.

4.3.7 Aptasensor selectivity to *Listeria innocua* using an interferent

Staphylococcus aureus experiment

The same principles and protocols were followed as discussed in Section 4.3.6

for viability experiments. The concentration of *Staphylococcus aureus* (ATTC 25923)

and *Listeria innocua* (NRCC B33076) ranging from 10 to 10^6 CFU/mL were used to

determine the selectivity of the biosensor to the *Listeria monocytogenes* aptamers used

to capture *Listeria* spp. The aptasensor was said selective to *Listeria innocua* if the

relative impedance change was higher for *Listeria innocua* than for *Staphylococcus*

aureus. The relative impedance comparison included: 1) impedance change measured

before and after washing off the bacteria from the aptasensor surface, and 2) impedance

change measured before and after loading each bacteria onto aptasensor surface. These

criteria were used to determine if the *Listeria monocytogenes* aptamers were selective to

Listeria spp. DEP was applied with the peak to peak voltage of 4.24 V_{pp} for 10 minutes

at 10 kHz. EIS test was run at frequency range of 1 Hz to 100 kHz at 12 points per decade and 100 mV potential.

4.3.8   Detection of *Listeria monocytogenes* in off-the-shelf product experiment

The aptasensor was tested for the detection of *Listeria monocytogenes* for concentrations ranging from 10 to 10^7 CFU/mL inoculated in in vegetable broth using DEP-EIS test .Vegetable broth was sterilized using thermal sterilization (121^oC for 15 min) to ensure that only the targeted bacteria were present during the testing. Control samples, i.e.; non-inoculated vegetable broth, were tested to determine the baseline for the aptamer coated IMEs biosensor using total impedance as the method to compare and quantify the inoculated sample with *L. monocytogenes*. The small volume set-up containing the aptasensor was first used with 350 µL of vegetable broth solution without bacteria for the baseline measurements followed by the addition of 50 µL increments of *Listeria monocytogenes* with concentrations ranging from 10 to 10^7 CFU/mL into the vegetable broth.

4.3.9   Microscopy imaging

Optical microscopy of stained bacteria is the only commonly method used to examine the alignment of bacteria during the DEP process (Cheng et al., 2007; Koo et al., 2009; Li & Bashir, 2002). Zeiss Axiophot microscope (Thornwood, NY) with dipping objective lens (Plan Apochromat 25x/0.8 magnification, Zeiss microscopy (Thornwood, NY)) and BPW solution was used for imaging studies. Images were collected using the CoolSNAP CF monochrome CCD camera from Roper Scientific, Inc. (Tucson, Arizona). BPW was used due to its colorless properties as compared to PBS

solution. Dipping objective lens were used to dip into the BPW solution to reduce the working distance from the lens to the IMEs as compare to regular objective lens. Live/Dead staining reagents were prepared using Marker Gene Technologies protocol (Marker Gene Technologies). Live and dead bacteria cultures of *Listeria innocua* were prepared by washing the cells three times in PBS solution. Briefly, 2 mL of 10^8 CFU/mL *Listeria innocua* in PBS were centrifuged at 13,000x g for 30 seconds. The bacteria cells were collected at the bottom of the vial and re-suspended in 2 mL of PBS solution. This procedure was repeated three times to wash the cells for proper bacteria staining. Both live and dead bacteria cells (200 μL) were re-suspended in 200 μL of live and dead staining dyes. Then, 30 μL of the stained bacteria cells were further diluted into 500 μL of BPW solution and used for imaging of live and dead *Listeria innocua*. The bacteria concentration used for imaging was 10^4 CFU/μL or 10^7 CFU/mL. The images were obtained before and after applying the DEP force at 10 kHz for 5 min and 4.24 V_{pp}. Real-time images were captured during the DEP test to see the alignment of the bacteria cells onto the aptamer coated IMEs. Images were also taken after washing the biosensor with DI water to monitor the bacteria attachment after applying the DEP test. The images were captured for both live and dead bacteria cells.

4.3.10 Statistical analysis

MatLAB v8.3 and statistical toolbox software (MarthWork, Inc., Natick, MA) was used for all statistical analyses. Means and standard deviations were calculated based on triplicate tests. Differences between variables was tested for significance using one-way analysis of variance (ANOVA) and significantly different means ($p < 0.05$) was

separated using Tukey's Honestly Significant Differences (HSD) test. The lower

detection limits was determined as a signal/noise ratio of 3, where noise is defined as the

standard deviation of the control test without bacteria (Tolba et al., 2012; J. Wang,

2006).

4.4   Results and Discussion

4.4.1   Detection of *Listeria innocua* using combined DEP-EIS

Figure 4.4A - 4.4C show the total impedance magnitude of captured *L. innocua*

onto the aptamer functionalized IMEs measured after various DEP frequencies were

applied including 500 Hz, 1, 10, 100, 600 kHz, and 1 MHz with the peak to peak voltage

of 4.24 V_{pp} for 30 minutes. The EIS signal was measured after the DEP signal was

turned off at various bacteria concentrations with the frequency sweeping from 1 Hz to 1

MHz, amplitude of 100 mV, and 12 points per decade points. In addition, a smaller

sample volume was dispensed over the biosensor surface. This allowed for direct contact

of the bacteria to the IMEs electrodes using a thin liquid layer on top of the IMEs;

therefore, improving the capture process. The total impedance versus log frequency is

shown in Figure 4.4A - 4.4C for bacteria concentrations of 10, 10^2, and 10^4 CFU/mL,

respectively.

The total impedance value increased as the applied DEP frequency increased for

all bacteria concentrations tested (Figure 4.4A – 4.4C) suggesting that applied DEP

signal captured the bacteria from the solution and trapped it onto the aptamer

functionalized IMEs surface. The theory discussed in Section 4.3.2 illustrated that

increased impedance with changing frequency from f_i to f_{i+1} was a result of an

additive process where bacteria was able to attach to the open ligand sites (aptamer binding sites) as the electrostatic forces were increased in magnitude. This trend showed that increasing DEP frequency signal led to bacteria accumulation at the aptamer binding sites despite of the polarity changes that might have occurred due to the nature of bacteria interaction with the DEP signal (Yang, 2009). In addition, this additive process showed the ability of the aptamer coated IMEs to not allow the bacteria to be released back to the solution proving that the bacteria to aptamer binding is strong regardless of the applied DEP signal. The binding affinity, K_D, of *Listeria monocytogenes* aptamers that binds to the membrane protein Internalin A at the targeted bacteria, *Listeria* spp., is 83.50 μM (GeneLink, 2004). The K_D values for both aptamers and antibodies are on similar magnitude order; however, aptamers offer the advantage of simple production and modification, reproducibility, and target versatility (Dong, Xu, Yong, Chu, & Wang, 2014). Figure 4.14 shows the imaging results of bacteria attachment to the aptamers after applying the DEP signal. These results led to an important conclusion that the functionalized *Listeria monocytogenes* aptamers that selectively bind to internalins proteins of the target bacteria is an excellent capture probe regardless of the frequency applied by the DEP signal. In other words, the aptamer coating was not compromised due to the effects of the electrical fields generated by DEP during the duration of the experiment because the aptamers were able to show increased impedance values as the frequency was changed.
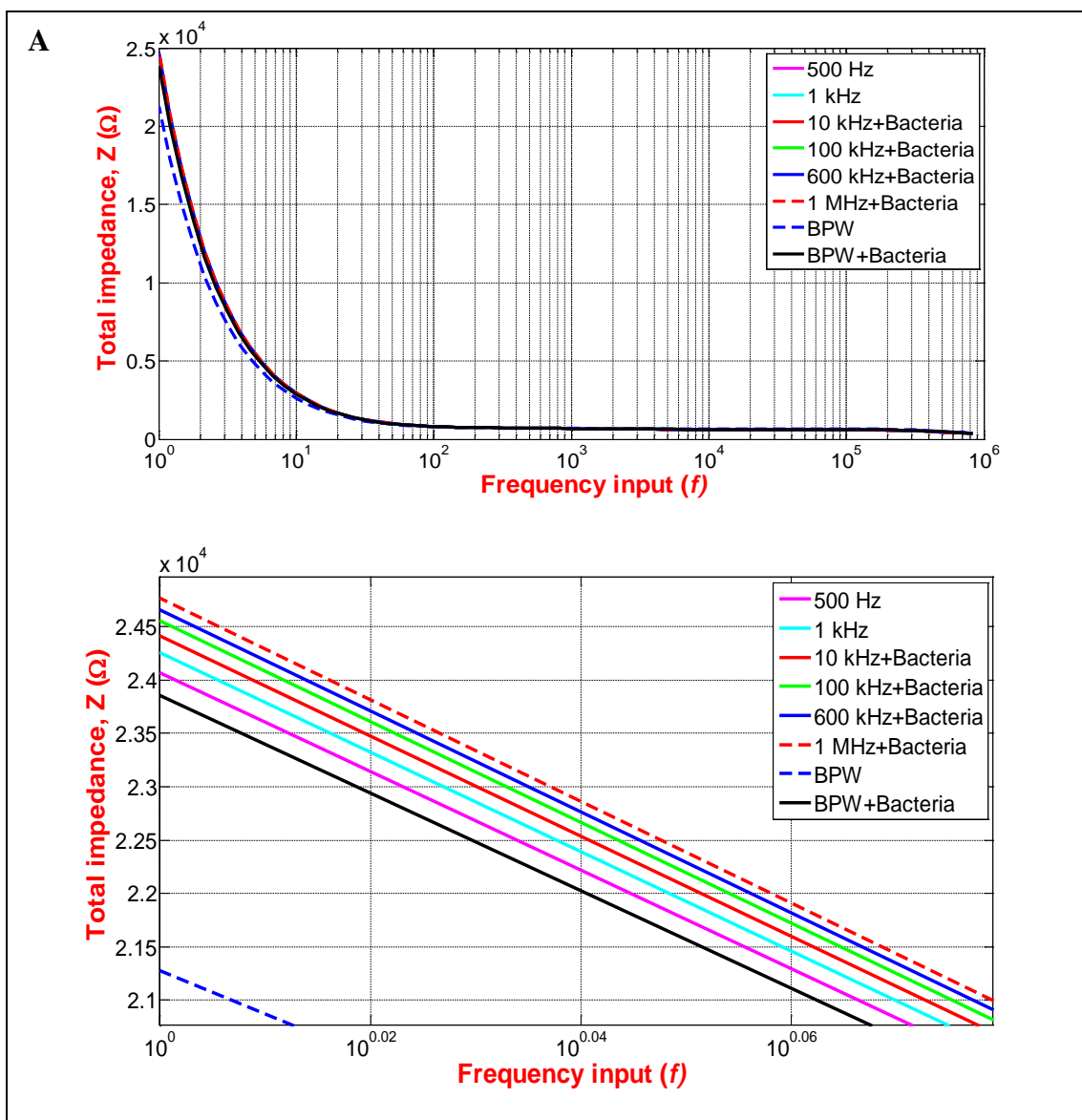
Figure 4.4. EIS curves followed by the DEP test at various frequencies at *L. innocua* concentration of (A) 10 CFU/mL, (B) 10^2 CFU/mL, and (C) 10^4 CFU/mL. BPW with dotted blue line on the graph demonstrates impedance measurement, $Z_{aptamer}$, of aptamer coated IMEs without bacteria concentration, i.e. 0 CFU/mL and without DEP force applied . The solid black line (BPW + bacteria) shows impedance measurement, Z_1 , without applying DEP force at bacteria concentration of 10 CFU/mL. Z_1 represents the biosensor baseline. The total impedance measurement, Z_f , of the captured bacteria onto the aptamer coated IMEs after applying DEP force at frequencies of 500 Hz, 1, 10, 100, 600 kHz, and 1 MHz shown as ($f_i, f_{i+1},...f_{i+5}$ + bacteria) on the graph.
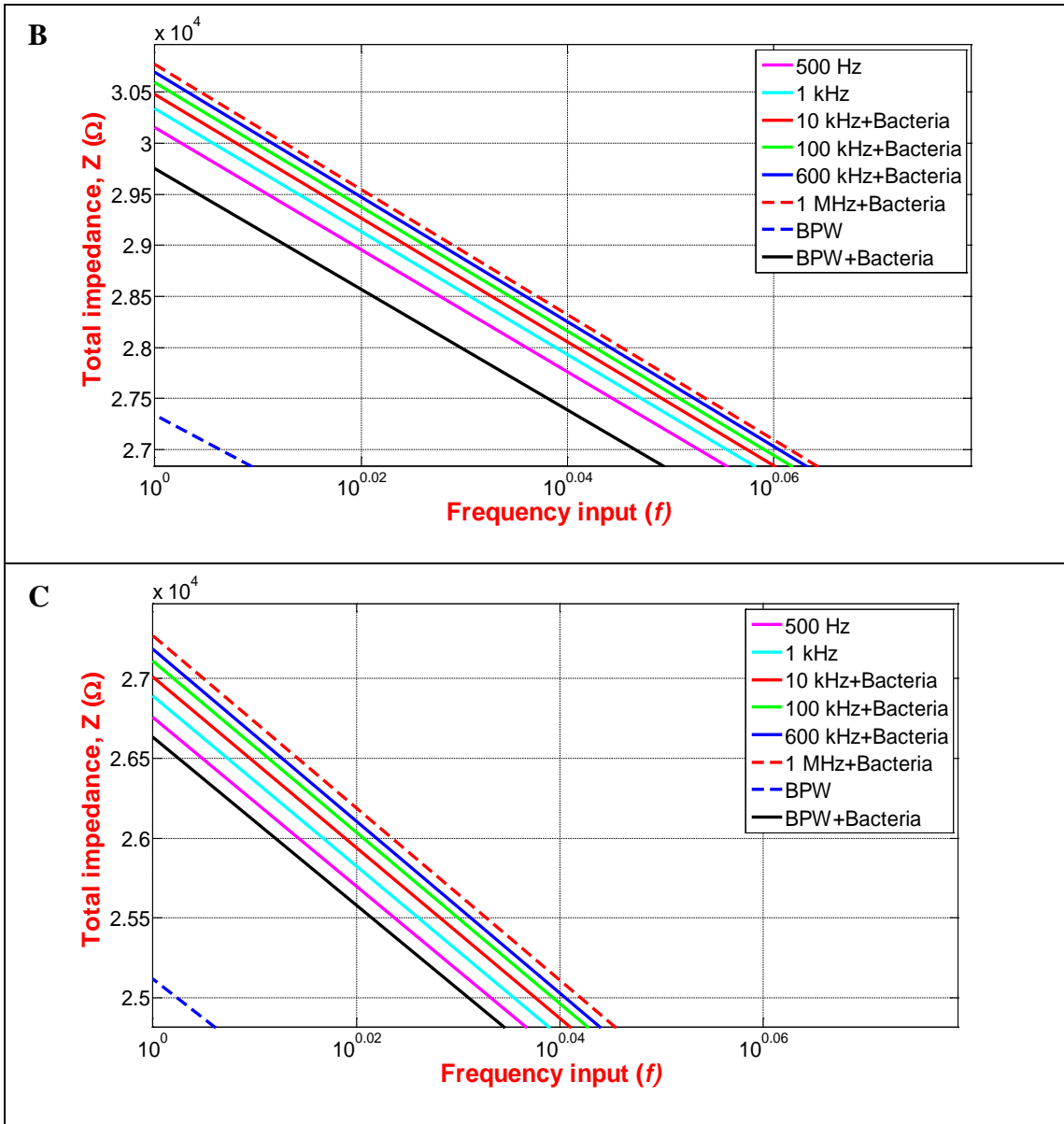
126

Figure 4.4. Continued.

127

Figure 4.5A – 4.5C show the impedance change, $\Delta Z = (Z_f - Z_1)$, in Ohms at the applied DEP frequencies of 500 Hz, 1, 10, 100, 600 kHz, and 1 MHz for bacteria concentration of 10, 10^2, and 10^4 CFU/mL, respectively. As mentioned above, Z_f was defined as total impedance measured by EIS following the DEP signal at a given frequency and Z_1 was the baseline impedance of an aptamer coated IMEs with a given bacteria concentration measured by EIS before applying the DEP signal. The graphs generated in Figure 4.5A - 4.5C illustrate the total impedance magnitude change versus log frequency scale for three bacteria concentrations. The graphs were classified into low, medium, and high frequency regions: 1) 500-1000 Hz, 2) 1-600 kHz, and 3) 600-1000 kHz. Within each region, the relationship between impedance change and frequency was linearly proportional at the three bacteria concentrations. These results further confirm that the increase in impedance is due to accumulation of bacteria at IMEs surface as the electrical field is increased by changing the frequencies through three regions.
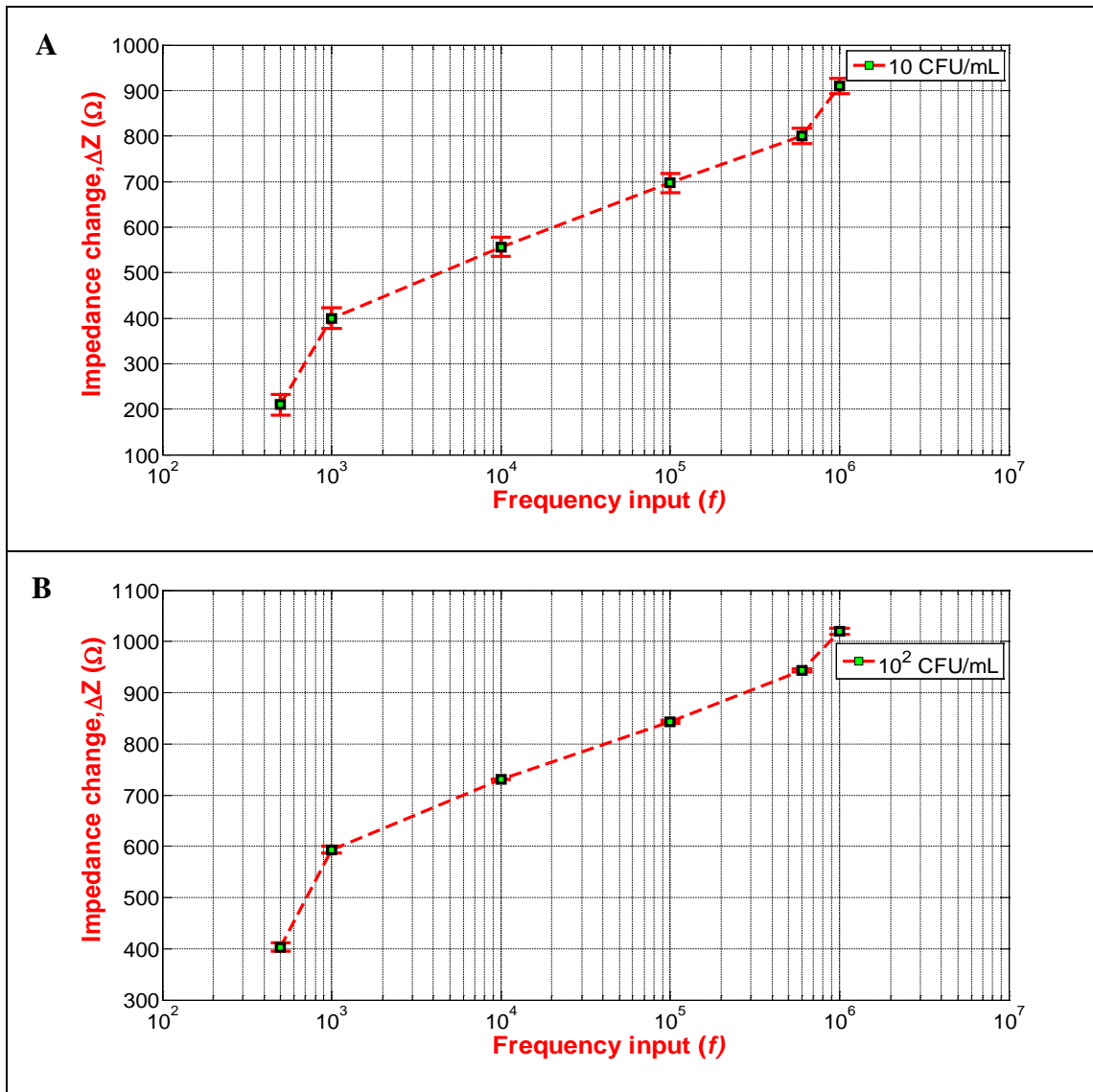
Figure 4.5. Impedance change vs. DEP frequency. ΔZ is relative to the baseline defined as aptamer coated electrodes with BPW bacteria solution before applying DEP signal at (A) 10 CFU/mL, (B) 10^2 CFU/mL, and (C) 10^4 CFU/mL.
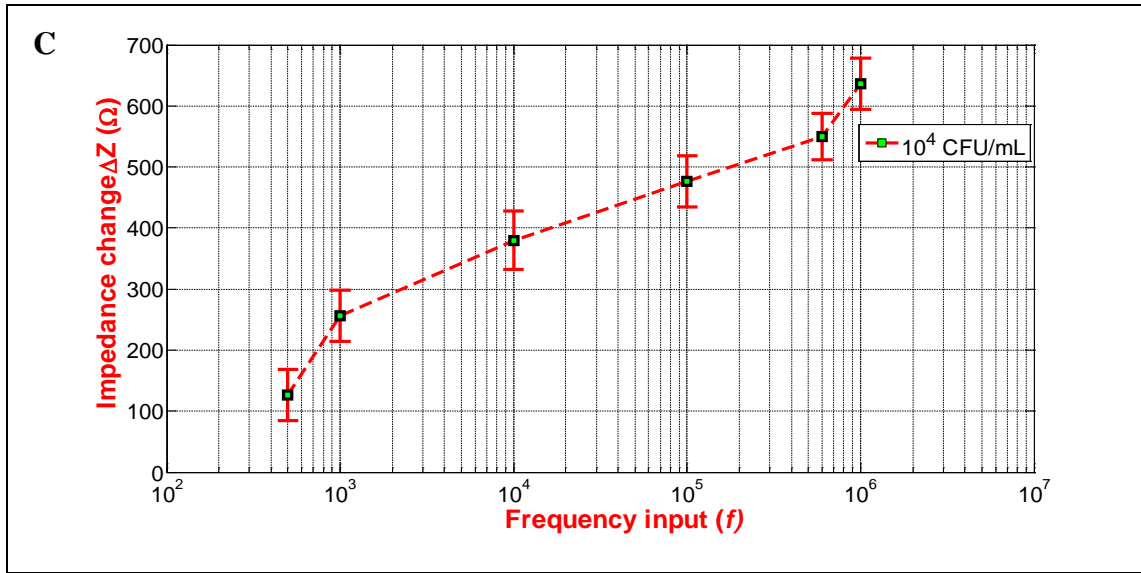
Figure 4.5. Continued.

A normalization factor was used to study the percentage increase in total impedance before and after applying DEP signal for the three bacteria concentrations studied. The normalization factor, N, is defined as a dimensionless quantity, and it is calculated by normalizing the impedance change as described on Equation 4.3:

$$N = [(Z_f - Z_1)/(Z_1 - Z_{aptamer})]*100 \qquad (4.3)$$

where $Z_{aptamer}$ is the impedance (Ohms) of the aptamer coated IMEs at zero bacteria concentration without DEP signal. These total impedances were measured from EIS test and the values were determined at 1 Hz based on the discussion in Chapter III. $Z_f - Z_1$ described the total impedance change (Ohms) occurred only due to applied DEP signal, which is measured at given frequency and bacteria concentration. $Z_1 - Z_{aptamer}$ described the impedance change only due to bacteria attachment onto the aptamer coated IMEs

130

before applying DEP signal. Therefore, the normalization Equation 4.3 expresses the percentage increase of bacteria due to applying DEP-EIS technique, and it is calculated relative to the EIS technique. The normalization curves of each concentration were shown in Figure 4.6A - 4.6C for bacteria concentration of 10, 10^2, and 10^4 CFU/mL, respectively. The sensitivity of DEP was obtained from the linear slopes in Figure 4.6A - 4.6C, where the slopes were in low, medium, and high frequency regions. Sensitivity is calculated based on the Equation 4.4 measured in percentage increase over log frequency [1/Hz]:

$$S = \frac{\Delta N}{\Delta \log(f)} = \frac{N_2 - N_1}{\log\left(\dfrac{f_2}{f_1}\right)} \tag{4.4}$$

Table 4.1, summarizes the sensitivity for each region for each bacteria concentration. The percent increase in each region at all bacteria concentrations was positive which signified the total impedance values have increased from the baseline, which measured impedance of bacteria on aptamer coated electrodes before applying DEP signal. Thus, proving that the DEP signal assisted to trap bacteria onto the aptamer coated IMEs further increasing the capture efficiency of the biosensor. Normalized percentage change of impedance in each frequency is shown in Table 4.1. The highest increase is observed in the frequency region of 1 – 600 kHz implying better capture efficiency as compare to the other frequency regions.
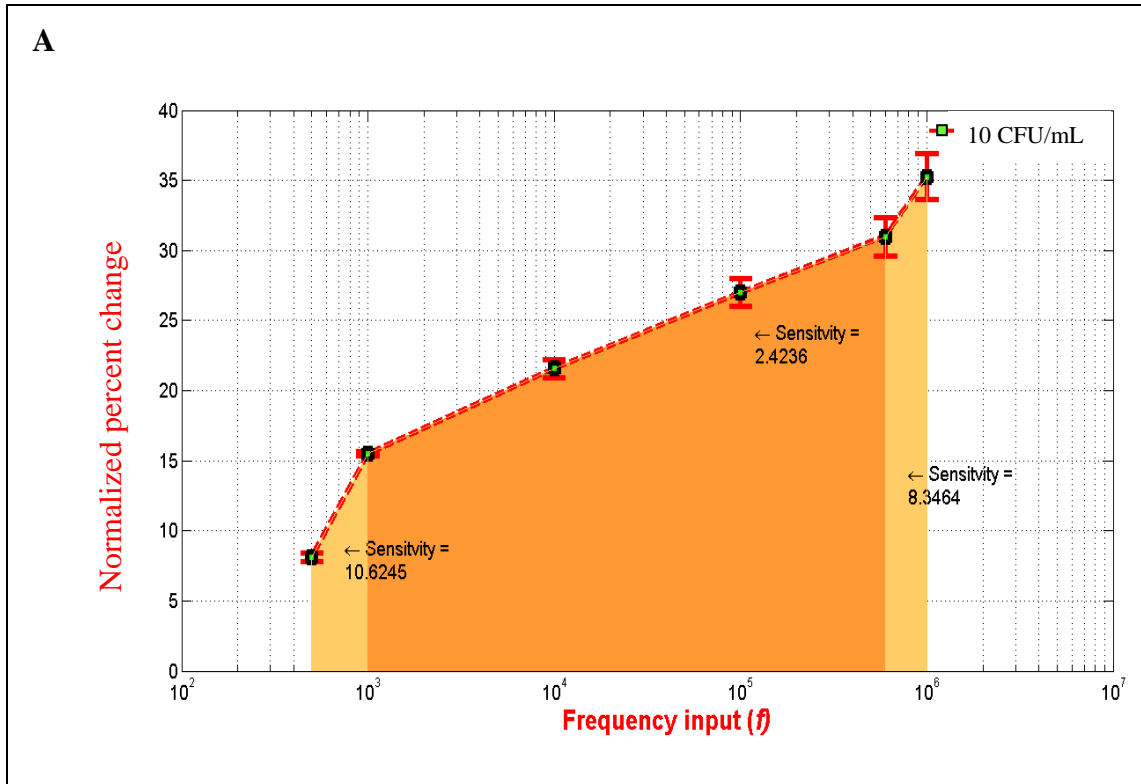
Figure 4.6. Normalized impedance and sensitivity with respect to the baseline with BPW solution at (A) 10 CFU/mL, (B) 10^2 CFU/mL, and (C) 10^4 CFU/mL.
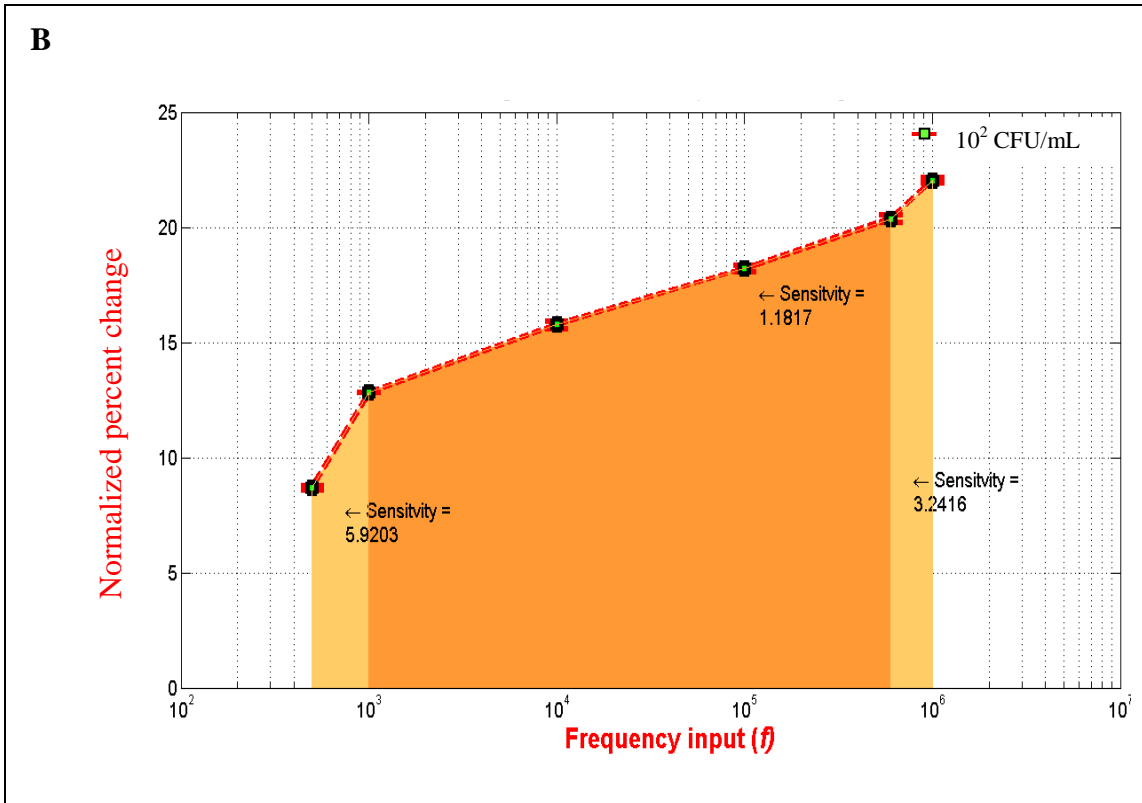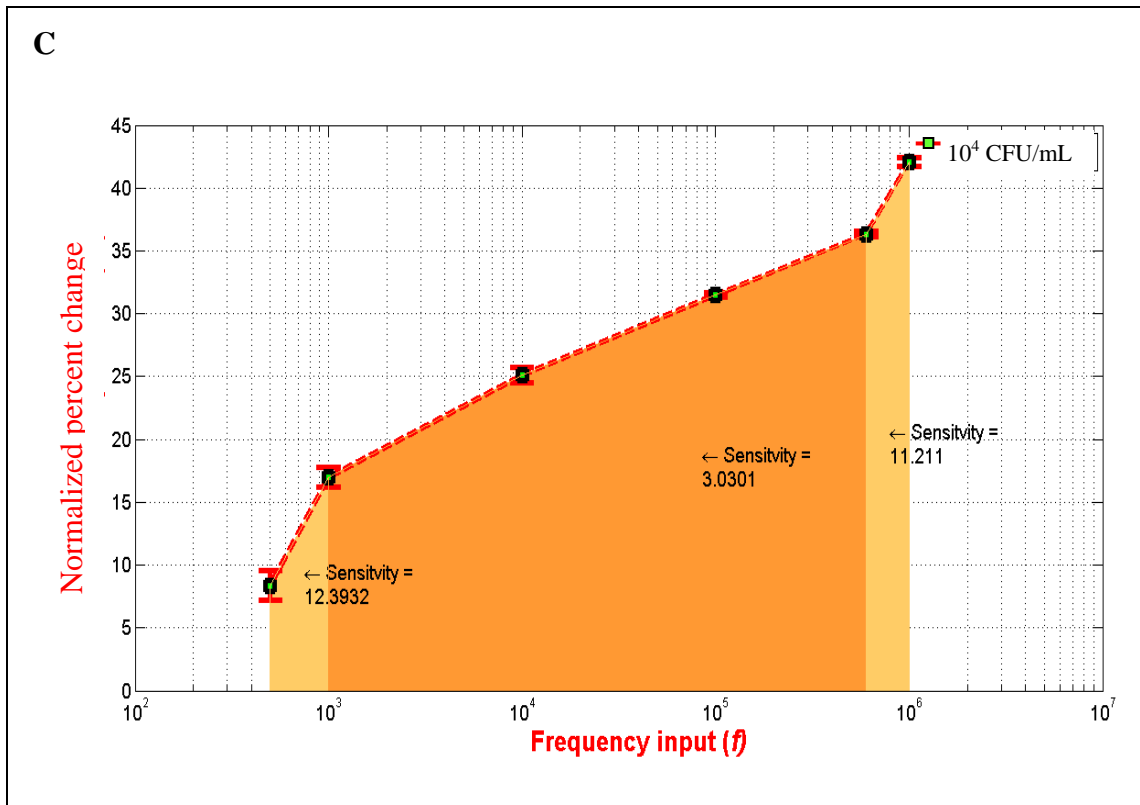
Figure 4.6. Continued.

Figure 4.6. Continued.

Table 4.1. DEP sensitivity values measured in impedance percentage increase over log frequency [1/Hz] at different frequency regions.

Listeria innocua concentration (CFU/mL)	Sensitivity for 500-1000 Hz	Normalized percent change between 500-1000 Hz	Sensitivity for 1-600 kHz	Normalized percent change between 1-600 kHz	Sensitivity for 600-1000 kHz	Normalized percent change between 600-1000 kHz
10	10.62	7.4	2.42	15.5	8.35	4.3
100	5.92	4.1	1.18	7.6	3.24	1.6
10000	12.39	8.6	3.03	19.3	11.21	5.7

134

4.4.2 Dynamic DEP impedance method characterization

Dynamic DEP impedance was measured while DEP signal was active to study the dynamic impedance response of the biosensor .The test was carried out to characterize biosensor response to dynamic DEP and impedance analysis, and whether its impedance measurement provides a conclusive indication of the capturing mechanism. Impedance versus time and impedance versus phase angle were generated to understand the conditions for the biosensor to reach steady state based on bacteria interactions with aptamer coated IMEs. Optimal time and frequency magnitude were determined for DEP force based on the dynamic impedance response results and later used to perform viability and selectivity experiments discussed in the following Sections 4.4.3 and 4.4.4. Figure 4.7A – 4.7F shows the impedance versus time and phase versus time plots at DEP frequencies of 500 Hz, 1, 10, 100, 600 kHz and 1 MHz with a bacteria concentration of 10^2 CFU/mL. The impedance versus time plots shows the impedance signal variance during an active DEP signal. The impedance standard deviations for DEP frequencies of 500 Hz, 1 kHz, 10 kHz, 100 kHz, 600 kHz, and 1 MHz were 863 Ω, 366 Ω, 9.7 Ω, 7.4 Ω, 163 Ω, and 40360 Ω, respectively. Peaks in impedance signal were observed at 1 MHz. The phase versus time plots for each DEP frequency can be described as scattered for 500 Hz, 1 kHz, and 100 kHz, steady for 10 kHz, and switching for 600 kHz and 1 MHz. At 500 Hz and 1 kHz, the phase was scattered between 180 to -180 degrees and at 10 kHz was steady at -90 degrees. At 100 kHz, the phase was scattered at zero degree. The phase was switching between 180 to -180 degrees with a distinct signal at zero for 600 kHz and 1 MHz.
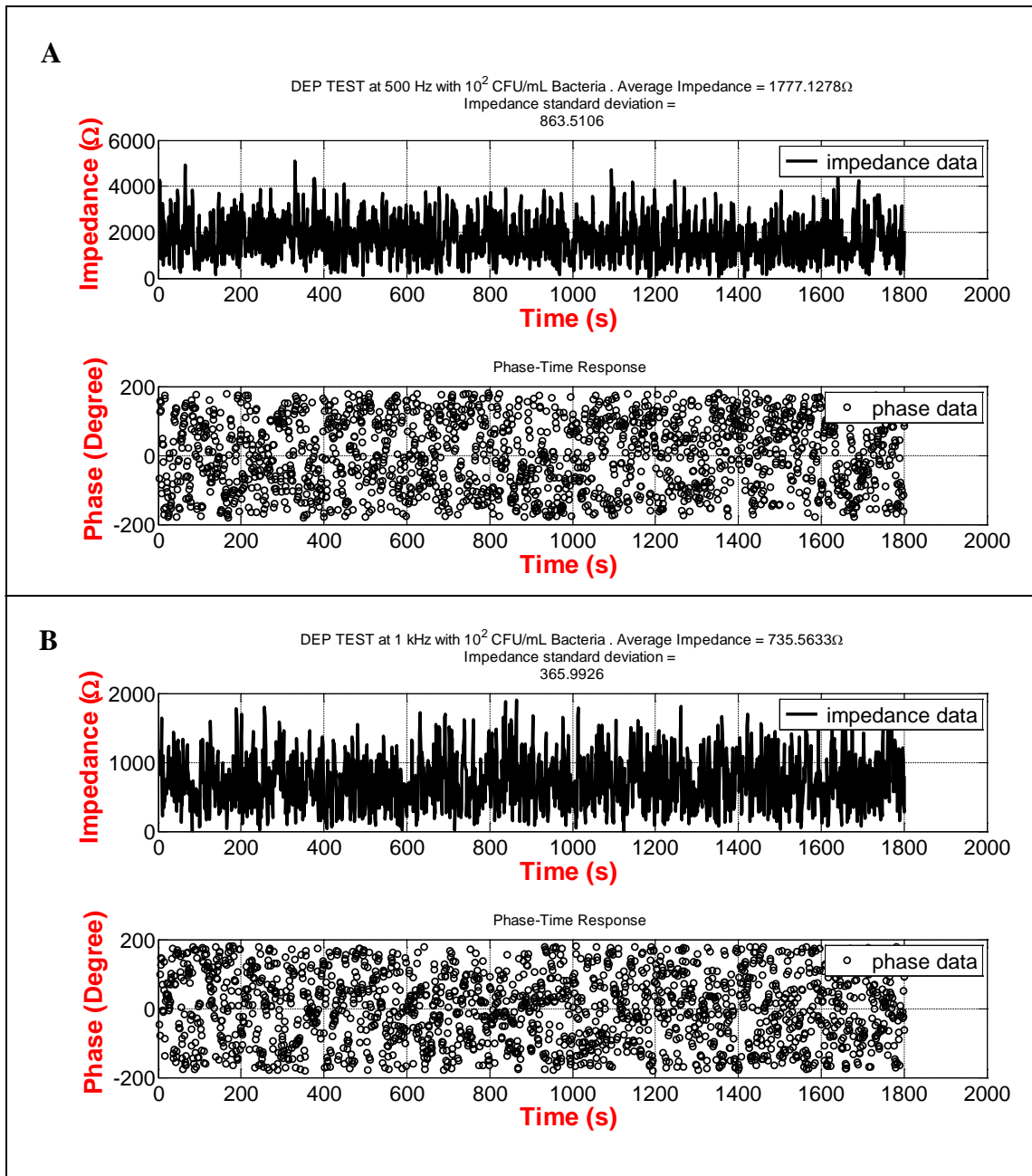
135

Figure 4.7. Impedance versus time and phase versus time are shown at DEP frequencies of (A) 500 Hz, (B) 1 kHz, (C) 10 kHz, (D) 100 kHz, (E) 600 kHz, and (F) 1 MHz for *L. innocua* at a concentration of 10^2 CFU/mL.

C

DEP TEST at 10 kHz with 10^2 CFU/mL Bacteria . Average Impedance = 112.9735Ω
Impedance standard deviation =
9.7126

Phase-Time Response

D

DEP TEST at 100 kHz with 10^2 CFU/mL Bacteria . Average Impedance = 125.8363Ω
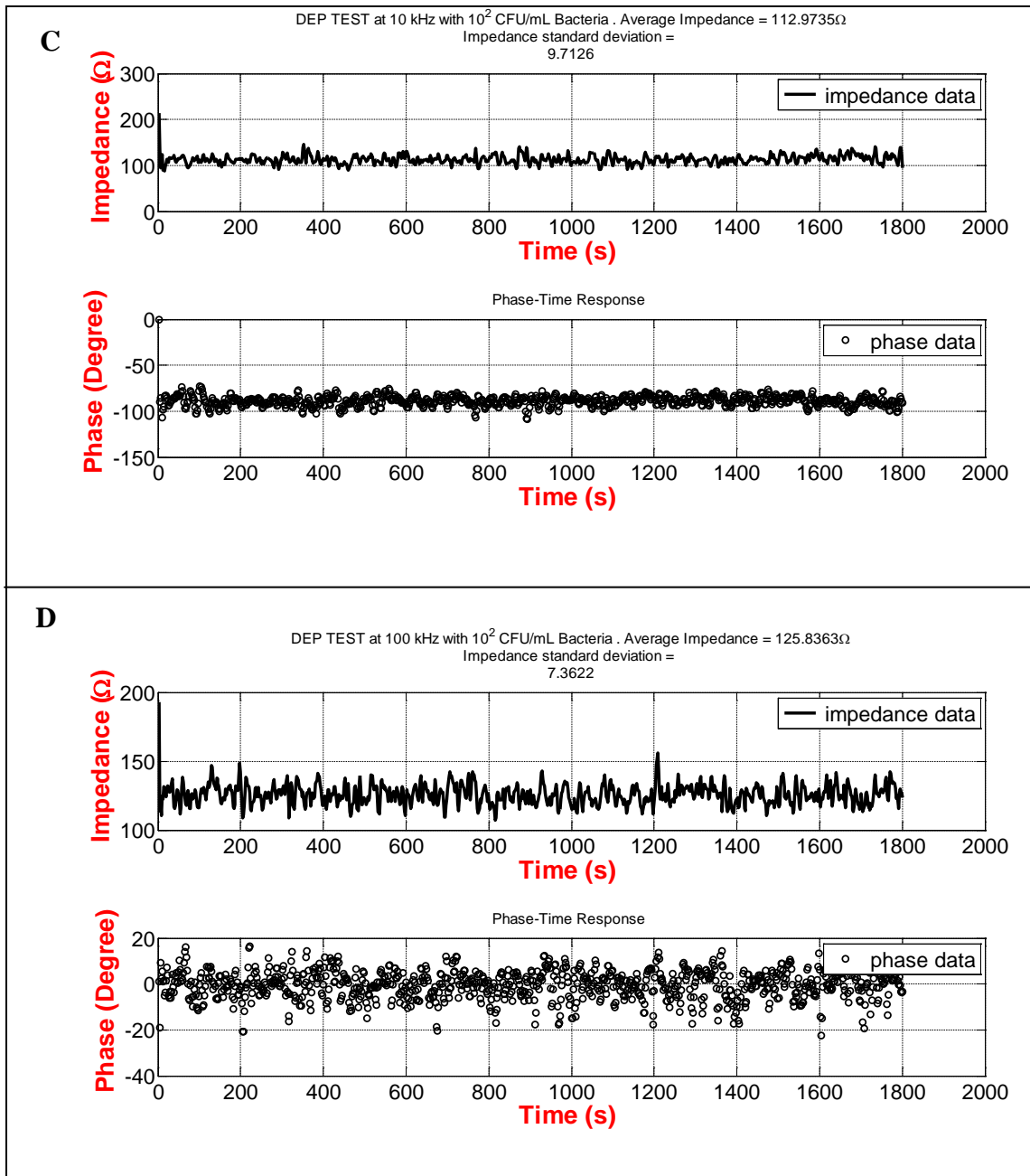Impedance standard deviation =
7.3622

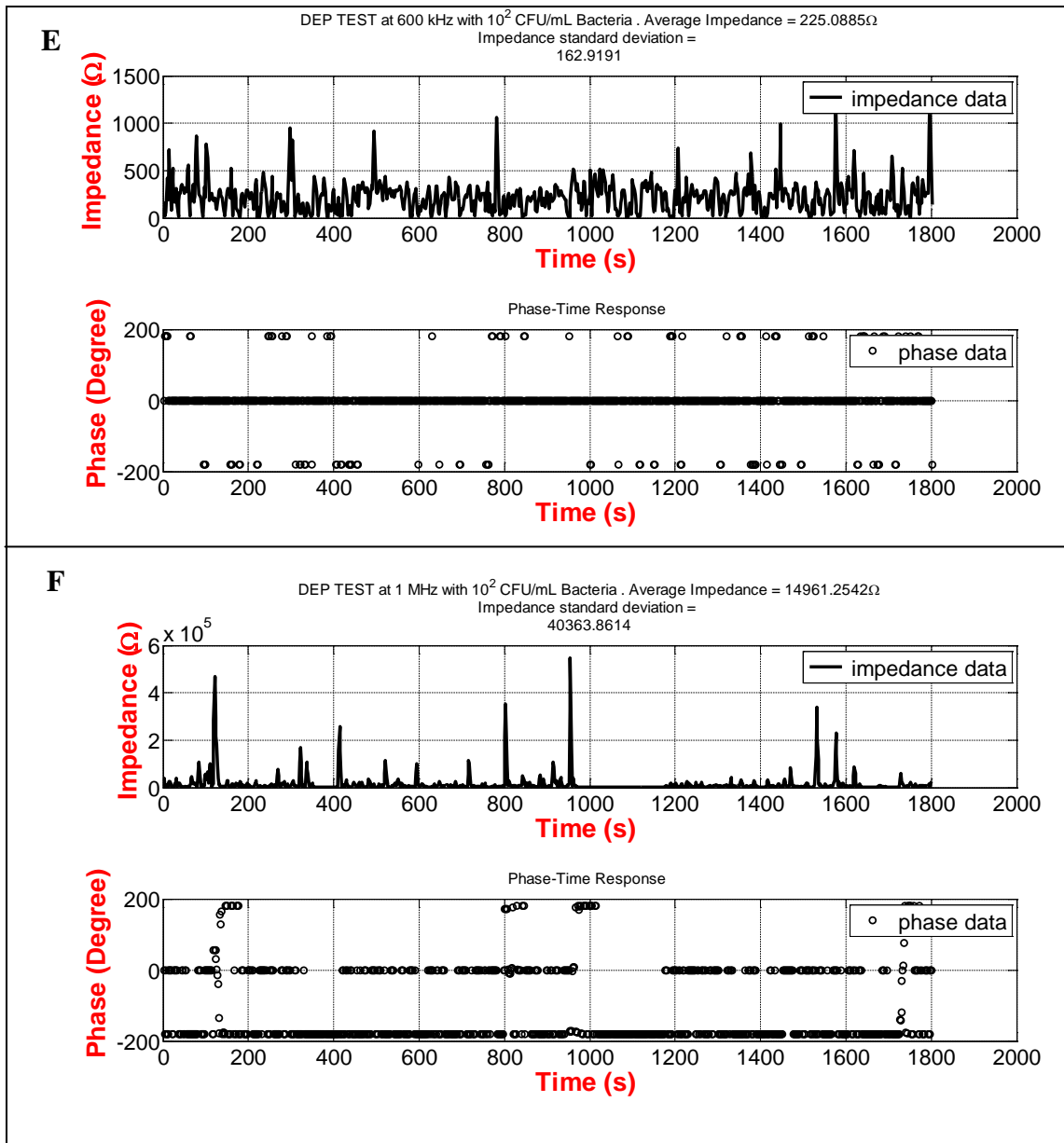Phase-Time Response

Figure 4.7. Continued.

Figure 4.7. Continued.

Figure 4.8A – 4.8F shows impedance versus phase plots at various DEP

frequencies. At 500 Hz and 1 kHz the plots were scattered and at 10 kHz the impedance

data was concentrated at -90 degrees phase and 100 Ω. At 100 kHz, the impedance data

was scattered between 20 to -20 degrees and the impedance showed an increasing trend

over phase. At 600 kHz, the impedance data was distinctively peaked at 180, -180, and

0 degrees. The same trend was observed at 1 MHz with some scattered points. Based on

Figure 4.7A – 4.7F and Figure 4.8A – 4.8F that show DEP frequencies signal results, the

frequency of 10 kHz was chosen because impedance was not changing over time for a

fixed bacteria concentration providing reliable and quantifiable results The impedance

signal was shown to be steady for 30 minutes at 10 kHz. The time frame of 10 minutes

was chosen to allow time for bacteria and aptamer interactions to take place. The system

readings are based on Control and Signal theory, -90 degree shift in the phase diagrams

indicated that the model could be represented by a first order linear dynamic system.

This system is stable with one pole representing the following transfer function written

in Laplace domain

$$Z(s) = \frac{K}{(s+a)}$$
(4.5)

where K is the system gain and $s = -a$ is the system pole. The solution of this system

is a decaying exponential function (Ogata, 2010). Secondly, it showed that the

impedance measurement readings had small variance. Unlike other frequencies, this

provided enough certainty in reading the impedance output. The behavior could be due

to electrostatic interference between the solution and the electric field generated by

comb fingers discussed in Figure 4.1. Similar trends as discussed in this section were seen in DEP signal for bacteria concentrations at 10 and 10^4 CFU/mL. The results are compiled in Appendix A showing the same trends.
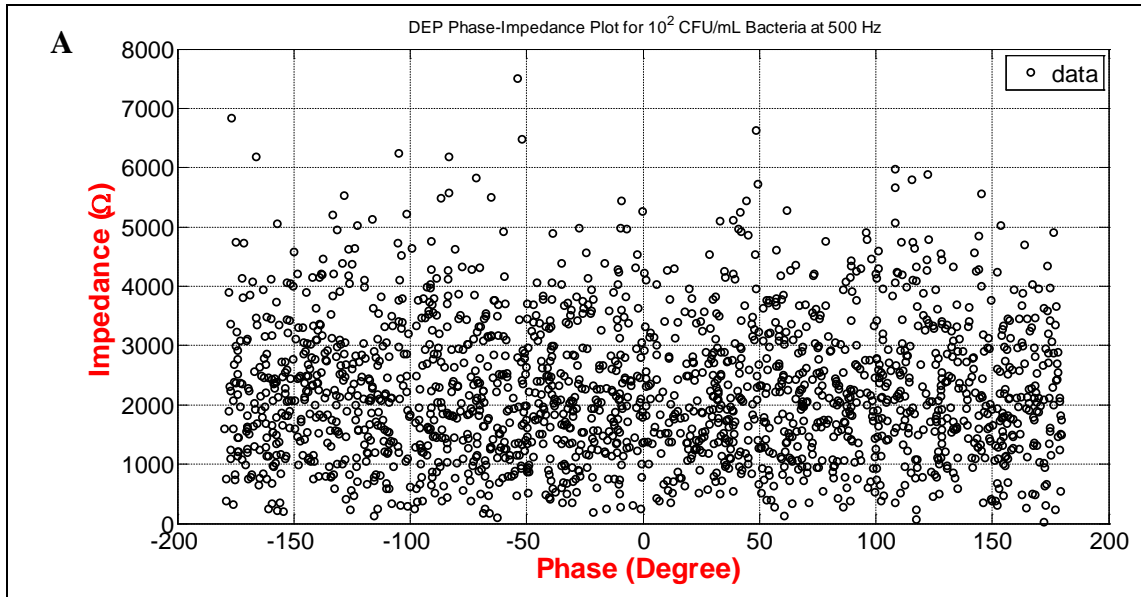

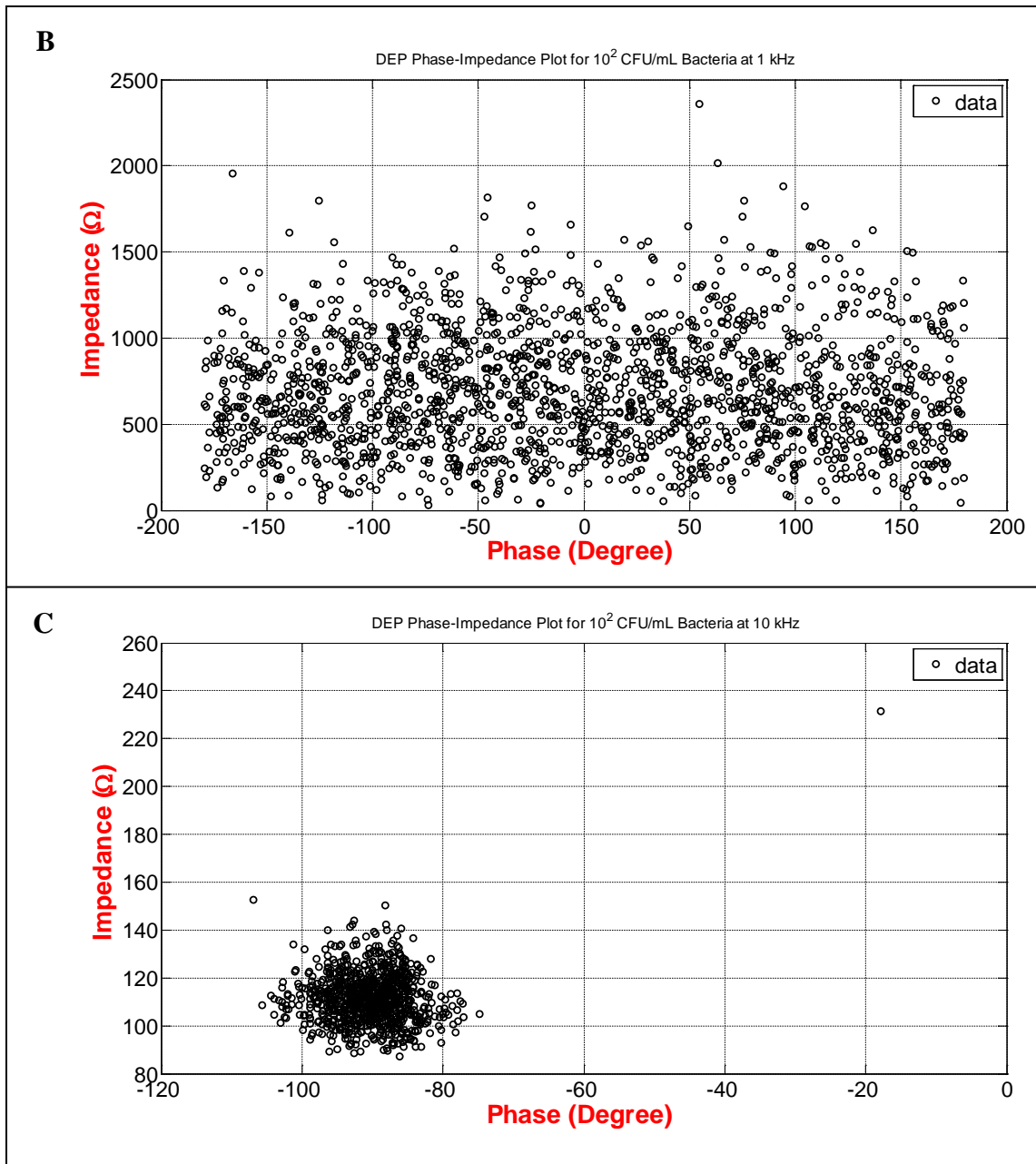Figure 4.8. Impedance versus phase are shown at (A) 500 Hz, (B) 1 kHz, (C) 10 kHz, (D) 100 kHz, (E) 600 kHz, and (F) 1 MHz DEP frequencies for *L. innocua* at a concentration of 10^2 CFU/mL. The legend data implies impedance data on the graph.
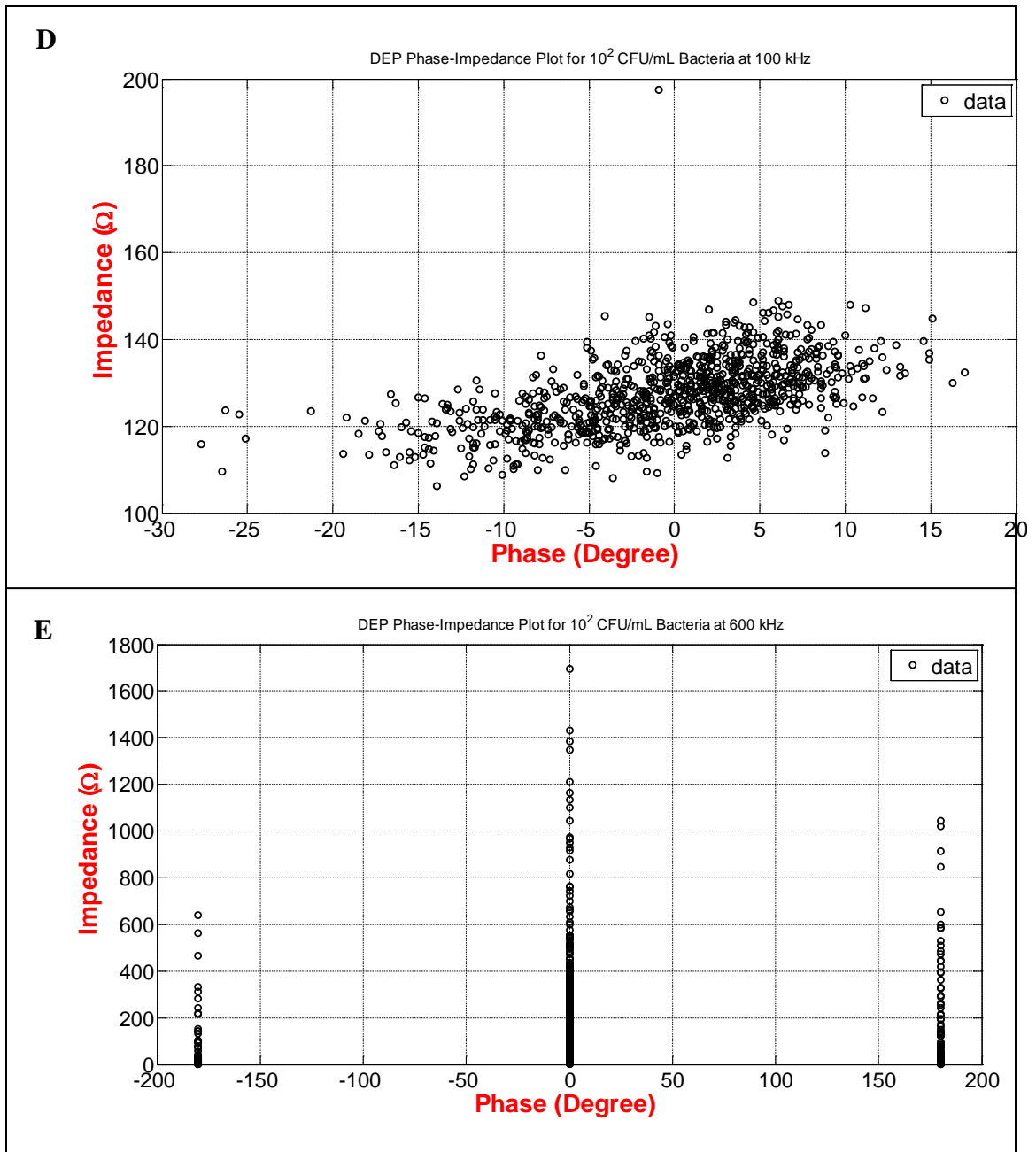
B

DEP Phase-Impedance Plot for 10^2 CFU/mL Bacteria at 1 kHz

C

DEP Phase-Impedance Plot for 10^2 CFU/mL Bacteria at 10 kHz

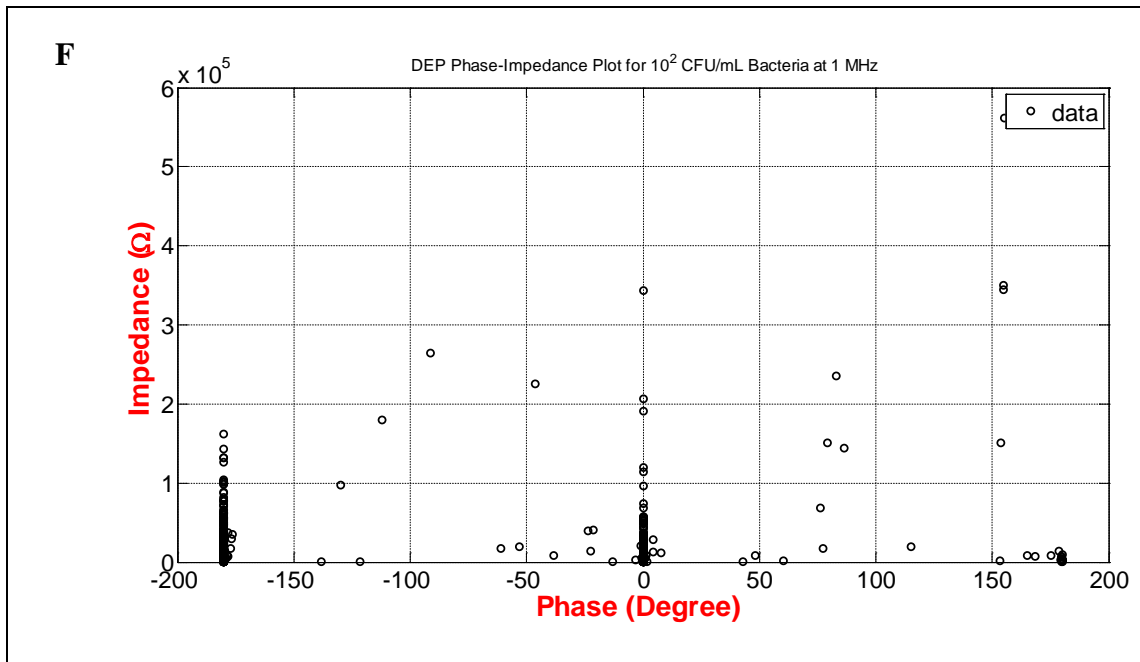Figure 4.8. Continued.

Figure 4.8. Continued.

Figure 4.8. Continued.

4.4.3 Aptasensor selectivity to viable and non-viable *Listeria innocua*
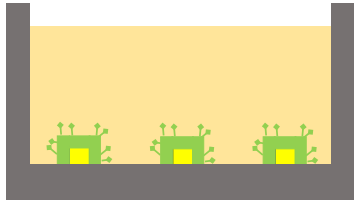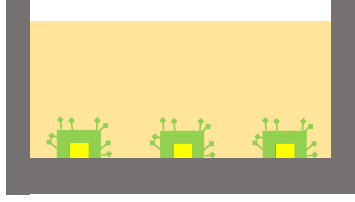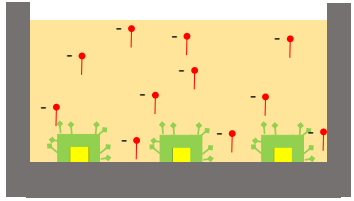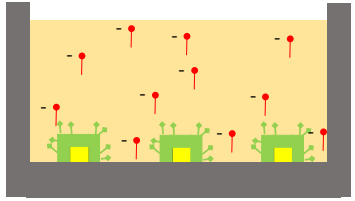
Figure 4.9 show the Bode plots (log frequency versus total impedance) generated

using the viability protocol discussed in Section 4.3.6. The viability procedures as

described in Table 4.2 included measuring the total impedance by EIS scan from 1 Hz to

1 MHz after applying the DEP signal at 10 kHz for 10 minutes. The biosensor was

cleaned with piranha solution before coating the IMEs with 800 nM aptamer

concentration. Table 4.2 also discusses the expected results based on the developed

procedures and the results that were achieved after running the experiments.

The results were used to develop two comparative methods to determine the biosensor

response to viable and non-viable *Listeria innocua* using DEP-EIS technique as

discussed below:

1) <u>Before washing</u>: Impedance measurements due to bacteria presence in both: the aptamers coated IMEs and in the BPW suspension. The impedance magnitude obtained in step 2 and 4 in Table 4.2 describes that the measurements were taken after the addition of viable and non-viable bacteria.

2) <u>After washing</u>: Impedance measurements solely due to the bacteria attachment to the aptamers coated IMEs after washing. The impedance measurements in step 3 and 5 as described in Table 4.2 provided the impedance magnitude after removing viable and non-viable bacteria suspension followed by rinsing the device.

Table 4.2. Viable and non-viable test procedures with comparison between expected and experimental data[**].

Procedures	Expected impedance results	Experimental impedance results
1) 350 µL of BPW solution without bacteria was used to determine the impedance of the aptamer coated IMEs biosensor by applying DEP and EIS (DEP-EIS) tests.	The resulting impedance, Z_{BPW}, would represent the overall impedance due to the aptamer coating on the IMEs surface, i.e., baseline.	The resulting impedance, Z_{BPW}, represented the overall impedance due to the aptamer coating on the IMEs surface.
2) 50 µL of non-viable *L. innocua* was added to the initial volume, 350 µL, followed by DEP-EIS test.	The resulting impedance, $Z_{non-viable}$, would represent the overall impedance due to the aptamer coating on IMEs and the presence of the non-viable bacteria in the BPW solution.	The resulting impedance, $Z_{non-viable}$, represented the overall impedance due to the aptamer coating on the IMEs and the presence of the non-viable bacteria in the BPW solution.

[**]

Non viable bacteria. Viable bacteria. Ligand site. Aptamer film. Electrode. Medium. Chamber.
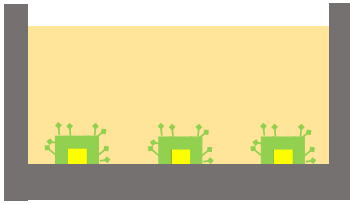
Table 4.2. Continued.
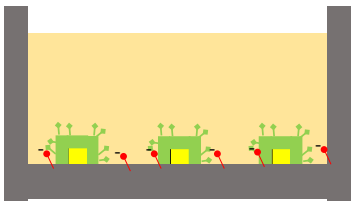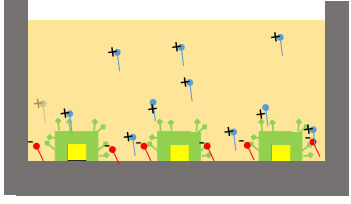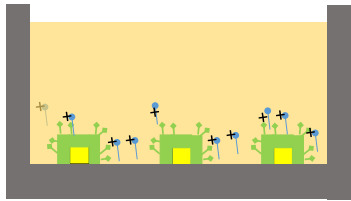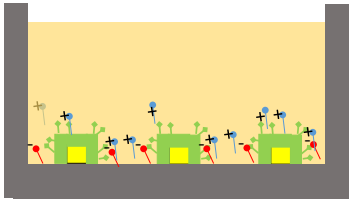
Procedures	Expected impedance results	Experimental impedance results
3) BPW solution with non-viable bacteria was removed and the device was rinsed with DI water. Next, BPW solution, 350 µL, without bacteria was added and DEP-EIS test was performed to record impedance value.	The resulting impedance, $Z_{washed\,non\,-\,viable}$, would represent the impedance of the aptamer coating on the IMEs surface; hypothetically it should be the same as Z_{BPW}, because non-viable bacteria should not be selective to the aptamers. 	The resulting impedance, $Z_{washed\,non\,-\,viable}$, represented the total impedance of the aptamer coating on the IMEs and bacteria trapped at the IMEs edges; therefore, the impedance was greater than Z_{BPW}.
4) 50 µL of viable, *L. innocua* was added to 350 µL and a final DEP-EIS test was performed.	The resulting impedance, Z_{viable}, would represent the impedance due to the aptamer coating and the protein binding of bacteria to the aptamers. 	The resulting impedance, Z_{viable}, represented the impedance due to the aptamer coating and viable bacteria binding, trapped non-viable bacteria at the IMEs edges, and the presence of viable bacteria in the suspension.

Table 4.2. Continued.

Procedures	Expected impedance results	Experimental impedance results
5) BPW with viable bacteria solution from step 4 was removed and the device was rinsed with DI water. BPW solution, 350 µL, without bacteria was added and DEP-EIS test was performed.	The resulting impedance, $Z_{washed\ viable}$, would represent the impedance of the aptamer coating with attached viable bacteria to aptamer coated IMEs; hypothetically it should be the same as Z_{viable}.	The resulting impedance, $Z_{washed\ viable}$, represented the impedance of the aptamer coating on the IMEs, viable bacteria attachment to the aptamers, and trapped non-viable bacteria at the IMEs edges. The washing process could possibly trap more live bacteria at the edges of the IMEs.

**

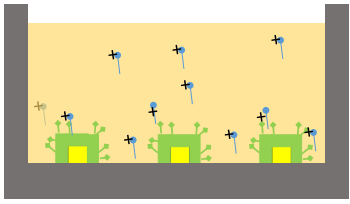⌐● Non viable bacteria. ⌐+ Viable bacteria. ▮ Ligand site. ▮ Aptamer film. ▮ Electrode. ▮ Medium. ▮ Chamber.

Figure 4.9, 4.10, and 4.11 shows the same trend for all bacteria concentrations that the total impedance increased as it was measured at each step mentioned in Table 4.2 reflecting experimental impedance results. Figure 4.12 shows the total impedance values measured as viable and non-viable bacteria were introduced into the BPW solution at 10, 10^2, and 10^3 CFU/mL. The experimental results represented in Figure 4.12 were different from the expected results because the total impedance comparisons did not take non-viable bacteria trapped at the edges of the IMEs into consideration. The

following comparison was developed to conclude the viability test. The impedance

difference from the step 1 was used to compare the magnitudes for the viable and non-

viable *L. innocua*. The impedance differences from $Z_{NV} - Z_{BPW}$ were compared to

$Z_V - Z_{BPW}$ and $Z_{washed\ NV} - Z_{BPW}$ to $Z_{washed\ V} - Z_{BPW}$. Figure 4.12 summarized these

comparisons and the same trends were observed between two sets at different bacteria

concentrations.

Average EIS Signals of 10 CFU/mL Measured After Each DEP TEST at 10 kHz
$Z_{Non\text{-}viable}\text{-}Z_{BPW} = 500 \pm 95.4112\ \Omega$
$Z_{Viable}\text{-}Z_{BPW} = 956.6667 \pm 78.1624\ \Omega$
$Z_{Washed\ Non\text{-}viable}\text{-}Z_{BPW} = 686.6667 \pm 83.9041\ \Omega$
$Z_{Washed\ Viable}\text{-}Z_{BPW} = 1273.3333 \pm 66.4236\ \Omega$
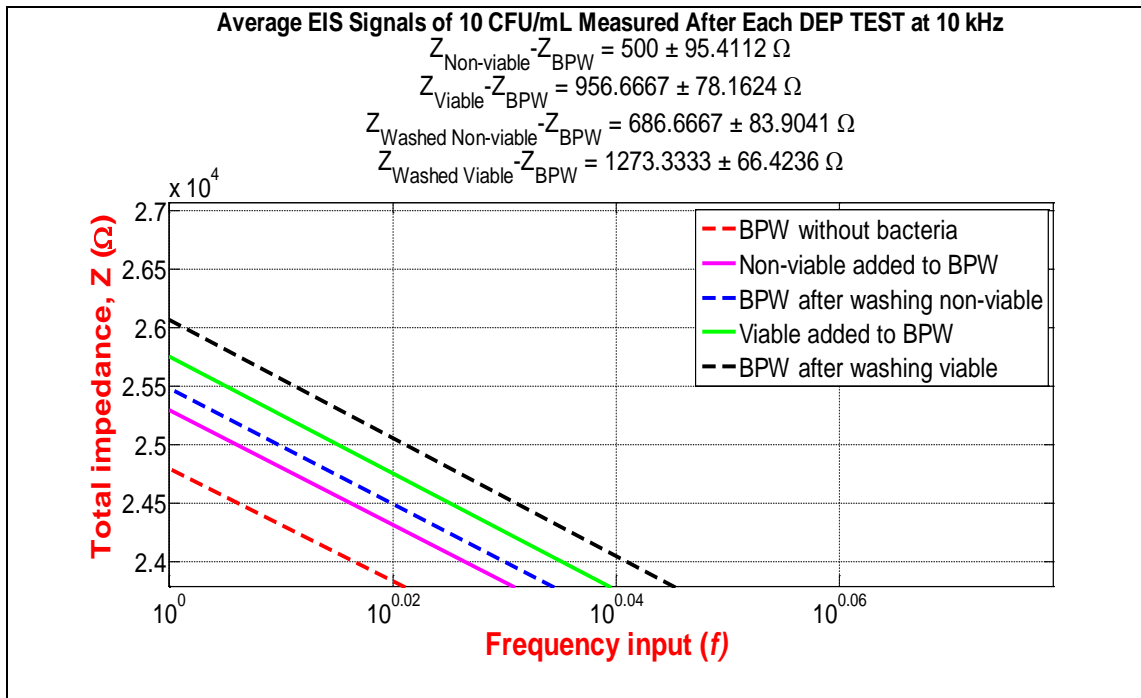
Figure 4.9. Total impedance measurements of viable and non-viable *L .innocua* for 10 CFU/mL after DEP-EIS test at 10 kHz for 10 min.
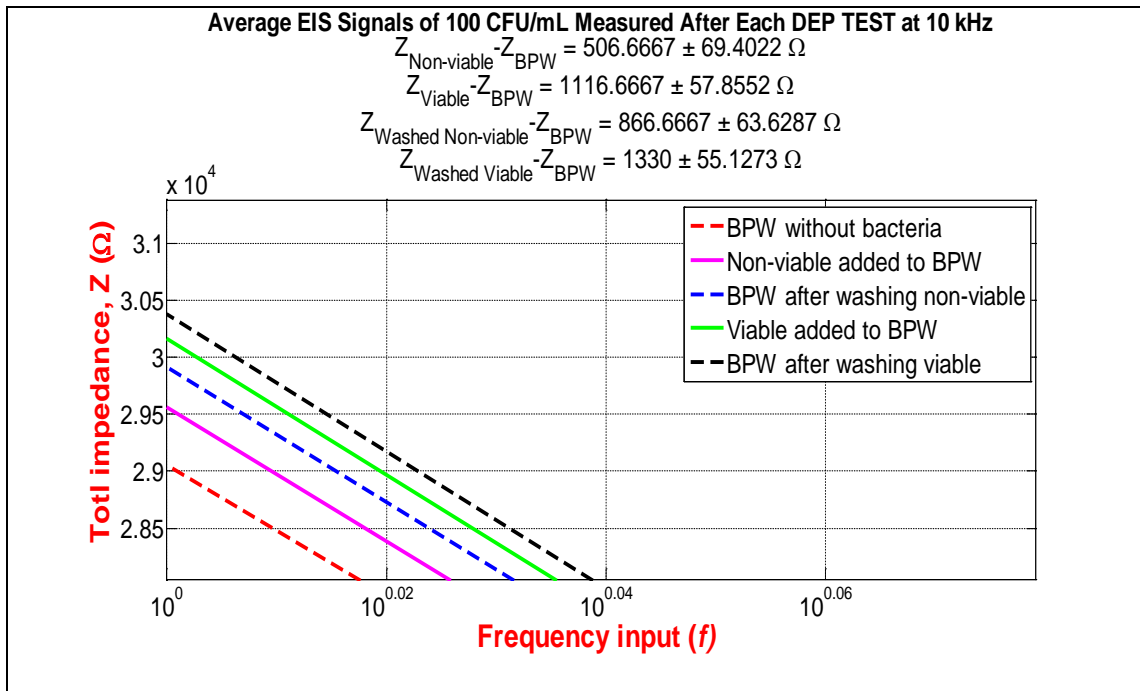
Figure 4.10. Total impedance measurements of viable and non-viable *L .innocua* for 100 CFU/mL after DEP-EIS test at 10 kHz for 10 min.
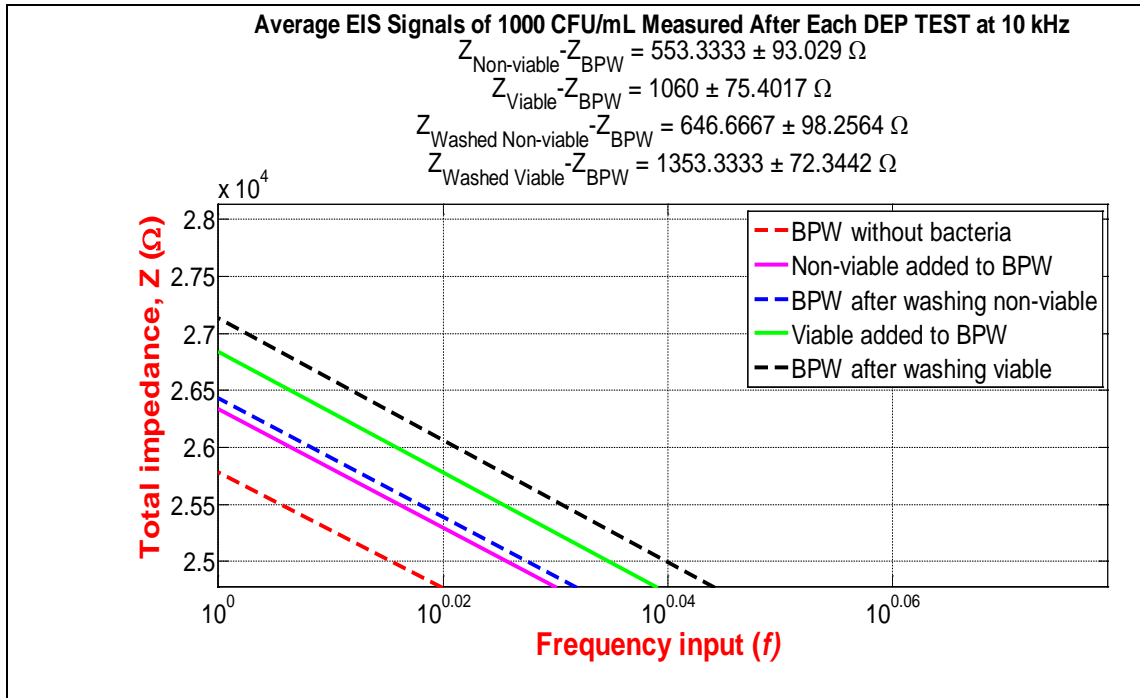
Figure 4.11. Total impedance measurements of viable and non-viable *L .innocua* for 1000 CFU/mL after DEP-EIS test at 10 kHz for 10 min.

The total impedance value of viable bacteria doubled as compared to the non-viable *L. innocua* at each concentration. The impedance change at 10 CFU/mL between non-viable and BPW solution without bacteria ($\Delta Z = Z_{NV} - Z_{BPW}$) was 500 ± 95.41 Ω and impedance change for viable ($\Delta Z = Z_V - Z_{BPW}$) was 957 ± 78.16 Ω. The biosensor total impedance after the washing steps for non-viable bacteria ($Z_{washed\ NV} - Z_{BPW}$) was 686 ± 83.90 Ω and for viable ($\Delta Z = Z_{washed\ V} - Z_{BPW}$) was 1273 ± 66.42 Ω. The total impedance difference, $Z_{NV} - Z_{BPW}$, for non-viable bacteria at 10, 10^2, and 10^4 CFU/mL were 500 ± 95.41 Ω, 507 ± 69.40 Ω, and 553 ± 93.03 Ω, respectively.
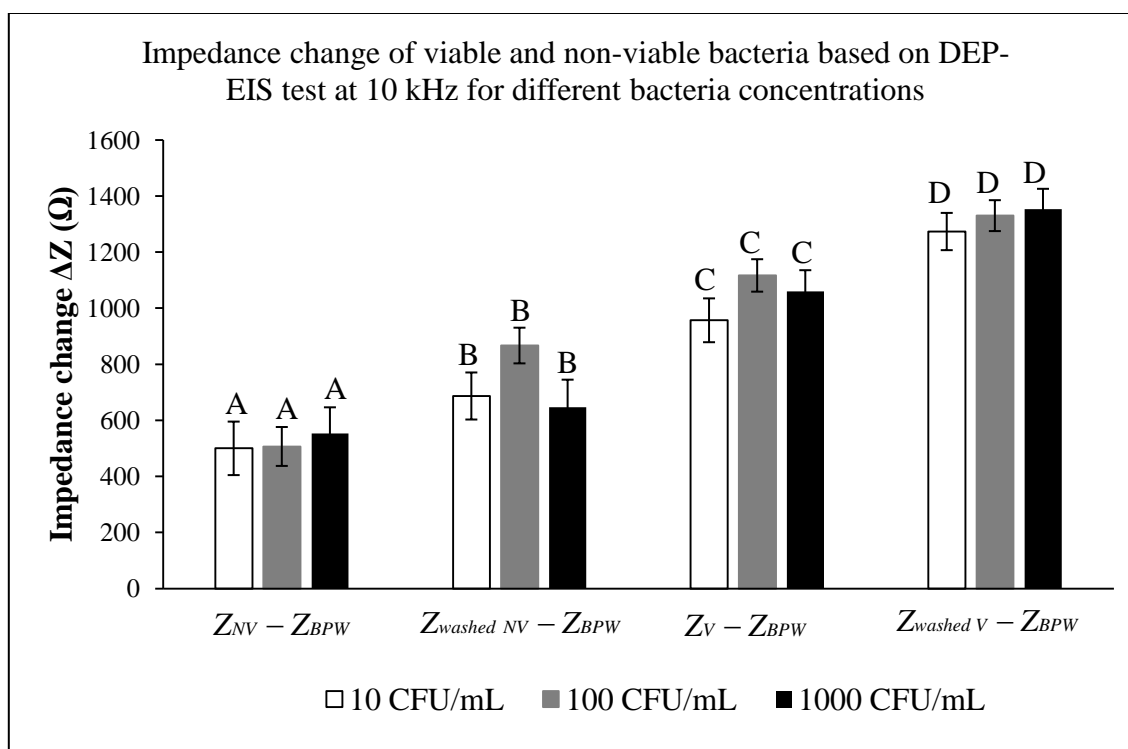
Figure 4.12. Impedance change of viable (Z_V, $Z_{washed\ V}$) and non-viable (Z_{NV}, $Z_{washed\ NV}$) *L. innocua* relative to aptamer coated IMEs impedance (Z_{BPW}) determined based on DEP-EIS technique at 10 kHz for different bacteria concentrations.

The total impedance of the system increased twice as much as when viable bacteria was introduced onto the aptamer coated IMEs, which demonstrated that the *Listeria monocytogenes* aptamers are in fact selective to recognize Internalin A on the membrane of *L. innocua* cell membrane. The total impedance values of viable and non-viable bacteria supported the hypothesis that the viable bacteria would selectively bind to the functionalized aptamers onto the IMEs surface; therefore changing the impedance twice as much as than the non-viable that did not bind to the aptamers. These results are

further confirmed by the Zeiss Axiophot microscopic images in Figure 4.13 and Figure

4.14. The optical results in Figure 4.13 shows that the non-viable *L. innocua* was washed

away from the top of the aptamer coated IMEs after washing and rinsing the biosensor.

However, the trapped non-viable bacteria were visible at the edges of the IMEs

increasing the impedance of the biosensor after washing due to the factors discussed in

Table 4.2. Figure 4.14 illustrates the attachment of the viable bacteria during the DEP

signal and after washing the biosensor. The *Listeria* stayed on the IMEs after cleaning

the biosensor; therefore, showing that the *Listeria monocytogenes* aptamers were

selective to viable *Listeria innocua* and not to the non –viable bacteria.
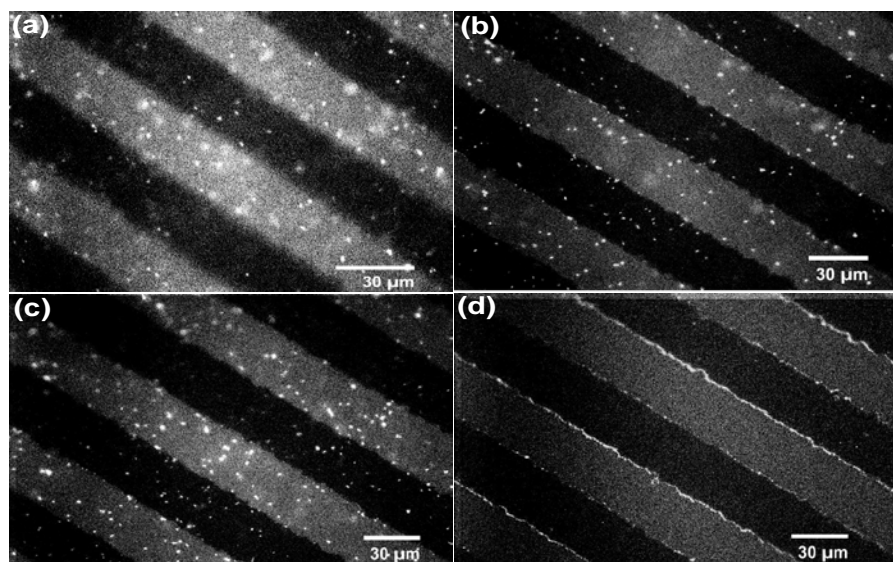
Figure 4.13. Detection of 10^7 CFU/mL non-viable *Listeria innocua* on aptamer coated
IMEs: (a) DEP is turned off. (b) During 10 kHz DEP force at 10 seconds. (c) During
10kHz DEP force at 290 seconds (d) After washing.
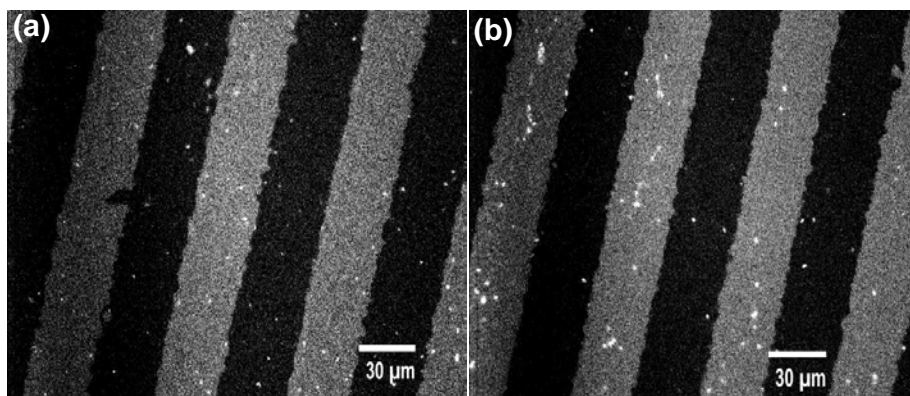
Figure 4.14. Detection of bacteria concentration 10^7 CFU/mL viable *Listeria innocua* onto the aptamer coated IMEs: (a) During 10 kHz DEP at 120 secs. (b) After washing.

In addition sensitivity value was determined between viable and non-viable bacteria for bacteria concentration from 10 - 10^3 CFU/mL before and after washing the biosensor as shown in Figure 4.15. The lower detection limits were summarized in Table 4.3. The sensitivity value before washing step for non-viable *L. innocua* was shown by the following equation: $\Delta Z = 11.57 \log(C_{NV}) + 466.7; R^2 = 0.8426$ and for viable *L. innocua* before washing step was given by the following equation:

$\Delta Z = 22.43 \log(C_V) + 941.2; R^2 = 0.4054$. The sensitivity value after washing step for viable *L. innocua* is given by the following equation:

$\Delta Z = 17.37 \log(C_{washed\,V}) + 1238.9; R^2 = 0.9451$. The sensitivity value after washing step for non-viable bacteria was shown to be negative due to the non-repeatable cleaning procedures which varied the bacteria attachment at the electrode edges and on top of the aptamer coated IMEs. The detection limit based on the logarithmic curve fitting was not

153

calculated due to the negative slope of the sensitivity value. From the aforementioned

sensitivity values, viable *Listeria* has higher sensitivity values as compared to the non-

viable bacteria further supporting the claim that aptamers are selective solely to viable

bacteria. The developed aptasensor assisted with DEP was able to detect the viable and

non-viable bacteria by using ΔZ measurement analysis with sensitivity values of 11.57

and 17.37 Ω/log(CFU/mL)] for non-viable and viable *Listeria* spp., respectively. The

lower detection limit was calculated to be 7.88 ± 0.073 and 7.44 ± 0.175 CFU/mL for

non-viable and viable *Listeria* spp., respectively within 12 minutes. The detection of

viable and non-viable bacteria by the aptasensor showed promising results and

improvement over the previously published work.
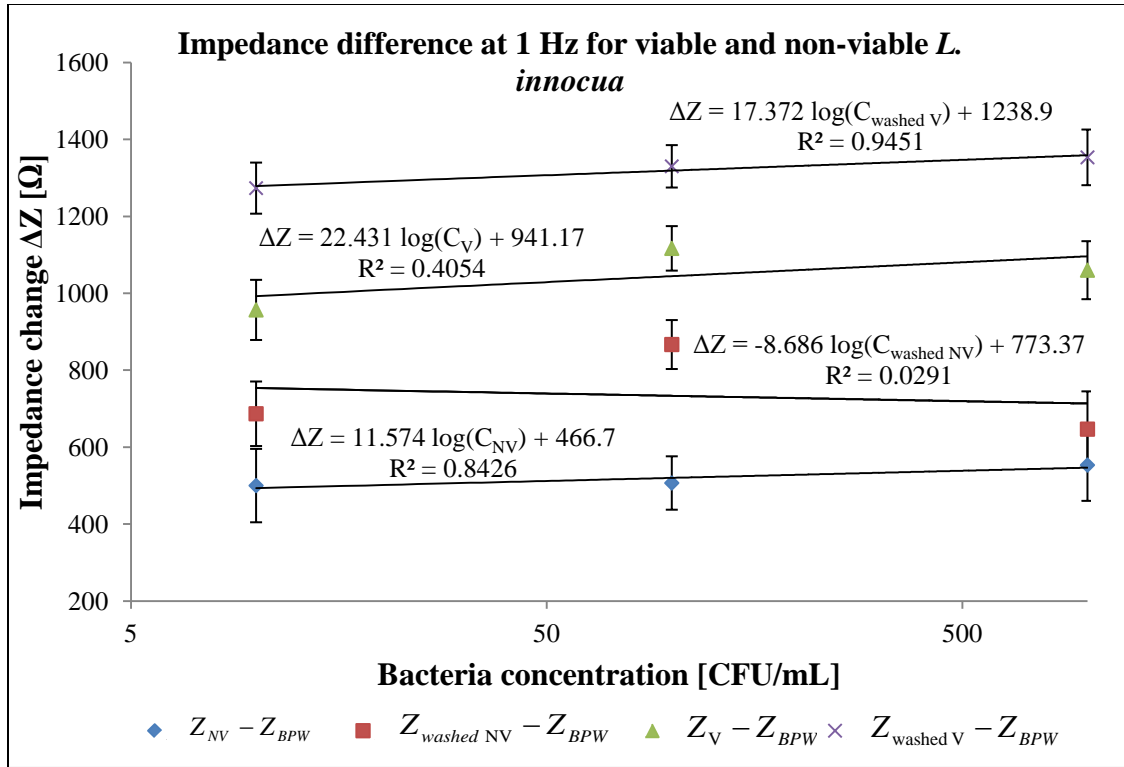
Figure 4.15. Impedance difference change measured at 1 Hz relative to the aptamer coated IMEs for viable and non-viable *L. innocua*.

Table 4.3. Sensitivity and lower limit detection limit of viable and non-viable *L. innocua* for three bacteria concentrations (10, 100, and 1000 CFU/mL).

Impedance difference [Ω]	Sensitivity [Ω/log(CFU/mL)]	Lower detection limit, LOD [CFU/mL]
$Z_{NV} - Z_{BPW}$	11.57	7.88
$Z_{washed\ NV} - Z_{BPW}$	-8.69	N/A
$Z_V - Z_{BPW}$	22.43	7.20
$Z_V - Z_{BPW}$	17.37	7.44

155

In summary, this method described the selectivity of the aptamer to viable

bacteria in the presence of non-viable bacteria, where the total impedance increase was

regarded to viable *Listeria innocua* attached onto the aptamer coated IMEs. This can be

explained by calculating $\Delta Z_{Diff} = (Z_{washed\,V} - Z_{washed\,NV})$, which eliminated the impedance

of non-viable bacteria, but counts the impedance increased by viable *Listeria innocua*.

Therefore, the biosensing method with *L. monocytogenes* coated aptamers IMEs would

be selective to viable bacteria if the difference ΔZ_{Diff} is greater than zero. For all

concentration, the values ΔZ_{Diff} were non-zero, indicating that the biosensor was

definitely selective to viable *Listeria* spp. bacteria. The values for ΔZ_{Diff} at 10 CFU/mL

was 586.60 ± 52.12 Ω, at 100 CFU/mL was 463.3 ± 26.14 Ω, and at 1000 CFU/mL was

706.6 ± 66.46 Ω.

The viability protocol was developed based on the selective binding nature of the

aptamers that allowed only viable bacteria attachment to the surface. This allowed the

testing of non-selective species to the aptamers during the same run and the impedance

measurements were recorded. The advantages of this protocol could be that it is a three

step test to detect viable and non-viable bacteria and no calibration curve of the

biosensor is required given that cleaning procedures are implemented to remove the

trapped bacteria. Typically, a calibration curve is obtained by running the biosensor in a

given solution where the baseline impedance is known. In this protocol, a field

technician can utilize the findings reported here to detect the pathogenic bacteria by

using three simple steps: 1) measure the impedance of the biosensor in a given solution

such as PBS or BPW in a small closed chamber 2) load a small sample volume of the

156

food product into the chamber, and then mechanically shake the chamber while the DEP force is activated. The electrical field attracts the polarized bacteria to the aptamer surface. Mechanical shaking generates kinetic motion in the fluid that assist the bacteria to enter in contact with the aptamer surface. Therefore, the total impedance will increase as a result of trapping bacteria onto the aptamer surface. 3) Dispense the fluid from previous step and replace it with the solution specified in step 1, then measure the impedance. If the impedance in step 3 is greater than step 1 then we detect viable *Listeria* spp. Otherwise, non-targeted bacteria species or non-viable *Listeria spp* .are present provided that cleaning procedures are implemented to remove the trapped bacterial cells at the electrode edges.

The disadvantage of this protocol is that it requires standardized cleaning protocol to remove bacteria at the edges of the IMEs without comprising the aptamer attachment onto the surface of IMEs and bacteria binding with the aptamer ligand sites. The cleaning procedures used in this protocol did not result in clean edges as shown in microscopy images and Table 4.2 discussion on expected result column. Some of the possible methods to improve the cleaning could include tunable ultrasound treatment, directed jet flow of water or blowing inert gas at optimal velocities.

The previous studies on viable and non-viable detection of *Listeria innocua* are discussed in Section 4.1 by (Li & Bashir, 2002). This research group reported the lower detection limit of 10^5 CFU/mL in DI water within 20 minutes based on the epifluoresence method while applying DEP force to separate the viable and non-viable bacteria onto the different regions of the electrodes. In other study by (Suehiro, Hamada,

et al., 2003), reported detection of viable and non-viable *E. coli* strain K12 bacteria suspended in 0.1 M mannitol solution using IMEs based on the difference of the electrical properties of live and dead bacteria. Optimal frequency of 1 MHz was determined at fixed voltage magnitude (3 V peak-to-peak) at which significantly conductance (μS) increase was observed for viable as compare to the non-viable bacteria cells. Using this DEP technique the conductance comparison between viable and non-viable bacteria was measured with the lower detection range of 5 x 10^5 CFU/mL from bacteria concentration ranging from 10^5 to 10^6 CFU/mL within 15 minutes.

The developed protocol based on the aptasensor in this study could be easily employed to detect viable from non-viable *Listeria* spp. based on the sensitivity values. Thus, potentially replacing standard colony counting methods by following the methods described in this study.

4.4.4 Aptasensor selectivity to *Listeria innocua* using an interferent *Staphylococcus aureus*

Figure 4.16A – 4.16F show the total impedance curves after applying the DEP-EIS technique to determine the aptasensor selectivity to *Listeria* spp. using *Staphylococcus aureus* as an interferent. The same rationale as viability protocol was applied to determine the specificity of the *Listeria monocytogenes* aptamer coated IMEs, which were designed to bind Internalin A protein found on the cell membrane of *Listeria* spp. and *S. aureus* was used to test the hypothesis instead of heat inactivated *L. innocua*. The detailed theory and explanations were discussed in Sections 4.3.7 and 4.4.3.

Protocols were discussed in Table 4.2 for the detection of viable bacteria and similar experimental procedures were followed to perform biosensor behavior to an interferent, *S. aureus*. In this study, the impedance measured with *S. aureus* was denoted as $Z_{S.aureus}$ before rinsing and $Z_{washed\ S.aureus}$ after washing the biosensor device measured in steps 2 and 3, respectively. Similarly, the impedance for *L. innocua* was characterized as $Z_{L.innocua}$ before washing and $Z_{washed\ L.innocua}$ after washing the biosensor.
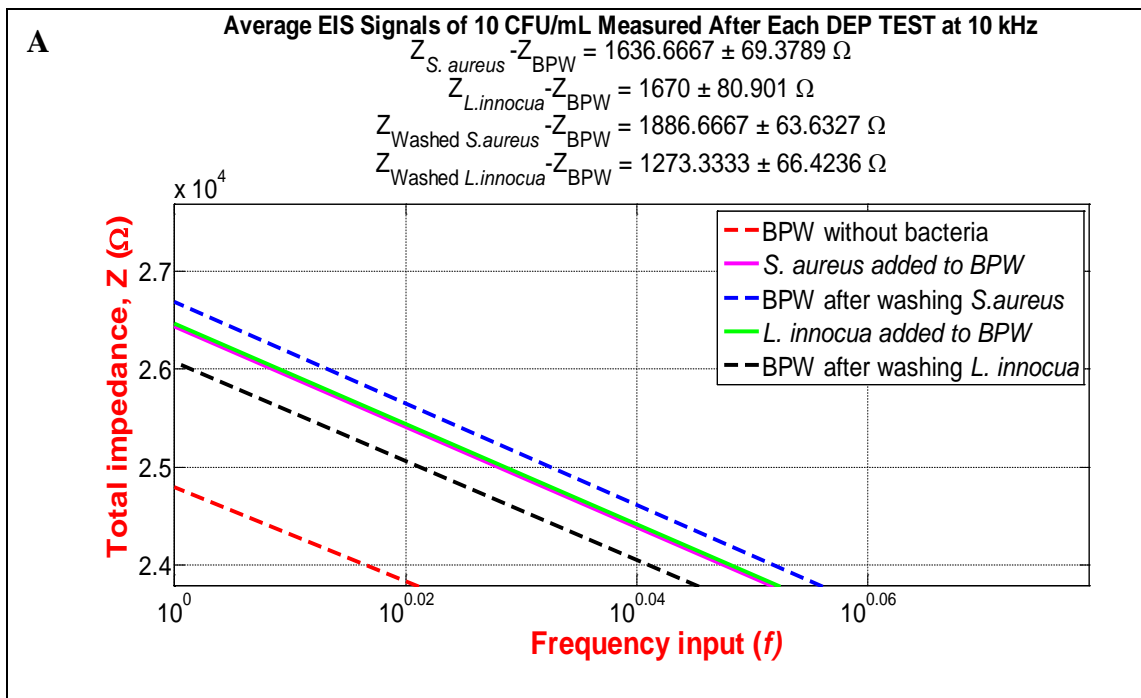
Figure 4.16. The total impedance measurements after DEP-EIS test at 10 kHz and different bacteria concentration of *L. innocua* and *S. aureus* (A) 10 CFU/mL, (B) 10^2 CFU/mL, (C) 10^3 CFU/mL, (D) 10^4 CFU/mL, (E) 10^5 CFU/mL, and (F) 10^6 CFU/mL.

159

Figure 4.16. Continued.

C

Average EIS Signals of 1000 CFU/mL Measured After Each DEP TEST at 10 kHz

$$Z_{S.\ aureus} - Z_{BPW} = 460 \pm 63.5989\ \Omega$$

$$Z_{L.innocua} - Z_{BPW} = 1123.3333 \pm 52.0944\ \Omega$$

$$Z_{Washed\ S.aureus} - Z_{BPW} = 2546.6667 \pm 54.8853\ \Omega$$

$$Z_{Washed\ L.innocua} - Z_{BPW} = 3010 \pm 46.3839\ \Omega$$

Legend:
- – – BPW without bacteria
- —— *S. aureus added to BPW*
- – – BPW after washing *S.aureus*
- —— *L. innocua added to BPW*
- – – BPW after washing *L. innocua*

Y-axis: **Total impedance, Z (Ω)** × 10⁴ (values 2.7, 2.8, 2.9, 3, 3.1)

X-axis: **Log Frequency input (*f*)** (10^0, $10^{0.02}$, $10^{0.04}$, $10^{0.06}$)

Figure 4.16. Continued.

161

D **Average EIS Signals of 10^4 CFU/mL Measured After Each DEP TEST at 10 kHz**

$Z_{S.\ aureus} - Z_{BPW} = -673.3333 \pm 81.1537\ \Omega$

$Z_{L.innocua} - Z_{BPW} = 1123.3333 \pm 52.0944\ \Omega$

$Z_{Washed\ S.aureus} - Z_{BPW} = -193.3333 \pm 60.6588\ \Omega$

$Z_{Washed\ L.innocua} - Z_{BPW} = 3010 \pm 46.3839\ \Omega$

Legend:
- BPW without bacteria
- S. aureus added to BPW
- BPW after washing S.aureus
- L. innocua added to BPW
- BPW after washing L. innocua

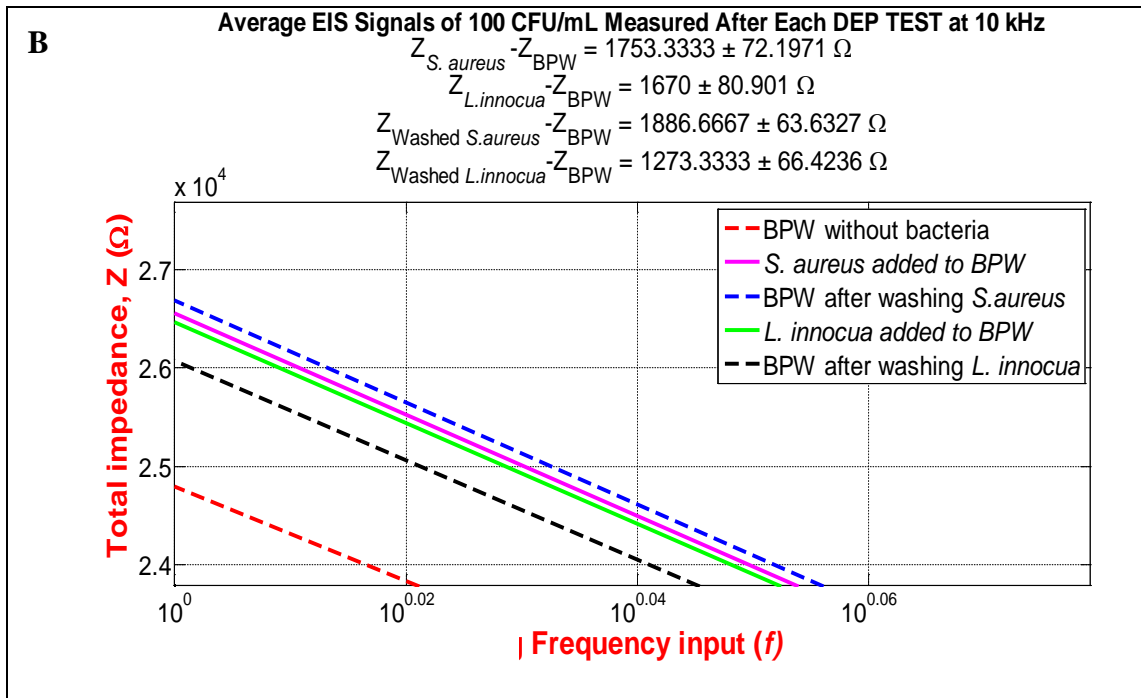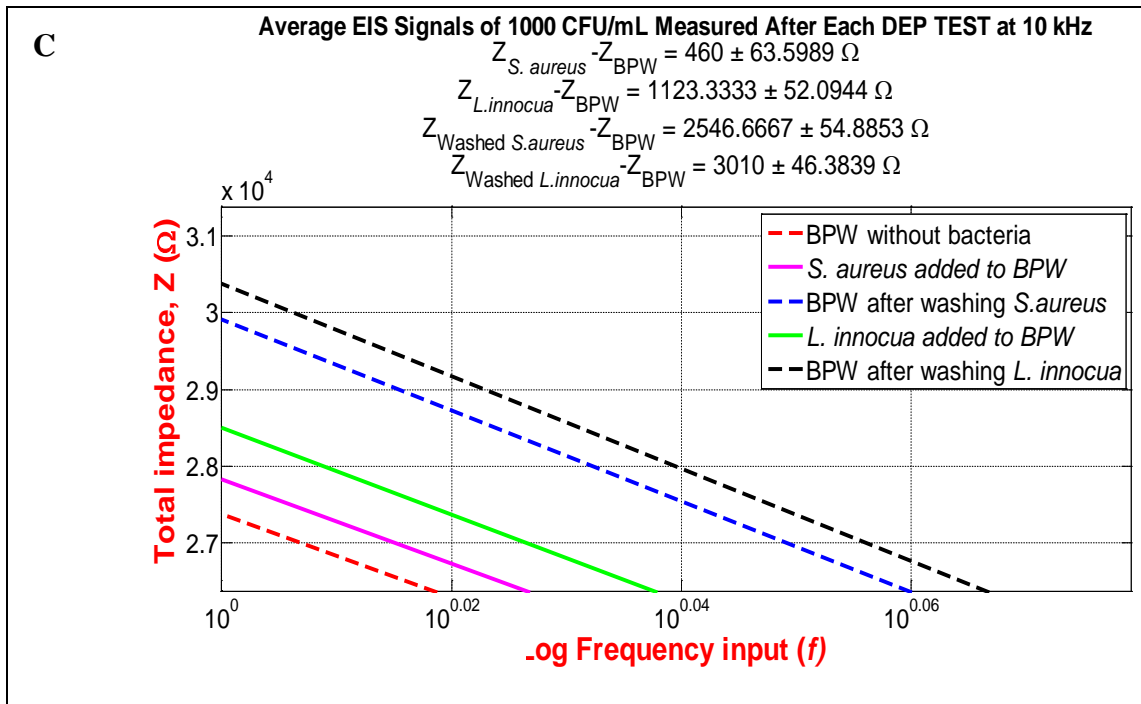Y-axis: Total impedance, Z (Ω) — x 10^4
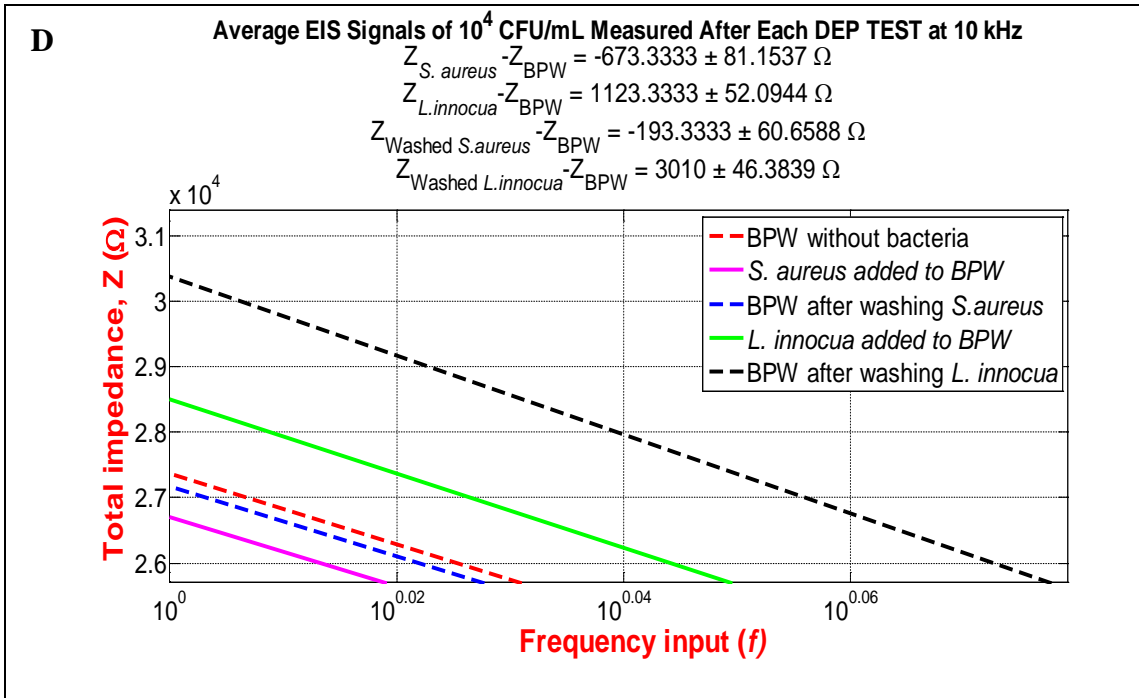
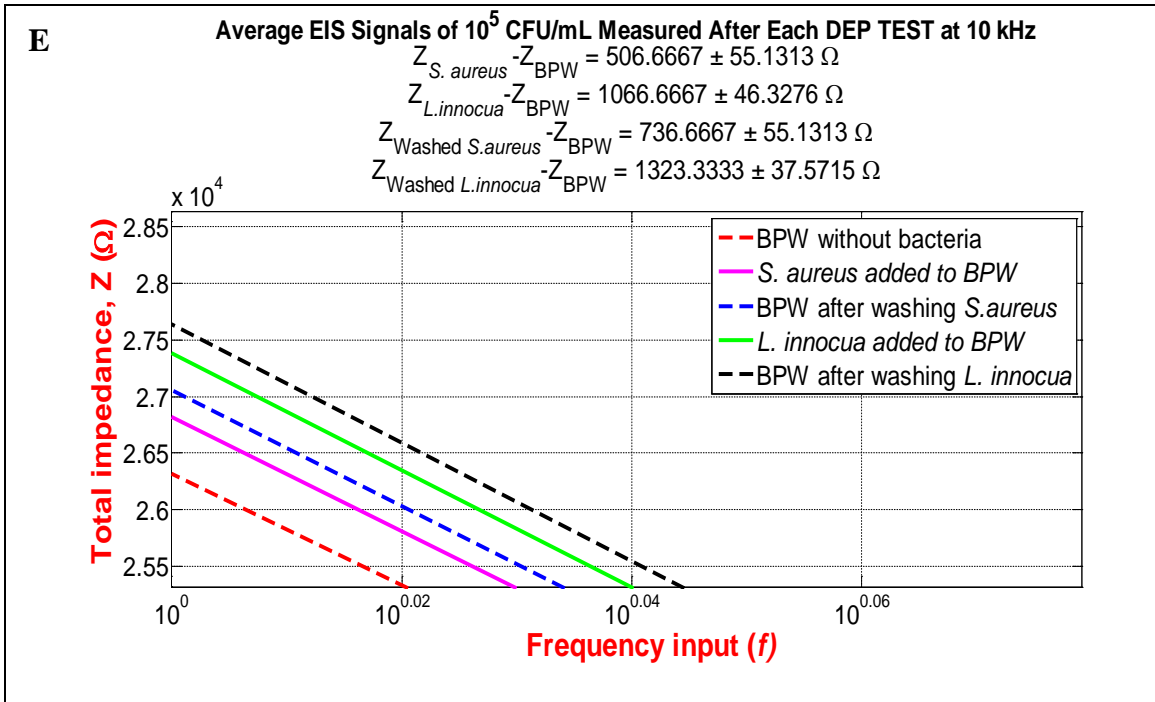X-axis: Frequency input (*f*)

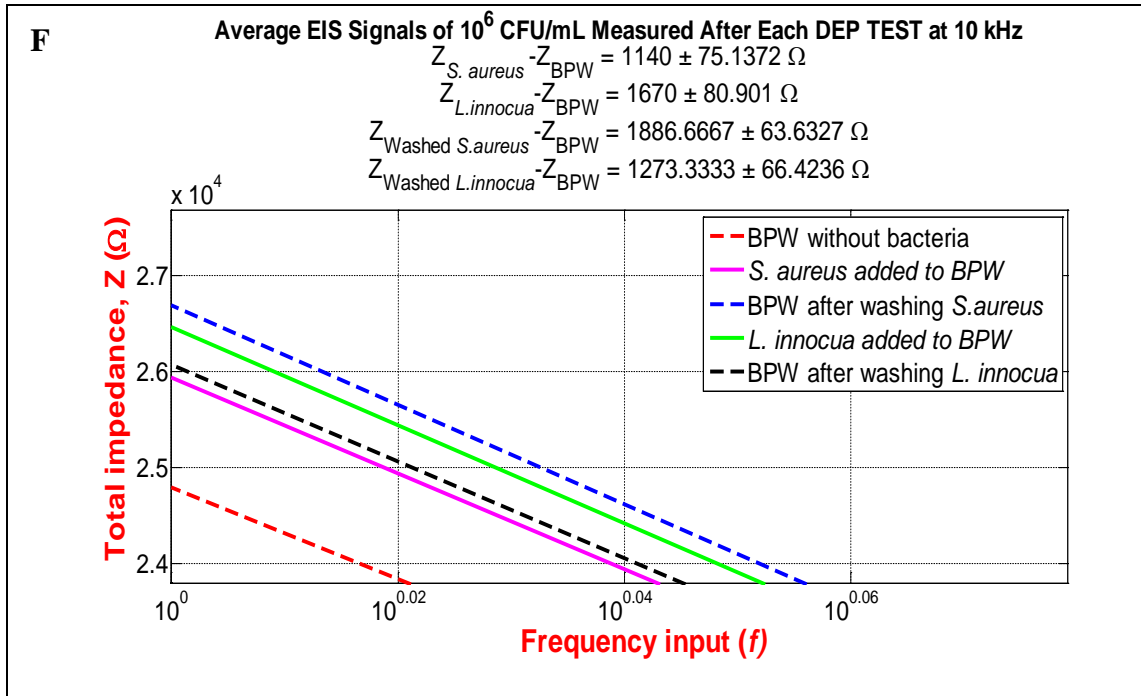Figure 4.16. Continued.

Figure 4.16. Continued.

Figure 4.16. Continued.

Figure 4.16A – 4.16F show the same trend as seen in viable and non-viable results, which illustrated that the total impedance measured at 1 Hz increased with increasing bacteria concentration from $10 – 10^6$ CFU/mL from before and after washing steps performed in the biosensor, as discussed in the Section 4.4.3. DEP-EIS technique was applied at DEP signal at 10 kHz for 10 minutes followed by the EIS scan from 1 Hz to 1 MHz. These results can be compared with the Table 4.2 discussion that showed that the impedance values did not show the expected results designed for the selectivity protocol. Figure 4.17 illustrates the impedance differences between *S. aureus* and *Listeria innocua*. The trend shows that the *Listeria innocua* impedance change values

(ΔZ) were significantly higher than the one for *S. aureus* from before and after washing

steps performed in the biosensor.
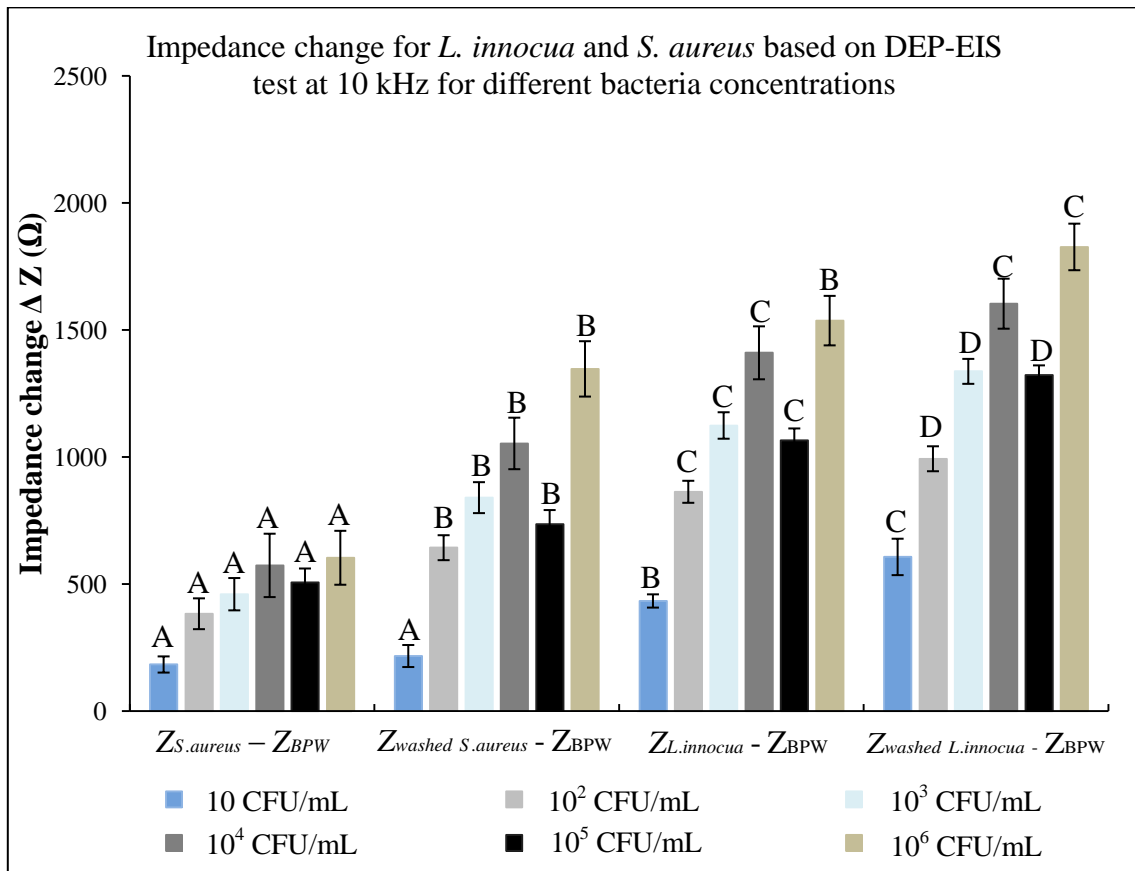
Figure 4.17. Impedance change of *S. aureus* ($Z_{S.aureus}$, $Z_{washed\ S.aureus}$) and *L. innocua* ($Z_{L.innocua}$, $Z_{washed\ L.innocua}$) relative to aptamer coated IMEs impedance (Z_{BPW}) determined based on DEP-EIS technique at 10 kHz for 10 min for bacteria concentrations ranging from 10 to 10^6 CFU/mL.

The impedance values supporting the hypothesis that *Listeria monocytogenes*

aptamers were selective to *Listeria* spp. $\Delta Z_{Diff} = Z_{washedL.innocua} - Z_{washedS.aureus}$ was

evaluated to describe the selectivity of aptamers to *Listeria innocua* with impedance difference contributed only by *Listeria innocua* in the presence of *S. aureus*. The values for ΔZ_{Diff} measured in Ohms for 10 CFU/mL is 390 ± 97.72, 10^2 CFU/mL is 350 ± 98.22, 10^3 CFU/mL is 497 ± 110.01, 10^4 CFU/mL is 550 ± 202.62, 10^5 CFU/mL is 587 ± 92.70 and 10^6 CFU/mL is 480 ± 200.55. The advantages and disadvantage of this protocol was discussed in the viability Section 4.4.3. The developed biosensor was able detect *Listeria* spp. in the presence of an interferent, *S. aureus*, from bacteria concentrations ranging from 10 to 10^6 CFU/mL. The sensitivity and lower detection limits values of *S. aureus* and *L. innocua* are shown in Figure 4.17 and Table 4.4 for before and after washing steps performed in the biosensor. Based on these results the sensitivity values are higher (P < 0.05) for *L. innocua* as compared to the *S. aureus* implying that the developed biosensor is more sensitivity to targeted bacteria *Listeria* spp. The sensitivity values over the bacteria concentration range of $10 - 10^6$ CFU/mL were calculated for *S. aureus* and *Listeria* spp. with the values of 32.05 and 91.28 Ω/log(CFU/mL)], respectively. The lower detection limit determined to be 6.74 ± 0.022 and 5.68 ± 0.025 CFU/mL for *S. aureus* and viable *Listeria* spp., respectively within 12 minutes. The developed aptasensor was also able to detect the impedance response at bacteria concentration of 10^7 CFU/mL; however, the results are not included in the linear range analysis. The results are shown in Appendix E for bacteria concentration at 10^7 CFU/mL for *Listeria innocua*.

Impedance difference at 1 Hz for *S. aureus* and *L. innocua*

$\Delta Z = 91.284 \log(C_{\text{after wash } L. innocua}) + 546.01$
$R^2 = 0.819$

$\Delta Z = 79.586 \log(C_{L. innocua}) + 430.83$
$R^2 = 0.7493$

$\Delta Z = 76.231 \log(C_{\text{after wash } S. aureus}) + 191.77$
$R^2 = 0.7354$

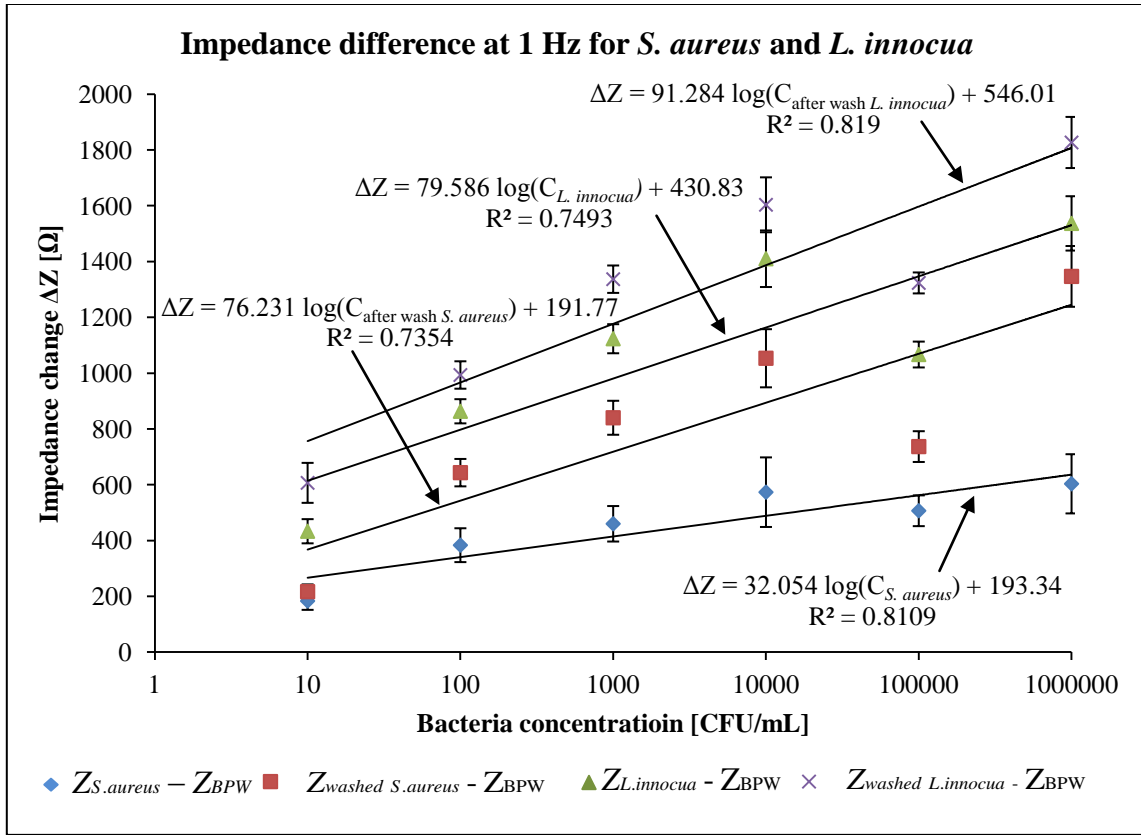$\Delta Z = 32.054 \log(C_{S. aureus}) + 193.34$
$R^2 = 0.8109$

Figure 4.18. Impedance difference change measured at 1 Hz relative to the aptamer coated IMEs for *S. aureus* and *L. innocua*.

Table 4.4. Sensitivity and lower limit detection limit of *Staphylococcus aureus* and *Listeria innocua* for different bacteria concentration.

Impedance difference [Ω]	Sensitivity [Ω/log(CFU/mL)]	Lower detection limit, LOD [CFU/mL]
$Z_{S.aureus} - Z_{BPW}$	32.05	6.74 ± 0.022
$Z_{washed\ S.aureus} - Z_{BPW}$	76.23	5.88 ± 0.024
$Z_{L.innocua} - Z_{BPW}$	79.59	5.83 ± 0.042
$Z_{washed\ L.innocua} - Z_{BPW}$	91.28	5.68 ± 0.025

In summary, the sensitivity for *Listeria* spp. were higher in the presence of *S. aureus*/ *L. innocua* than non-viable/viable *L. innocua* with the values of 91.28 and 17.37 [Ω/log(CFU/mL)] respectively. The aptasensor has a better sensitivity in the presence of *S. aureus* as compared to non-viable *L. innocua* because *S. aureus* has less interference with the viable *L. innocua* than in the presence of non-viable *L. innocua*. This might be due to the increased charge polarity of heated treated cells as compared to viable *S. aureus* and *L. inncoua*.

4.4.5 Detection of *Listeria monocytogenes* in off-the-shelf product

Figure 4.19 and Figure 4.20 show the Bode and Nyquist plots for *Listeria monocytogenes* detection in off-shelf vegetable broth using DEP-EIS technique. The aptamer concentration of 800 nM was used to functionalize the IMEs to determine the baseline of the biosensor with vegetable broth. EIS scan was used to measure the total impedance changes due to the increasing concentration of the bacteria from 10 to 10^7 CFU/mL. The presence of the *Listeria monocytogenes* resulted in an increase in impedance magnitude which could be measured at 1 Hz. The total impedance spectrum from Bode and Nyquist plots showed the increasing trend with the increasing concentration of the bacteria at lower frequencies from 1 to 10 Hz. Nyquist plot showed the imaginary (Z'') versus the real (Z') impedance values from high to low frequency. At higher frequencies, the total impedance values converged and similar trend was shown in the Bode plot. Significant change was observed at the lower frequencies; therefore, 1 Hz was chosen to calculate the impedance changes for the sensitivity and lower detection limit of the aptasensor.
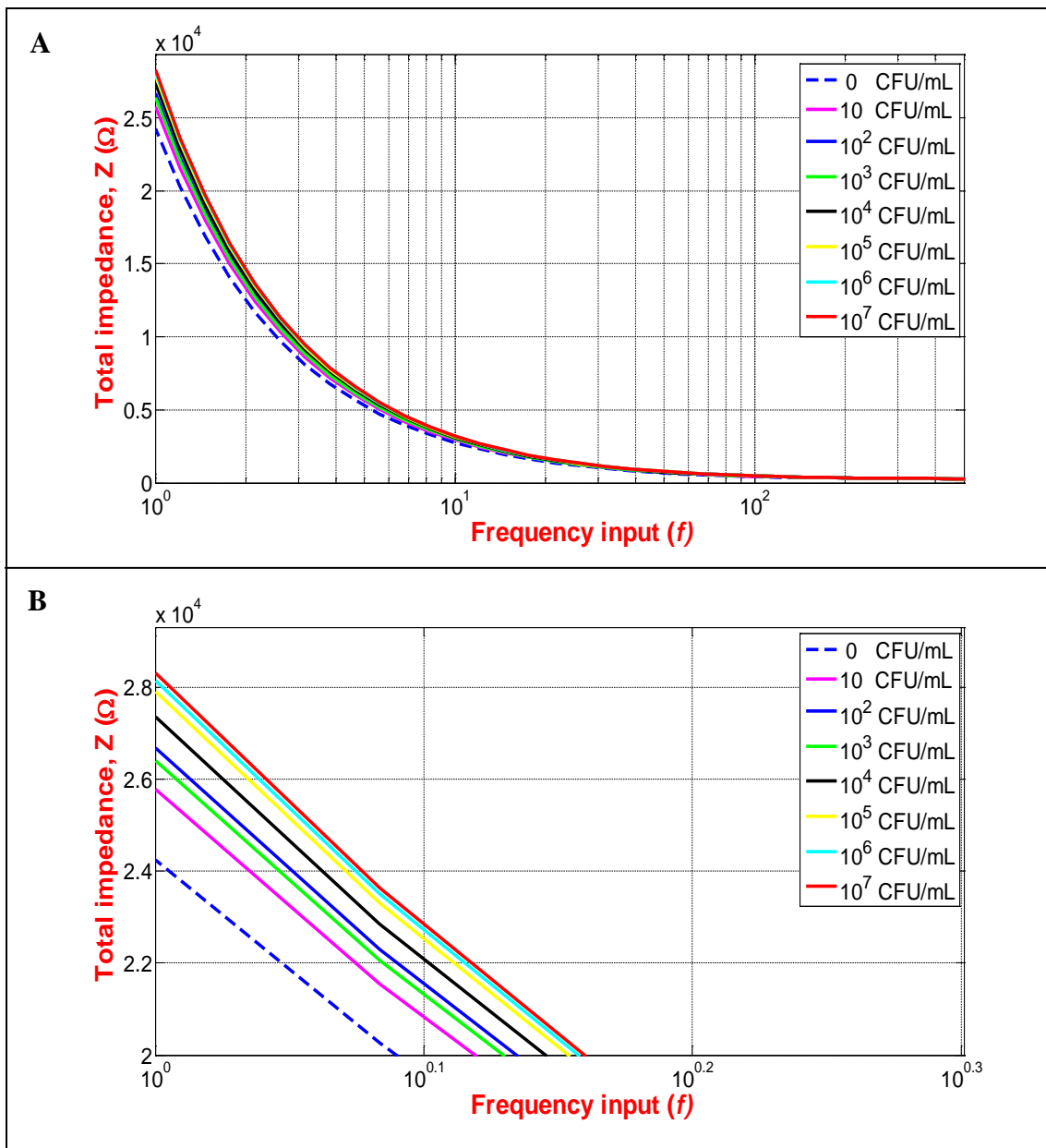
Figure 4.19. Detection of *L. monocytogenes* in vegetable broth solution after applying 10 kHz DEP signal for 10 min. (A) The total impedance versus log frequency obtained from EIS analysis. (B) The total impedance values at 1 Hz from the Bode plot.
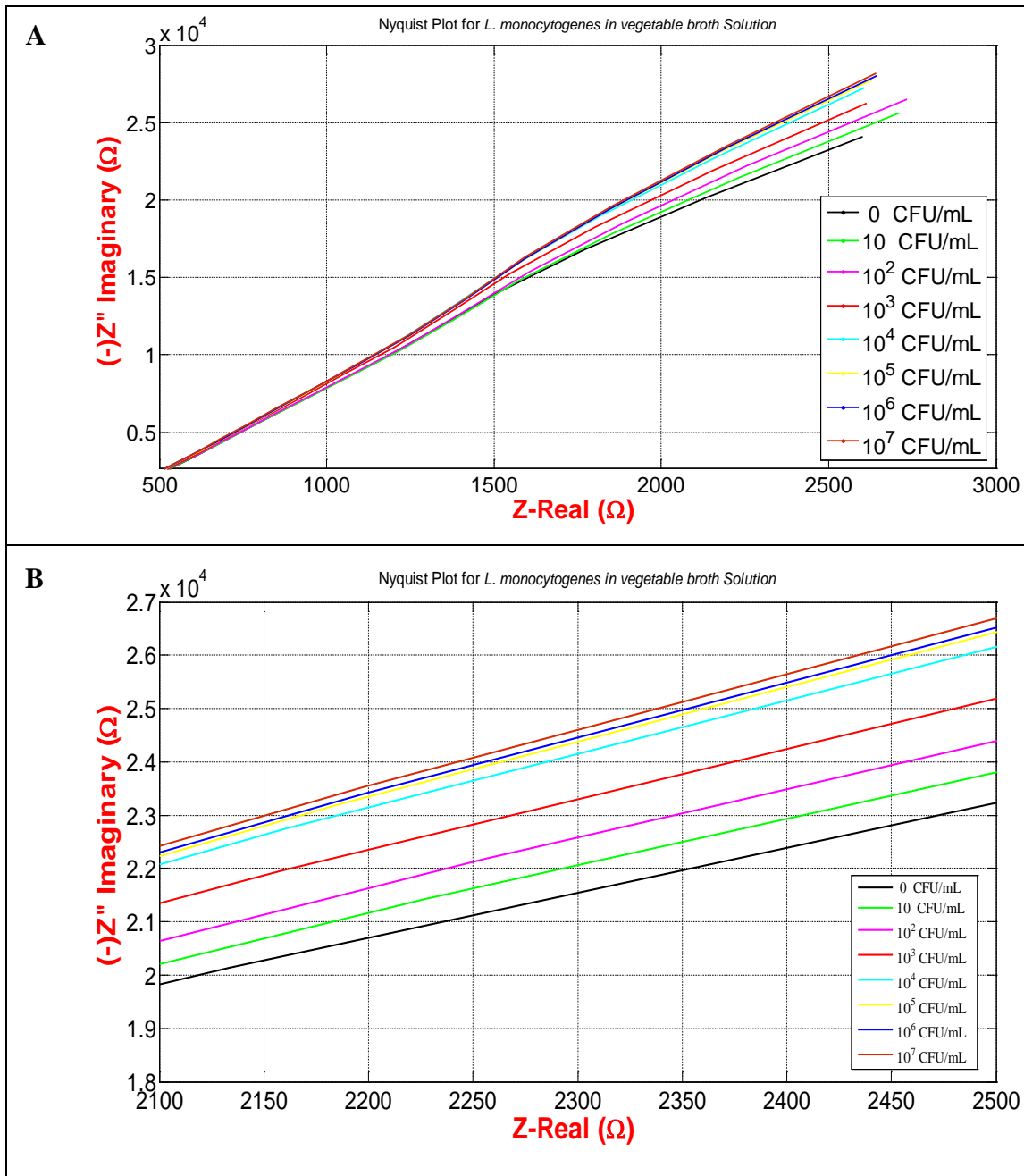
Figure 4.20. (A) Nyquist plot of *L. monocytogenes* detection in vegetable broth after applying 10 kHz DEP signal for 10 min. (B) the total impedance values at 1 Hz. Z' is real impedance and Z'' is imaginary impedance representing resistance and capacitance of the biosensor.

The lower detection limit (LDL) was calculated based on the signal to noise ratio of 3 where noise and signal were defined as $Z_{apatmer}$ (baseline experiment, 0 CFU/mL of *L. monocytogenes*) and $Z_{bacteria}$, respectively. Figure 4.21 showed the impedance change with respect to the baseline of the biosensor with respect to the aptamer coated IMEs. A logarithmic relationship was found between ΔZ (Ohms) and the bacteria concentration (CFU/mL) to be $(\Delta Z = 186.51\ln(C_{L.innocua}) + 1268; R^2 = 0.9272)$. The sensitivity was determined to be 186.51 ± 23.37 (Ω/[CFU/mL]). The lower detection limit and the standard deviation of the aptasensor for *L. monocytogenes* were found to be 4.82 ± 0.01 CFU/mL. The total detection time from introducing the bacteria samples to impedance (DEP-EIS technique) measurements was 12 minutes.

Impedance difference at 1 Hz in vegetable broth

$$y = 186.51\log(C_{bacteria}) + 1268.4$$
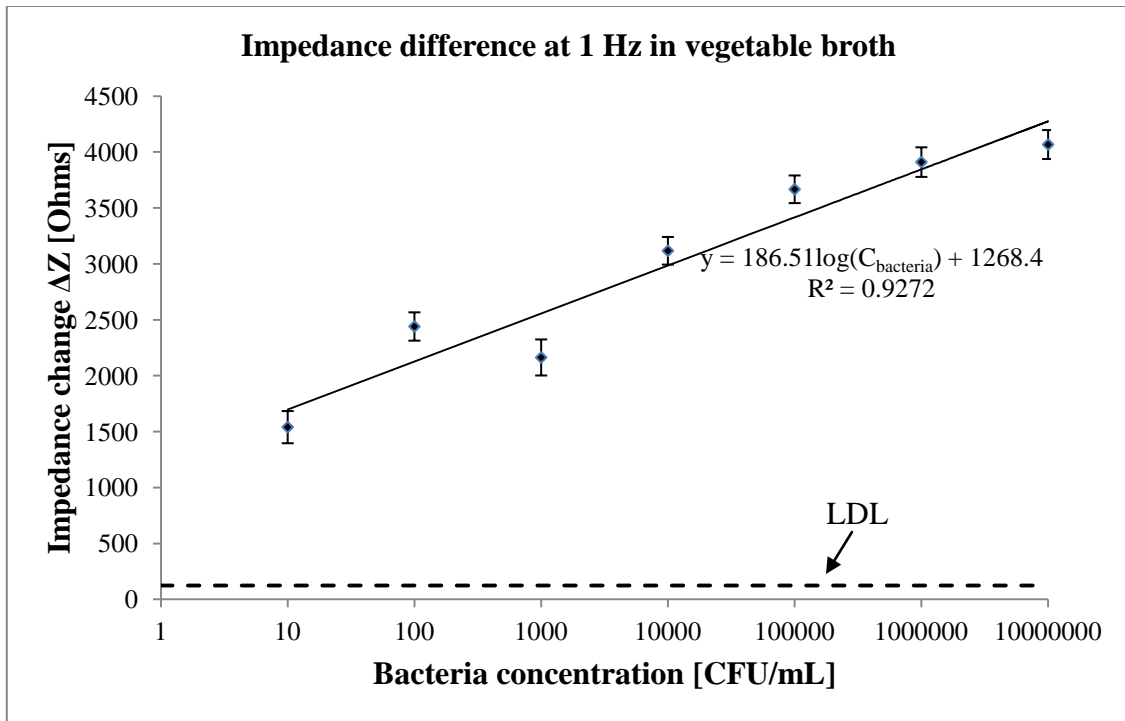$$R^2 = 0.9272$$

Figure 4.21. Calibration curve of *L. monocytogenes* obtained by plotting impedance difference from baseline versus bacteria concentration suspended in vegetable broth. Total impedance was measured at 1 Hz. Lower detection limit (LDL) of *L. monocytogenes* in vegetable broth solution using aptamers functionalized IMEs shown as dashed line.

The developed impedimetric aptasensor was able to capture *Listeria* spp. using dielectrophoresis technique which had a lower detection limit (4.82 ± 0.01 CFU/mL) and shorter detection time (12 min) as compared to the biosensors reported in the literature as discussed in section 4.1. In a study performed by Yang et al. (2006), a flow-through microchannel was designed for DEP capture of *Listeria* cells using fluorescence detection in brain heart infusion broth (BHI). The device consisted of IMEs in a polydimethylsiloxane (PDMS) microchannel that demonstrated the bacteria capture

172

efficiency was between 87-92% for concentrations ranging from 10^5 to 10^7 CFU/mL. The DEP capture efficiency was directly related to the flow rate, as the flow rate was increased the capture efficiency was decreased. In the same study performed by (Yang et al., 2006), IMEs were functionalized with a biotinylated-BSA-streptavidin-biotinylated monoclonal antibody sandwich structure for the detection of *L. monocytogenes*. The capture efficiency using the DEP chamber was between 20-30% with the range of 10^3 to 10^6 CFU/ mL. In another study that used IME-based DEP device to trap and detect the *Listeria* cells was developed by (Gómez-Sjöberg et al., 2005). A microfluidic chamber was incorporated to use DEP force to trap the *Listeria* onto the IMEs surface to detect their metabolic activity by impedance measurements. The detection range of bacteria was from 10^4 to 10^5 CFU/mL and detection time was 1 hour. (Koo et al., 2009) reported DEP enhanced biochip for the detection of *Listeria monocytogenes* by immobilizing a heat shock protein 60 (Hsp60) onto the surface of the electrodes. The capture efficiency of Hsp60-coated biosensor was increased by 60% when 5 minutes of DEP was applied at 1 kHz for 1 hour incubation time. The lower detection limit was 10^7 CFU/mL for the bacteria concentration ranging from 10^6 to 10^7 CFU/mL within approximately 3 hours. Their biosensor was unable to detect 10^6 CFU/mL. Compare to these studies the developed aptamer based biosensor showed significantly rapid, lower detection limits and broader range of detection.

4.5   Conclusion

DEP-EIS techniques were applied in this chapter for the detection of the viable and non-viable bacteria. DEP assisted aptasensors were shown to improve the sensitivity

over the non-applied DEP signal at three different bacteria concentrations. The normalized impedance percent change was calculated over three frequency regions from low (500 – 1000 Hz) to medium (1 – 600 kHz) to high (600 – 1000 kHz). The average percent change over medium region was determined to be 14.13 % over bacteria concentration of 10, 10^2, and 10^4 CFU/mL implying maximum capture efficiency of bacteria cells in 1 – 600 kHz range. The developed aptasensor assisted with DEP was able to detect viable and non-viable bacteria by using impedance difference measurement analysis with sensitivity value of 17.37 Ω/log(CFU/mL)] *Listeria* spp. The lower detection limit was calculated to be 7.44 ± 0.075 CFU/mL for viable *Listeria* spp. within 12 minutes. These sensitivity and detection limits values of viable and non-viable bacteria by aptasensor showed significant improvement over the previously published work and promising results to implement the biosensor in the field to detect viable bacteria cells and potentially replacing traditional methods of plate counting *S. aureus* was used as an interferent to detect the *Listeria* spp. in BPW solution over the bacteria concentration range of 10 – 10^6 CFU/mL. The developed biosensor showed that it was capable of distinguishing the two bacteria using impedance difference analysis with sensitivity value of 91.28 Ω/log(CFU/mL)] for   *Listeria* spp. The lower detection limit was calculated to be 5.68 ± 0.025 CFU/mL for viable *Listeria* spp. within 12 minutes. The sensitivity values in viability and selectivity experiments were higher for viable *Listeria* spp. in the selectivity test demonstrating the biosensor response in the presence of *S. aureus*/*L. innocua* and viable/non-viable *L. innocua*. This might be due to the increased charge polarity of heated treated cells as compared to viable *S. aureus* and *L.*

174

inncoua. Finally, impedimetric aptamer based biosensor using DEP-EIS technique demonstrated that it was able to detect *Listeria monocytogenes* in off-the-shelf product, vegetable broth, with the detection limit of 4.82 ± 0.01 CFU/mL in 12 min for bacteria ranging from 10 to 10^7 CFU/mL. Based on these results, the developed biosensor showed significant improvement compared to previously published biosensors and it could be employed to detect other pathogenic bacteria.

CHAPTER V

SUMMARY AND CONCLUSIONS

In this thesis, lab-on-a-chip biosensors for selective detection of foodborne pathogen, *Listeria* spp., using aptamers as biorecognition agents were investigated. *Listeria* was chosen as a model target due to its significant impact on the agricultural, food industries and human health.

The lab-on-a-chip impedimetric biosensor was developed based on the platinum interdigitated microelectrodes array (IMEs) for the detection of pathogenic bacteria to achieve enhanced sensitivity and response time. The biosensors were fabricated using microfabrication lithographic techniques with four different Pt-IMEs electrode gaps including 15, 25, 50, and 100 μm. The electrode performance was characterized by using electrochemical techniques including cyclic voltammetry (CV) to determine electroactive surface area (ESA) and direct current potential amperometry (DCPA) for sensitivity calculations in reversible redox species. The electrode gaps including 25, 50, and 100 μm were successfully fabricated whereas the electrodes with 15 μm gap showed to have short-circuited connection between interdigitated electrodes by making a conductive path across two electrodes of different combs due to fabrication limitations of the mylar mask resolution. The fabrication limits of 15 μm electrode gap could be resolved by using chrome mask designed to achieve higher resolution. A direct relationship was observed between surface area and sensitivity with 25, 50, and 100 μm electrode gaps. The electroactive surface area and sensitivity was increased as the electrode gap was decreased. The potentiostat was unable to read current response due to

high current density flow on the electrode surface of Pt-IME device with 25 μm

electrode gap. An instrument that would cover larger range of current can be used to

detect the changes at the 25 μm electrode gap or a current divider setup can be

implemented to reduce the current flow between the electrodes. Based on the results

from CV and DCPA electrochemical techniques, the electrodes with 50 μm gap were

selected for the detection of the bacteria.

Platinum interdigitated microelectrodes (IMEs) array with electrode gap size of

50 μm was used and functionalized with *Listeria monocytogenes* aptamers, selective to

protein internalin A, via metal-thiol self-assembly for *Listeria* spp. detection in 17 mL

phosphate buffer saline (PBS, pH 7.4). Thiol labeled aptamers for *L. monocytogenes*

consisted of 47-mer and are designed to target the internalin A (InlA) protein on *Listeria*

spp. cell membrane. Electrochemical impedance spectroscopy analysis (EIS) was able to

detect the surface modification due to aptamers attachment and protein binding of

Listeria innocua; providing a direct technique for *Listeria* spp. detection without the

need for label amplification or sample pre-concentration steps. The frequency spectrum

from 1 to 100 kHz was applied to understand the behavior of the attached aptamers to

the Pt-IMEs based on the impedance difference, ΔZ , that was used to compare

impedance from the bare Pt-IMEs. The ΔZ data suggested that aptamers attachment

were significant at 1 Hz between the bare and aptamer coated IMEs and no impedance

differences above 10 Hz were observed. Therefore, impedance values at 1 Hz were

analyzed for aptamer concentrations. The loading of biorecognition element, *Listeria*

monocytogenes aptamers, onto the Pt-IMEs surface was optimized using covalently

177

adsorption of six aptamer concentrations including 100, 150, 200, 300, 400, and 800 nM. DTT reduction protocol was used to modify disulfide *Listeria* thiol aptamers to form two free thiols that provided strong bond with the platinum IMEs. The DTT reduction of aptamers was observed to be a crucial step for the capturing of the bacteria onto the electrodes, without performing DTT protocol the aptamers were washed away from the IMEs when the biosensor was rinsed. The developed aptasensor was saturated at 800 nM aptamer concentration which was used to functionalize the IMEs surface to detect the targeted bacteria. The use of the aptamers allowed the developed aptasensor to have lower detection limits of 5.39 ± 0.21 CFU/ml, sensitivity of 268.1 ± 25.40 (Ohms/log [CFU/mL]), and faster response of 17 minutes than a similar previously designed biosensors based on antibodies.

In addition, to label-free impedimetric methods, dielectrophoresis (DEP) technique was used to improve the capture efficiency of foodborne pathogens of the aptamer-functionalized biosensor by using reduced sample volumes (350 μL) at an optimized frequency signal and DEP force. DEP act as magnet to polarized bacteria, however; the DEP electrostatic field size is typically narrow, and would only collect polarized bacteria that are at a close distance to the electrodes surface. A unique combination of DEP and EIS techniques was utilized to develop the procedure to detect viable and non-viable *Listeria* spp. and detection of *Listeria* bacterial cells in the presence of an interferent, *S. aureus*.

DEP force was applied with varying frequency and EIS with frequency spectrum from 1 to 1 MHz was used to measure the impedance at 1 Hz. The optimal operating

178

settings of the biosensor were determined by varying the frequencies ranging from 0.5, 1, 10, 100, 600 kHz to 1 MHz. DEP assisted aptasensors were shown to improve the sensitivity over the non-applied DEP force at 10, 10^2, and 10^4 CFU/mL. The normalized impedance percent change was calculated over three frequency regions from low (500 – 1000 Hz) to medium (1 – 600 kHz) to high (600 – 1000 kHz) and impedance percentage change over the medium region was determined to be 14.13 %. These results implied that frequency region from 1 – 600 kHz should be used to maximize the bacteria capture efficiency. Optimal DEP force at 10 kHz frequency and 4.24 V_{pp} (peak-to-peak voltage) was applied to conduct the experiments for viability and selectivity. The developed aptasensor assisted with DEP was able to detect the viable and non-viable bacteria by using ΔZ measurement analysis with sensitivity values of 11.57 and 17.37 Ω/log(CFU/mL)] for non-viable and viable *Listeria* spp., respectively. The lower detection limit was calculated to be 7.88 ± 0.073 and 7.44 ± 0.075 CFU/mL for non-viable and viable *Listeria* spp., respectively within 12 minutes. The detection of viable and non-viable bacteria by the aptasensor showed promising results and improvement over the previously published work. *S. aureus* was used as an interferent to detect *Listeria* spp. in BPW solution over the bacteria concentration range of 10 – 10^6 CFU/mL and sensitivity were calculated for *S. aureus* and *Listeria* spp. with the values of 32.05 and 79.59 Ω/log(CFU/mL)], respectively. The lower detection limit determined to be 6.74 ± 0.022 and 5.68 ± 0.025 CFU/mL for *S. aureus* and viable *Listeria* spp., respectively within 12 minutes. Finally, impedimetric aptamer based biosensor using DEP-EIS technique demonstrated that it was able to detect *Listeria monocytogenes*

179

bacteria ranging from 10 to 10^7 CFU/mL in an off-the-shelf product, vegetable broth, with the detection limit of 4.82 ± 0.01 CFU/mL within 12 min with one of the lowest detection limits and detection times reported to date.

In this study, real-time, highly sensitive, rapid and portable aptamer based biosensors demonstrated to detect *Listeria* spp. and could be used in future food safety applications replacing traditional methods such as total viable counts (TVC), enzyme-linked immunosorbent assay (ELISA), and polymerase chain reaction (PCR). These methods are considered to be long and time consuming. The developed biosensor could be implemented in field conditions to detect foodborne pathogens in food products to ensure food safety and to promote public health. The simple designing method of the aptasensor described in these studies could be easily modified to detect other foodborne pathogens by changing the aptamer specificity. The designed aptasensor offers another advantage of reusing the interdigitated microelectrodes array by simple cleaning steps to regenerate the IMEs for different measurements. Consequently, the developed aptasensors has the potential to be available at a competitive cost of any commercialized biosensor, making it feasible to be implemented in the food industry for rapid screening of foodborne pathogens.

CHAPTER VI

FUTURE RECOMMENDATIONS

Based on the findings in this research further improvement on the aptamer based biosensors could be achieved by addressing the following issues:

a) Cleaning procedures should be studied to remove the attached bacteria from the aptamer ligand sites coated on the surface of the interdigitated microelectrodes array without comprising the aptamer integrity. This would eliminate the need to coat the aptamer layer onto IMEs before each test. Also, the shelf-life and reusability of aptamer coated IMEs should be studied.

b) The behavior of 15 μm and 25 μm electrode gaps should be studied by improving the fabrication mask resolution to achieve these electrode gaps and by replacing current instrumentation set-up that would cover larger range of current to detect the changes at the electrode surface.

c) Further cleaning procedures using microfluidic device should be explored to remove the bacteria from the edges of the electrodes during the detection of interference and viable/non-viable studies and to reduce the number of steps to detect viable/non-viable and distinguish interferents.

d) The mixture sample of interferents including non-viable and *S. aureus* should be studied to understand whether applied DEP force attracts more viable or non-viable bacteria cells using the developed biosensor. The calibrations curved can be generated at different concentrations of viable and non-viable bacteria.

Validate the developed aptasensor response in terms of false positives and negatives.

e) The detection of foodborne pathogens could be expanded based on using the developed aptasensor by changing the specificity of the aptamers and test on other food samples should be studied to obtain more information on biosensor performance and validate its use in food safety applications.

f) The detection of multiple bacteria on one chip could be explored by developing multiplex biosensors using aptamers as a biorecognition element.

REFERENCES

Alocilja, E. C., & Radke, S. M. (2003). Market analysis of biosensors for food safety. *Biosensors and Bioelectronics, 18*(5), 841-846.

Anekwe, T. D., & Hoffmann, S. (2013). Recent estimates of the cost of foodborne illness are in general agreement. Available at: http://search.proquest.com/openview/275d6cb2fcd17b19d0fc482ff636f4b6/1?pq-origsite=gscholar

Arora, P., Sindhu, A., Dilbaghi, N., & Chaudhury, A. (2011). Biosensors as innovative tools for the detection of food borne pathogens. *Biosensors and Bioelectronics, 28*(1), 1-12.

Artault, S., Blind, J., Delaval, J., Dureuil, Y., & Gaillard, N. (2001). Detecting *Listeria monocytogenes* in food. *International Food Hygiene, 12*(3), 23.

Babacan, S., Pivarnik, P., Letcher, S., & Rand, A. (2002). Piezoelectric flow injection analysis biosensor for the detection of *Salmonella typhimurium*. *Journal of Food Science, 67*(1), 314-320.

Balamurugan, S., Obubuafo, A., Soper, S. A., & Spivak, D. A. (2008). Surface immobilization methods for aptamer diagnostic applications. *Analytical and Bioanalytical Chemistry, 390*(4), 1009-1021.

Bierne, H., Sabet, C., Personnic, N., & Cossart, P. (2007). Internalins: a complex family of leucine-rich repeat-containing proteins in *Listeria monocytogenes*. *Microbes and Infection, 9*(10), 1156-1166.

Buzrul, S., & Alpas, H. (2004). Modeling the synergistic effect of high pressure and heat on inactivation kinetics of *Listeria innocua*: a preliminary study. *FEMS Microbiology Letters, 238*(1), 29-36.

Cartwright, E. J., Jackson, K. A., Johnson, S. D., Graves, L. M., Silk, B. J., & Mahon, B. E. (2013). *Listeriosis* outbreaks and associated food vehicles, United States, 1998–2008. *Emerging Infectious Disease, 19*(1), 1-9.

Centers for Disease Control and Prevention (CDC). (2011a). Multistate outbreak of *Listeriosis* linked to whole cantaloupes from Jensen Farms, Colorado. Available at: http://www.cdc. gov/listeria/outbreaks/cantaloupes-jensen-farms/082712/index. html

Centers for Disease Control and Prevention (CDC). (2011b). Surveillance for foodborne disease outbreaks--United States, 2008. *Morbidity and Mortality Weekly Report, 60*(35), 1197.

Centers for Disease Control and Prevention (CDC). (2013a). Incidence and trends of infection with pathogens transmitted commonly through food-foodborne diseases active surveillance network, 10 US sites, 1996-2012. *Morbidity and Mortality Weekly Report, 62*(15), 283.

Centers for Disease Control and Prevention (CDC). (2013b). Trends in foodborne illness in the United States. Available at: http://www.cdc.gov/Features/dsfoodsafetyreport/

Centers for Disease Control and Prevention (CDC). (2014a). Multistate outbreak of *Listeriosis* linked to Roos Foods dairy products (final update). Available at: http://www.cdc.gov/listeria/outbreaks/cheese-02-14/

Centers for Disease Control and Prevention (CDC). (2014b). Oasis Brands, Inc. cheese recalls and investigation of human *Listeriosis* cases (final update). Available at: http://www.cdc.gov/listeria/outbreaks/cheese-10-14/index.html

Centers for Disease Control and Prevention (CDC). (2015a). Multistate outbreak of *Listeriosis* linked to Blue Bell creameries products. Available at: http://www.cdc.gov/listeria/outbreaks/ice-cream-03-15/

Centers for Disease Control and Prevention (CDC). (2015b). Multistate outbreak of *Listeriosis* linked to commercially produced, prepackaged caramel apples made from Bidart Bros. Apples (final update). Available at: http://www.cdc.gov/listeria/outbreaks/caramel-apples-12-14/

Centers for Disease Control and Prevention (CDC). (2015c). Multistate outbreak of *Listeriosis* linked to soft cheeses distributed by Karoun Dairies, Inc. Available at: http://www.cdc.gov/listeria/outbreaks/soft-cheeses-09-15/

Centers for Disease Control and Prevention (CDC). (2015d). Wholesome Soy Products, Inc. sprouts and investigation of human *Listeriosis* cases (final update). Available at: http://www.cdc.gov/listeria/outbreaks/bean-sprouts-11-14/index.html

Chaturvedi, P., Vanegas, D., Taguchi, M., Burrs, S., Sharma, P., & McLamore, E. (2014). A nanoceria–platinum–graphene nanocomposite for electrochemical biosensing. *Biosensors and Bioelectronics, 58*, 179-185.

Chemburu, S., Wilkins, E., & Abdel-Hamid, I. (2005). Detection of pathogenic bacteria in food samples using highly-dispersed carbon particles. *Biosensors and Bioelectronics, 21*(3), 491-499.

Cheng, I.-F., Chang, H.-C., Hou, D., & Chang, H.-C. (2007). An integrated dielectrophoretic chip for continuous bioparticle filtering, focusing, sorting, trapping, and detecting. *Biomicrofluidics, 1*(2), 021503.

CH Instruments Model 600E Series User Manual. (2014). *Model 600E Series Electrochemical Analyzer/Workstation*. CH Instruments, Inc. Austin, TX.

Cohen, A. E., & Kunz, R. R. (2000). Large-area interdigitated array microelectrodes for electrochemical sensing. *Sensors and Actuators B: Chemical, 62*(1), 23-29.

Cunningham, A. (1998). *Introduction to Bioanalytical Sensors*. United States of America: John Wiley & Sons, Inc.

Daniels, J. S., & Pourmand, N. (2007). Label-free impedance biosensors: opportunities and challenges. *Electroanalysis, 19*(12), 1239-1257.

Dastider, S. G., Barizuddin, S., Dweik, M., & Almasri, M. (2013). A micromachined impedance biosensor for accurate and rapid detection of *E. coli* O157: H7. *Royal Society of Chemistry Advances, 3*(48), 26297-26306.

Dong, Y., Xu, Y., Yong, W., Chu, X., & Wang, D. (2014). Aptamer and its potential applications for food safety. *Critical Reviews in Food Science and Nutrition, 54*(12), 1548-1561.

Duncan, T. V. (2011). Applications of nanotechnology in food packaging and food safety: barrier materials, antimicrobials and sensors. *Journal of Colloid and Interface Science, 363*(1), 1-24.

Dutse, S. W., & Yusof, N. A. (2011). Microfluidics-based lab-on-chip systems in DNA-based biosensing: an overview. *Sensors, 11*(6), 5754-5768.

Elzanowska, H., Abu-Irhayem, E., Skrzynecka, B., & Birss, V. I. (2004). Hydrogen peroxide detection at electrochemically and sol-gel derived Ir oxide films. *Electroanalysis, 16*(6), 478-490.

Ercole, C., Del Gallo, M., Mosiello, L., Baccella, S., & Lepidi, A. (2003). *Escherichia coli* detection in vegetable food by a potentiometric biosensor. *Sensors and Actuators B: Chemical, 91*(1), 163-168.

Fan, X., White, I. M., Shopova, S. I., Zhu, H., Suter, J. D., & Sun, Y. (2008). Sensitive optical biosensors for unlabeled targets: a review. *Analytica Chimica Acta, 620*(1), 8-26.

Fortineau, N., Trieu-Cuot, P., Gaillot, O., Pellegrini, E., Berche, P., & Gaillard, J.-L. (2000). Optimization of green fluorescent protein expression vectors for in vitro and in vivo detection of *Listeria monocytogenes*. *Research in Microbiology, 151*(5), 353-360.

Gamry Instruments Application Note. (2015). Basics of electrochemical impedance spectroscopy. Available at: http://www.gamry.com/application-notes/EIS/basics-of-electrochemical-impedance-spectroscopy/

Gandhi, M., & Chikindas, M. L. (2007). *Listeria*: a foodborne pathogen that knows how to survive. *International Journal of Food Microbiology, 113*(1), 1-15.

GeneLink. (2004). *Oligo Reconstitution*. Available at: http://www.genelink.com/Literature/ps/R26-6400-XXA.pdf

GeneLink. (2011). *Thiol Modified Oligo Disulfide Reduction Protocol*. Available at: http://www.genelink.com/Literature/ps/Thiol_Oligo_reduction_V2.1_PT26-6419.pdf

GeneLink. (2014). *Gold Solid Surface Thiol Oligo Conjugation*. Available at: http://www.genelink.com/Literature/ps/PS_Gold_Surface_Thiol_Conjugation_V2.2.pdf

Gómez-Sjöberg, R., Morisette, D. T., & Bashir, R. (2005). Impedance microbiology-on-a-chip: microfluidic bioprocessor for rapid detection of bacterial metabolism. *Journal of Microelectromechanical Systems, 14*(4), 829-838.

Gómez, R., Bashir, R., & Bhunia, A. K. (2002). Microscale electronic detection of bacterial metabolism. *Sensors and Actuators B: Chemical, 86*(2), 198-208.

Grieshaber, D., MacKenzie, R., Voeroes, J., & Reimhult, E. (2008). Electrochemical biosensors-sensor principles and architectures. *Sensors, 8*(3), 1400-1458.

Hoffman, A. D., Gall, K. L., Norton, D. M., & Wiedmann, M. (2003). *Listeria monocytogenes* contamination patterns for the smoked fish processing environment and for raw fish. *Journal of Food Protection, 66*(1), 52-60.

Iliuk, A. B., Hu, L., & Tao, W. A. (2011). Aptamer in bioanalytical applications. *Analytical Chemistry, 83*(12), 4440-4452.

Kärkkäinen, R. M., Drasbek, M. R., McDowall, I., Smith, C. J., Young, N. W., & Bonwick, G. A. (2011). Aptamers for safety and quality assurance in the food industry: detection of pathogens. *International Journal of Food Science & Technology, 46*(3), 445-454.

Kim, S. K., Hesketh, P. J., Li, C., Thomas, J. H., Halsall, H. B., & Heineman, W. R. (2004). Fabrication of comb interdigitated electrodes array (IDA) for a microbead-based electrochemical assay system. *Biosensors and Bioelectronics, 20*(4), 887-894.

Kissinger, P. T., & Heineman, W. R. (1983). Cyclic voltammetry. *Journal of Chemical Education, 60*(9), 702.

Koo, O. K., Liu, Y., Shuaib, S., Bhattacharya, S., Ladisch, M. R., Bashir, R., & Bhunia, A. K. (2009). Targeted capture of pathogenic bacteria using a mammalian cell receptor coupled with dielectrophoresis on a biochip. *Analytical Chemistry, 81*(8), 3094-3101.

Labib, M., Zamay, A. S., Kolovskaya, O. S., Reshetneva, I. T., Zamay, G. S., Kibbee, R. J., . . . Berezovski, M. V. (2012). Aptamer-based impedimetric sensor for bacterial typing. *Analytical Chemistry, 84*(19), 8114-8117.

Lasseter, T. L., Cai, W., & Hamers, R. J. (2004). Frequency-dependent electrical detection of protein binding events. *Analyst, 129*(1), 3-8.

Laureyn, W., Nelis, D., Van Gerwen, P., Baert, K., Hermans, L., Magnee, R., . . . Maes, G. (2000). Nanoscaled interdigitated titanium electrodes for impedimetric biosensing. *Sensors and Actuators B: Chemical, 68*(1), 360-370.

Lazcka, O., Del Campo, F. J., & Munoz, F. X. (2007). Pathogen detection: a perspective of traditional methods and biosensors. *Biosensors and Bioelectronics, 22*(7), 1205-1217.

Lee, C.-S., Kim, S. K., & Kim, M. (2009). Ion-sensitive field-effect transistor for biological sensing. *Sensors, 9*(9), 7111-7131.

Leonard, P., Hearty, S., Brennan, J., Dunne, L., Quinn, J., Chakraborty, T., & O'Kennedy, R. (2003). Advances in biosensors for detection of pathogens in food and water. *Enzyme and Microbial Technology, 32*(1), 3-13.

Leonard, P., Hearty, S., Quinn, J., & O'Kennedy, R. (2004). A generic approach for the detection of whole *Listeria monocytogenes* cells in contaminated samples using surface plasmon resonance. *Biosensors and Bioelectronics, 19*(10), 1331-1335.

Li, H., & Bashir, R. (2002). Dielectrophoretic separation and manipulation of live and heat-treated cells of *Listeria* on microfabricated devices with interdigitated electrodes. *Sensors and Actuators B: Chemical, 86*(2), 215-221.

Luo, C., Lei, Y., Yan, L., Yu, T., Li, Q., Zhang, D., . . . Ju, H. (2012). A rapid and sensitive aptamer-based electrochemical biosensor for direct detection of *Escherichia coli* O111. *Electroanalysis, 24*(5), 1186-1191.

Marker Gene Technologies, Inc. Product Information Sheet. (2015). *MarkerGene Live: Dead/Cytotoxity Assay Kit Product M0795*. Eugene, OR: Marker Gene Technologies, Inc.

Milillo, S. R., Friedly, E. C., Saldivar, J. C., Muthaiyan, A., O'bryan, C., Crandall, P. G., . . . Ricke, S. C. (2012). A review of the ecology, genomics, and stress response of *Listeria innocua* and *Listeria monocytogenes*. *Critical Reviews in Food Science and Nutrition, 52*(8), 712-725.

Min, J., & Baeumner, A. J. (2004). Characterization and optimization of interdigitated ultramicroelectrode arrays as electrochemical biosensor transducers. *Electroanalysis, 16*(9), 724-729.

Muhammad-Tahir, Z., & Alocilja, E. C. (2003). Fabrication of a disposable biosensor for *Escherichia coli* O157: H7 detection. *IEEE Sensors Journal, 3*(4), 345-351.

Murphy, N., McLauchlin, J., Ohai, C., & Grant, K. (2007). Construction and evaluation of a microbiological positive process internal control for PCR-based examination of food samples for *Listeria monocytogenes* and *Salmonella enterica*. *International Journal of Food Microbiology, 120*(1), 110-119.

Nayak, M., Kotian, A., Marathe, S., & Chakravortty, D. (2009). Detection of microorganisms using biosensors—a smarter way towards detection techniques. *Biosensors and Bioelectronics, 25*(4), 661-667.

Ogata, K. (2010). *Modern Control Engineering* (5th ed.)*.* Upper Saddle River, N.J.: Prentice Hall.

Ohk, S., Koo, O., Sen, T., Yamamoto, C., & Bhunia, A. (2010). Antibody–aptamer functionalized fibre-optic biosensor for specific detection of *Listeria monocytogenes* from food. *Journal of Applied Microbiology, 109*(3), 808-817.

Park, S., Zhang, Y., Wang, T.-H., & Yang, S. (2011). Continuous dielectrophoretic bacterial separation and concentration from physiological media of high conductivity. *Lab on a Chip, 11*(17), 2893-2900.

Prodromidis, M. I. (2010). Impedimetric immunosensors—a review. *Electrochimica Acta, 55*(14), 4227-4233.

Radke, S. M., & Alocilja, E. C. (2004). Design and fabrication of a microimpedance biosensor for bacterial detection. *IEEE Sensors Journal, 4*(4), 434-440.

Radke, S. M., & Alocilja, E. C. (2005a). A high density microelectrode array biosensor for detection of *E. coli* O157: H7. *Biosensors and Bioelectronics, 20*(8), 1662-1667.

Radke, S. M., & Alocilja, E. C. (2005b). A microfabricated biosensor for detecting foodborne bioterrorism agents. *IEEE Sensors Journal, 5*(4), 744-750.

Rahimi, M., & Mikkelsen, S. R. (2011). Cyclic biamperometry at micro-interdigitated electrodes. *Analytical Chemistry, 83*(19), 7555-7559.

Schlech, W. F., & Acheson, D. (2000). Foodborne *Listeriosis*. *Clinical Infectious Diseases, 31*(3), 770-775.

Shangguan, D., Tang, Z., Mallikaratchy, P., Xiao, Z., & Tan, W. (2007). Optimization and modifications of aptamers selected from live cancer cell lines. *ChemBioChem, 8*(6), 603-606.

Shearer, A. E., Strapp, C. M., & Joerger, R. D. (2001). Evaluation of a polymerase chain reaction-based system for detection of *Salmonella enteritidis*, *Escherichia coli* O157: H7, *Listeria* spp., and *Listeria monocytogenes* on fresh fruits and vegetables. *Journal of Food Protection, 64*(6), 788-795.

Shi, J., McLamore, E. S., Jaroch, D., Claussen, J. C., Mirmira, R. G., Rickus, J. L., & Porterfield, D. M. (2011). Oscillatory glucose flux in INS 1 pancreatic β cells: a self-referencing microbiosensor study. *Analytical Biochemistry, 411*(2), 185-193.

Song, S., Wang, L., Li, J., Fan, C., & Zhao, J. (2008). Aptamer-based biosensors. *TrAC Trends in Analytical Chemistry, 27*(2), 108-117.

Stephan, R., Schumacher, S., & Zychowska, M. A. (2003). The VIT® technology for rapid detection of *Listeria monocytogenes* and other *Listeria* spp. *International Journal of Food Microbiology, 89*(2), 287-290.

Stoltenburg, R., Reinemann, C., & Strehlitz, B. (2007). SELEX—a (r)evolutionary method to generate high-affinity nucleic acid ligands. *Biomolecular Engineering, 24*(4), 381-403.

Stulík, K., Amatore, C., Holub, K., Marecek, V., & Kutner, W. (2000). Microelectrodes: definitions, characterization, and applications (technical report). *Pure and Applied Chemistry, 72*(8), 1483-1492.

Su, X.-L., & Li, Y. (2004). A self-assembled monolayer-based piezoelectric immunosensor for rapid detection of *Escherichia coli* O157: H7. *Biosensors and Bioelectronics, 19*(6), 563-574.

Suehiro, J., Hamada, R., Noutomi, D., Shutou, M., & Hara, M. (2003). Selective detection of viable bacteria using dielectrophoretic impedance measurement method. *Journal of Electrostatics, 57*(2), 157-168.

Suehiro, J., Hatano, T., Shutou, M., & Hara, M. (2005). Improvement of electric pulse shape for electropermeabilization-assisted dielectrophoretic impedance

measurement for high sensitive bacteria detection. *Sensors and Actuators B: Chemical, 109*(2), 209-215.

Suehiro, J., Noutomi, D., Shutou, M., & Hara, M. (2003). Selective detection of specific bacteria using dielectrophoretic impedance measurement method combined with an antigen–antibody reaction. *Journal of Electrostatics, 58*(3), 229-246.

Suehiro, J., Ohtsubo, A., Hatano, T., & Hara, M. (2006). Selective detection of bacteria by a dielectrophoretic impedance measurement method using an antibody-immobilized electrode chip. *Sensors and Actuators B: Chemical, 119*(1), 319-326.

Thévenot, D. R., Toth, K., Durst, R. A., & Wilson, G. S. (2001). Electrochemical biosensors: recommended definitions and classification. *Biosensors and Bioelectronics, 16*(1), 121-131.

Tokarskyy, O., & Marshall, D. L. (2008). Immunosensors for rapid detection of *Escherichia coli* O157: H7—perspectives for use in the meat processing industry. *Food Microbiology, 25*(1), 1-12.

Tolba, M., Ahmed, M. U., Tlili, C., Eichenseher, F., Loessner, M. J., & Zourob, M. (2012). A bacteriophage endolysin-based electrochemical impedance biosensor for the rapid detection of *Listeria* cells. *Analyst, 137*(24), 5749-5756.

Torres-Chavolla, E., & Alocilja, E. C. (2009). Aptasensors for detection of microbial and viral pathogens. *Biosensors and Bioelectronics, 24*(11), 3175-3182.

Van Benschoten, J. J., Lewis, J. Y., Heineman, W. R., Roston, D. A., & Kissinger, P. T. (1983). Cyclic voltammetry experiment. *Journal of Chemical Education, 60*(9), 772.

Vanegas, D. C., Taguchi, M., Chaturvedi, P., Burrs, S., Tan, M., Yamaguchi, H., & McLamore, E. S. (2014). A comparative study of carbon–platinum hybrid nanostructure architecture for amperometric biosensing. *Analyst, 139*(3), 660-667.

Varshney, M., & Li, Y. (2007). Interdigitated array microelectrode based impedance biosensor coupled with magnetic nanoparticle–antibody conjugates for detection of *Escherichia coli* O157: H7 in food samples. *Biosensors and Bioelectronics, 22*(11), 2408-2414.

Varshney, M., & Li, Y. (2009). Interdigitated array microelectrodes based impedance biosensors for detection of bacterial cells. *Biosensors and Bioelectronics, 24*(10), 2951-2960.

Varshney, M., Li, Y., Srinivasan, B., & Tung, S. (2007). A label-free, microfluidics and interdigitated array microelectrode-based impedance biosensor in combination with nanoparticles immunoseparation for detection of *Escherichia coli* O157: H7 in food samples. *Sensors and Actuators B: Chemical, 128*(1), 99-107.

Velusamy, V., Arshak, K., Korostynska, O., Oliwa, K., & Adley, C. (2010). An overview of foodborne pathogen detection: In the perspective of biosensors. *Biotechnology Advances, 28*(2), 232-254.

Wang. (2001). Glucose biosensors: 40 years of advances and challenges. *Electroanalysis, 13*(12), 983.

Wang, He, M., & Shi, H.-C. (2007). Novel indirect enzyme-linked immunosorbent assay (ELISA) method to detect total *E. coli* in water environment. *Analytica Chimica Acta, 590*(2), 224-231.

Wang, J. (2006). *Analytical Electrochemistry* (3rd ed.). Hoboken, N.J.: John Wiley & Sons, Inc.

Wang, R., Ruan, C., Kanayeva, D., Lassiter, K., & Li, Y. (2008). TiO_2 nanowire bundle microelectrode based impedance immunosensor for rapid and sensitive detection of *Listeria monocytogenes*. *Nano Letters, 8*(9), 2625-2631.

Wang, Y., Ye, Z.,Ying, Y. (2012). New trends in impedimetric biosensors for the detection of foodborne pathogenic bacteria. *Sensors, 12*(3), 3449-3471. doi: 10.3390/s120303449

Wu, W., Zhang, J., Zheng, M., Zhong, Y., Yang, J., Zhao, Y., . . . Wang, Q. (2012). An aptamer-based biosensor for colorimetric detection of *Escherichia coli* O157: H7. *Public Library of Science One, 7(11)*, e48999. doi:10.1371/journal.pone.0048999

Yang, L. (2009). Dielectrophoresis assisted immuno-capture and detection of foodborne pathogenic bacteria in biochips. *Talanta, 80*(2), 551-558.

Yang, L. (2012). A review of multifunctions of dielectrophoresis in biosensors and biochips for bacteria detection. *Analytical Letters, 45*(2-3), 187-201.

Yang, L., Banada, P. P., Chatni, M. R., Lim, K. S., Bhunia, A. K., Ladisch, M., & Bashir, R. (2006). A multifunctional micro-fluidic system for dielectrophoretic concentration coupled with immuno-capture of low numbers of *Listeria monocytogenes*. *Lab on a Chip, 6*(7), 896-905.

Yang, L., & Bashir, R. (2008). Electrical/electrochemical impedance for rapid detection of foodborne pathogenic bacteria. *Biotechnology Advances, 26*(2), 135-150.

Yang, L., & Li, Y. (2005). AFM and impedance spectroscopy characterization of the immobilization of antibodies on indium–tin oxide electrode through self-assembled monolayer of epoxysilane and their capture of *Escherichia coli* O157: H7. *Biosensors and Bioelectronics, 20*(7), 1407-1416.

Yang, L., Li, Y., & Erf, G. F. (2004a). Interdigitated array microelectrode-based electrochemical impedance immunosensor for detection of *Escherichia coli* O157: H7. *Analytical Chemistry, 76*(4), 1107-1113.

Yang, L., Li, Y., Griffis, C. L., & Johnson, M. G. (2004b). Interdigitated microelectrode (IME) impedance sensor for the detection of viable *Salmonella typhimurium*. *Biosensors and Bioelectronics, 19*(10), 1139-1147.

Yoon, J.-Y., & Kim, B. (2012). Lab-on-a-chip pathogen sensors for food safety. *Sensors, 12*(8), 10713-10741.

Zhang, X., & Yadavalli, V. K. (2011). Surface immobilization of DNA aptamers for biosensing and protein interaction analysis. *Biosensors and Bioelectronics, 26*(7), 3142-3147.

Zoski, C. G. (2006). *Handbook of Electrochemistry* (1st ed.). Amsterdam, The Netherlands: Elsevier.

APPENDIX A

PROJECT TIMELINE
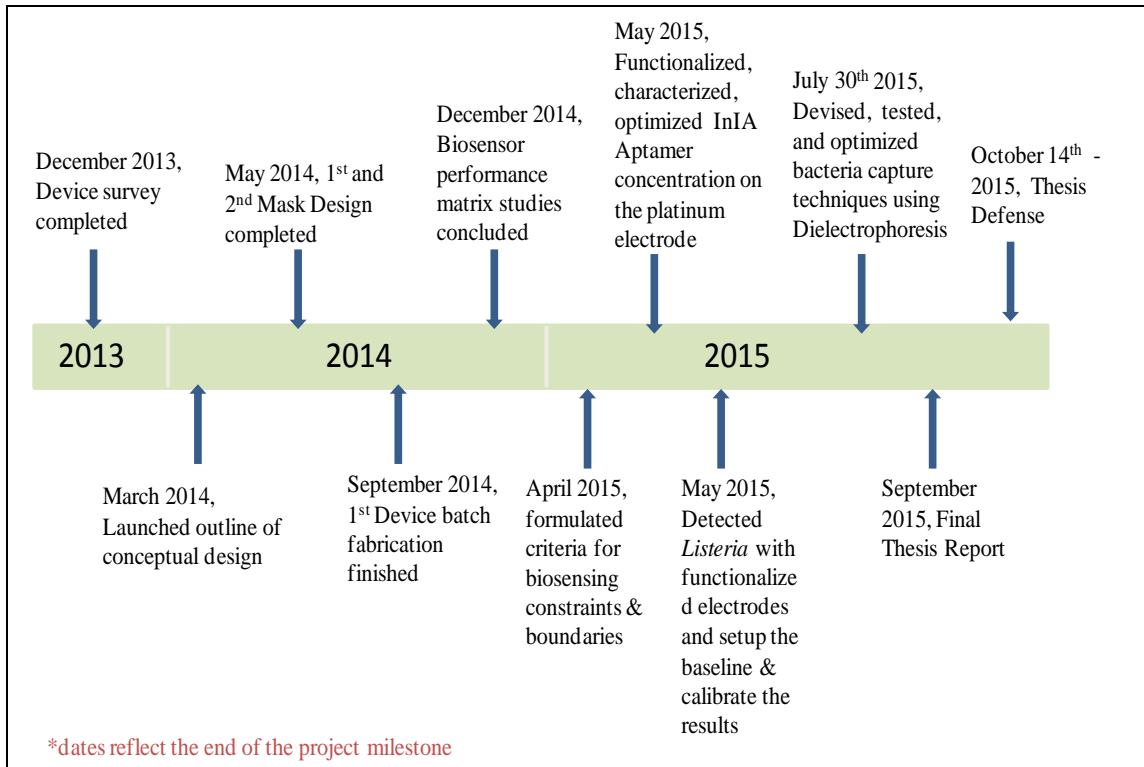
Figure A.1. Project milestones.

APPENDIX B

DUAL LAYER LIFT OFF PROCESS

Purpose
Dual layer lift off process provides cleaner process with fine resolution as compared to standard lift-off process for depositing thin layer of metals.

Equipment
1. Photoresist Spinner and Hotplate
2. Karl Suss MA6 Mask Aligner
3. Lesker PVD 75 Ebeam Evap

Materials
1. LOR 3A: Non UV sensitive polymer
2. AZ 5214 E: Positive photoresist
3. AZ 726 MIF: Standard photoresist developer
4. AZ 400T: Photoresist Stripper
5. Metals: Chromium (Cr) and platinum (Pt)

Process
1. Substrate Preparation:
    a. Clean the glass substrate with piranha solution with 3:1 ratio. Keep the substrate in the solution for 30 minutes to 1 hour and run it under DI water for 5-10 minutes.
    b. Dry the substrate with N_2 gun and then place it on the hotplate at 150ºC for 10 minutes.

2. Spin-coat LOR 3A:
    a. Coat the substrate with LOR 3A. Make sure to center the wafer and avoid any bubbles while dispensing the material to get a uniform coating.
    b. Dispense 5ml of LOR 3A and follow the process parameters in Table B.1.

Table B.1. Process details for LOR 3A

Thickness	1µm
Spin Speed	2000 rpm for 40 secs
Soft Bake	165 °C for 8 mins on a hot plate

3. Remove the wafer from the hot plate and let it cool before proceeding to the next step.

4. Spin-coat AZ 5214E
   a. Continue coating with AZ 5214E on top of LOR 3A layer and follow the process parameters in Table B.2.

Table B.2. Process parameters for AZ 5214E

Thickness	1.3µm
Spin Speed	4000 rpm for 45 secs
Soft Bake	110 °C for 2mins
Exposure	90 mJ/cm^2 (25 secs) soft contact
Develop	Agitate in AZ 720 MIF developer for 3 mins. Then run the substrate under DI water for 1 minute and dry with N_2 gun
Descuum	O_2 plasma for 5secs at 200W with 4% oxygen flow rate or 150 Torr

5. Deposit the metals using a PVD 75 E-beam evaporator. The thickness of Cr is 15nm at 0.3Å/s and Pt is 90nm at 0.5 Å/s. Follow the detailed procedure for the PVD 75 in the operator's manual and parameters are discussed in Appendix B of this document.

6. Lift-off in AZ 400T at 60°C on the hotplate for about 30 mins. Make sure to agitate the solution and rinse the wafer thoroughly once the lift-off process is done.

7. Inspect the wafer under the microscope to ensure proper metal lift-off from the patterns. If there is any remaining resist, put the wafer in the resist remover.

APPENDIX C

METAL DEPOSITION – E-BEAM EVAPORATOR

Metal Deposition – Lesker PVD 75 E-beam Evaporator

Purpose

Thin film layer metal deposition is used by e-beam evaporation. This appendix describes

the parameters used for silicon substrate for the Lesker PVD 75.

Material and equipment

1) Platinum pellets, Pt, 99.99% pure
2) Titanium
3) Patterned 4 inch silicon wafer
4) Kapton tape
5) Crucible

Process

1. Log into the machine and in the logbook.

2. Start PC vent or run recipe and PC vent. Making sure HV for E beam should be off while venting.

3. Run "Load Unload" recipe to open the e-beam and substrate shutter. The shutters for the e-beam and substrate will open, and the substrate holder will rotate to the home position to enable removal from the rotation rod.

4. Discharge unsafe charge around the e-gun using ground rod.

5. Load the patterned wafers by removing the substrate holder plate at the top of the vacuum chamber.

6. Load the wafers onto the substrate holder with the screw-down clips and Kapton tape making sure the sample do not fall when the holder plate upside down.

7. After fixing the wafers onto the holder plate, load substrate holder plate and samples into vacuum chamber.

8. Change or load crucible(s) with platinum and titanium. The crucible indexer will not work when the chamber is open while it is in the default auto mode.

a. Use manual mode to select the crucible position to change or refill the metal pellets.
   b. Use pocket 2 to load titanium and pocket 3 for platinum.
   c. Use care to avoid touching any e-gun surfaces while loading the new crucible.
   d. Inspect the condition of all crucibles before running the recipe. Do not use if the crucibles are cracked, or have holes in them to avoid overheating of the gun. With the crucible removed, inspect the copper surfaces of the e-gun for contamination or damage. Immediately notify a staff person if there is any damage or contamination of the e-gun, or if a new crucible is needed.
   e. When all crucibles have been loaded, rotate the e-gun pockets back to the original crucible using manual mode and then change to auto mode. Now the crucible indexer will automatically adjust the position.
   f. Change any labels in the e-gun software to properly identify the materials in each pocket/crucible. Change P2 to titanium and P3 to platinum.

9. Check the film thickness sensor 1 in the software under "View – Sensor Settings." If life is less than 40% then change the crystal.

10. Close the chamber.

11. Start "PC Pump" recipe on the main vacuum menu screen to begin evacuation pump.

12. Roughing pump will automatically start the evacuation process followed by the turbo pump as the pressure drops.

13. Select a process run recipe for metal deposition once the chamber pressure reaches 5×10^{-6} Torr.

14. Set substrate temperature to 25°C.

15. Select "P2 Ti rotation" recipe and open the Sigma software (SQP) to set the deposition rate and other parameters.

16. Select Ti process and film in SQP.

17. Edit Deposition Process: Set Point (rate): 1 Å/S; Final thickness : 0.150 kÅ; Set Sensor Tooling : 120%

18. Set the gun profile parameters: Melt power to 15% and Deposition power to 10%.

19. Close the SQP software after setting all the process changes.

20. Press "Run Recipe"

21. After the deposition of titanium is done, follow steps from 15 through 20 to deposit platinum film without breaking the vacuum.

22. Select "P3 Pt rotation" recipe and set Pt process and film in SQP.

23. Edit Deposition Process: Set Point (rate): 0.6 Å/S; Final thickness : 1 kÅ; Set Sensor Tooling : 120%

24. Set the gun profile parameters: Melt power to 30% and Deposition power to 40%.

25. Press "Run Recipe."

26. Once the deposition of two metals is done, vent the chamber to unload the samples.

27. Run "Load Unload" recipe to vent the chamber.

28. Discharge unsafe charge and make sure the substrate holder plate is not hot before removing the samples. If the plate is hot, wait 10-15 minutes.

29. Unload the substrate holder plate and remove the samples. Remove platinum crucible from the pocket.

30. Load the substrate holder plate and close the chamber.

31. Run post roughing process to pump down the chamber. Select "Roughing" recipe and press run recipe.

32. Leave system under rough down pressure and logout from the machine.

APPENDIX D

DIELECTROPHORESIS DYNAMIC

This appendix shows the results for 10 and 10^4 CFU/mL bacteria concentration for DEP

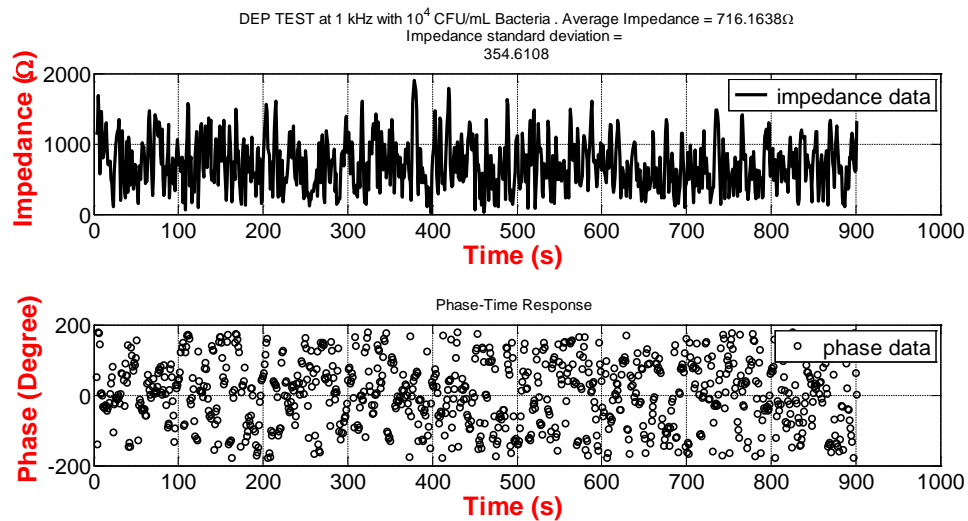impedance method characterization in section 5.4.2.
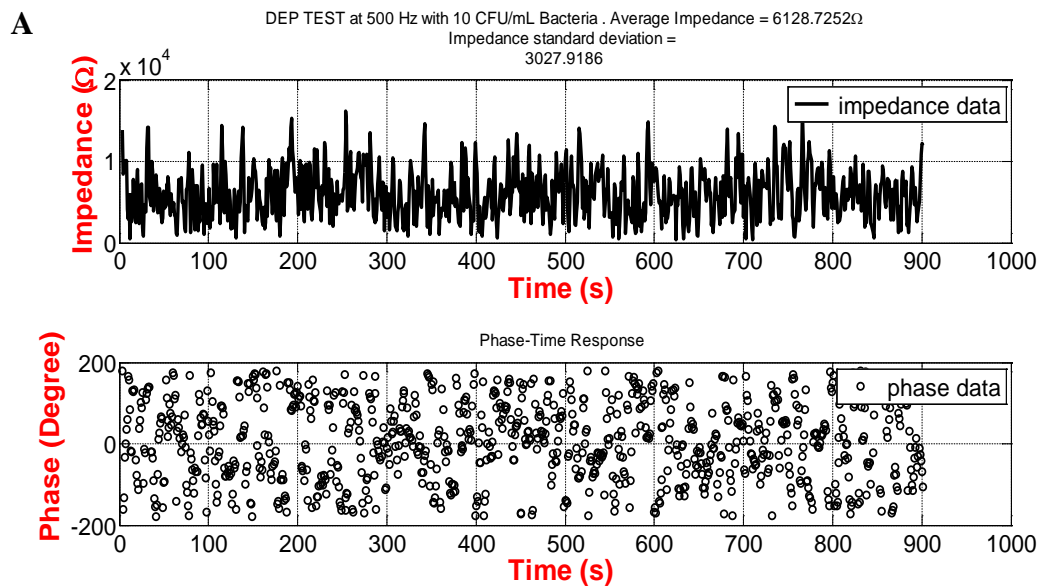
Figure D.1. Impedance versus time and phase versus time are shown at DEP frequencies of (A) 500 Hz, (B) 1 kHz, (C) 10 kHz, (D) 100 kHz, (E) 600 kHz, and (F) 1 MHz for *L. innocua* at a concentration of 10 CFU/mL.
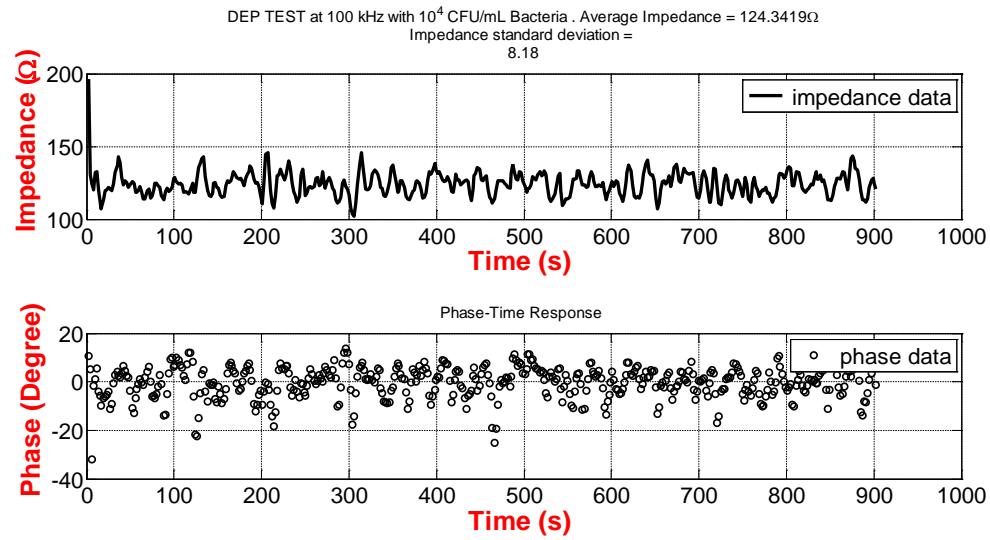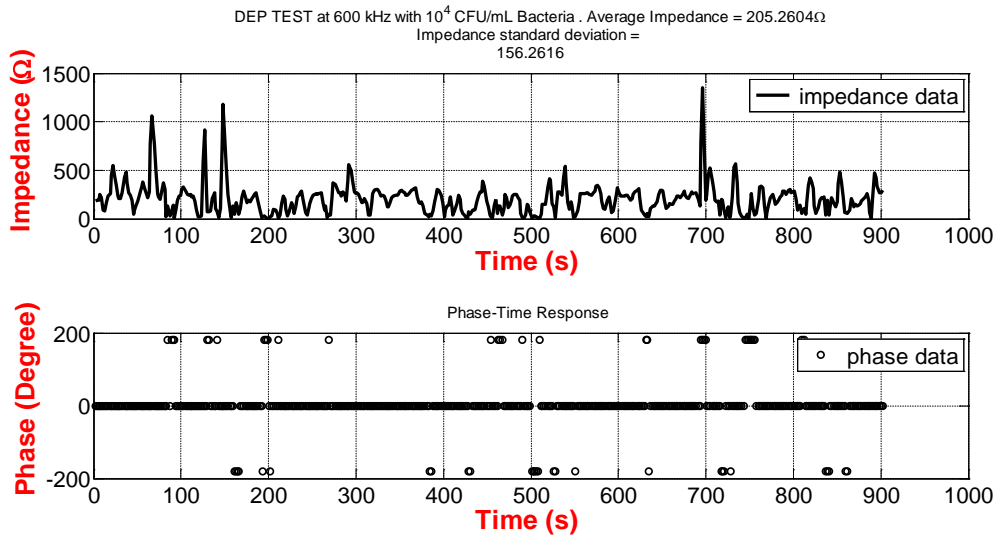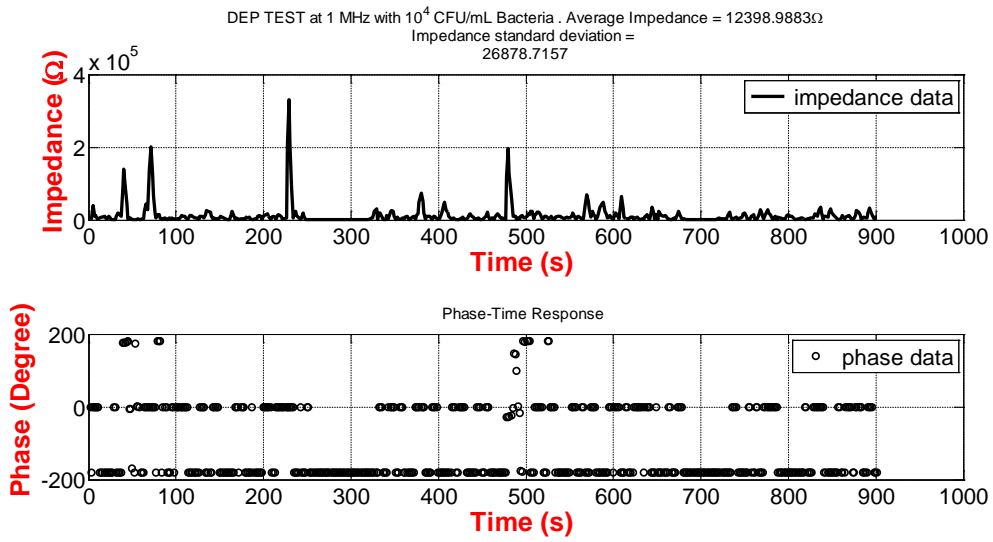
B
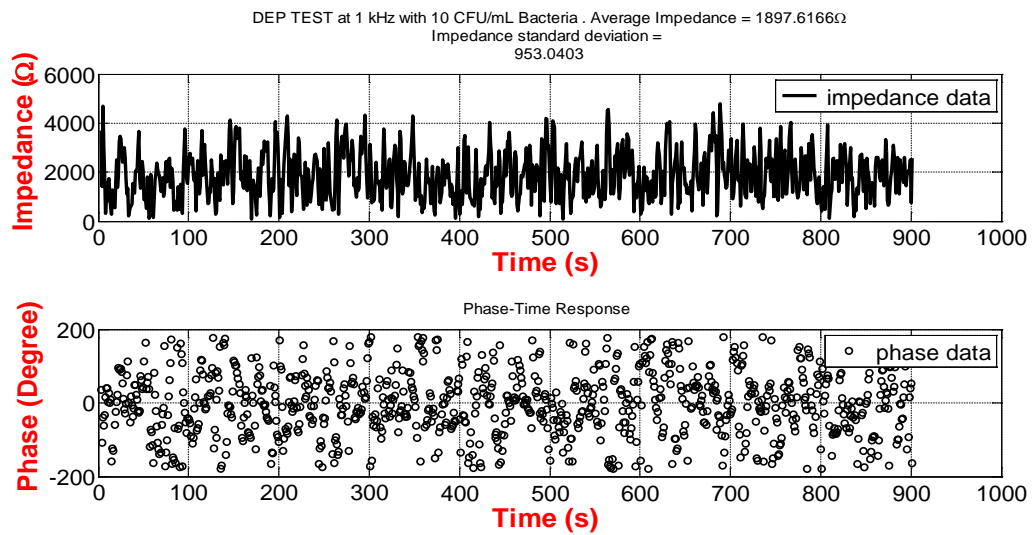
C
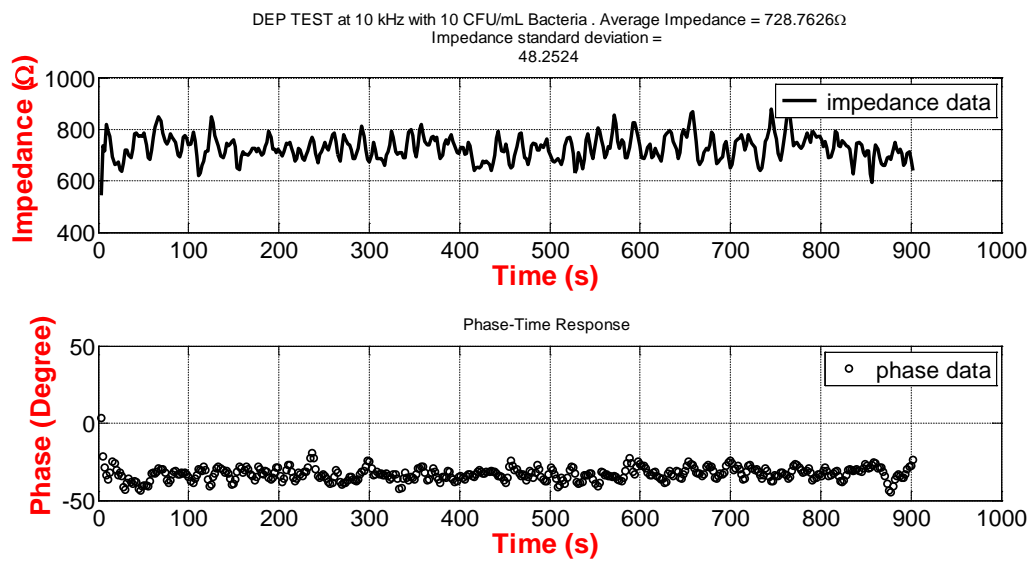
Figure D.1. Continued.

D
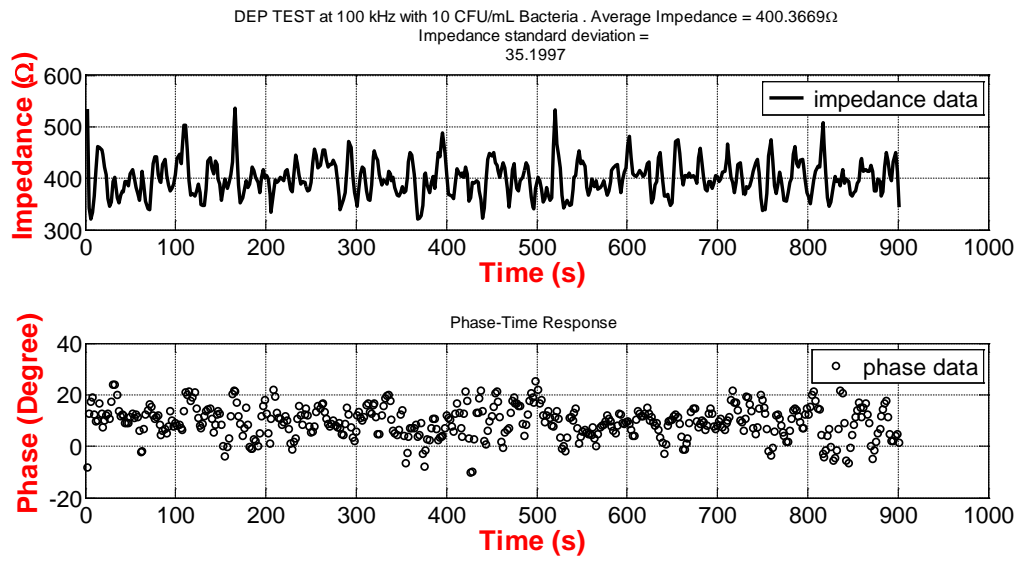
E
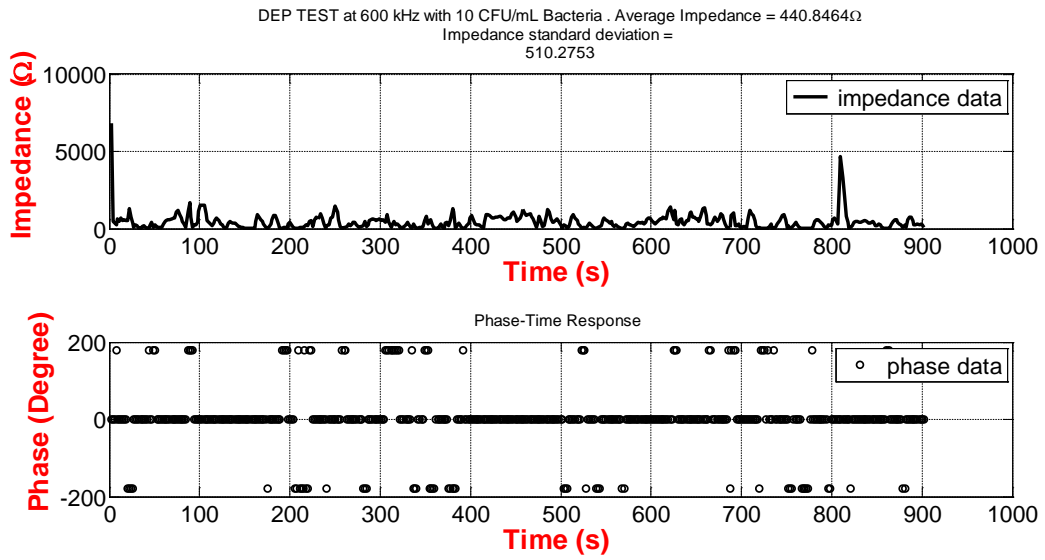
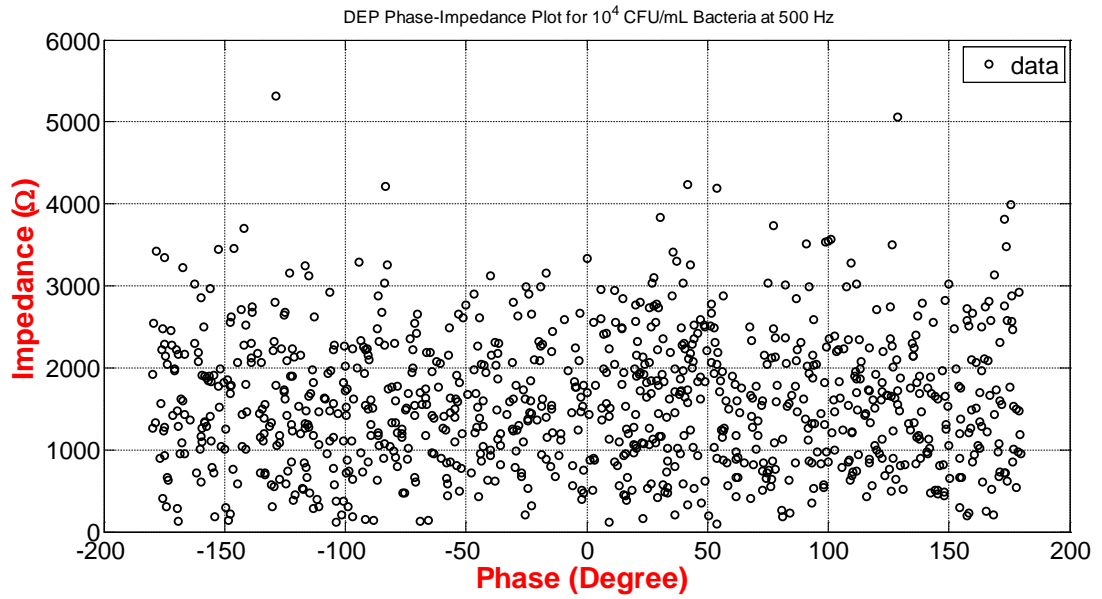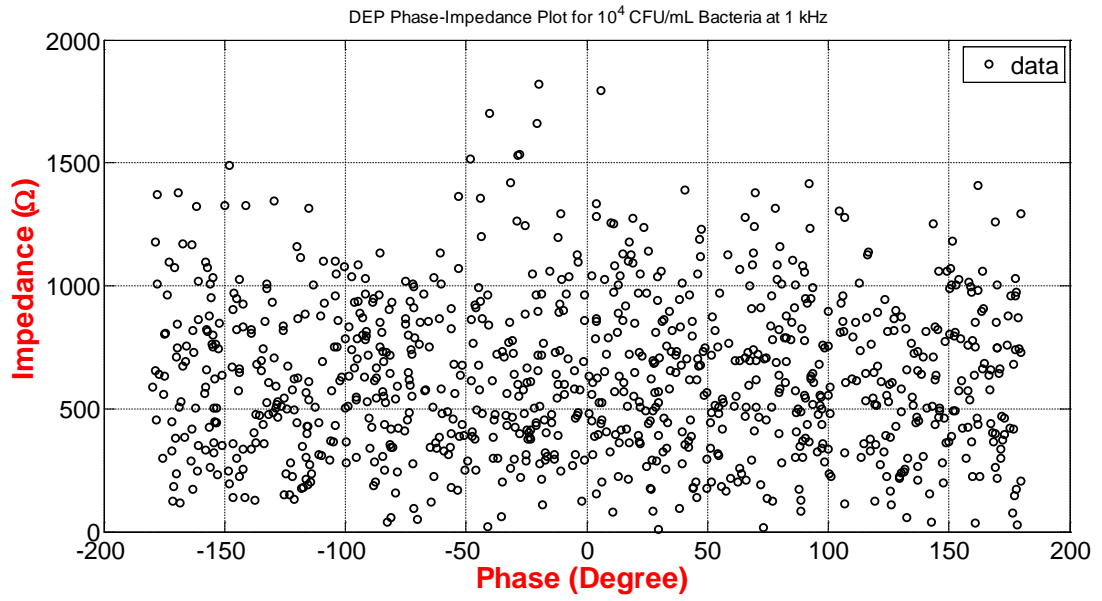Figure D.1. Continued.

F
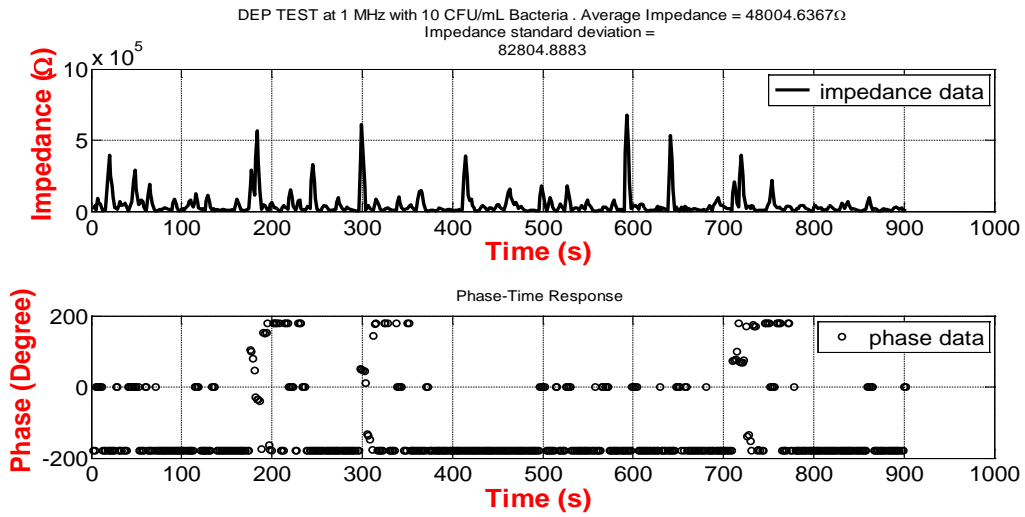
Figure D.1. Continued.

A
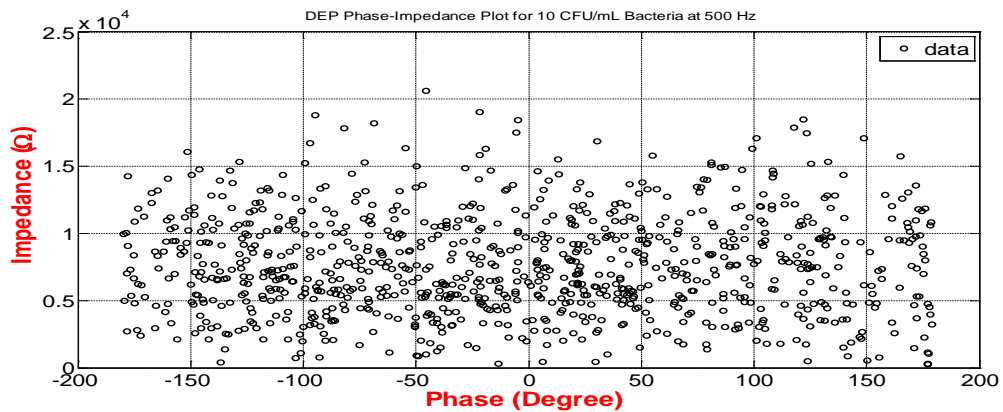
Figure D.2. Impedance versus phase are shown at (A) 500 Hz, (B) 1 kHz, (C) 10 kHz, (D) 100 kHz, (E) 600 kHz, and (F) 1 MHz DEP frequencies for *L. innocua* at a concentration of 10 CFU/mL. The legend data implies impedance data on the graph.

202

B
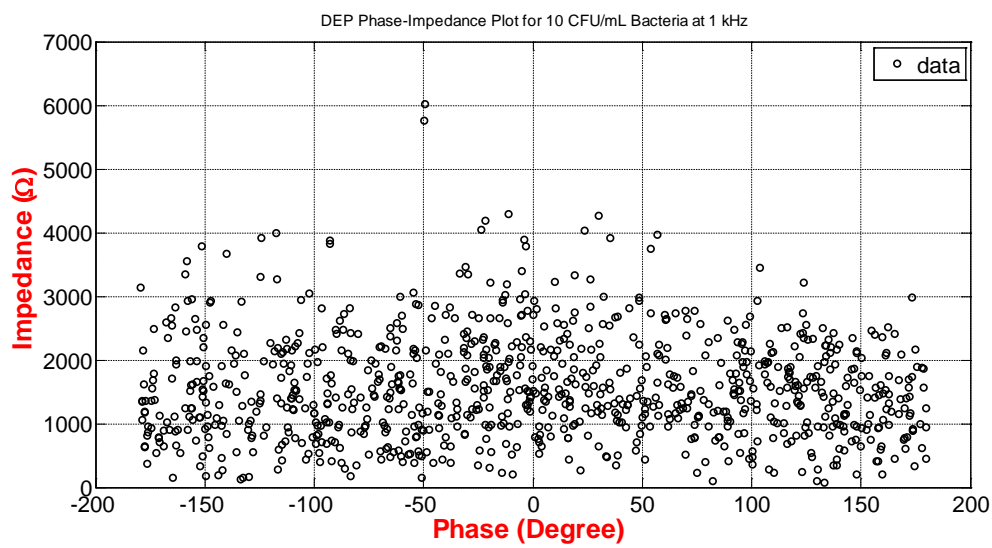
C
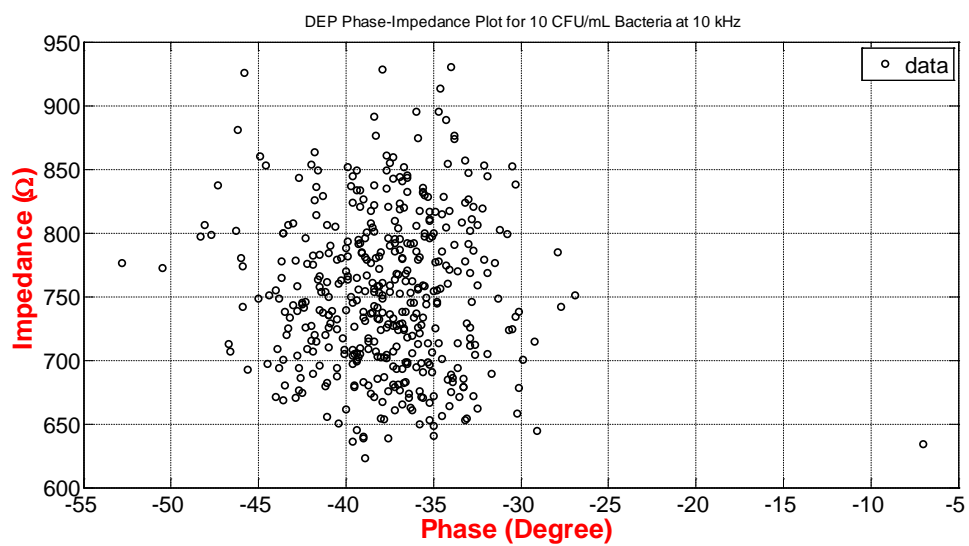
Figure D.2. Continued.

D
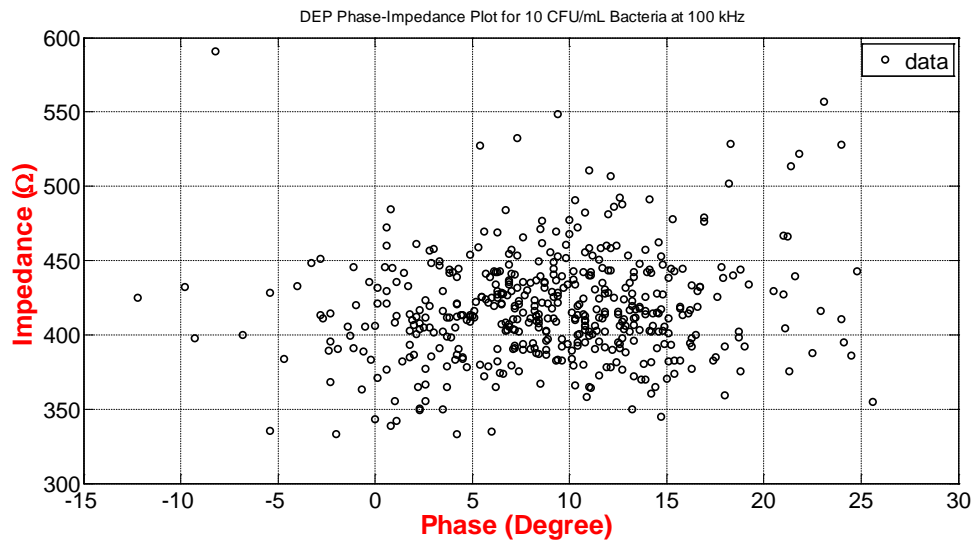
E
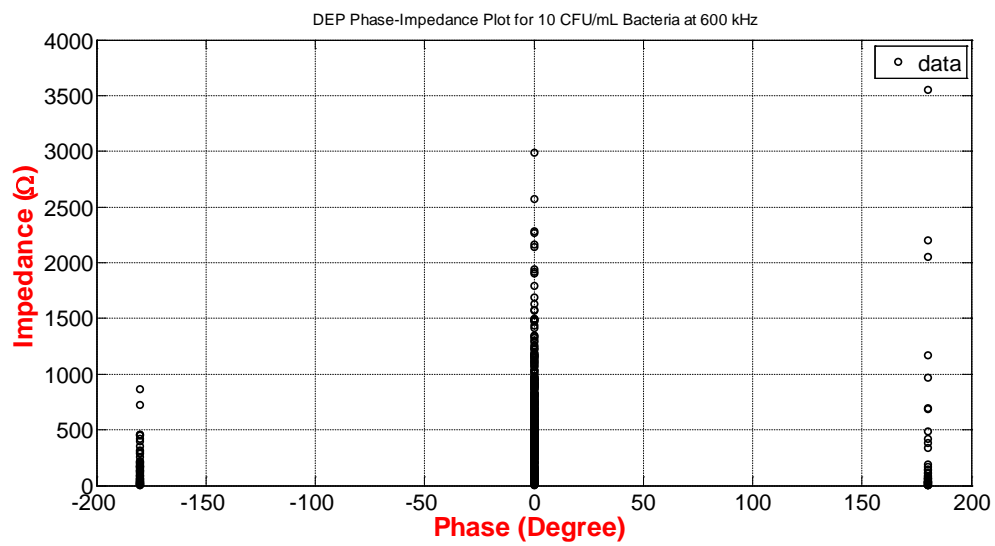
Figure D.2. Continued.

F

Figure D.2. Continued.
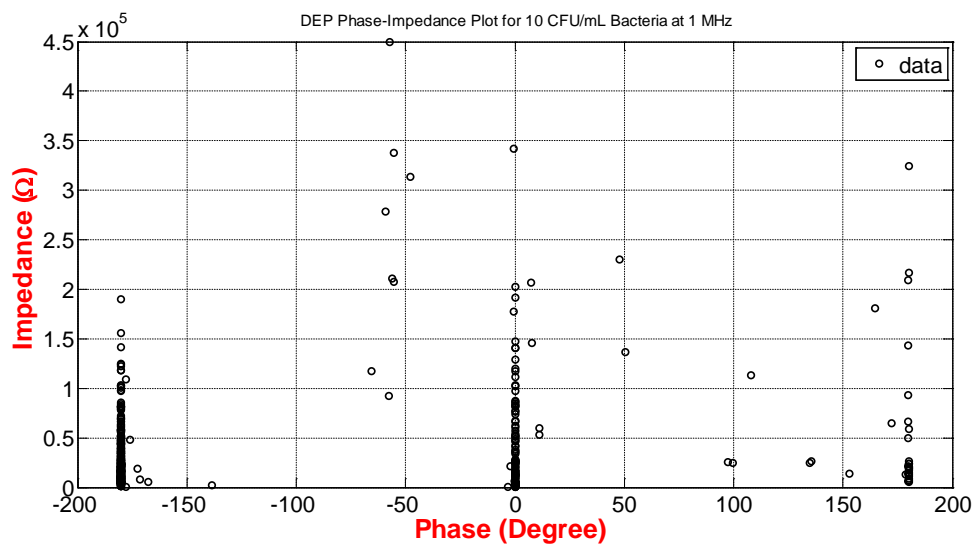
A
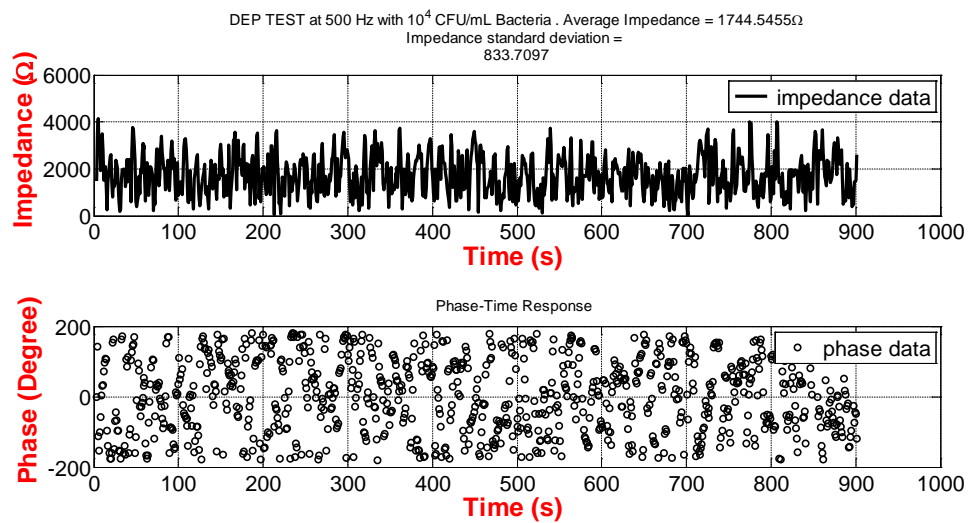
B

Figure D.3. Impedance versus time and phase versus time are shown at DEP frequencies of (A) 500 Hz, (B) 1 kHz, (C) 10 kHz, (D) 100 kHz, (E) 600 kHz, and (F) 1 MHz for *L. innocua* at a concentration of 10 CFU/mL.

C
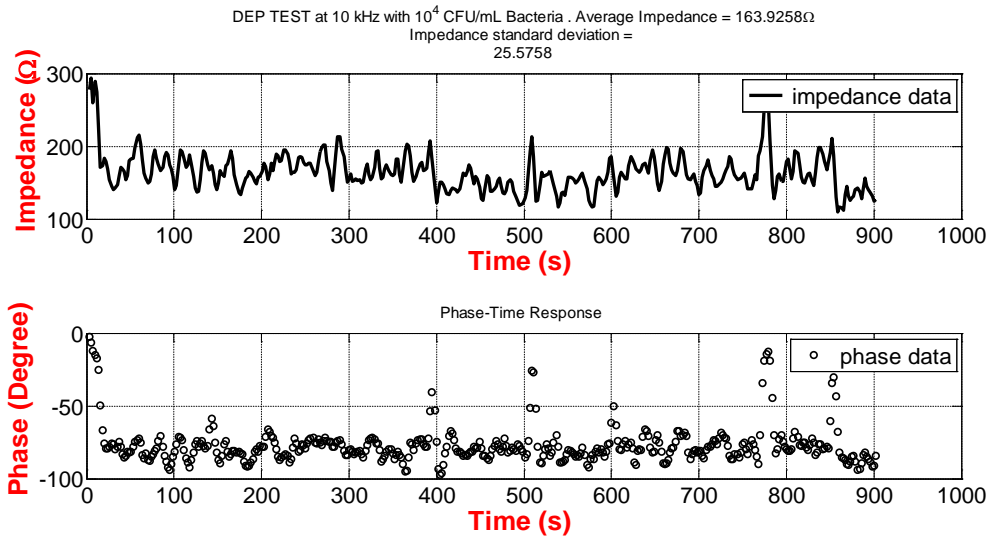
D

Figure D.3. Continued.

E

F

Figure D.3. Continued.

A

Figure D.4. Impedance versus phase are shown at (A) 500 Hz, (B) 1 kHz, (C) 10 kHz, (D) 100 kHz, (E) 600 kHz, and (F) 1 MHz DEP frequencies for *L. innocua* at a concentration of 10 CFU/mL. The legend data implies impedance data on the graph.
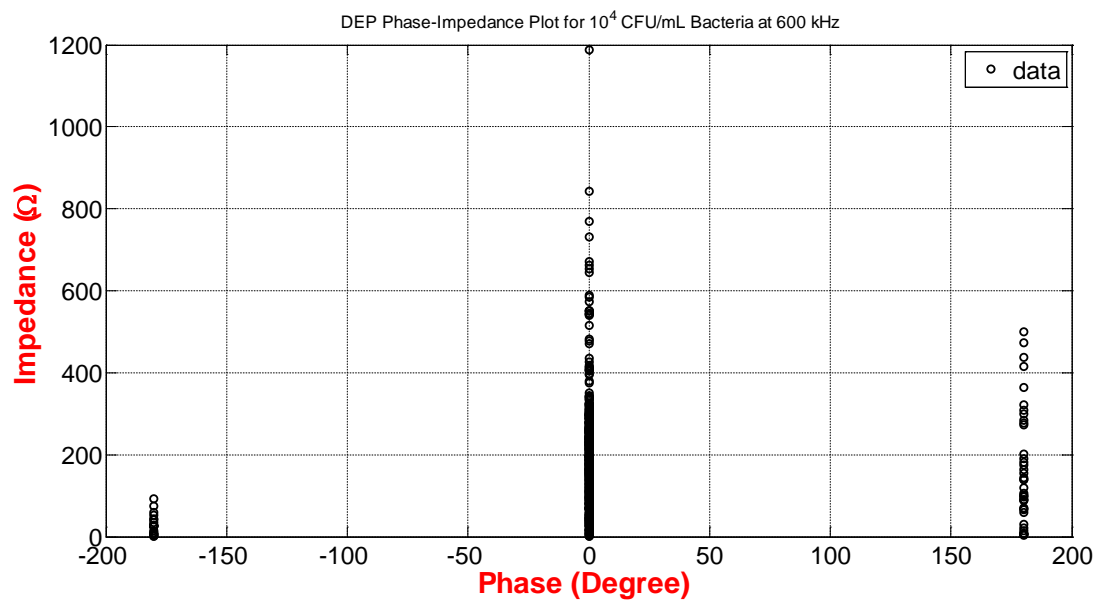
B

C
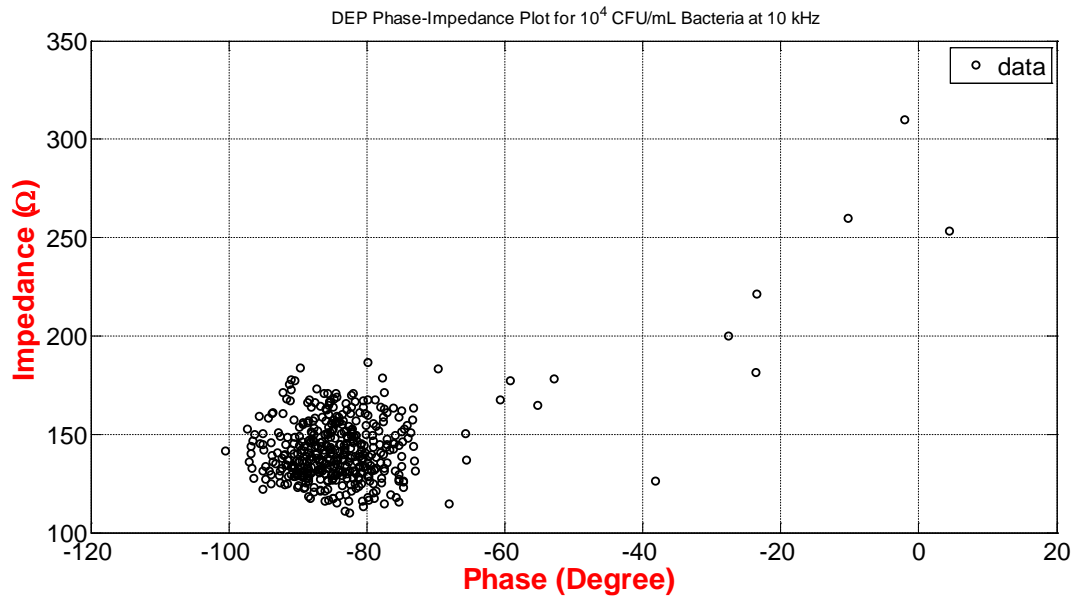
Figure D.4. Continued.
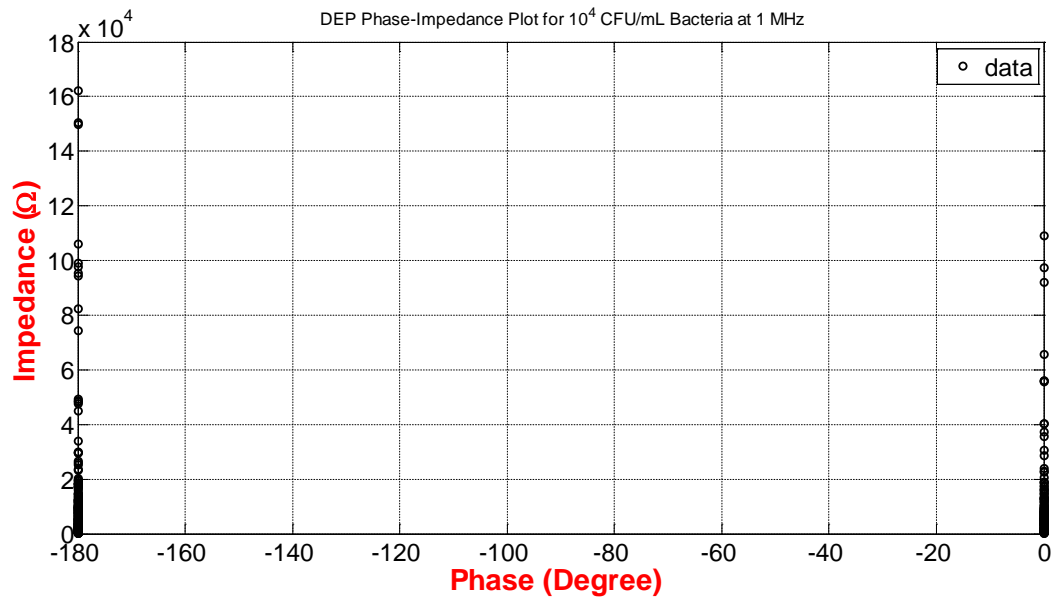
D
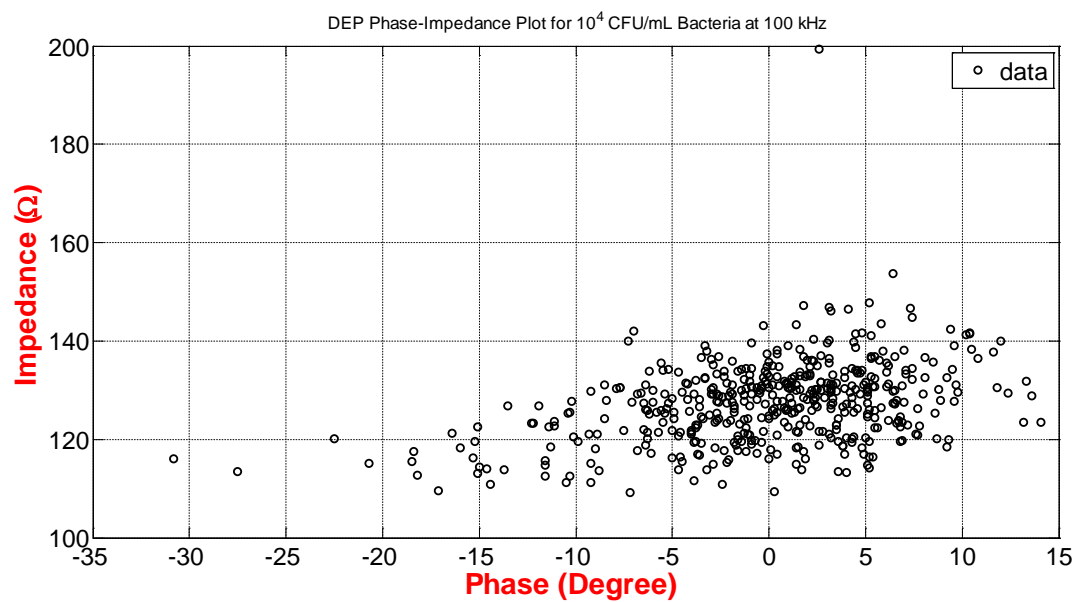
E

Figure D.4. Continued.

F

Figure D.4. Continued.

APPENDIX E

SELECTIVITY DATA

This appendix shows the results for 10^7 CFU/mL bacteria concentration for selectivity of

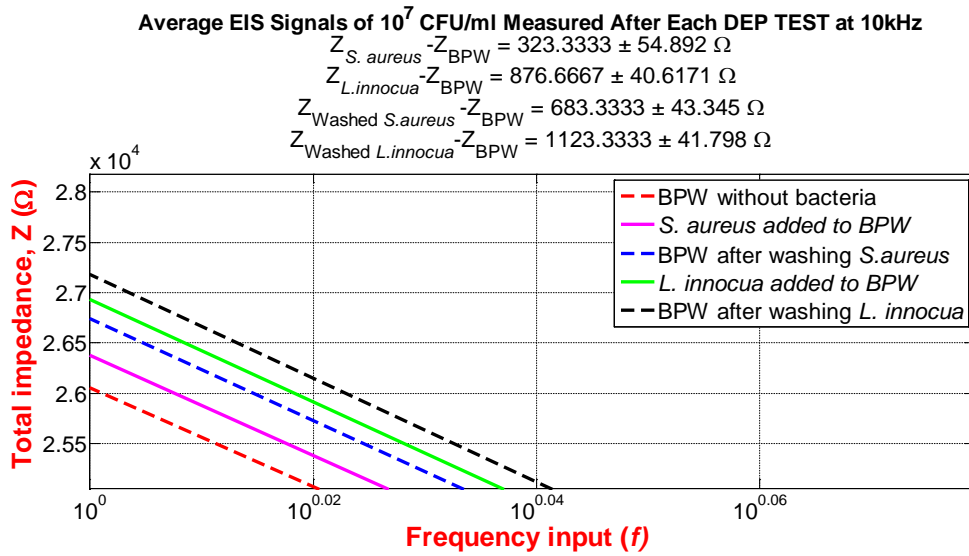*S. aureus* which were not included in the linear range sensitivity calculations.

Figure E.1. The total impedance measurements after DEP-EIS test at 10 kHz and 10^7 CFU/mL bacteria concentration of *L. innocua* and *S. aureus*.
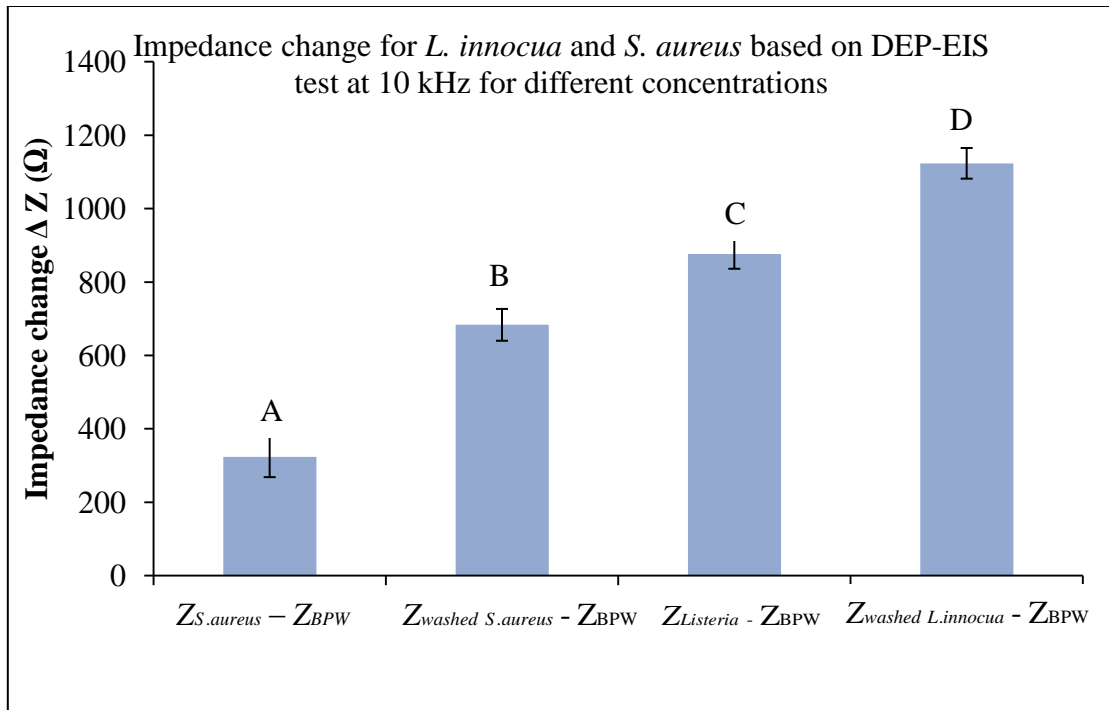
Figure E.2. Impedance change of *S. aureus* ($Z_{S.aureus}$, $Z_{washed\ S.aureus}$) and *L. innocua* ($Z_{L.innocua}$, $Z_{washed\ L.innocua}$) relative to aptamer coated IMEs impedance (Z_{BPW}) determined based on DEP-EIS technique at 10 kHz for 10 min for bacteria concentration of 10^7 CFU/mL.